



HAL
open science

Characterization of fascia lata mechanical behavior and contribution to its numerical modelling

Yuliia Sednieva

► **To cite this version:**

Yuliia Sednieva. Characterization of fascia lata mechanical behavior and contribution to its numerical modelling. Biomechanics [physics.med-ph]. Université de Lyon, 2021. English. NNT : 2021LYSE1326 . tel-03783572

HAL Id: tel-03783572

<https://theses.hal.science/tel-03783572>

Submitted on 22 Sep 2022

HAL is a multi-disciplinary open access archive for the deposit and dissemination of scientific research documents, whether they are published or not. The documents may come from teaching and research institutions in France or abroad, or from public or private research centers.

L'archive ouverte pluridisciplinaire **HAL**, est destinée au dépôt et à la diffusion de documents scientifiques de niveau recherche, publiés ou non, émanant des établissements d'enseignement et de recherche français ou étrangers, des laboratoires publics ou privés.



N°d'ordre NNT : 2021LYSE1326

THESE de DOCTORAT DE L'UNIVERSITE DE LYON
opérée au sein de
l'Université Claude Bernard Lyon 1

Ecole Doctorale N° 162
(Mécanique, Energétique, Génie civil et Acoustique)

Spécialité de doctorat : Mécanique
Discipline : Biomécanique

Soutenue publiquement le 16/12/2021, par :

Yuliia SEDNIEVA

**Caractérisation mécanique du fascia lata et
contribution à sa modélisation numérique**

Devant le jury composé de :

LAPORTE Sébastien	Professeur des Universités, Arts et Métiers ParisTech	Président
CHAGNON Grégory	Professeur des Universités, Univ Grenoble Alpes	Rapporteur
MASSON Catherine	Directrice de Recherche, Université Gustave Eiffel	Rapporteuse
BEYER Benoit	PhD, Université Libre de Bruxelles	Examineur
LAFON Yoann	Maître de Conférences, UCB Lyon 1	Examineur
BRUYERE-GARNIER Karine	Directrice de Recherche, Univ Gustave Eiffel	Directrice de thèse
GRAS Laure-Lise	Maître de Conférences, UCB Lyon 1	Co-directrice de thèse
VISTE Anthony	Maître de Conférences, UCB Lyon 1 Praticien Hospitalier, Hospices Civils de Lyon	Co-directeur de thèse

THESE de DOCTORAT DE L'UNIVERSITE DE LYON
opérée au sein de
l'Université Claude Bernard Lyon 1

Ecole Doctorale N° 162
(Mécanique, Energétique, Génie civil et Acoustique)

Spécialité de doctorat : Mécanique
Discipline : Biomécanique

Soutenue publiquement le 16/12/2021, par :

Yuliia SEDNIEVA

**Characterization of fascia lata mechanical
behavior and contribution to its numerical
modelling**

Devant le jury composé de :

LAPORTE Sébastien	Professeur des Universités, Arts et Métiers ParisTech	Président
CHAGNON Grégory	Professeur des Universités, Univ Grenoble Alpes	Rapporteur
MASSON Catherine	Directrice de Recherche, Université Gustave Eiffel	Rapporteuse
BEYER Benoit	PhD, Université Libre de Bruxelles	Examineur
LAFON Yoann	Maître de Conférences, UCB Lyon 1	Examineur
BRUYERE-GARNIER Karine	Directrice de Recherche, Univ Gustave Eiffel	Directrice de thèse
GRAS Laure-Lise	Maître de Conférences, UCB Lyon 1	Co-directrice de thèse
VISTE Anthony	Maître de Conférences, UCB Lyon 1 Praticien Hospitalier, Hospices Civils de Lyon	Co-directeur de thèse

Université Claude Bernard – LYON 1

Président de l'Université	M. Frédéric FLEURY
Président du Conseil Académique	M. Hamda BEN HADID
Vice-Président du Conseil d'Administration	M. Didier REVEL
Vice-Président du Conseil des Etudes et de la Vie Universitaire	M. Philippe CHEVALLIER
Vice-Président de la Commission de Recherche	M. Petru MIRONESCU
Directeur Général des Services	M. Pierre ROLLAND

COMPOSANTES SANTE

Département de Formation et Centre de Recherche en Biologie Humaine	Directrice : Mme Anne-Marie SCHOTT
Faculté d'Odontologie	Doyenne : Mme Dominique SEUX
Faculté de Médecine et Maïeutique Lyon Sud - Charles Mérieux	Doyenne : Mme Carole BURILLON
Faculté de Médecine Lyon-Est	Doyen : M. Gilles RODE
Institut des Sciences et Techniques de la Réadaptation (ISTR)	Directeur : M. Xavier PERROT
Institut des Sciences Pharmaceutiques et Biologiques (ISBP)	Directrice : Mme Christine VINCIGUERRA

COMPOSANTES & DEPARTEMENTS DE SCIENCES & TECHNOLOGIE

Département Génie Electrique et des Procédés (GEP)	Directrice : Mme Rosaria FERRIGNO
Département Informatique	Directeur : M. Behzad SHARIAT
Département Mécanique	Directeur M. Marc BUFFAT
Ecole Supérieure de Chimie, Physique, Electronique (CPE Lyon)	Directeur : Gérard PIGNAULT
Institut de Science Financière et d'Assurances (ISFA)	Directeur : M. Nicolas LEBOISNE
Institut National du Professorat et de l'Education	Administrateur Provisoire : M. Pierre CHAREYRON
Institut Universitaire de Technologie de Lyon 1	Directeur : M. Christophe VITON
Observatoire de Lyon	Directrice : Mme Isabelle DANIEL
Polytechnique Lyon	Directeur : Emmanuel PERRIN
UFR Biosciences	Administratrice provisoire : Mme Kathrin GIESELER
UFR des Sciences et Techniques des Activités Physiques et Sportives (STAPS)	Directeur : M. Yannick VANPOULLE
UFR Faculté des Sciences	Directeur : M. Bruno ANDRIOLETTI

RÉSUMÉ

Les pathologies du genou liées au sport sont nombreuses et impliquent, pour partie, la bandelette iliotibiale (ITT). Il s'agit d'un renforcement d'une partie du fascia profond de la cuisse, nommé fascia lata. Le fascia lata est un tissu conjonctif fibreux composé de fibres d'élastine et de réseaux de fibres de collagène présents dans différentes couches de tissu. Il a un rôle stabilisateur de l'articulation et permet le transfert des efforts entre les muscles, mais les propriétés et mécanismes de déformation de ce tissu restent mal connus. Dans ce contexte, les mécanismes de déformation du fascia lata lors de mouvements physiologiques du genou ont été étudiés. Des données quantitatives des champs de déformation du fascia lata ont été obtenues *in situ* mettant en évidence des mécanismes de déformation en traction, compression et aussi cisaillement. Par conséquent, le comportement mécanique d'échantillons isolés de fascia lata a été analysé avec des essais de cisaillement de type large bande et traction de biais, incluant l'étude de la cinématique des fibres de collagène. Une première contribution à la modélisation en éléments finis du comportement du fascia a également été proposée. Enfin, comme l'état de déformation naturel du fascia lata contribue à une bonne mobilité du genou, une étude *in situ* a été mise en place pour évaluer l'impact sur les déformations du fascia et mobilités articulaires d'une technique chirurgicale de relâchement des tensions, dite de pie-crusting appliquée à l'ITT et pouvant être recommandée dans des cas pathologiques. L'ensemble du travail réalisé apporte donc de nouveaux éléments dans l'étude du comportement mécanique du fascia lata.

Mots clefs : *Fascia lata, mécanismes de déformation, flexion du genou, cinématique des fibres, membrane biologique fibreuse, essai de cisaillement, technique chirurgicale de pie-crusting.*

ABSTRACT

There are many sports-related knee injuries, some of which involve the iliotibial band (ITT). This is a thicker part of the deep fascia of the thigh, called fascia lata. The fascia lata is a fibrous connective tissue composed of elastin fibers and networks of collagen fibers present in different layers of tissue. It has a stabilizing role in the joint and allows the transfer of forces between muscles, but its properties and strain mechanisms remain poorly understood. In this context, the strain mechanisms of the fascia lata during physiological knee movements were studied. Quantitative data of fascia lata strain fields were obtained *in situ* highlighting strain mechanisms in tension, compression, and shear. Therefore, the mechanical behavior of isolated fascia lata samples was analyzed with shear tests such as bias extension tests and traction of a large band tissue. The study of collagen fiber kinematics was also included. A first contribution to the finite element modelling of fascia behavior was also proposed. Finally, as the natural state of deformation of the fascia lata contributes to good knee mobility, an *in situ* study was set up to evaluate the impact on joint mobility and strain levels on fascia of a surgical tension-release technique, known as pie-crusting, applied to the ITT and which may be recommended in pathological cases. All the work carried out therefore provides new elements in the study of the mechanical behavior of fascia lata.

Keywords: *Fascia lata, strain mechanisms, knee flexion, fiber kinematics, fibrous biological membrane, shear test, surgical technique of pie-crusting.*

ACKNOWLEDGEMENTS

This is a ‘fruit’ of three years of work. I remember starting this journey and thinking what it is going to feel like to go through the doctorate. I am here, and now I can surely say it worth it! I cannot make it without two great woman who supported me through all the way, whose expertise was invaluable in formulating the research questions and methodology, helping me to find the answers to all difficult, and sometimes not that much, questions. As you may understand, I thank my supervisors, Karine Bruyère-Garnier and Laure-Lise Gras. Your insightful feedback pushed me to sharpen my thinking and brought my work to a higher level. Thank you especially for your assistance during this thesis work. I greatly appreciated our innumerable meetings, which allowed me to progress and to succeed.

A big thank you to my co-supervisor Anthony Viste, who made me discover the first anatomical dissection, was patient with the explanations, and made the consultations. Leïla Ben Boubaker, we were not able to perform all the amount of the experiments without you. I thank you for your precious help in carrying out the tests and always-positive mood. Thank you, Richard Roussillon and Stéphane Ardizzone, for your technical support.

I want to thank Alexandre Naaim for sharing with me his knowledge about motion analysis and contributing to current study. Thank you, Eva and Elvige, for the contribution into this work they made during master internships. Thank you, Melanie Ottenio, for your help with the equations. Thank you, Louis, for helping me during and after the experiments. I wish I can write here all the names, but I am limited by space, therefore, thank you, all the students and members of the LBMC for being supportive, creating a good atmosphere, and for all your pastries on Fridays! Also, thank you to all the members of the jury for accepting to judge this work.

Of course, I cannot be here if not the great support and trust in me of my husband Lyes, my family, and my closest friends! Thank you, my love, for being always here for me, reminding that I am strong, loving me, and believing in me. Thank you, mom, dad, Artem, Valerii, my grandparents, Nastya, uncle, Alena, Hazal, Maxime, Anna, and all people I love for being a part of my life, your kindness, your calls, and support help me every day!

I will never forget my first article writing, participation to the French speaking conference, experiment at the Anatomy laboratory, and many more. This was a great part of my life! Therefore, at the end I would like to thank two people who taught me biomechanics, supervised my first internship, whose encouragement bring me to the ‘fascia lata’. Thank you, Batiste Sandoz and Damien Subit.

Have a good reading!

TABLE OF CONTENTS

RÉSUMÉ	4
ABSTRACT	5
ACKNOWLEDGEMENTS	6
TABLE OF CONTENTS	7
TABLE OF FIGURES.....	11
LIST OF TABLES	19
ABBREVIATIONS.....	20
INTRODUCTION	21
CHAPTER I	25
STATE OF THE ART AND OBJECTIVES.....	25
1.1. State of the art	25
1.1.1. Anatomy and function of deep fascia	25
1.1.2. Microstructural anatomy of fascia lata	27
1.1.2.1. Thickness	27
1.1.2.2. Collagen fibers distribution.....	29
1.1.3. Mechanical properties of fascia lata	31
1.1.3.1. Mechanical behavior under tensile test.....	31
1.1.3.2. Mechanical behavior under shear loading	34
1.1.3.3. Age and sex effect.....	35
1.1.4. Constitutive models of fascia lata’s mechanical behavior and use in FE modeling	35
1.2. Synthesis and Objectives.....	38
CHAPTER II.....	40
STRAIN MECHANISM DURING KNEE FLEXION MOVEMENT.....	40
CHAPTER III	55
MECHANICAL PROPERTIES OF FASCIA DURING A SHEAR LOADING.....	55
3.1. Introduction.....	55
3.2. Materials and Methods	55
3.2.1. Specimen Preparation	55
3.2.1.1. Bias test specimen preparation.....	57
3.2.1.3. Specimen preparation for a bi-photon microscopy	58
3.2.2. Testing procedures.....	58

3.2.2.1.	Mechanical test setup	58
3.2.2.2.	Video setup	59
3.2.2.3.	Loading conditions.....	59
3.2.3.	Strain field measurements	59
3.2.3.1.	Bias test.....	59
3.2.3.2.	Large band test.....	60
3.2.4.	Fibers kinematics.....	61
3.2.5.	Bi-photon microscopy	62
3.3.	Results	63
3.3.1.	Mechanical behavior	63
3.3.1.1.	Bias test.....	63
3.3.1.2.	Large band test.....	65
3.3.2.	Fiber Distribution.....	66
3.3.2.1.	Bias test.....	66
3.3.2.2.	Large band test.....	67
3.3.3.	Bi-photon microscopy	69
3.4.	Discussion	70
CHAPTER IV.....		73
FINITE ELEMENT (FE) MODELING OF FASCIA SAMPLE’S MECHANICAL BEHAVIOR.....		73
4.1.	Introduction.....	73
4.2.	Materials and Methods	73
4.2.2.	Material model: constitutive law	75
4.2.3.	Data fitting.....	78
4.3.	Results	78
4.3.1.	Stress-strain distribution during the uniaxial tensile simulations.....	78
4.3.2.	Stress-strain distribution during the bias test simulation	79
4.3.3.	Stress-strain distribution during the large band test simulation	81
4.4.	Discussion and Perspectives.....	82
CHAPTER V.....		84
ITT STRAIN RELEASE AND KNEE MOBILITY		84
5.1.	Introduction.....	84
5.2.	Materials and Methods	84
5.2.1.	Specimen Preparation	84

5.2.2.	Anatomical Frames Acquisition and Motion Analysis	85
5.2.3.	Passive leg movements	87
5.2.4.	Strain field measurements by DIC	88
5.2.5.	Pie-crusting Technique	89
5.3.	Test Conduction.....	90
5.4.	Results	91
5.4.1.	Static strain analysis	91
5.4.2.	Ranges of motion.....	95
5.4.2.1.	Flexion-extension leg movements	95
5.4.2.2.	Rotation leg movements	96
5.4.2.3.	Varus-valgus leg movements (abduction-adduction)	97
5.4.3.	Strains after movements	99
5.4.4.	Strain mechanisms during movements.....	101
5.4.4.1.	Strain along the thigh	101
5.4.4.1.1.	Leg flexion movement	101
5.4.4.1.2.	Leg rotation and varus-valgus movements	102
5.4.4.2.	Principal strains.....	103
5.4.4.2.1.	Leg flexion movement	103
5.4.4.2.2.	Leg rotation and varus-valgus movements	104
5.5.	Discussion	107
	CONCLUSIONS	109
	BIBLIOGRAPHY.....	112
	APPENDIX I	123
	Additional results to the Chapter II	123
	Materials and Methods	123
	Results	123
	Knee Angular Velocity	123
	Strain Analysis	124
	Average strains	124
	Strain Mechanisms	127
	Strain rates.....	127
	Discussion.....	128

APPENDIX II	129
Additional results to the Chapter III	129
APPENDIX III	131
Additional results to the Chapter V	131

TABLE OF FIGURES

CHAPTER I

<i>Figure 1.1-1. On the left, the examples of fascias (in grey) all over the body (Bordoni and Myers 2020) and on the right, a schematic drawing of fascias (superficial and deep) anatomy in the leg. Where: A – skin, B – superficial fascia, C – peripheral layer of deep fascia; D – intermuscular layer of deep fascia, DAT – deep adipose tissue, SAT – superficial adipose tissue (Ali, Srinivasan, and Peh 2014).</i>	<i>25</i>
<i>Figure 1.1-2. Confocal microphotograph of the deep fascia of lower limb showing collagen fibers on application of fluorescein dye using laser scanning multiphoton confocal microscope (Radiance 2000) (Bhattacharya et al. 2010).</i>	<i>26</i>
<i>Figure 1.1-3. (A) Lateral view of the muscles of the anterior region of the hip, including the iliotibial tract, iliac crest, lateral intermuscular septum, and a linea aspera (Themes 2016b; 2016a); (B) location of the ITT and identification of its insertions on the distal site of the leg (subject 2021_098, LBMC).</i>	<i>26</i>
<i>Figure 1.1-4. Images of fascia lata visible by ultrasound (A)(C. Stecco et al. 2011a) and by histological analysis with HE stain (B), highlighting the thin layer of fibroelastic tissue in the external side of the fascia lata (C. Stecco et al. 2008).</i>	<i>27</i>
<i>Figure 1.1-5. SHG images of fascia tissue in (A) forward and (B) backward direction. (C) Fascia sample topography (5μm scan) taken with AFM.</i>	<i>29</i>
<i>Figure 1.1-6. Zoom on the lateral view of the area along the ITT showing longitudinal (in green color) and transversal (in red color) collagen fibers from tested subject (LBMC).</i>	<i>30</i>
<i>Figure 1.1-7. (A) Classification of the fibers' orientations and (B) typical image of the fascia lata. i: longitudinal (inferior to superior), ii: transverse (anterior to posterior or medial to lateral), iii: M/L- or A/P- diagonal (medial-superior to lateral-inferior or anterior–superior to posterior-inferior), iv: L/M- or P/A- diagonal (lateral-superior to medial-inferior or posterior-superior to anterior-inferior) (Otsuka et al. 2018).</i>	<i>30</i>
<i>Figure 1.1-8. Mechanical tests for the fascia lata: (a) loading–unloading cycles (b) with the typical results of (c) stiffness, (d) Young's modulus, and (e) hysteresis loop. (Otsuka et al. 2018)</i>	<i>32</i>
<i>Figure 1.1-9. Cauchy stress versus stretch from pure shear and uniaxial tensile tests of deep fascia lata samples harvested from the sheep (Ruiz-Alejos et al. 2016).</i>	<i>34</i>
<i>Figure 1.1-10. Experimental uniaxial (in the longitudinal and transverse direction) and biaxial stress-strain curves and corresponding predicted responses based on the one constant and two constant models (Weiss 1994).</i>	<i>36</i>

Figure 1.1-11. Results from the uniaxial tensile tests (circles and squares) and the constitutive model (solid and dashed lines) (Ruiz-Alejos et al. 2016)..... 37

Figure 1.1-12. Contour plot of the displacement along the loading direction during the pure shear tests superposed to the displacement map obtained by FE simulation (Ruiz-Alejos et al. 2016)..... 37

CHAPTER III

Figure 3.2-1. (A) Example of samples location for large band (on the left) and bias tests (on the right) respectively on internal and external sides of the fascia lata harvested from the corresponding left leg of subjects 2021_133 and 2021_107. (B) Minor and major principal strain directions on the external surface of fascia lata measured in Sednieva et al. (2020). .. 56

Figure 3.2-2. Representation of the testing sample of fascia lata for a bias test with the identification of its dimensions..... 57

Figure 3.2-3. Representation of the testing sample of fascia lata for a large band test with the identification of its dimensions..... 58

Figure 3.2-4. The configurations of the loading cell on the INSTRON machine (on the left) and the fixture (on the right) for the bias and large band tests. 58

Figure 3.2-5. Example of speckle applied on the surface of fascia lata sample for the bias test (on the left) and the calibration grid for a 2D calibration (on the right). 60

Figure 3.2-6. Example of speckle applied on the surface of fascia lata sample for the large band test (on the left) and the calibration grid for a 3D calibration (on the right)..... 61

Figure 3.2-7. Example of an image (0% strain) obtained for the observation of fibers for the large band test (left) (sample 133_L_03) and bias test (right) (front face of sample 107_L_07). 61

Figure 3.2-8. Examples of the colored detected fibers perpendicular to the shading (SW – South-West, SE – South-East) for the large band test (on the left) (sample 133_L_03) and bias test (on the right) (front face of sample 107_L_07) with color gradient scale for fiber detection. 62

Figure 3.2-9. Example of the histograms for the two types of shading (South-West and South-East) associated with longitudinal and transverse fiber directions with the curve of the maximum values between the two shadows. The results of the left are from the large band test (sample 133_L_03) and on the right – from the bias test (front face of sample 107_L_07) at 0% stretch. 62

Figure 3.3-1. Nominal stress versus global and local strain curves for samples 107_L_06 (left) and 107_L_08 (right). 63

Figure 3.3-2. Strain field on the front (top) and back faces (bottom) of 107_L_06 (left) and 107_L_08 (right) samples at 10% deformation. The white arrows represent the main

<i>deformation directions. Square area in the middle of the sample named R0 shows the average value of corresponding strain.</i>	<i>64</i>
<i>Figure 3.3-3. Correlation results on the front (top) and back faces (bottom) of 308_L_03 sample at 10% deformation. The white arrows represent the main deformation directions.</i>	<i>65</i>
<i>Figure 3.3-4. Nominal stress versus global and local strain curves for 133_R_02 sample. ...</i>	<i>65</i>
<i>Figure 3.3-5. Strain field on the front (internal) faces of 133_R_02 (left) and 133_L_04 (right) samples for a 9% local deformation. The white arrows represent the main deformation directions. Square area in the middle of the sample named R0 shows the average value of corresponding strain.</i>	<i>66</i>
<i>Figure 3.3-6. Longitudinal and transverse fibers detection on the samples during bias test at 0%, 6%, and 10% displacements. Colors of detected fibers correspond to the angles from the gradient scale for fiber detection (Figure 3.2-8).</i>	<i>66</i>
<i>Figure 3.3-7. The amount of fibers corresponding to a given angle for 0%, 6%, and 10% global deformation detected on the 107_L_05 (left) and 107_L_07 (right) samples during bias test.</i>	<i>67</i>
<i>Figure 3.3-8. Reorientation of the main collagen fibers networks along the sample global stretch of 107_L_05 (only longitudinal fibers detected) and 107_L_07 samples (both longitudinal and transverse fibers detected).</i>	<i>67</i>
<i>Figure 3.3-9. Longitudinal and transverse fibers detection on the samples during large band test at 0% and 8% displacements. Colors of detected fibers correspond to the angles from the gradient scale for fiber detection (Figure 3.2-8).</i>	<i>68</i>
<i>Figure 3.3-10. The amount of fibers corresponding to a given angle for first three cycles at 0% and 8% local deformation detected on the 133_R_01 (top) and 133_L_03 (bottom) samples.</i>	<i>69</i>
<i>Figure 3.3-11. The transverse and longitudinal fibers orientation along the global strain of the 133_R_01 sample. First three cycles are in red, green and black colors respectively and the rest 6 cycles are in blue color.</i>	<i>69</i>
<i>Figure 3.3-12. Human ITT (107_R_05 sample) observation with bi-photon microscopy. Green color corresponds to the elastin fibers (on the left) and blue color to the collagen fibers (on the right). Size of the bar is 50 μm. White arrow is showing the direction of the corresponding fiber.</i>	<i>70</i>

CHAPTER IV

Figure 4.2-1. Boundary conditions of uniaxial tensile (top), bias (middle) and large band (bottom) models of fascia lata samples with corresponding longitudinal (blue) and transverse (pink) material directions. Black crosses highlight fixed nodes and by red triangles indicate

<i>translational nodes. On the fibers' identifications, red arrow shows the material principal direction.</i>	<i>75</i>
<i>Figure 4.2-2. Representation of longitudinal (on the left) and transverse (on the right) uniaxial tensile tests.</i>	<i>76</i>
<i>Figure 4.3-1. Stress-strain curves for longitudinally (left) and transversally (right) loaded one-fiber network model from: the experimental data (Ruiz-Alejos et al. 2016), analytically fitted Two Coefficient model, and FE model.</i>	<i>79</i>
<i>Figure 4.3-2. Contour plots of the E_{xx}, principal (E_1 and E_2) and maximal shear ($\max E_{xy}$) strains distributions on the front and back faces of the experimental sample obtained at 10% stretch during bias test.</i>	<i>80</i>
<i>Figure 4.3-3. Contour plots of the strains distributions in the longitudinal and transverse layers along the loading direction (which is chosen to be the bisector of two fibers directions) during bias test simulation obtained at the 10% strain.</i>	<i>80</i>
<i>Figure 4.3-4. Nominal stress-stretch curve of the bias test simulation.</i>	<i>81</i>
<i>Figure 4.3-5. Contour plots of the E_{yy}, principal (E_1 and E_2) and maximal shear ($\max E_{xy}$) strains distributions for the experimental sample (front face only) during the large band test at the 6% strain.</i>	<i>81</i>
<i>Figure 4.3-6. Contour plots of the Y-stress, E_{yy}, principal (E_1 and E_2) and maximal shear ($\max E_{xy}$) strains distributions in longitudinal and transverse layers along the loading direction (which is chosen to be aligned with the bisector of two fibers directions) during large band simulation, obtained at the 6% strain.</i>	<i>82</i>
<i>Figure 4.3-7. Nominal stress-strain curve of the large band test simulation.</i>	<i>82</i>

CHAPTER V

<i>Figure 5.2-1. Body preparation: (A) tripods drilled into the major anatomical points for motion analysis (subject 2021_073), (B) speckles pattern for digital image correlation (DIC) (subject 2021_098).</i>	<i>85</i>
<i>Figure 5.2-2. Experimentation area: motion analysis cameras (white) and Photron cameras for the DIC (red).</i>	<i>86</i>
<i>Figure 5.2-3. Diagram showing locations of the anatomical landmarks (black circles), and the reflective markers (yellow circles) on the left leg, and an example of the orientation of the anatomical reference frame for the femur. ME, LE, and FH corresponds to medial malleolus, lateral malleolus, and fibula head, respectively.</i>	<i>86</i>
<i>Figure 5.2-4. Lateral view of the flexion-extension movement of the left leg with identification of the iliotibial tract (ITT) and reference image of 47°, which is defining the zero-strain position.</i>	<i>87</i>

Figure 5.2-5. Schematically illustrated leg movements: (A) common lateral view with knee flexion angles identifications for both movements, (B) varus-valgus (adduction-abduction) and (C) rotation. Reference knee flexion angles are indicated in orange font. 88

Figure 5.2-6. Example of the image recorded by Photron camera with identifications of ITT insertions and area for the pie-crusting (subject 073_L)..... 88

Figure 5.2-7. Lateral view of the right extended leg (subject 073) with identification of defined areas 2 and 3 on the iliotibial tract (ITT) (on the left) from the areas corresponding to those from Otsuka et al. (2020) (on the right). 89

Figure 5.2-8. Illustrations of: A – leg position with identification of ITT and cuts for a pie-crusting technique in lateral view; B – identifications of: initial (case I), after pie-crusting state (case A), after ITT dissection from tibial insertion (case B). 90

Figure 5.4-1. Subjects 219_L and 073_R x-axis strains evolutions along the time during the pie-crusting technique and ITT dissection on areas 2 (green) and 3 (orange). Scale range is the same for pie-crusting (on the left) and ITT dissection (on the right) plots. 92

Figure 5.4-2. E_{xx} after the pie-crusting and before the ITT dissection on the areas 2 and 3 for each leg of all subjects. 93

Figure 5.4-3. (A) Distribution maps of the E_{xx} strain after pie-crusting (left) and before ITT dissection (right) on the ITT from subjects 219_L (top) and 073_L (bottom) with three extensometers (white lines): E_0 in the longitudinal direction of the ITT, E_1 and E_2 in the transverse direction of the ITT. (B) Displacement measured with the corresponding extensometer (E_0 , E_1 , and E_2) for all subjects. 94

Figure 5.4-4. Subject 098_R flexion-extension movements knee joint angles with statistical data (range, mean values) during the initial, after pie-crusting, after ITT dissection cases. 95

Figure 5.4-5. Flexion-extension movements knee joint angles' ranges (from the minimum to the maximum angle) for all subjects and all cases (initial, after pie-crusting, after ITT dissection from tibial insertion). 96

Figure 5.4-6. Subject 098_R rotation movements knee joint angles' with statistical data (range and mean values) when the leg was flexed at approximately 0° , 20° , and 50° during the initial, after pie-crusting, and after ITT dissection cases. 97

Figure 5.4-7. Rotation movements knee joint angles' ranges (from the minimum to the maximum angle) for all subjects and all cases (initial, after pie-crusting, after ITT dissection from tibial insertion) when the leg was flexed at approximately 0° , 20° , and 50° . R and L in the subject number legend identifies the right and the left leg, respectively..... 97

Figure 5.4-8. Subject 098_R varus-valgus movements' knee joint angles with statistical data (range, mean values) when the leg was flexed at approximately 0° , 20° , and 50° during the initial, after pie-crusting, and after ITT dissection cases. 98

Figure 5.4-9. Varus-valgus movements' knee joint angles' ranges (from the minimum to the maximum angle) for all subjects and all cases (initial, after pie-crusting, after ITT dissection from tibial insertion) when the leg was flexed at approximately 0°, 20°, and 50°. R and L in the subject number legend identifies the right and the left leg, respectively. 98

Figure 5.4-10. Comparison of the average E_{xx} along the static extended positions of the leg between subjects on the areas 2 (top) and 3 (bottom). Dashed red vertical lines indicate the strains after pie-crusting (PC) and before the ITT dissection (ITT diss). F – flexion, V_0/R_0 , V_{20}/R_{20} , V_{50}/R_{50} , correspondingly, varus valgus/rotation when knee is extended (0°), flexed at 20° and 50° 100

Figure 5.4-11. Subject 219_L mean E_{xx} strain along time (top) and along flexion knee angle (bottom) during leg flexion movements on both areas. The curves in blue color are representing the results on the area 2, and the curves in magenta color are representing the results on the area 3..... 101

Figure 5.4-12. Knee rotation movements for leg 2019_L : mean value of x-axis– strain (E_{xx}) along the time on the area 2 (mid-thigh) and area 3 (closer to the pie-crust zone)s that are closer and further from the pie-crusting and ITT dissection, corresponding to area 3 (magenta) and area 2 (blue). 102

Figure 5.4-13. Subject 219_L principal strains and maximal shear strain distributions with the knee flexion angles during flexion-extension movement for areas 2 and 3. Bold and dashed lines are corresponding to the strains from the area 2 and 3, respectively. In blue – minor principal strain E_1 , in red – major principal strain E_2 , in black - maximal shear strain $\max E_{xy}$. The range and mean values of corresponding strain and of angles is on the top of the graphs. 104

Figure 5.4-14. Average maximal shear $\max E_{xy}$, principal major E_1 and minor E_2 strains change with the rotation and adduction-abduction knee angle during subject 219_L rotation and subject 073_L varus-valgus movements, respectively. Rotations and varus-valgus movements with different knee flexion angles (0°, 20°, and 50°) for initial, after pie-crusting, and after ITT dissection cases on the areas 2 and 3 along the ITT..... 105

Figure 5.4-15. Subject 098_R E_1 strain against E_2 strain in absolute value during rotation and varus-valgus movements with flexed knee at 0°, 20°, and 50° along the areas 2 and 3 on the ITT. 106

APPENDIX I

Figure 1. Averaged angular velocities and corresponding standard deviations (grey area) over the knee angles for left L (top) and right R (bottom) legs from all subjects. Data was filtered using a forward-backward linear filter. Filter coefficients were obtained from a low-pass digital Butterworth filter (3rd order, cut off frequency of 2Hz) that was first applied on data. Even though angular velocity was applied manually, results show good reproducibility for each subject. Inter-subject variability can be observed because of subjects' different knee mobility and associated range of motion.....123

Figure 2. Maximal shear strain distribution $\max E_{xy}$ on the ITT, at knee angles of $20 \pm 0.5^\circ$, $60 \pm 0.5^\circ$, and $90 \pm 0.5^\circ$ for all subjects (Test 1). White arrows show the direction of the major E_1 and minor E_2 principal strains, which are perpendicular to each other.....124

Figure 3. Mean strain distributions over the knee angles for the ITT. In blue, mean major principal strain E_1 , in red, minor principal strain E_2 , and in black maximal shear strain $\max E_{xy}$. For each test, all cycles are plotted. Vertical dashed line represents the knee position chosen as reference: 47° . Three other vertical lines locate knee angles of 20° , 60° , and 90°125

Figure 4. Average curves for mean major principal strain E_1 (bold) and mean minor principal strain E_2 (dashed) over the knee angles on the ITT.....126

Figure 5. Average curves for mean major principal strain E_1 against negative mean minor principal strain E_2 for ITT. Results are presented for each subject and average of the test. Blue curves and light blue areas correspond respectively to average values and standard deviation obtained for a knee angle lower than the reference position of 47° : extended knee. Red curves and orange areas correspond respectively to average values and standard deviation obtained for a knee angle greater than the reference position of 47° : flexed knee. Dashed line represents the $y = x$ curve, when points are along this line, pure shear can be observed.....127

Figure 6. Averaged strain rates and corresponding standard deviation over the knee angles for all subjects on the ITT. Blue curves and grey areas correspond respectively to average strain rate and standard deviation for major strain E_1 . Red curves and orange areas correspond respectively to average strain rate and standard deviation for minor strain E_2 . Data was filtered using a forward-backward linear filter. Filter coefficients were obtained from a low-pass digital Butterworth filter (3rd order, cut off frequency of 2Hz) that was first applied on data.....128

APPENDIX II

Figure 1. Reorientation of the main fibers along the global stretch measured on the front and (or) on the back faces of the large band samples. * A synchronization error may give this curve shape for samples 133_L_05 and 133_R_05.....129

Figure 2. Reorientation of the main fibers along the global stretch measured on the front and (or) on the back faces of the bias samples.....130

APPENDIX III

Figure 1. X-axis strains evolutions along the time during the pie-crusting technique and ITT dissection on areas 2 (green) and 3 (orange) for remaining subjects. Scale range is the same for pie-crusting (on the left) and ITT dissection (on the right) plots.....132

Figure 2. Flexion-extension movements knee joint angles with statistical data (range, mean values) during the initial, after pie-crusting, after ITT dissection cases for all remaining subjects.

Figure 3. Rotation movements knee joint angles' with statistical data (range and mean values) when the leg was flexed at approximately 0° , 20° , and 50° during the initial, after pie-crusting, and after ITT dissection cases for all remaining subjects.

Figure 4. varus-valgus movements' knee joint angles with statistical data (range, mean values) when the leg was flexed at approximately 0°, 20°, and 50° during the initial, after pie-crusting, and after ITT dissection cases for all remaining subjects.....138

Figure 5. Mean E_{xx} strain along time (top) and along flexion knee angle (bottom) during leg flexion movements on both areas. The curves in blue color are representing the results on the area 2, and the curves in magenta color are representing the results on the area 3 for all remaining subjects.....139

Figure 6. Knee rotation movements for all remaining subjects: mean value of x-axis– strain (E_{xx}) along the time on the area 2 (mid-thigh) and area 3 (closer to the pie-crust zone)s that are closer and further from the pie-crusting and ITT dissection, corresponding to area 3 (magenta) and area 2 (blue).....141

Figure 7. Knee varus-valgus movements for all subjects: mean value of x-axis– strain (E_{xx}) along the time on the area 2 (mid-thigh) and area 3 (closer to the pie-crust zone)s that are closer and further from the pie-crusting and ITT dissection, corresponding to area 3 (magenta) and area 2 (blue).....143

Figure 8. Principal strains and maximal shear strain distributions with the knee flexion angles during flexion-extension movement for areas 2 and 3. Bold and dashed lines are corresponding to the strains from the area 2 and 3, respectively for all remaining subjects. In blue – minor principal strain E_1 , in red – major principal strain E_2 , in black - maximal shear strain $maxE_{xy}$. The range and mean values of corresponding strain and of angles is on the top of the graphs.

Figure 9. Average maximal shear $maxE_{xy}$, principal major E_1 and minor E_2 strains change with the rotation and adduction-abduction knee angle during rotation movement. Rotations and varus-valgus movements with different knee flexion angles (0°, 20°, and 50°) for initial, after pie-crusting, and after ITT dissection cases on the areas 2 and 3 along the ITT. * E_1 – maximum principal strain (blue), E_2 – minimum principal strain (red), $maxE_{xy}$ – maximal shear strain (black).....149

Figure 10. Average maximal shear $maxE_{xy}$, principal major E_1 and minor E_2 strains change with the rotation and adduction-abduction knee angle during varus-valgus movement. Rotations and varus-valgus movements with different knee flexion angles (0°, 20°, and 50°) for initial, after pie-crusting, and after ITT dissection cases on the areas 2 and 3 along the ITT. * E_1 – maximum principal strain (blue), E_2 – minimum principal strain (red), $maxE_{xy}$ – maximal shear strain (black).....153

Figure 11. E_1 strain against E_2 strain in absolute value during rotation movement with flexed knee at 0°, 20°, and 50° along the areas 2 and 3 on the ITT for all remaining subjects.....155

Figure 12. E_1 strain against E_2 strain in absolute value during varus-valgus movement with flexed knee at 0°, 20°, and 50° along the areas 2 and 3 on the ITT for all remaining subjects..157

LIST OF TABLES

<i>Table 1.1-1. Gross anatomy of fascia lata: human and goat data.....</i>	28
<i>Table 1.1-2 Mechanical properties of fascia lata (means \pm S.D. or min – max range) presented in the literature. Where: Long. – longitudinal fiber direction, Trans. – transverse fiber direction.</i>	33
<i>Table 1.1-3. Constitutive models of fascia lata presented in the literature.</i>	36
<i>Table 1.1-4. Examples of available FE models of deep fascias of the leg.</i>	38
<i>Table 4.2-1. The parameters for the models.</i>	74
<i>Table 4.3-1. Material coefficients for the longitudinal Cauchy stress-strain curve, describing the fascia lata’s behavior.</i>	78
<i>Table 5.2-1. List of the recordings corresponding to leg movements performed on each leg during the experiment.....</i>	91
<i>Table 5.4-1. Average values of the ratio $\Delta L/L_0$ measured from three extensometers with standard deviation (std), averaged for all subjects.....</i>	95
<i>Table 5.4-2. Ranges of joints’ angles (rotation and abduction) averaged from all the subjects corresponding to rotation and varus-valgus movements when the knee was flexed at approximately 0°, 20°, and 50°.....</i>	99
<i>Table 5.4-3. Average and standard deviation (std) of maximum (max) and minimum (min) values of the E_{xx} strain from all subjects during flexion-extension movements for all cases.</i>	102
<i>Table 5.4-4. Average of the E_{xx} strain range and mean values from all subjects during rotations and varus-valgus movements with varying knee flexion angles for all cases.</i>	103

APPENDIX I

<i>Table 1. Mean, standard deviation (SD) and maximum relative standard deviations (RSD) for the ITT, for each subject, both legs, and for both major E_1 and minor E_2 strains. * RSD were calculated considering the five cycles and the three performed tests. Italicized values are mean values for the three subjects and both legs.....</i>	126
---	-----

APPENDIX III

<i>Table 1. Average of principal and maximal shear strains range, mean, and standard deviation values from all subjects on both areas of the interest for all cases and both rotation and varus-valgus knee movements. * Cases I, A, and B corresponds to the initial, after pie-crusting, and after ITT dissection from the tibial insertion, respectively. Std – standard deviation.....</i>	131
--	-----

ABBREVIATIONS

AOI	area of the interest
BMI	body mass index
ITB	iliotibial band
ITT	iliotibial tract
ITBS	iliotibial band syndrome

INTRODUCTION

Nowadays, sport is a style of life for many of us. In any sport, there are many positive effects on the body and health, nevertheless, knee injury is one of the commonly occurring injuries in sports, and it accounts 41 – 42.1% of all sport injuries (Sancheti et al. 2010; Taunton et al. 2002). In a ten years study made by Majewski et al. (2006), from 17397 patients with injuries, 37% had 39.8% of injuries related to the knee joint. Almost a half of them (43.1%) were young people from 20 to 29 years old, and the proportion of men and women was 68.1% and 31.6%, respectively.

It is no matter if you are a professional athlete or just a beginner, very common knee injury named iliotibial band syndrome (ITBS) is a common overuse injury of runners (Fairclough et al. 2007). Iliotibial band (ITB), also named iliotibial tract (ITT) is a thickened part of the lateral side of the fascia lata, the deep fascia of the thigh, passing through the knee.

The number of runners, harassed by the ITBS have grown from 1.6% – 12% reported by Richards et al. (2003) up to 22% documented by Fredericson and Weir (2006) just in 3 years in the US. ITBS injury is also occurring in the athletic population participating in tennis, soccer, skiing, and weight lifting (Beals and Flanigan 2013; Hadeed and Tapscott 2019), cyclists (Strauss et al. 2011; Farrell, Reisinger, and Tillman 2003; Holmes, Pruitt, and Whalen 1993; Wanich et al. 2007), football players (Martens, Libbrecht, and Burssens 1989); military recruits (Hadeed and Tapscott 2019; Strauss et al. 2011). In the non-active population the ITBS is slightly more common in women than men, and seldom (Hadeed and Tapscott 2019), when the study of Foch et al. (2015) suggests that it is twice as likely to afflict women compared to men.

One of the first symptoms of ITBS is a lateral knee pain particularly at 30° knee flexion (Charles and Rodgers 2020; Ferber et al. 2010; Sangkaew 2007; Noble 1979), which will renew as soon as activity being restarted. This specific flexion angle is related to the pain, as it is when the contact between the ITT and lateral epicondyle causes anterior-posterior friction of the ITT on the lateral femoral condyle during knee flexion and extension activities (Charles and Rodgers 2020; Fairclough et al. 2007; Strauss et al. 2011; Lavine 2010).

The study of Hamill et al. (2008) indicates that a major factor in the development of iliotibial band syndrome is the strain rate, but, there are many more theories regarding the nature of the lateral knee pain, such as inflammation of the ITT's bursa, or the compression of a fat pad located between the ITT and the femur (Hadeed and Tapscott 2019; Fairclough et al. 2007). In addition, it was found that biomechanical factors resulting in increasing the strain of the ITT are contributing to the development of this injury (Hamill et al. 2008). Because of the ITT attachments to the bones, knee adduction and internal rotation movements can lead to increased strain and tension on the ITT. It is believed that strain on the ITT and friction of the ITT sliding over the lateral femoral epicondyle is the cause of ITBS (Orava, 1978; Noble, 1980).

To prevent knee injuries, an accurate diagnosis is essential. When knee injuries occur, two treatments exist: non-invasive (Baker and Fredericson 2016; Michael Fredericson and Weir 2006; Gunter, Schweltnus, and Fuller 2004; Schweltnus et al. 1991) and surgical. The non-invasive treatments can include manual therapy techniques (M. Fredericson, Guillet, and Debenedictis 2000), anti-inflammatory medication and corticosteroid injection (Michael Fredericson and Weir 2006; Gunter, Schweltnus, and Fuller 2004; Schweltnus et al. 1991).

They found to give a treatment with quite high rates of recovery that may vary from 44 to 91.7%, depending on the complication of the syndrome and the length of the conservative management (Beals and Flanigan 2013). Nevertheless, there are insensitive cases, occurring quite often. In this case, surgery is needed, and is shown to be very effective (100% recovery) (Beals and Flanigan 2013). The surgical treatment can be as follows: arthroscopic technique (resection of the fibrous attachments to the femur and the associated fat, without a resection of the ITT) (Michels et al. 2009); surgical release of the posterior fibers of the ITT by a 2-cm incision at the level of ITT's tibial insertion (Noble 1979); the excision of abrading posterior distal ITT fibers (Holmes, Pruitt, and Whalen 1993); mesh technique (Sangkaew 2007), which may also be named in the literature as a pie-crusting (PC) technique and represents itself as small (one-two millimeter long) multiple incisions (perpendicular to the fibers of the ITT in the area overlying the lateral femoral epicondyle) (Bruzzone et al. 2010; Elkus et al. 2004; Jabalameli et al. 2016; He, Cai, and Zhang 2018; Politi and Scott 2004), and more others.

The pie-crusting technique is often used to release the strains of the ITT during a total knee arthroplasty to correct the varus/valgus deformity of the knee and align it with the axis of the leg, by balancing soft tissues (Ranawat et al. 2005; Freeman, Sculco, and Todd 1977). This is also a common technique for the correction only of valgus deformity, when the knee is tighten laterally in flexion and extension, or only in extension (Buechel 1990; Elkus et al. 2004; Matsuda, Lustig, and van der Merwe 2017; Whiteside 2002). One study in the literature reported that varus instability and knee pain caused an isolated ITT rupture (Pandit et al. 2014).

The ITT and fascia lata itself are connected to different bones and ligaments (Zaghloul 2018), serve as areas of insertion for neighboring thigh muscle fibers (Stecco et al. 2013; Zaghloul 2018), limit the changes in shape of underlying tissues (Langevin and Huijing 2009), enable the sliding and gliding of muscles (and tendons) against each other and against other structures (Van der Wal 2009). They must be fully investigated and studied as they serve important roles in the body, like movement coordination (Barker, Briggs, and Bogen 2004), pelvic and lower extremity stability (Evans 1979; Merican and Amis 2009; Birnbaum et al. 2004; Kaplan 1958; Kwak et al. 2000), transmit mechanical forces between muscles (Klingler et al. 2014; C. Stecco et al. 2014; Huijing 2009; Wilke et al. 2018), etc.

Because of all the attachments of fascia lata, changes of the knee joints angles (flexion/extension, internal/external rotations, adduction/abduction) will lead consequently to the deformation in three dimensions, creating tension, compression, and shear mechanisms through the tissue (Hamill et al. 2008).

Fascia lata is a connective tissue with two types of fibers, elastin and collagen, which are making possible to keep an underlying structure in position. Hence, tension within the tissue can be supported by 2 main collagen fibers orientations, which are forming an angle of 67 – 80° between two adjacent layers in the goat fascia lata (Pancheri et al. 2014). As for any biological soft tissue, several sample tests should be done to describe the biomechanical behavior of the tissue. Although, there are uniaxial (Fischer et al. 2020; Gratz 1931; Henderson et al. 2014; Zwirner et al. 2019) and biaxial tensile (Eng et al. 2014a; Pancheri et al. 2014) tests done on the fascia lata or ITT isolated samples, and few pure shear tests (Ruiz-Alejos et al. 2016), the full description of the mechanical behavior of the fascia lata is still incomplete. Mechanism of the collagen fibers reorientation during the physiological movement is also missing in the literature. Depending on the angle of the collagen fibers, the parameters such as ultimate load,

stress, elastic modulus, etc., can change (Henderson et al. 2014). Moreover, quantitative information about the fascia lata's strain mechanisms during leg movements or during surgical intervention is not well described.

Knowing the structure, mechanical properties, and loadings of fascia lata, the next step, would be to create a model of it, in order to use for different simulations. There are several rigid body musculoskeletal models (Chèze, Moissenet, and Dumas 2012; Hamill et al. 2008; Piazza and Delp 2001; McLean, Su, and van den Bogert 2003) and finite element models (Al-Dirini et al. 2016; Savonnet, Wang, and Duprey 2018; Stelletta, Dumas, and Lafon 2017; Mo et al. 2019) of the leg that include muscles, bones, ligaments and tendons. Nevertheless, fascia lata is missing. There is a big interest in the models, which can be used by clinicians prior to the surgery, which must be patient specific and show the predicted post-operative results (Klein Horsman et al. 2007). For example, there is a recent musculoskeletal model with total knee arthroplasty (Tzanetis et al. 2021), where soft tissue balancing is expected, but the ITT is not included to this model.

In this context, the thesis work presented in this manuscript aims first at obtaining quantitative data of fascia lata deformation during physiological knee movements from *ex vivo*, but *in situ*, experiments; and then at analyzing more deeply its mechanical behavior with tests on isolated samples including the investigation of the collagen fibers' kinematics. A first contribution to the FE modelling of the behavior of fascia samples was also proposed. As the natural strain state of fascia lata contributes to a good knee mobility, a specific *in situ* study of the impact of ITT pie-crusting, that may be recommended in pathological cases, has also been performed.

Therefore, the manuscript is consisting of five chapters: (I) Background and objectives, (II) Strain mechanism during knee flexion movement, (III) Mechanical properties of fascia lata during a shear loading, (IV) Finite element modeling of fascia lata sample, (V) ITT strain release and knee mobility.

Chapter I outlines the fascia lata findings in the literature, including the identification and differentiation between deep fascia, fascia lata, and ITT, their structure, functions, and mechanical properties. Here are also discussed published clinical studies on the ITT. With rapid growth of the finite element modeling, limited amount of fascia lata models found in the literature are presented. In addition, specific objectives of the work are defined based on the gaps on fascia lata information (geometry, loadings, mechanical behavior) within the literature review.

Chapter II presents the published article (Sednieva et al. 2020) with additional results obtained after publication (Appendix I). Three (plus three later) cadaveric subjects were submitted to a physiological leg movement (knee flexion-extension) with the interest to quantify and define strain mechanism on the surface of fascia lata. Fascia lata's strain levels were investigated in three areas: anterior fascia, lateral fascia, and ITT.

To identify mechanical properties, chapter III includes shear tests on fascia samples taken from different locations of fascia lata. The main interest and the contribution of these tests is to perform shear tests as this is the strain mechanism highlighted with *in situ* tests. In this configuration, we would then obtain a characterization of fascia mechanical properties representative of these *in situ* loadings. Here, we presented the description of the samples, the methodology of the tests, bi-photon microscopy method, strain field measurements, fiber

distributions. Bias extension and large band tests were performed, meaning that the load was applied to the bisector of two fibers networks (longitudinal and transverse). Fibers orientations and distribution during the loadings were studied as we suppose that layers of fascia lata may slide in between during the deformation of the tissue, and that fibers orientations are highly oriented in the direction of the applied force. As these mechanisms may be related to microscopic arrangement of fibers, an attempt to study the tissue microstructure was performed.

The chapter IV describes the simple finite element model of the fascia lata with the longitudinal and transverse directions of fibers subjected to the load along the bisector of two fibers networks. The geometry of the tested samples was modeled in the commercial software LS-PrePost. The soft tissue (091) transversely isotropic hyperelastic material was chosen for the fascia lata. Coefficients of the isotropic Mooney-Rivlin matrix reinforced by fibers material are evaluated analytically and then numerically to fit the experimental data from shear tests.

The ITT strain release and its effect on the knee mobility are examined in the chapter V. The pie-crusting technique is commonly used for the ITT strain release during knee surgery. We hypothesized that strain release after the pie-crusting technique and the ITT dissection will affect the range of knee motion, by correcting the knee axis and increasing the range of varus-valgus and rotation angles. It was thus used on three female cadaveric subjects for the strain release on the area of the ITT, between lateral epicondyle (femur) and Gerdy's tubercle (tibia), to study the motion angles (adduction-abduction, internal-external rotations) before and after the surgical intervention. Moreover, we studied the affection of the motion and strains after cutting the ITT at its origin on the tibia.

The last chapter VII contains the conclusions of the work and its future developments.

CHAPTER I

STATE OF THE ART AND OBJECTIVES

1.1. State of the art

1.1.1. Anatomy and function of deep fascia

Fascias can be either loose or dense connective tissues present all over the body (*Figure 1.1-1*). Within this research project, the focus is on dense fascias, and especially deep fascia. They are surrounding muscles and groups of muscles, connecting them to each other and to the bones.

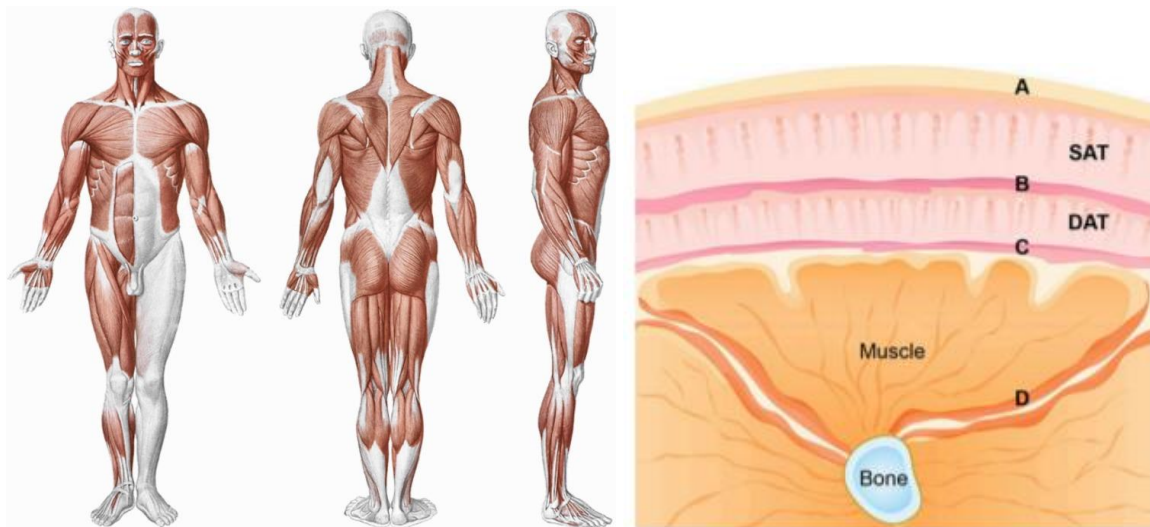


Figure 1.1-1. On the left, the examples of fascias (in grey) all over the body (Bordoni and Myers 2020) and on the right, a schematic drawing of fascias (superficial and deep) anatomy in the leg. Where: A – skin, B – superficial fascia, C – peripheral layer of deep fascia; D – intermuscular layer of deep fascia, DAT – deep adipose tissue, SAT – superficial adipose tissue (Ali, Srinivasan, and Peh 2014).

Deep fascia is a biological well-organized composite material, with different layers mainly made of collagen and elastin fibers (Stecco et al. 2011). Between these layers, the substance matrix is composed of a proteoglycan reinforced by collagen type I (Rivard et al. 2011) (*Figure 1.1-2*) and elastin fibers (Pancheri et al. 2014). In addition, all three types of blood vessels (arterioles, capillaries, and venules), mast cells, myofibroblasts and myofibrils can be observed in fascia's layers (Bhattacharya et al. 2010).

It has been shown that fascia contribute to the pressure in the muscular compartments (Garfin et al. 1981), and to muscle force transmission (Snoeck et al. 2014). They transmit mechanical forces between muscles (Klingler et al. 2014; C. Stecco et al. 2014; Huijing 2009) and they also participate in movement coordination (Barker, Briggs, and Bogeski 2004), limb stabilization (Stahl 2010), and elastic energy storage (Bennett et al. 1986). Therapies directed to fascia may improve balance and posture (DellaGrotte et al. 2008). It is also known that fascia is playing a role of a reservoir of water and ions for surrounding tissue (C. Stecco et al. 2011a).

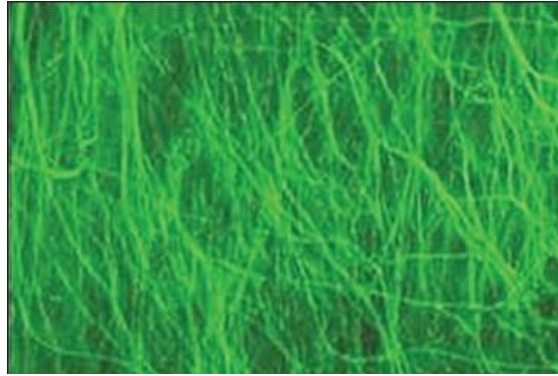


Figure 1.1-2. Confocal microphotograph of the deep fascia of lower limb showing collagen fibers on application of fluorescein dye using laser scanning multiphoton confocal microscope (Radiance 2000) (Bhattacharya et al. 2010).

Regarding the lower limb, fascia lata is a deep fascia enveloping muscles of the thigh (Figure 1.1-3). Tensor fasciae latae muscle fibers come down in line with the transversal fibers of the fascia lata and insert on them; the gluteus maximus muscle attaches to the upper part of the longitudinal fibers of the fascia lata (Evans 1979). In the postmortem, fascia lata can be easily separated from the muscle due to the thin layer of loose tissue between them (Stecco et al. 2013). Therefore, muscle is attached to the fascia only in some regions, while in other places loose connective tissue is between the muscle and fascia, this tissue is a gel-like substance permitting the sliding of the muscle under the fascia lata (C. Stecco et al. 2008).

The fascia lata presents a thicker region in the lateral and posterior-lateral sides named iliotibial tract (ITT) or iliotibial band (Stecco et al. 2013). It is enclosing tensor fasciae latae and anchoring this muscle to the iliac crest (Figure 1.1-3). The gluteus maximus is also inserted upon the ITT. Therefore, its origins are at the lateral condyle of the tibia at Gerdy's tubercle and the iliac crest, more specifically, the anterolateral iliac tubercle portion of the external lip of the iliac crest (C. Stecco 2014). It is also attached to the linea aspera (a ridge of roughened surface on the posterior surface of the shaft of the femur (White, Black, and Folkens 2012)) of the femur through the lateral intermuscular septum (it separates the anterior compartment of the thigh from the posterior compartment) (A. Stecco et al. 2009a; Terry, Hughston, and Norwood 1986).

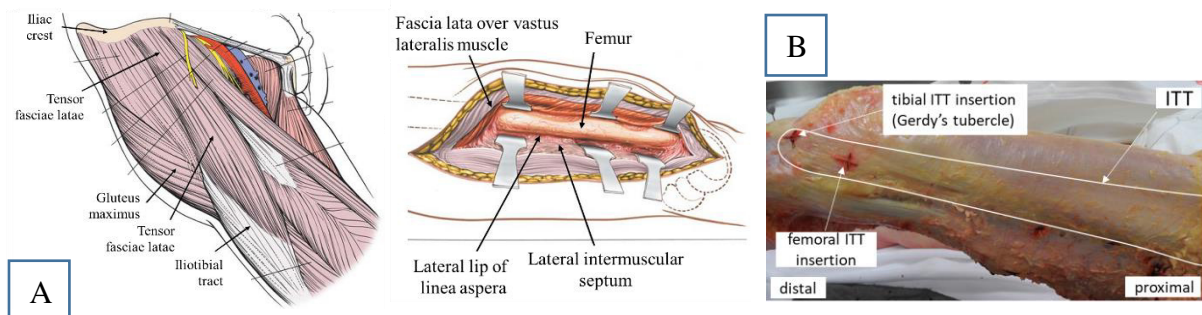


Figure 1.1-3. (A) Lateral view of the muscles of the anterior region of the hip, including the iliotibial tract, iliac crest, lateral intermuscular septum, and a linea aspera (Themes 2016b; 2016a); (B) location of the ITT and identification of its insertions on the distal site of the leg (subject 2021_098, LBMC).

Because the ITT is crossing two joints, it has significant contribution to pelvic and lower extremity stabilities (Merican and Amis 2009; Birnbaum et al. 2004; Kwak et al. 2000). Thus,

the stability effect on the knee varies with the hip position. The elastic tenseness of the ITT resists adduction, it might create the maximal resistance when the pelvis sags ; during the walk, ITT's abduction action is bearing nearly a half of the body weight; while standing, it allows us to rest (Evans 1979). In addition, the ITT participates in the force transmission (Stecco et al. 2013), which can be explained by the tensor fasciae latae and the gluteus maximus insertions on the ITT (Birnbbaum et al. 2004).

At the knee level, ITT has a role in stabilizing rotation during knee flexion (Matsuda, Lustig, and van der Merwe 2017). It is also responsible for the stability of the lateral compartment of the knee (Kaplan 1958; Evans 1979). Moreover, it was found that the ITT's forces can affect knee kinematics (Kwak et al. 2000), and its tension affects patellofemoral and tibiofemoral kinematics (Merican and Amis 2009).

1.1.2. Microstructural anatomy of fascia lata

1.1.2.1. Thickness

Fascia lata is a bi-layered tissue with the transverse and longitudinal collagen fiber directions. However, Stecco et al. (2011a) showed three layers with the ultrasound (*Figure 1.1-4A*), suggesting that the full thickness of the fascia lata is proportional to the number of layers of which it is composed. Nevertheless, to our best knowledge it is the only one study where fascia lata was containing three layers. The same study shows the presence of a loose connective tissue between the layers of fascia lata. The thickness of this loose connective tissue is measured as $15 \pm 16 \mu\text{m}$ in the superficial layer, and $19 \pm 13 \mu\text{m}$ in the deep layer. The presence of two thin layers (mean thickness $23 \mu\text{m}$) of fibroelastic tissue on the external and internal sides of the fascia lata was observed with a histological study (*Figure 1.1-4B*).

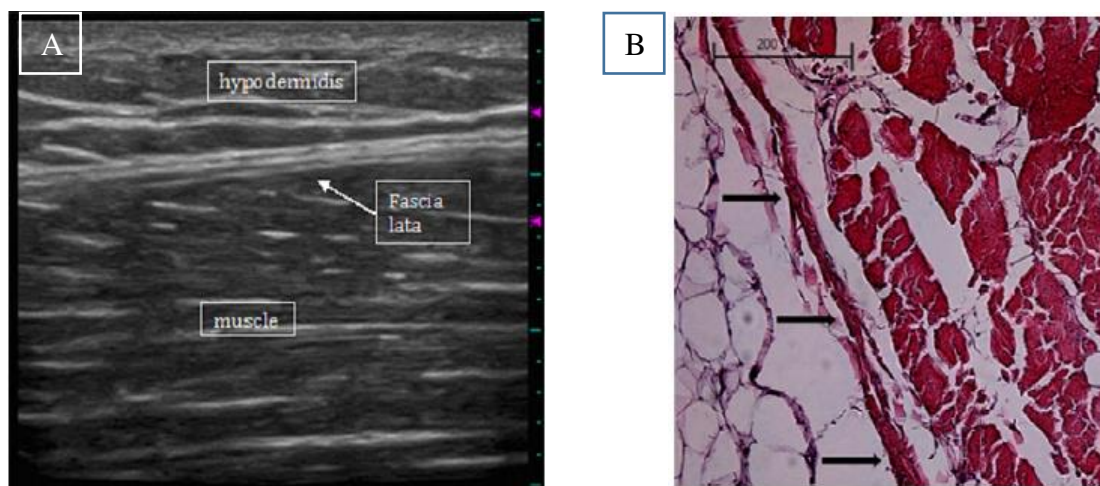


Figure 1.1-4. Images of fascia lata visible by ultrasound (A)(C. Stecco et al. 2011a) and by histological analysis with HE stain (B), highlighting the thin layer of fibroelastic tissue in the external side of the fascia lata (C. Stecco et al. 2008).

Site dependency was also documented by other studies reported in the literature (*Table 1.1-1*). Some of them measured the thickness of both fascia lata's layers and some separated them. High variability can be observed among all these values: at the lateral site ($0.8 \pm 0.2 \text{ mm}$) it is much thicker than on the other sites ($0.2\text{--}0.3 \text{ mm}$) (Otsuka et al. 2018). Also, the fascia lata is thinner in the proximal region, and thicker near the knee ($926 \pm 156 \mu\text{m}$) (C. Stecco et al. 2008).

Table 1.1-1. Gross anatomy of fascia lata: human and goat data

Parameter	Value	Reference	Species	Methodology
Mean thickness (±SD), µm	926 ± 156	(Stecco et al. 2008)	human	histology
	541 ± 23 – <i>Inguinocrural region</i> 874 ± 62 – <i>Middle third of the thigh</i> 1419 ± 105 – <i>Distal third of the thigh</i>	(Stecco et al. 2009)		thickness gauge
	188 ± 38	(Stecco et al. 2011)		ultrasound
	2000 ± 500 – <i>Lateral site</i>	(Rahnemai-Azar et al. 2016)		digital calipers
	800 ± 150 – <i>Lateral site</i> 280 ± 50 – <i>Anterior site</i> 190 ± 40 – <i>Medial site</i>	(Otsuka et al. 2018)		ultrasound
	830 – 950 – <i>Anterior site</i> 930 – 950 – <i>Posterior site</i>	(Wilke et al. 2019)		digital calipers
	600 – 900 – <i>Lateral site</i>	(Beck et al. 2020)		
	910 ± 20 – <i>Lateral site</i> 560 ± 12 – <i>Anterior site</i> 675 ± 155 – <i>Posterior site</i>	(Otsuka et al. 2021)		ultrasound
	320 ± 20	(Eng et al. 2014a)		goat
	Each of layers mean thickness (±SD), µm	54.2 ± 16 – <i>Superficial layer</i> 38 ± 12 – <i>Middle layer</i> 40 ± 10 – <i>Deep layer</i>	(C. Stecco et al. 2011a)	human
218.0 ± 22.7 – <i>longitudinal layer</i> 94.7 ± 6.5 – <i>transversal layer</i>		(Eng et al. 2014a)	SEM	
246.4 ± 42.8 – <i>longitudinal layer</i> 61.3 ± 8.7 – <i>transversal layer</i>		(Pancheri et al. 2014)	goat	inverted light microscopy

The difference in the fascia lata thickness reported by Stecco et al. (2008) and Stecco et al. (2011a) may be explained by the methods used to measure the thickness, from the harvested samples and ultrasound, respectively (Table 1.1-1). Moreover, the impact on the results may be related to the location of the measurement along fascia lata: posterior region and middle third of the anterior region were studied in 2008, and proximal quarter of the anterior region in 2011.

Later, Otsuka et al. (2021) carried on the measurements of fascia lata thickness with the connection to the surrounding tissues, and observed a large individual variation in the fascia lata thickness even in the same region of the thigh. As the result of the study, the thickness of the fascia lata showed partial positive correlations with the height, body mass, and the

underlying muscle thickness, and corresponding joint torque. They suggest that muscle thickness and strength exert greater influence on the morphology of fascia lata.

As fascia lata has insertions on the underlying muscles, when they change in the volume during the contraction or the relaxation (Bhattacharya et al. 2010), the mechanical stresses they produce change the stiffness of fascia lata, it becomes stiffer with the contraction (Otsuka et al. 2018). It was found *in vivo* that young people, who have larger muscles, have thicker fascia lata, especially on the anterior site (Wilke et al. 2019).

Collagen fibers in the longitudinal direction are thicker in size compared to those in the transverse direction, 127.0 ± 9.2 nm and 94.9 ± 8.9 nm respectively (Eng et al. 2014a). The size of fibers was measured using scanning electron microscopy (SEM); other possible techniques are second harmonic generation (SHG) microscopy that can be associated to multiphoton imaging that allow to observe elastin. These last techniques are often used for imaging extracellular matrix (ECM) of biological structures (Monaghan et al. 2016), such as fascias (Guo et al. 2018; Rivard et al. 2011), tissues rich in collagen (Szotek et al. 2012; Stoller et al. 2003; Tan et al. 2004), cartilage (Yeh et al. 2005; Mansfield et al. 2008), tendon (Cury et al. 2016; Takasugi, Inoue, and Akahori 1976), etc.

Rivard et al. (2011) used SHG microscopy and Atomic Force Microscope (AFM) on the fascia harvested *in situ* from the anterior tibialis muscle (lower part of the leg) of the mice. Both techniques give the image with visible fibers and their fibrils (*Figure 1.1-5*). Even the thickness of this fascia was about $10 \mu\text{m}$, what is much lower than thickness of fascia lata, this fascia is also mainly composed of collagen type I. The diameter of a single collagen fibril was around 30 nm with the 67 nm periodicity of the banding pattern.

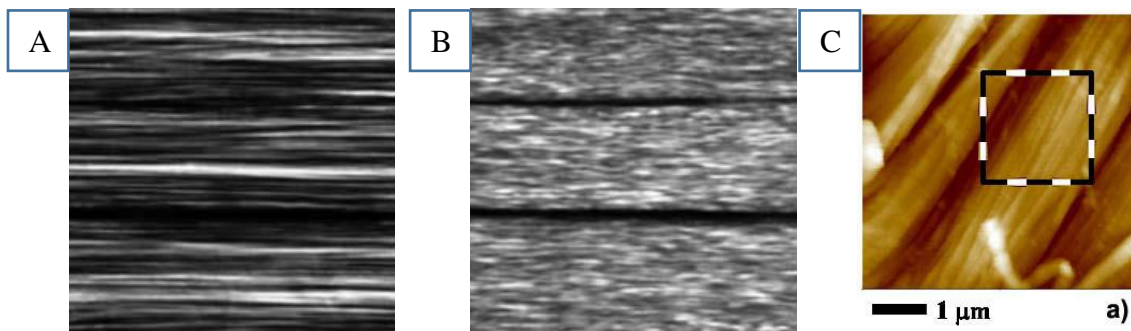


Figure 1.1-5. SHG images of fascia tissue in (A) forward and (B) backward direction. (C) Fascia sample topography ($5\mu\text{m}$ scan) taken with AFM (Rivard et al. 2011).

1.1.2.2. Collagen fibers distribution

Meanwhile, not only the thickness is site dependent, but also the collagen fiber directions (Otsuka et al. 2018). Two fibers orientations can be easily observed on the ITT (*Figure 1.1-6*) with the eye only: the transverse fibers attached to the back of the femur as the lateral intermuscular septum and the longitudinal fibers going from the iliac crest above to the tibia below. Nevertheless, the longitudinal fibers of the fascia lata do not attach to the linea aspera of the femur, but only transverse fibers (Evans 1979).

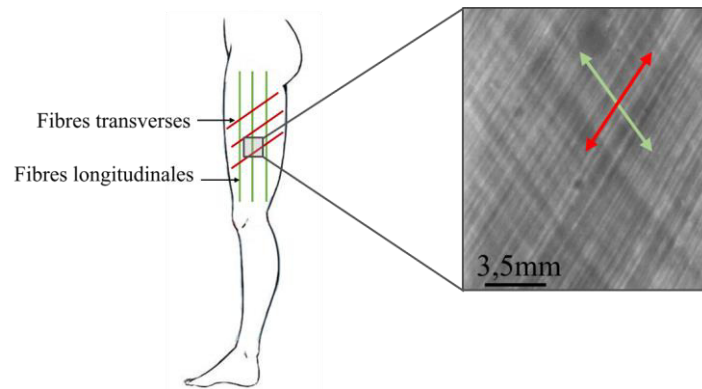


Figure 1.1-6. Zoom on the lateral view of the area along the ITT showing longitudinal (in green color) and transversal (in red color) collagen fibers from tested subject (LBMC).

The collagen fibers network of the fascia lata can be visible by multi-photon microscopy as already done on various fibrous membranes (Rezakhaniha et al. 2012; Jayyosi, Coret, and Bruyère-Garnier 2016; Jayyosi et al. 2017) or with high resolution photos adapted to a stereomicroscope and post processed using available techniques and software (Otsuka et al. 2018). Using the light microscopy the angles between fibers in adjacent layers for fascia lata were obtained to be $67 - 80^\circ$ for the goat fascia lata (Pancheri et al. 2014), what is close to the crural fascia $78 \pm 4.3^\circ$ reported by Benetazzo et al. (2011), but lower than $80 - 90^\circ$ reported by Stecco et al. (2009).

By classifying fiber directions into longitudinal, transverse, and two opposite diagonal directions (Figure 1.1-7), a higher proportion of longitudinal fibers was observed on all the sites except for the posterior site (Otsuka et al. 2018). However, the percentage of transversely directed fibers was significantly higher than that of the posterior-superior to anterior-inferior (P/A) diagonally directed fibers and the medial-superior to lateral-inferior (M/L) diagonally directed fibers.

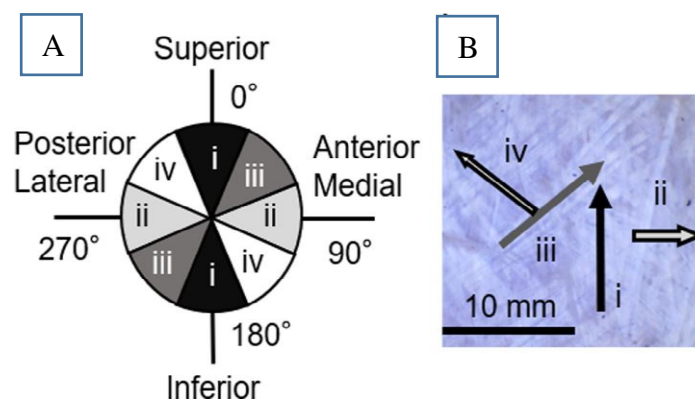


Figure 1.1-7. (A) Classification of the fibers' orientations and (B) typical image of the fascia lata. i: longitudinal (inferior to superior), ii: transverse (anterior to posterior or medial to lateral), iii: M/L- or A/P- diagonal (medial-superior to lateral-inferior or anterior-superior to posterior-inferior), iv: L/M- or P/A- diagonal (lateral-superior to medial-inferior or posterior-superior to anterior-inferior) (Otsuka et al. 2018).

To conclude, fibers' orientations have an impact on the behavior of the tissue: for greater fiber angle orientation, the fibers are more resistant to reorientation as the fascia is stretched longitudinally (Chaudhry et al. 2012). They found that reinforced fascia is always in tension as

the stretch is applied. However, some elements within fascia are under compression (Findley et al. 2012).

1.1.3. Mechanical properties of fascia lata

The structure of collagen fibrous tissues determines the response of the tissue to mechanical stress. Collagen is the main component that resist to tension. Elastin also resist tension but behaves similar to a rubber, after the stretching it will recoil as soon as the force is removed. The combination of these two fiber networks is responsible for the non-linear and anisotropic behavior of the deep fascia. Fascia is subjected to complex three-dimensional loadings *in vivo* that include tension, compression, and shear (Chaudhry et al. 2008; Gardiner and Weiss 2000). Different tests can be found in the literature to characterize its mechanical properties, such as tensile and shear tests.

1.1.3.1. Mechanical behavior under tensile test

Deep fascia mechanical properties have been evaluated in several uniaxial tensile tests (Gratz 1931; Butler et al. 1984; Hammer et al. 2012; 2016; Steinke et al. 2012; Eng et al. 2014a; C. Stecco et al. 2014; Henderson et al. 2014; Ruiz-Alejos et al. 2016; Otsuka et al. 2018; Zwirner et al. 2019; Fischer et al. 2020) or biaxial tensile tests (Eng et al. 2014a; Pancheri et al. 2014) performed in the main fiber direction on deep fascia isolated samples.

If comparing uniaxial and biaxial testing, the second is considered as a more realistic loading of deep fascia than uniaxial tension, and tests to failure can help to understand the mechanical behavior of the deep fascia under larger strains (Pancheri et al. 2014).

The stress-strain curves for fascia lata are consistent with those typically observed for soft tissues (Ruiz-Alejos et al. 2016). They are nonlinear curves with a toe region for small strain levels where fibers align with the tension direction, then stress increases exponentially with strain and, finally, the tissue behaves linearly, when fibers are stretched until rupture (*Figure 1.1-8*). A Young's modulus (E) is usually computed from the linear region. Mechanical characteristics of fascia lata may vary upon authors (*Table 1.1-2*). For instance, different tensile strain at failure obtained with uniaxial test can be found : 9 % (Gratz 1931), from 9.7 to 10.3 % (Hammer et al. 2012; 2016), 15 % (Zwirner et al. 2019) on a human ITT, 8 % (Eng et al. 2014a) on a goat fascia lata.

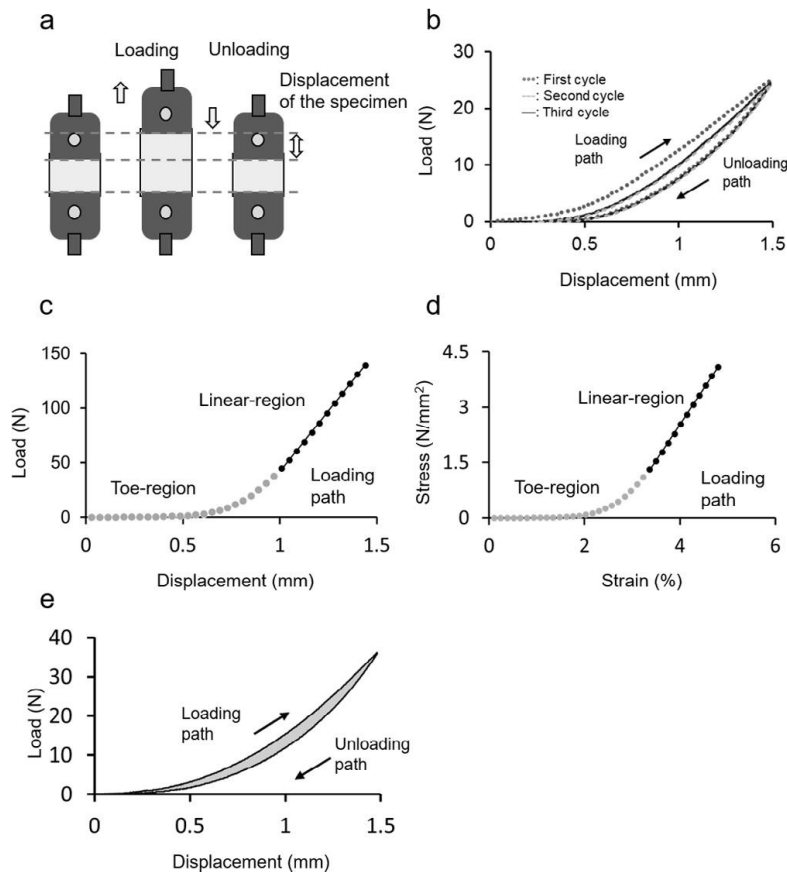


Figure 1.1-8. Mechanical tests for the fascia lata: (a) loading–unloading cycles (b) with the typical results of (c) stiffness, (d) Young’s modulus, and (e) hysteresis loop. (Otsuka et al. 2018)

Young’s modulus of fascia lata is also varying a lot in the literature, but this might be explained by the sites of the fascia’s from where samples were taken: highest value of Young’s modulus is found on the lateral site of the fascia lata in the direction of longitudinal fibers, contrary to the fibers in the transverse direction (Otsuka et al. 2018). Lower value of Young’s modulus is saying about the softer tissue (Hammer et al. 2012), therefore, longitudinal samples are found to be stiffer than transverse samples (Table 1.1-2). For the stiffness of the ITT reported in the literature, there is no consistency in the value: 17 N/mm (Birnbaum et al. 2004), 73.2 ± 24.1 N/mm (Rahnemai-Azar et al. 2016). It was observed, for the longitudinally oriented samples of the goat fascia lata, the stiffness was 4.4 times greater than for the transverse samples (Eng et al. 2014a). Additionally, the stiffness is varying depending on the site (higher values on the lateral site for the longitudinally oriented fibers, contrary to the transversally oriented fibers, stiffer samples from the anterior site compared to those from a medial site) (Otsuka et al. 2018).

Expectedly, the mechanical response of the fascia lata in tension depends on the direction of loading, where anisotropy resulting in greater stiffness when the fascia lata is pulled in the direction of its longitudinal fibers (Ruiz-Alejos et al. 2016). Stiffening of fascia lata can be related to a decrease of elastin and elastin cross-links as described for ligaments (Osakabe et al. 2001).

Table 1.1-2 Mechanical properties of fascia lata (means \pm S.D. or min – max range) presented in the literature. Where: Long. – longitudinal fiber direction, Trans. – transverse fiber direction.

Study	Species	Samples #	Test	Strain rate (sec ⁻¹)	Young's modulus (MPa)		Ultimate stress (MPa)		Hysteresis (%)		Ultimate stretch (%)	
					Long.	Trans.	Long.	Trans.	Long.	Trans.	Long.	Trans.
Eng et al. (2014a)	Goat	10	planar biaxial	0.0015	263.5 \pm 16.3	52.2 \pm 4.7	9.4 \pm 1.1	1.9 \pm 0.3	14.8 \pm 1.6	10.1 \pm 1.3	8	
Butler (1984)	Human	18	tensile test to failure	1	397.5 \pm 17.1		78.7 \pm 4.6		–		27 \pm 1.1	
Otsuka et al. (2018)	Human	68	tensile strength test	0.014 – 0.056	173.75 \pm 102.15	22.55 – 19.35	–		33.3 \pm 6.2	34.1 \pm 5.6	–	
Pancheri et al. (2014)	Goat	20	uniaxial and planar biaxial extension	0.0015	–		38.4 \pm 10.3		–		10 – 18	
Hammer et al. (2012)	Human	38	tensile test to failure	?	84.7 \pm 30.24 – 369.13 \pm 191.47		35.8 \pm 16.4		–		9.7 – 10.3	
Gratz (1931)	Human	1	uniaxial tension	?	57.58 (calculated)		54.2		–		9	
Zwirner et al. (2019)	Human	33	uniaxial tension until failure	0.0025	408 \pm 232		29 \pm 17		–		15	
Fischer et al. (2020)	Human	20	uniaxial tension	0.1	0.73 \pm 0.44		37.66 \pm 18.87		–		10 – 22.29	

Mechanical hysteresis is analyzed in order to investigate the viscoelastic property of the tissue. The values of hysteresis for the human fascia lata with longitudinally and transversally oriented fibers, respectively, are two and three times higher than for the goat's fascia lata (Table 1.1-2). The hysteresis is significantly greater in the longitudinal than transverse orientation for the goat samples, but slightly higher in transverse direction for the human samples. The last is expected to be greater in the transverse orientation and can be explained by the smaller size of the fibrils with higher surface area-to-volume ratio, increasing shear stresses that result from interactions between the fibrils and the matrix components (Parry 1988). Hence, fibers orientation has significant influence on different parameters, such as ultimate load, stress, elastic modulus and hysteresis (Henderson et al. 2014).

1.1.3.2. Mechanical behavior under shear loading

Tension states have already been discussed above and to the best of our knowledge, compression tests has not been performed yet. However, not many studies have been made to study shear mechanisms of deep fascia, while shearing is induced in soft tissues in numerous physiological settings (Taber 2004). That kind of tests may be hard to perform (Gardiner and Weiss 2000). For example, in order to have a state of pure shear, tissue must be extended in one direction by some amount of stretch λ , while simultaneously compressed in a lateral direction by λ^{-1} , with the third orthogonal direction remaining fixed in length and free from traction (Freed 2009).

The shear behavior affects load transfer between microstructural parts of the tissue (Gardiner and Weiss 2000), stretch along the fibers could cause the stress in the ground matrix, or vice versa (Weiss 1994). There is one study presented in the literature with pure shear loading done on fascia lata samples from the sheep (Ruiz-Alejos et al. 2016). The obtained results (*Figure 1.1-9*) demonstrate that mechanical response of fascia lata stretched along its longitudinal fibers is stiffer than when it is stretched along its transverse fibers. The stress in longitudinal and transverse direction corresponding to 6% strain is respectively 0.91 MPa and 0.18 MPa. Accordingly, the stresses from the uniaxial tension test were found to be 3.21 MPa and 1.01 MPa.

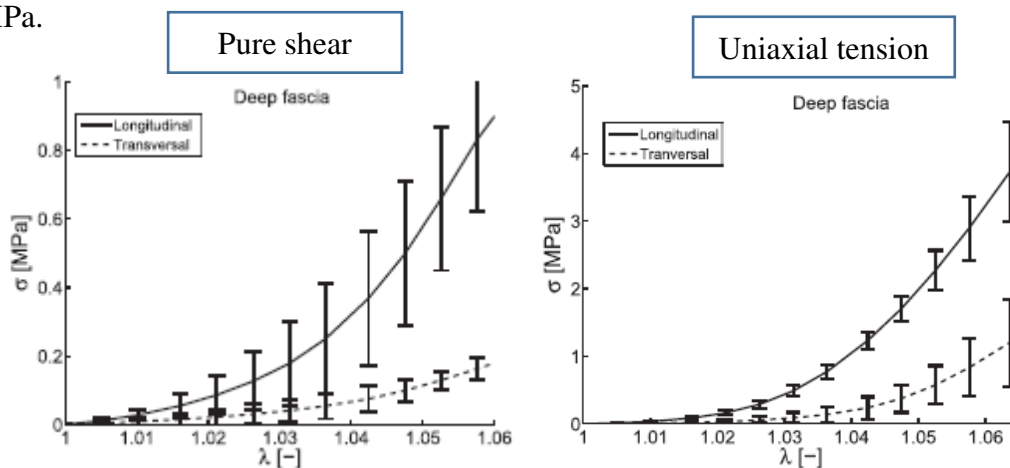


Figure 1.1-9. Cauchy stress versus stretch from pure shear and uniaxial tensile tests of deep fascia lata samples harvested from the sheep (Ruiz-Alejos et al. 2016).

Therefore, the fascia lata is stiffer when subjected to simple tension compared to pure shear. Similar results were reported by Pancheri et al. (2014), where the samples of goat fascia lata were tested under planar biaxial extension. All the tests, tensile and pure shear, show that fascia lata is much stiffer in the longitudinal direction compared to the transverse direction. The structure of fascia lata results are consistent with the biaxial response, in which the longitudinally oriented fibers reinforce the tissue to withstand higher loads (Pancheri et al. 2014).

Hence, shear loading will help to understand how fibers move depending on loading direction compared to fiber initial orientation, also it will give an information on the interaction between the layers, for instance if there is sliding of the layers of one on the other. According to the study presented by Stecco et al. (2008), there is a thin layer of loose connective tissue between two adjacent layers with different fiber orientations.

1.1.3.3. Age and sex effect

Tensile tests on samples performed by Hammer et al. (2012) did not reveal any sex differences, however, *in vivo* study done by Otsuka et al. (2018) showed that females have higher and lower Young's modulus than males in the longitudinal and transverse directions respectively. The proportion of the transversal fibers is 1.3 times higher in females compared to males at the middle site of the thigh (Otsuka et al. 2018). Although, no difference of ultimate stress was found between females and males (Hammer et al. 2012).

Aging has an effect on the fascia lata's properties as well (Steinke et al. 2012; Hammer et al. 2012). The collagen content is decreasing with age in all soft tissues, for skin (Czekalla et al. 2017), for ligaments (Osakabe et al., 2001), and for tendons (Couppé et al. 2009; Guilbert et al. 2016). In addition, female group with the age have a higher decrease of collagen (Osakabe et al. 2001). Meanwhile, Couppé et al. (2009) showed that even if the tissue is poor on collagen with the age, cross-linking increased, and mechanical properties are maintained.

Nevertheless, stiffening with increasing age is reported to be related to a decrease of elastin, an increase of collagen-crosslinks, and loss of body water (Hammer et al. 2012). The Young's modulus for fascia lata was found to be much greater for the old population compared to the young one (Hammer et al. 2012).

Zwirner et al. (2019) showed that for the ITT, tensile parameters did not depend on age, except for a strain at failure in the male group; other anthropometric parameters such as height should be considered when looking at fascia mechanical properties, especially for males, as longer ITT can withstand higher forces before the failure during uniaxial tensile test; thereby, it is well related to tensile properties.

1.1.4. Constitutive models of fascia lata's mechanical behavior and use in FE modeling

In the creation of the mathematical or constitutive model of fascia lata's mechanical behavior (*Table 1.1-3*), it is very important to remember its anisotropy. Not less important is to take into account the large elastic deformations, representing the non-linear behavior of the fibers during stretching of the fascia lata.

Two mathematical models were published by Chaudhry et al. (2008; 2007) in order to be used in the manual therapy field helping to determine the amount of required force during a fascia lata extension. The results they got suggest that compression and shear alone, within the normal physiologic range, cannot directly deform the fascia lata. Moreover, in order to produce 1% compression and 1% shear, fascia lata requires very large forces "far outside the human physiologic range". Later, Chaudhry et al. (2012) created a mathematical model of fiber reorientation for highly elastic, transversely isotropic, incompressible material at large displacements valid for the human fascia reinforced by the collagen fibers.

Table 1.1-3. Constitutive models of fascia lata presented in the literature.

Parameters	Data	Tests	Material
Ruiz-Alejos et al. (2016)	Sheep fascia lata	Uniaxial Pure shear	Anisotropic and hyperelastic
Pancheri et al. (2014)	Goat fascia lata	Uniaxial Biaxial	Anisotropic and hyperelastic (Demiray 1972)
Weiss (1994)	Human fascia lata	Uniaxial Biaxial	Transversely isotropic hyperelastic neo-Hookean (refers as 'One Coefficient model') and Mooney-Rivlin (refers as 'Two Constant model') (Mooney 1940)
Chaudhry et al. (2007)		Uniaxial	Viscoelastic (Fung 1984)
Chaudhry et al. (2008)		(Gratz 1931)	Isotropic (Demiray 1972)

Constitutive models presented by Weiss (1994) were developed to describe and predict the behavior of fascia lata, ligaments, and tendons. They propose two models based on the strain energy function, which is composed by the behaviors of the ground matrix, collagen fibers, and their interactions. Within the first model, called “One coefficient model”, the behavior of the ground matrix is described by the Neo-Hookean material model, while in the second model called “Two Coefficient model”, it is defined by Mooney-Rivlin material model. The coefficients (the first and second Mooney-Rivlin constants, constant scaling the collagen exponential stresses, constant controlling rate of rise of collagen exponential stress, and the modulus of straightened collagen fibers) identified from uniaxial tensile data were used to predict the response of the biaxial tests. The prediction ability of both, one- and two-coefficient models, were similar with a good agreement for the uniaxial tensile tests and at low stretches ($\lambda < 1.04$) for the biaxial tensile test, but at higher stretch values, the predicted models showed stiffer results compared to the experimental data (*Figure 1.1-10*). This big difference of strain values for the stretches higher than 1.04 was linked to the possibility of the lateral contraction during the biaxial tests, which would result in a less stiff response more evident at higher stretches. The possibility to overcome this issue may be performance of shear tests.

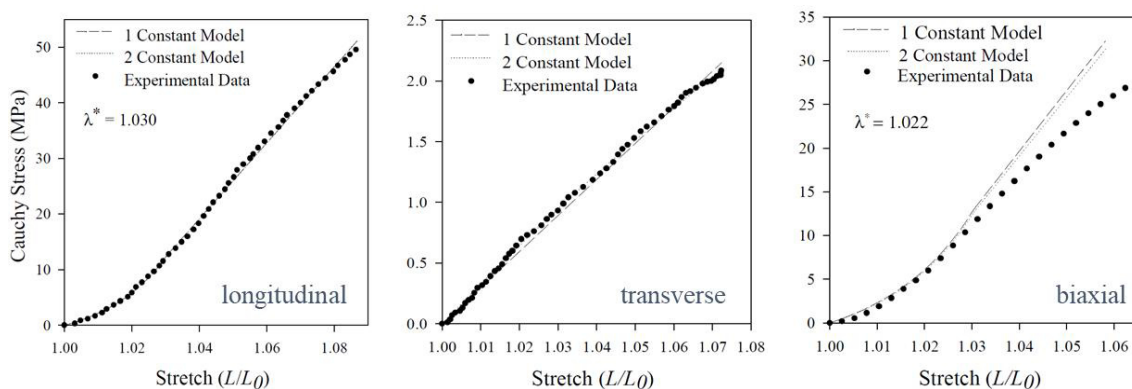


Figure 1.1-10. Experimental uniaxial (in the longitudinal and transverse direction) and biaxial stress-strain curves and corresponding predicted responses based on the one constant and two constant models (Weiss 1994).

Pancheri et al. (2014) proposed a hyperelastic material constitutive law (based on Holzapfel (2002) and Ogden (1997)) describing mechanical response in uniaxial and planar biaxial extension, which includes the thickness of the layers and the orientations of the fibers in those

two layers. The model with the coefficients found from the biaxial tension tests was validated showing a good fit of the simulation response to the experimental data. Good agreement with the uniaxial experimental data was also achieved up to 6% of stretch in the two directions, what suggests that this is an elastic limit in the uniaxial tension tests on the fascia lata samples.

Another model of anisotropic hyperelastic material created by Ruiz-Alejos (2016) was applied to pure shear data and was used for a finite element simulation of the behavior of the fascia lata. For both longitudinal and transversal data fitting (*Figure 1.1-11*), the model was calculated with the same set of parameters assuming that the behavior of the collagen fibers is the same in longitudinal and transversal directions, and only the number of the fibers is different. Moreover, they included the deformation gradient, which means that the direction of the fibers in the adjustment layers are not orthogonal and changing with the stretch. With the error calculation, the parameters underestimation was evident for the longitudinal data. Authors did not present the fitting curves for the planar pure shear tests.

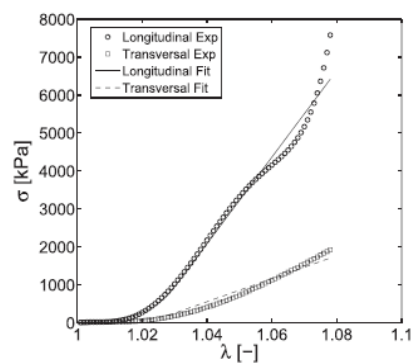


Figure 1.1-11. Results from the uniaxial tensile tests (circles and squares) and the constitutive model (solid and dashed lines) (Ruiz-Alejos et al. 2016).

The results of the pure shear FE simulation and the corresponding measured displacement map on fascia sample are illustrated on the *Figure 1.1-12*. The coefficients for the material model were the same as earlier (fitting the uniaxial data). The curves from the FE simulation slightly overestimated the load, but the total response and the stiffness were close to the experimental results.

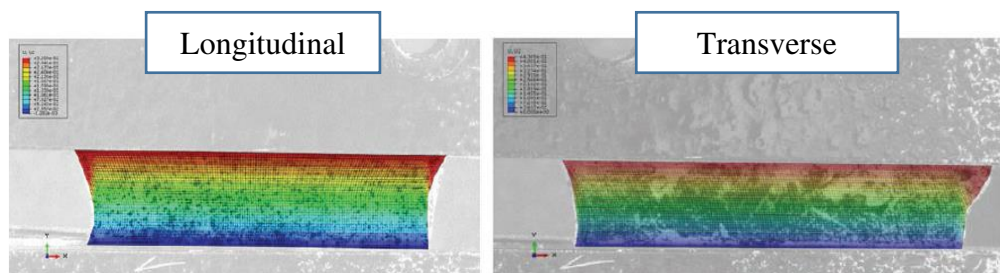


Figure 1.1-12. Contour plot of the displacement along the loading direction during the pure shear tests superposed to the displacement map obtained by FE simulation (Ruiz-Alejos et al. 2016).

Most of the leg's FE models including deep fascias deal with plantar or crural fascias (*Table 1.1-4*). In addition, almost all are isotropic and linearly elastic materials with varying element types.

Table 1.1-4. Examples of available FE models of deep fascias of the leg.

Study	Behavior law	Fascia	Element type	Young's modulus (MPa)	Poisson's ratio	Thickness (mm)
Cheung et al. (2008)	homogeneous, isotropic, and linearly elastic	Plantar	Tension-only truss	350	-	2
Pavan et al. (2017)	hyperelastic fiber-reinforced material	Crural	4-node membrane	constitutive modeling		0.3
Ruiz-Alejos et al. (2016)	anisotropic and nonlinearly elastic	Fascia lata samples	8-node brick elements	constitutive modeling (Table 1.1-3)		
Chen et al. (2015)	homogeneous, isotropic, and linear elastic	Plantar	solid	350	0.45	2
Chen et al. (2019)	linearly elastic	Profundal	linear triangular shell (S3R)	190	0.4	0.2
	linearly elastic	Plantar	Slip ring connector	-	-	-
Gu et al. (2013)	isotropic and linearly elastic	Plantar	Tetrahedral solid	350	0.4	-
Guo et al. (2018)	linearly elastic, homogeneous, and isotropic	Plantar	8-node 3D-hexahedral elements	350	-	0.65
Birnbaum et al. (2004)	linearly elastic	ITT	spring elements	170	-	-

There is almost nothing validated specifically for the fascia lata, except the model above and the model of the ITT presented by Birnbaum et al. (2004). Here, the ITT was modeled as a construction of five parallel spring elements with each spring rigidity of 3.4 N/mm and a proximal and distal conduction. The position of the ITT was created accordingly to the *in vivo* investigation of its anatomic location. The main objective was to obtain the accurate location of the ITT and its material characteristics including biomechanical properties. The loading capacity of the ITT averaged 17 N/mm with averaged tissue lengthening of 65 mm. Hence, this is the first model which includes ITT and the influence of it on the hip joint. Therefore, it can be used for the measurement of the forces created by the ITT onto the great trochanter during total hip replacement.

1.2. Synthesis and Objectives

Most approaches of soft tissue modeling failed due to missing data on their material properties (García et al. 2000; Majumder, Roychowdhury, and Pal 2007). With the FE model of the upper leg where contacts between muscles were defined by contact laws, Stelletta et al. (2016; 2017) showed that in order to properly reproduce muscle activation in three dimensions, these connections were not enough to replicate transverse loadings. They therefore suggest that including connective tissues and fascias in the model would improve its response. To do so, mechanical behavior and strain levels of fascias for both passive and active movements are required to be implemented in such models.

Therefore, the first objective of the study was to understand and quantify the strain mechanisms and the strain rates that the fascia lata of the leg can experience during passive knee flexion-extension movement. We assessed these strain mechanisms on the fascia lata's external surface using digital image correlation. The strain changes on the fascia lata were linked with the joint angles during the leg movements to describe and understand the mechanisms of the tissue behavior. This was never done previously, but it seemed important to define what experimental conditions should be applied when performing tests on isolated samples.

Then, the second objective of the thesis was to analyze fascia lata's mechanical behavior from tests on isolated samples. It has been seen in the literature review, that the mechanical response of fascia lata was mainly studied in tension for different strain levels and at different strain rates but supposedly they do not reflect the physiological state of the fascia lata. To go further, we thus proposed to look at the response of fascia lata under shear loadings. Bias extension tests and large band tests were thus proposed. Furthermore, the directions of the fibers have an influence on the tissues parameters, and due to the literature, the only reported angle between collagen fibers network are based on the data obtained from the goat fascia lata (Pancheri et al. 2014). Therefore, we investigated the fibers kinematics (orientations and distributions) in each of the fascia lata's layers during the shear loadings. Hypotheses related to bias extension tests such as supposing that fibers layers are not sliding on each other had to be checked, for instance by measuring strain fields on both sides of the tissue (internal and external). Additionally, few observations of the microstructure of the tissue were performed by bi-photon microscopy.

The best way to combine all the results from this research and to go further in the understanding of fascia lata's behavior is to assess an associated constitutive law. For that, a finite element model of fascia lata samples was created to reproduce the tensile tests found in the literature and the shear tests performed in this thesis.

To relate the strain state of fascia lata *in situ* and the one observed during mechanical tests on isolated samples, the analysis of *in situ* strain release by cutting may be a first approach. We choose to analyze the impact of a surgical technique named pie-crusting on the strain state on the surface of the ITT. This technique is widely used by surgeons to balance the soft tissues in the varus-valgus knee deformities. We assessed quantitatively the impact of pie crusting on ITT strain release and strain mechanisms, and on knee mobility.

CHAPTER II

STRAIN MECHANISM DURING KNEE FLEXION MOVEMENT

This chapter is composed with the open access article Sednieva et al. (2020) ("<https://doi.org/10.3389/fbioe.2020.00750>") and the additional results from three subjects which were studied after the publication are added into the APPENDIX I.



Strain Assessment of Deep Fascia of the Thigh During Leg Movement: An *in situ* Study

Yulia Sednieva¹, Anthony Viste^{1,2}, Alexandre Naaim¹, Karine Bruyère-Garnier¹ and Laure-Lise Gras^{1*}

¹ Univ Lyon, Université Claude Bernard Lyon 1, Univ Gustave Eiffel, IFSTTAR, LBMC UMR_T9406, Lyon, France, ² Hospices Civils de Lyon, Hôpital Lyon Sud, Chirurgie Orthopédique, Pierre-Bénite, France

Fascia is a fibrous connective tissue present all over the body. At the lower limb level, the deep fascia that is overlying muscles of the outer thigh and sheathing them (fascia lata) is involved in various pathologies. However, the understanding and quantification of the mechanisms involved in these sheathing effects are still unclear. The aim of this study is to observe and quantify the strain field of the fascia lata, including the iliotibial tract (ITT), during a passive movement of the knee. Three fresh postmortem human subjects were studied. To measure hip and knee angles during knee flexion-extension, passive movements from 0° to around 120° were recorded with a motion analysis system and strain fields of the fascia were acquired using digital image correlation. Strains were computed for three areas of the fascia lata: anterior fascia, lateral fascia, and ITT. Mean principal strains showed different strain mechanisms depending on location on the fascia and knee angle. For the ITT, two strain mechanisms were observed depending on knee movement: compression is observed when the knee is extended relative to the reference position of 47°, however, tension and pure shear can be observed when the knee is flexed. For the anterior and lateral fascia, in most cases, minor strain is higher than major strain in absolute value, suggesting high tissue compression probably due to microstructural fiber rearrangements. This *in situ* study is the first attempt to quantify the superficial strain field of fascia lata during passive leg movement. The study presents some limitations but provides a step in understanding strain mechanism of the fascia lata during passive knee movement.

Keywords: deep fascia of the thigh, digital image correlation, motion analysis, strain, *in situ* study, iliotibial tract, biomechanics

INTRODUCTION

Pathologies of the musculoskeletal system have become a major public health issue, especially due to an aging and sedentary population. Osteoarticular pathologies such as osteoporosis or musculoskeletal disorders lead to disability and loss of autonomy. In the lower limb, for instance, several pathologies such as osteoarthritis, iliotibial band syndrome, inflammatory lesions, joint disorders, traumatic injuries etc. may significantly affect a patient's quality of life. To develop

OPEN ACCESS

Edited by:

Ciaran Knut Simms,
Trinity College Dublin, Ireland

Reviewed by:

Charles S. Chung,
Wayne State University, United States
Niels Hammer,
Medical University of Graz, Austria

*Correspondence:

Laure-Lise Gras
laure-lise.gras@univ-lyon1.fr

Specialty section:

This article was submitted to
Biomechanics,
a section of the journal
Frontiers in Bioengineering and
Biotechnology

Received: 06 February 2020

Accepted: 11 June 2020

Published: 29 July 2020

Citation:

Sednieva Y, Viste A, Naaim A,
Bruyère-Garnier K and Gras L-L
(2020) Strain Assessment of Deep
Fascia of the Thigh During Leg
Movement: An *in situ* Study.
Front. Bioeng. Biotechnol. 8:750.
doi: 10.3389/fbioe.2020.00750

a greater understanding of these pathologies and to provide better health care, clinicians are increasingly using biomechanical modeling (Chèze et al., 2012). Musculoskeletal models allow the study of everyday life movements – walking, climbing stairs, getting up from a chair – thanks to kinematic and dynamic analyses, and can therefore provide a thorough evaluation of patients' functional status.

Dynamic multi rigid body models of the lower limb (Moissenet et al., 2014) can predict musculotendinous forces within the joints as well as ligament and contact forces. However, the main limitation of these models is that muscles are represented only by their main lines of action. They are unable to reproduce forces induced transversely (Huijing, 2009) by a muscle's activation on other muscles, bones and joints via fascias, epimysium and connective tissues.

To overcome this limitation, finite element models of the lower extremity including contractile muscular volumes (Stelletta et al., 2016, 2017) or for one specific muscle (Westman et al., 2019) have been developed. Nevertheless, even though these models include detailed geometry and mechanical properties of muscles, improvements are still needed to increase their biofidelity in reproducing the complex passive mechanical action of soft connective tissues, especially the fascias. These passive structures sheath muscles and muscular compartments; exert a stress or pressure on them and thus participate in force transmission in both longitudinal and transverse directions during muscle activation (Huijing, 2009; Snoeck et al., 2014; Eng and Roberts, 2018). With their finite element model of the upper leg where contacts between muscles were defined by contact laws, Stelletta et al. (2016, 2017) showed that in order to properly reproduce muscle activation in three dimensions, these connections were not enough to replicate transverse loadings. They therefore suggest that including connective tissues and fascias in the model would improve its response. To do so, mechanical behavior, and strain levels of fascias for both passive and active movements are required to be implemented in such models.

Fascias can be either loose or dense connective tissues. Deep fascias are multi-layered dense fibrous connective tissues, mainly made of collagen and elastin fibers (Stecco et al., 2011), and surround muscles and groups of muscles. It has been shown that they contribute to the pressure in the muscular compartments (Garfin et al., 1981), and to muscle force transmission (Snoeck et al., 2014), they transmit mechanical forces between muscles (Huijing, 2009); they also participate in movement coordination (Barker et al., 2004), limb stabilization (Stahl, 2010), and elastic energy storage (Bennett et al., 1986).

Many studies have been carried out to characterize the mechanical behavior of deep fascias in relationship with their microstructure. These tissues are anisotropic, non-linear viscoelastic materials (Findley et al., 2015). *In vitro* tests and associated constitutive models have been proposed to characterize these tissues (Eng et al., 2014; Ruiz-Alejos et al., 2016; Otsuka et al., 2018). Presented results are obtained from animal tissue (Eng et al., 2014; Ruiz-Alejos et al., 2016) or human tissue (Stecco et al., 2014; Otsuka et al., 2018). They were obtained from unidirectional (Pavan et al., 2015; Ruiz-Alejos et al., 2016;

Otsuka et al., 2018) or biaxial (Eng et al., 2014; Pancheri et al., 2014) tensile tests performed until rupture or at high strain levels (Stecco et al., 2014; Ruiz-Alejos et al., 2016). Pure shear loading (Ruiz-Alejos et al., 2016) was also studied and used to identify a constitutive law.

Biaxial testing aims at reproducing a more realistic loading of deep fascias than uniaxial tension, and tests to failure help to understand the mechanical behavior of the deep fascias under large strains. However, the mechanical behavior (mechanism, level of strain) of the deep fascias during movement is relatively unknown.

In this study, we focus on the fascia lata, which overlies the muscles of the outer thigh. It is involved in various pathologies, such as iliotibial band syndrome (Fairclough et al., 2006; Huang et al., 2013), compartment syndrome (Nau et al., 2000), varus-valgus of the knee (Clarke et al., 2005; Nikolopoulos et al., 2015), and traumatic injuries. As part of the fascia lata, the iliotibial tract (ITT) shows complex interactions with muscles and skeletal structure of the lower limb, and has a major role in the knee joint stability (Fairclough et al., 2006; Vieira et al., 2007).

The aim of this study is to observe and quantify the strain field of the external surface of the fascia lata, including the ITT, during a passive movement of knee flexion-extension. Collected data could then be useful to perform adequate sample testing and develop constitutive laws of fascia to be implemented in numerical models dedicated to clinical applications. This analysis is based on *in situ* testing and involves movement analysis and strain field measurement using stereovision and digital image correlation.

MATERIALS AND METHODS

Specimen Preparation

Three fresh postmortem human subjects from the Department of Anatomy of the University of Rockefeller (DAUR), Lyon, France, were instrumented for motion analysis of the left leg and the measurement of the strain field on fascia lata during knee flexion-extension movement. Ethical approval was not required for this study since it is not required by French law. The cadaver subjects were obtained after the deceased gave their informed consent to donate them to science during their lifetime (law article R2213-13). The authors ensure that these experiments were performed with respect for these remains, and in correct health and safety conditions. These subjects were in average 92.3 years-old (± 2.5), measured 161 cm (± 2.6 cm), weighted 45.5 kg (± 12.3 kg) and had a BMI of 13.6, 16.6, and 22.3 kg/m², respectively. Subjects were considered as fresh since no specific body preservation was performed: no injection of any embalming solution, no freezing. After death, bodies were kept at 4°C until testing. The duration between time of death and time of test was 6 days (5 days postmortem and 1 additional day for body preparation) for subject 2019_285, it was 5 days (4 + 1 days postmortem) for subject 2019_300 and 3 days (2 + 1 days postmortem) for subject 2019_308. The average postmortem interval was 4.7 days.

For motion analysis, six rigid tripods with attached markers (four reflective markers of 10 mm diameter fixed to a rod) were

screwed in the right and left areas of the pelvis, in both femurs, and in both tibias (Figure 1A). Particular attention was paid to the position of the tripods in the femur. They were implanted in the medial condyles in order to avoid any interference with the lateral and anterior areas of the thigh where soft tissue strains were measured.

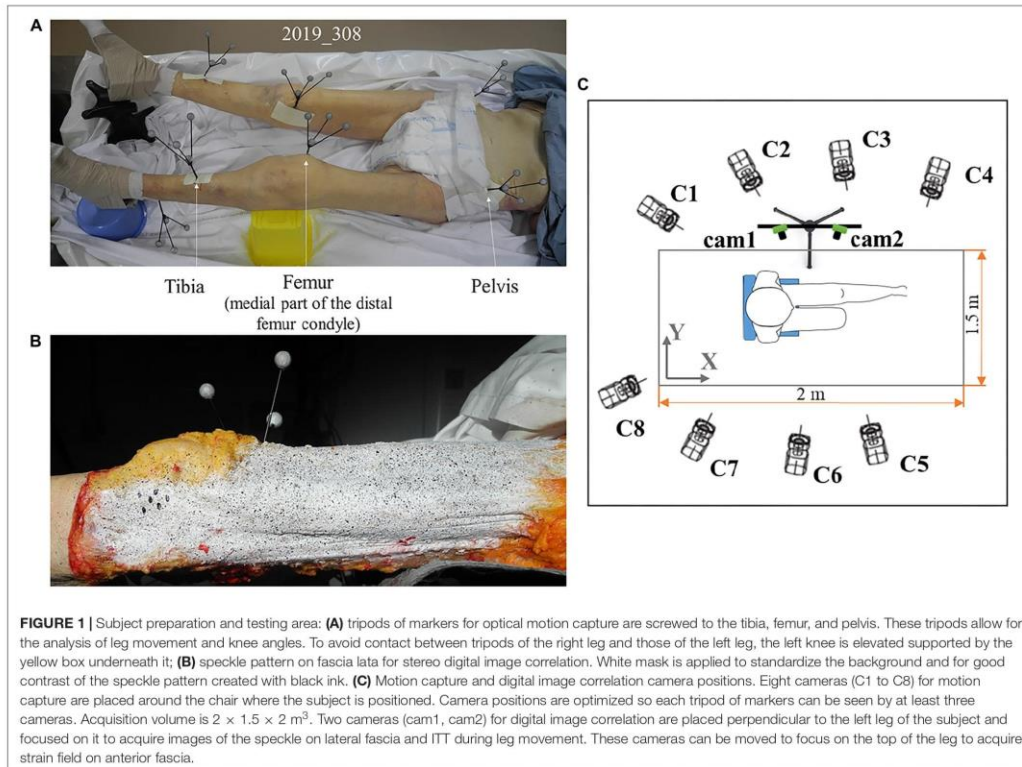
In order to measure the superficial strain of the deep fascia lata by using the digital image correlation, a random speckle pattern was applied to the surface of the fascia lata after skin and fat removal (Figure 1B). To do this, the fascia lata was covered with a thin layer of white clown makeup to standardize the background and obtain good contrast, speckles were then created using a toothbrush and black ink to apply droplets on the white surface (Podwojewski et al., 2014, 2013). The washable white makeup layer could be easily removed without damaging the tissue, and therefore it was possible to redo the pattern until an appropriate speckle size or density for digital image correlation was obtained. Initially, speckles were created on the anterior area of the fascia lata, and after testing with observation of this area, speckles were created on the lateral side of the fascia for the new testing. This procedure allowed for correct tissue hydration, keeping it in saline solution

when not being tested. It also reduced the risk of erasing the speckle during testing.

During tests, the body was placed on a specific chair at ambient temperature. This chair facilitated the installation of the subject lying on its back with buttocks at the edge of the seat, and then back rest support reproducing a seated posture, both legs were suspended allowing full knee flexion.

Anatomical Frames Acquisition and Motion Analysis

The acquisition was performed using an optical motion capture system – Optitrack – with 8 cameras (1280 × 1024) recording at 100 Hz. The 8 cameras were oriented in order to cover a volume of interest ($2 \times 1.5 \times 2 \text{ m}^3$) where each tripod could be seen by at least three cameras at the same time during the leg movement from extension to flexion (Figure 1C). Considering the volume of interest (Eichelberger et al., 2016) and the optical motion capture system used (Carse et al., 2013), eight cameras were sufficient to accurately measure leg kinematics. Each tripod screwed into the lower limbs meant that a technical frame for each body segment could be defined, to follow its position during



movement. In order to define the anatomical frame relative to these technical frames, anatomical markers were palpated with an additional tripod when the body was lying on its back. Each tripod consisted of four markers fixed to a rod.

The tip position of the additional tripod used for palpation was previously calibrated. Calibration was performed by pointing three points of known positions. As in the lying position the posterior superior iliac spine was inaccessible, it was supposed that the mid sacrum marker was positioned vertically relative to the middle of the left and right anterior superior iliac spine on the seat plane. All anatomical points are listed in **Table 1**. Joint kinematics were then calculated using the anatomical frame and Euler sequences recommended by the International Society of Biomechanics (Wu et al., 2002) using MATLAB. During acquisition, hip angle varied: for subject 2019_285 it was $24.84 \pm 10.75^\circ$, for subject 2019_300 it was $26.71 \pm 9.45^\circ$ and for subject 2019_308 it was $20.38 \pm 8.63^\circ$.

Digital Image Correlation

In order to obtain the 3D surface strain field of the thigh fascia, a digital image correlation set-up was required. A pair of low noise cameras were rigidly mounted and fixed in place during system calibration and subsequent data acquisition (**Figure 1C**). The cameras used for these tests were GO-5000-USB from JAI's Go Series (maximum frame rate: 62 Hz) with objective KOWA LM12HC with lenses of 12.5 mm and an f-stop range of $f/14$ to $f/16$. Image size was 2560×2048 px. The frame rate for the acquisition was set to 50 Hz, two times lower than for the motion analysis recording. This chosen frame rate allowed an easier synchronization and correspondence between strain measurements and knee angles, while it resulted in at least 300 data points for each flexion or extension knee movement. The depth of field was optimized by closing the diaphragms as much as possible: an aperture of $f/16$ was kept consistent during and between acquisitions, permitting a correct focus on the area of interest although slight changes in the distance between the area of interest and the cameras. The light was adjusted to optimize image quality and for a sharp contrast. Owing to this configuration, strains in planes closer or further from the cameras' focal plane were captured thanks to clear high-quality images. Care was taken to match cameras center points. Calibration was carried out using a calibration grid adapted to the size of the field of view with a 5 Hz frame rate.

TABLE 1 | List of anatomical points and associated anatomical frames.

Anatomical points

Left and right anterior superior iliac spine
 Left and right greater trochanter
 Left and right lateral epicondyle
 Left and right medial epicondyle
 Left and right fibula head
 Left and right tibial tuberosity
 Left and right lateral malleolus
 Left and right medial malleolus

Data processing was carried out with VIC-3D software. For the area of the ITT and lateral fascia, the size of pixels was 0.19 mm; for the anterior fascia, the size of pixels was 0.18 mm. The subset was chosen equal to 31 and the step at 7.

For this strain analysis, a hip angle of $26.52 \pm 3.85^\circ$ (respectively 25.23° , 30.41° , and 23.91° for each subject) and knee flexion of $47 \pm 0.5^\circ$ was considered as a reference image for strain analysis. This angle for the knee was chosen due to the position of the body with zero gravity (Mount et al., 2003).

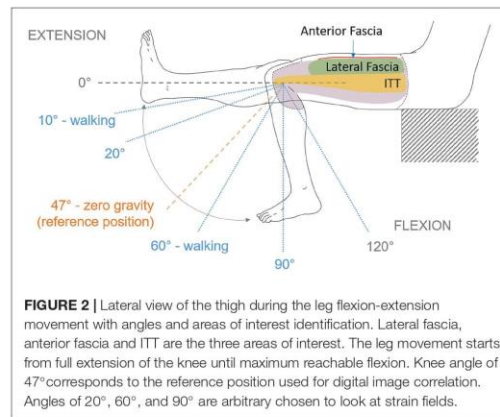
For the lateral view, the area of interest was divided into "ITT area" and "above ITT area" named "lateral fascia" (**Figure 2**). The anterior view area of the fascia was entirely post processed and named "anterior fascia." Major principal (E_1), minor principal (E_2) and maximum shear ($\max E_{xy}$) Green-Lagrange strains were extracted.

Test Conductions

The knee extension-flexion range of motion was applied to the left leg manually from 0° (full extension) to 120° (flexion) (**Figure 2**). These movements were chosen in order to cover the possible positions of the leg during daily life activities (walking, step climbing, etc.) and stretching.

During the leg movement, care was taken to avoid subject contact with the experimental setup, keeping the femur parallel to the digital image correlation system and as motionless as possible to stay in the field of view, and to maintain focus on the surface of interest. Movements were recorded with the anterior area of the fascia lata as region of interest for the digital image correlation. The digital image correlation system was then moved to record strains on the lateral side of the fascia. For each area of interest, three tests consisting of five cycles of knee flexion-extension were performed. Cycles were applied continuously. A waiting time of 10 min was observed between tests.

Motion analysis and digital image correlation acquisitions were synchronized using a common trigger box sending a rising edge square signal to both systems. All the data extracted from motion analysis and digital image correlation were processed



using a custom-made script in Python. Due to the stretching of knee area during knee flexion and creation of folds during the full extension, strain could not be computed on a sufficient number of points in this area. Therefore, the knee area was excluded from fascia strain computations.

RESULTS

Knee Angular Velocity

Figure 3 illustrates the knee angular velocity recorded during movement for each subject and for each digital image correlation configuration: observing the anterior fascia and observing both the lateral fascia and ITT. Although leg movement was applied manually, angular velocity was relatively reproducible throughout the five cycles of each configuration and over the three tests for each subject. Relative standard deviations (RSD) ranged from 21 to 28% with a mean value of 24% for tests on anterior fascia. For tests performed on lateral fascia and ITT, they ranged from 18 to 25% with a mean value of 22.5%. Maximum angular velocities in flexion (positive values) and in extension (negative values) were close in absolute value, with an average difference of 7 deg/sec considering the three subjects and two configurations. For each subject, the angular velocities were also similar between the two configurations, with an average difference in maximum velocity during flexion of 8 deg/sec.

Strain Analysis

Average Strains

Shear strain fields obtained for three knee angles are given for all areas of fascia and ITT and for each subject and for three knee angles (20°, 60°, and 90°), as shown in Figure 4.

Figures 5–7 illustrate the average strains computed along the five cycles of the three tests performed on each subject, on the area of the anterior fascia, the lateral fascia and the ITT, respectively. For each subject, we can observe a good reproducibility of results over the five cycles and the three tests, except on the lateral area of the fascia for which we can see a larger dispersion of the minor strain levels along the cycles. As for RSD, each area of the fascia for both major and minor strains are presented in Table 2. For tests on the anterior fascia, RSD were in average ranging from 20 to 53%. Similar results were obtained for the lateral fascia, with RSD ranging from 20 to 39%. Results were less dispersed for the ITT with RSD ranging in average from 15 to 25%. For all curves, maximum RSD was obtained for knee angles around the reference position of 47°, which can be seen on Figures 5–7.

For the subject 2019_285, on both the lateral and anterior areas of the fascia, we measured lower strains compared to the other subjects. For a knee angle of 90° (flexion), the average shear strain values on the fascia did not exceed 2%. Strains of the ITT are also lower in full extension of the knee. The specific behavior of this subject was associated to a subjective observation of knee rigidity in rotation and varus-valgus during the experiment compared to the other subjects. Moreover, full extension of the knee was limited for this subject compared to the others with a minimum knee angle of 0° while it was around –15° for other subjects.

For each subject, average curves obtained for the different areas of fascia and ITT are illustrated in Figure 8. A large inter-subject variability of fascia and ITT behavior is observed. This can be related to the variability of anthropometries of the three subjects, specifically in terms of BMI or to other physical conditions that could affect soft tissue mechanical behavior.

Strain Mechanisms

Despite the apparent inter-subject variability, the evolutions of major and minor strains along the knee flexion-extension movement seem vertically mirrored in many cases. To analyze the E_1/E_2 ratio, Figure 9 illustrates E_1 against ($-E_2$). On this figure, two phases of the movement corresponding to postures closer to knee flexion (i.e., knee angles > the reference knee angle of 47°) and the postures closer to knee extension (i.e., knee angles < the reference knee angle of 47°), are illustrated with two different colors.

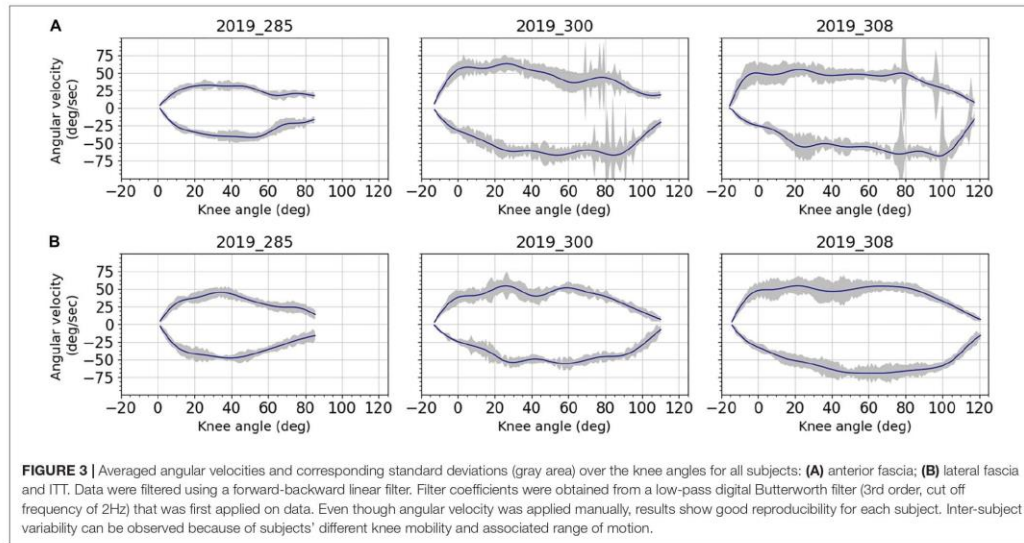
On the anterior fascia (Figure 9A), for subject 2019_285, for which strain levels are lower, a tension mechanism is observed with a maximum average tensile strain around 1.5% and a lower absolute value of compressive strain around 0.5%. For subjects 2019_300 and 2019_308, absolute value of the compressive strain is greater than the average tensile strain when the knee is more flexed relative to the reference knee angle (red curves, knee angle > reference angle).

On the lateral fascia (Figure 9B), for the subjects 2019_300 and 2019_308, the same analysis as for the anterior fascia can be made, and compressive strain can reach up to 15% in absolute value. For the subject 2019_285, for which strain levels are lower, the strain mechanism of the fascia is pure shear with a ratio $E_1/(-E_2)$ equal to 1 when the knee is more flexed relative to the reference knee angle (red curves, knee angle > reference angle).

On the ITT (Figure 9C), the two phases of knee movement show different strain mechanisms for subjects 2019_285 and 2019_308. When the knee is more flexed relative to the reference knee angle (red curves, knee angle > reference angle), even if a tensile strain larger than the compressive strain may be observed, we can observe pure shear with a curve gradient close to 1. For subject 2019_300, the two phases of movement do not differentiate between strain mechanisms so clearly, but we can also observe some pure shear. Considering all tests, strain measurements on ITT show maximum tensile strain between 2 and 15% and compressive strain between 4 and 13% in absolute values.

Strain Rates

Strain rates measured on the various areas of the fascia lata during movement are illustrated in Figure 10. As for the strains, the strain rate measurements are very low on the anterior and lateral fascia for the subject 2019_285. Considering all the other tests, the maximum strain rates in flexion (positive values) and in extension (negative values) of the knee were close in absolute value, with an average difference of 1%/sec for E_1 strain rate and 1.5% for E_2 strain rate. Concerning the anterior and lateral fascia, these maximum strain rates can reach 6.3%/sec for E_1 and 8.1%/sec



for E_2 . As for the ITT, they can reach 10.5%/sec for E_1 and 11.2%/sec for E_2 .

DISCUSSION

This *in situ* study is the first attempt to quantify the superficial strain field of fascia lata during passive leg movement. Motion analysis, stereovision and digital image correlation were combined to measure major, minor and maximum shear Green-Lagrange strains. These measurements were performed on three different locations of fascia lata: anterior, lateral and ITT.

The strain measurement by 3D surface digital image correlation in these conditions is challenging. Specific care was taken to get good quality images. A large depth of field was needed to limit the unfocused area on the view of the anterior fascia area, as this area could have a pronounced curved shape. Lighting and exposure time were optimized to avoid, as much as possible, shiny areas due to the water content in the tissue, and the fascia had to be kept hydrated. In-depth hydration could not be controlled, but to ensure good surface hydration of the fascia along the tests, a sheet of saline-solution soaked paper systematically covered the fascia between tests. This protocol was performed to avoid loss of fluid that may affect fascia mechanical properties such as its stiffness (Schleip et al., 2012).

White makeup, mainly made of talc, glycerin and water, was also used to facilitate digital image correlation. This specific water-based makeup was indeed chosen because of its assumed lower effect on tissue hydration, however, its osmotic effect on fascia tissue remains unknown to the best of the authors' knowledge. Connective tissue water content may affect its mechanical properties, and thus strain measurements. For

instance, Chimich et al. (1992) showed that the viscoelastic behavior of ligaments soaked in phosphate-buffered saline solution was altered; Basser et al. (1998) used the osmotic stress technique to evaluate the relationship between hydration and the tensile stress in the collagen network. Thornton et al. (2001) showed that ligaments creep behavior increased with increased tissue hydration; and Masic et al. (2015) looked at changes in tensile forces resulting from osmotic pressure in tendon collagen. In the present study, we can consider that the water content within the fascia before application of the white mask was close to the natural one since cadaveric subjects were not frozen and only stored at 4°C before body preparation. However, water content is difficult to assess *in situ* on the whole specimens' leg after application of makeup. Therefore, the osmotic effect of this white makeup on fascia water content and mechanical properties should be further investigated through tests on isolated samples, following an experimental protocol as proposed by Hammer et al. (2014) with the use of osmotic stress technique to assess the water content in ITT samples.

Moreover, another difficulty was to apply the knee flexion-extension without compromising the movement analysis or the strain field analysis on the fascia. This movement was applied manually by moving the ankle to avoid any constraint due to attachment of the femur or the lower leg but did not prevent from some variation of the angle between the pelvis and the femur. As the fascia lata involves both hip and knee joints, this hip angle variation could lead to the generation of strain noise that may contribute to the lack of reproducibility of mean strain during movement. To improve the set-up and increase reproducibility, a controlled device could be developed in order to guide the movement of the knee. With such system, it would then be possible to do the analysis without the optical motion

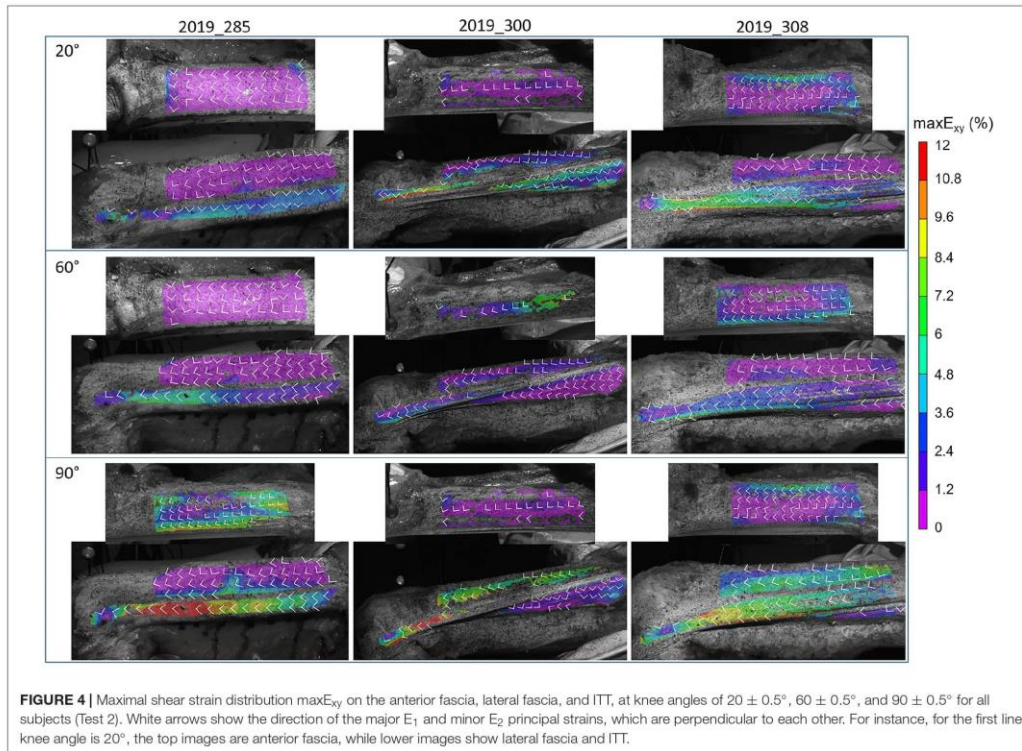


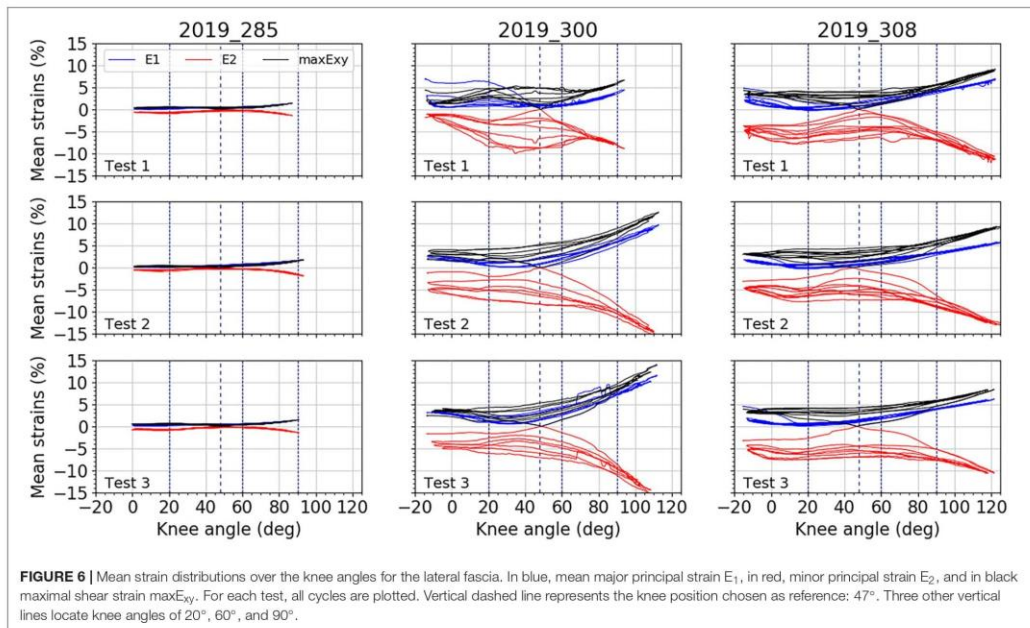
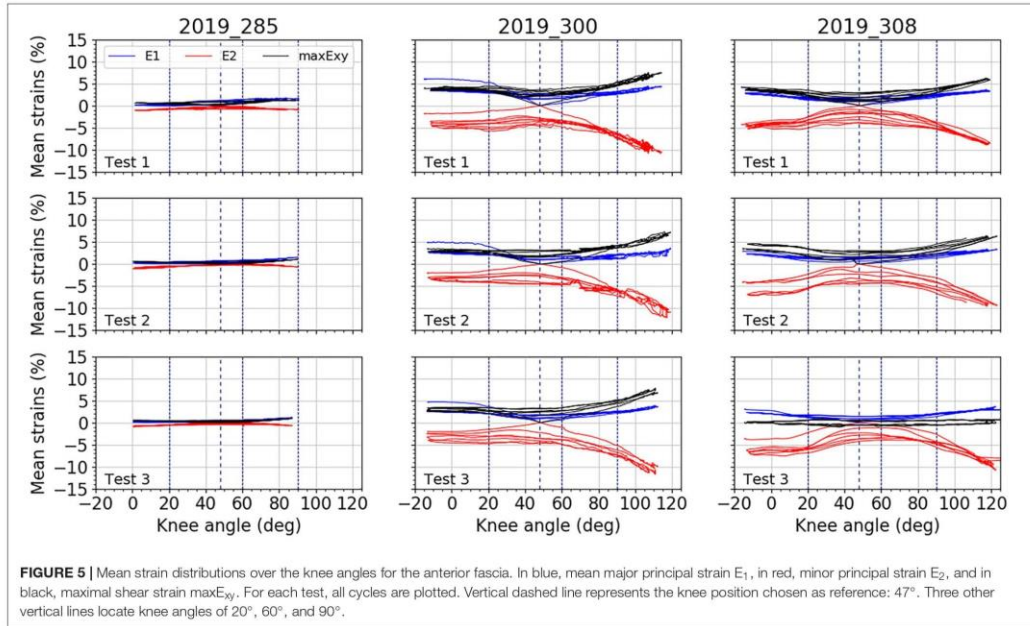
FIGURE 4 | Maximal shear strain distribution $\max E_{xy}$ on the anterior fascia, lateral fascia, and ITT, at knee angles of $20 \pm 0.5^\circ$, $60 \pm 0.5^\circ$, and $90 \pm 0.5^\circ$ for all subjects (Test 2). White arrows show the direction of the major E_1 and minor E_2 principal strains, which are perpendicular to each other. For instance, for the first line knee angle is 20° , the top images are anterior fascia, while lower images show lateral fascia and ITT.

capture system; only synchronization between stereovision and the new device would be needed. The challenge would be to have a device adaptable to different subjects' anthropometries and that will not affect knee kinematics. Nevertheless, despite the manual application of movement, knee angular velocity was relatively reproducible, and representative of the movement surgeons could perform to test knee stability during surgery.

Cadaveric subjects were used in this study and hence the effect of postmortem storage on tissue mechanical properties may affect the presented results. The fascia lata is composed of highly oriented collagen fibers in different layers connected to each other with an extracellular matrix composed of proteoglycans (Pancheri et al., 2014). Both components may have deteriorated with death. Tuttle et al. (2014) investigated the effect of postmortem time on rabbit skeletal muscle mechanical and biochemical properties. As for collagen content, results indicate that it remained unaffected over 7 days postmortem. Another study by Nishimura et al. (1996) looked at the content of proteoglycans sheathing collagen fibrils and fibers. They showed that for beef stored at 4°C , proteoglycans content decreased by 40% within 7 days postmortem. In the present study, the maximum duration between time of death and time of test was 6 days, and during this period, subjects were kept at

4°C . Therefore, based on existing literature, we can hypothesize that for fascia lata the collagen content remained constant but that the links or lubricant between collagen fibers were degraded. This would probably imply that strain measurements are underestimated compared to what would be experienced *in vivo* on living tissue, since the viscosity properties provided by proteoglycans and that allow fibers to glide, progressively disappeared; but the impact on postmortem storage on fascia properties should be further investigated.

This study was performed on only three subjects. These subjects were geriatric people, presenting three different BMI and knee mobility ranges. At this stage of the study, inclusion criteria regarding for instance BMI, age or leg pathology were not considered, since the aim of the study was to get a first overview of the fascia strain field without preconditions. Nevertheless, the physical condition of these subjects prior to death could affect the results. Unfortunately, such information (regarding physical conditions or medical records as well as cause of death) of donors is unavailable, but we can still observe that two subjects had a low BMI suggesting muscular atrophy due to aging also known as sarcopenia, or due to a body weight loss related to cachexia. Such pathologies affect muscle tissue and its ability to contract (Muscaritoli et al., 2010; Tournadre et al., 2019). Moreover,



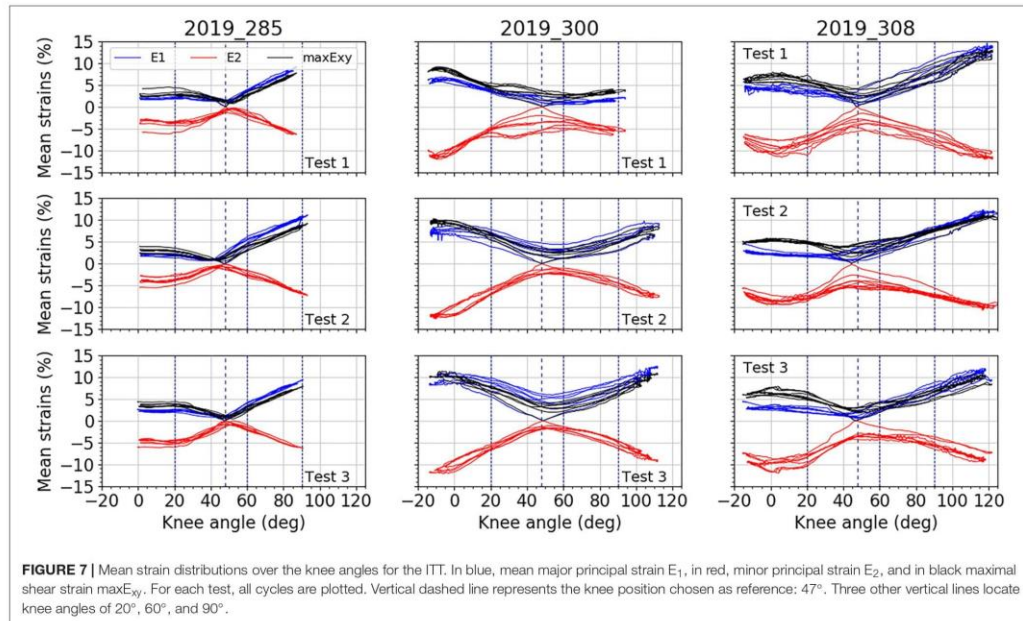


FIGURE 7 | Mean strain distributions over the knee angles for the ITT. In blue, mean major principal strain E_1 , in red, minor principal strain E_2 , and in black maximal shear strain $maxE_{xy}$. For each test, all cycles are plotted. Vertical dashed line represents the knee position chosen as reference: 47° . Three other vertical lines locate knee angles of 20° , 60° , and 90° .

TABLE 2 | Mean, standard deviation (SD) and maximum relative standard deviations (RSD) for each area of fascia, for each subject, and for both major E_1 and minor E_2 strains.

Fascia area	Subject #	mean RSD for E_1 (%)	SD RSD for E_1 (%)	max RSD for E_1 (%)	mean RSD for E_2 (%)	SD RSD for E_2 (%)	max RSD for E_2 (%)
Anterior	2019_285	43	26	81	53	71	100
	2019_300	22	13	60	21	12	48
	2019_308	20	13	55	21	13	62
	mean	28.3			31.7		
Lateral	2019_285	29	15	54	26	16	71
	2019_300	31	20	71	25	15	57
	2019_308	39	33	71	20	13	57
	mean	33			23.7		
ITT	2019_285	15	9	43	19	12	54
	2019_300	21	13	56	25	20	85
	2019_308	20	14	77	16	11	55
	mean	18.7			20		

RSD were calculated considering the five cycles and the three performed tests. Experimental results were overall less dispersed for ITT area. Italicized values are mean values for the three subjects.

age, gender and body weight have also been reported to affect collagen content within tissues and their mechanical properties. For patellar tendon, Couppé et al. (2009) showed that collagen content decreased with age while cross-linking increased, but that mechanical properties were maintained. For ligaments (Osakabe et al., 2001) and tendons (Guilbert et al., 2016), collagen was also found to decrease with age, but gender differences were also noticed with a higher decrease in the female group (Osakabe et al., 2001). Specifically regarding fascia, Zwirner et al. (2019) showed

that for the iliotibial tract, tensile parameters did not depend on age, except for strain at failure in the male group; but other anthropometric parameters such as height should be considered when looking at fascia mechanical properties. Nonetheless, Wilke et al. (2019) used ultrasound measurements on young and older volunteers to show that fascia thickness changes with aging, depending on its location in the body and that fascia mechanical properties were affected. These changes are supposed to affect joint range of motion (decrease or enhance) but interactions

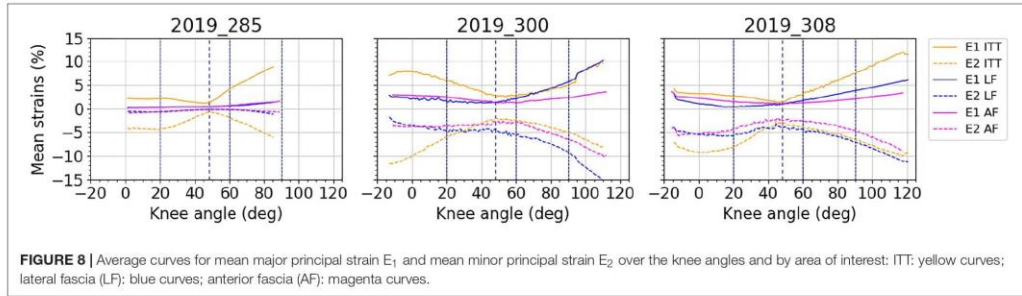


FIGURE 8 | Average curves for mean major principal strain E_1 and mean minor principal strain E_2 over the knee angles and by area of interest: ITT: yellow curves; lateral fascia (LF): blue curves; anterior fascia (AF): magenta curves.

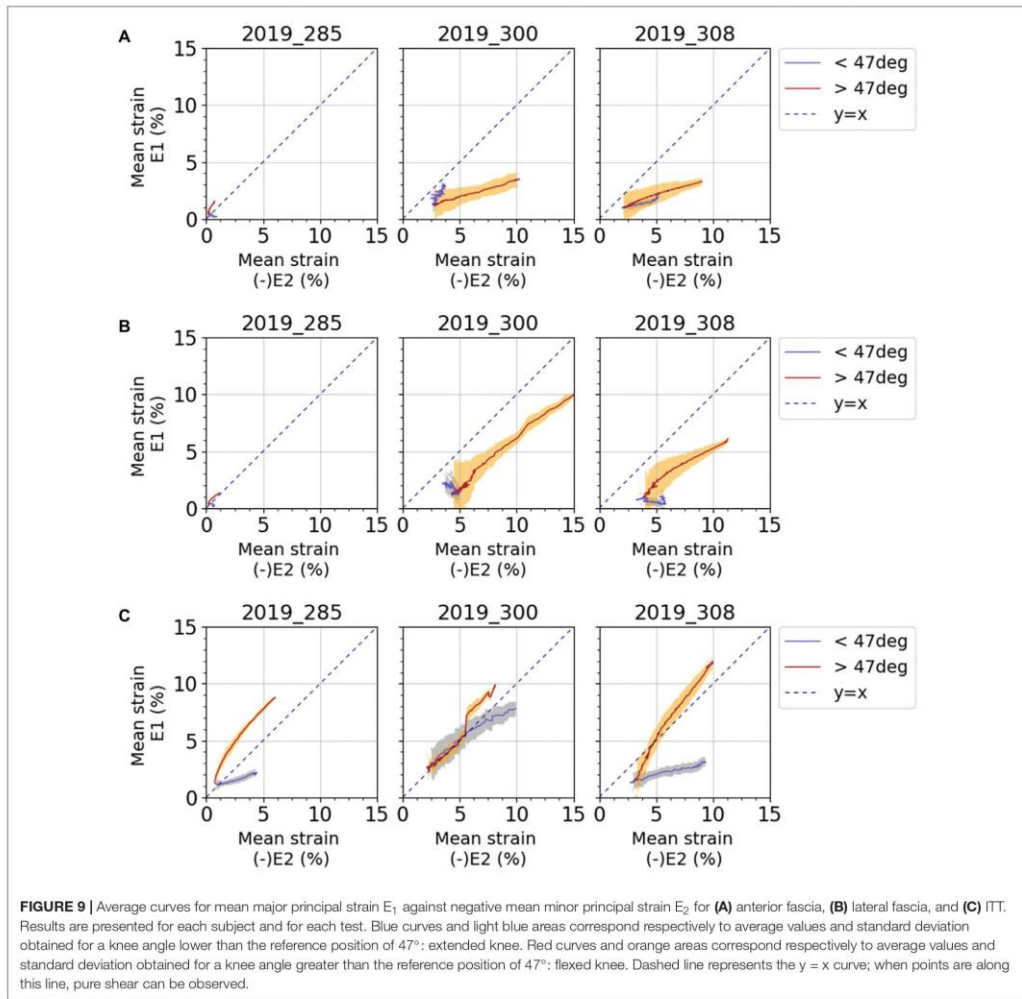
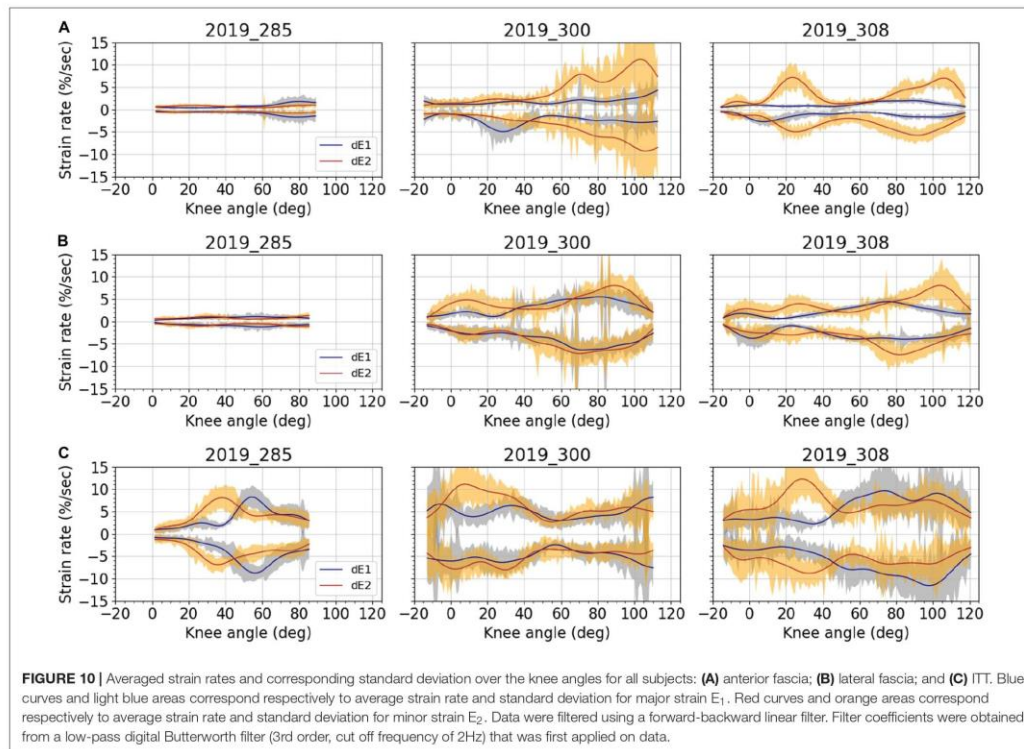


FIGURE 9 | Average curves for mean major principal strain E_1 against negative mean minor principal strain E_2 for (A) anterior fascia, (B) lateral fascia, and (C) ITT. Results are presented for each subject and for each test. Blue curves and light blue areas correspond respectively to average values and standard deviation obtained for a knee angle lower than the reference position of 47° : extended knee. Red curves and orange areas correspond respectively to average values and standard deviation obtained for a knee angle greater than the reference position of 47° : flexed knee. Dashed line represents the $y = x$ curve; when points are along this line, pure shear can be observed.



between fascial thickness, age, body mass and flexibility should be further investigated. Therefore, even though physical condition of donors is unknown, fascia thickness or collagen content were not measured and the effect of age has been partially evaluated in the literature, we should acknowledge that this might have an influence on our results; especially for subject 2019_285 that had a higher BMI and a lower knee range of motion than the other two subjects, suggesting a stiffer fascia. However, regardless of these limitations and variability between subjects, interesting tendencies regarding measured strain levels and observed strain mechanisms can still be highlighted.

In comparison with the existing data in the literature, we can first consider the level of the fascia lata strains. The maximum value of 10 and 12% for the average major principal strain measured respectively on the lateral fascia and ITT are higher than the 9% reported by Gratz (1931; human iliotibial tract), the 9.7–10.3% reported by Hammer et al. (2012, 2014, 2016; human iliotibial tract) as tensile strain at failure, and the 8% reported by Eng et al. (2014; goat fascia lata) as damage tensile strain. It is still lower than the 15% reported by Zwirner et al. (2019; human iliotibial tract) as tensile strain at failure. However, it is smaller than the maximum tensile strain applied by Stecco et al. (2014) who performed tensile tests up to 30% on human crural fascia.

It is also smaller than the 40.6% in the proximal-distal direction and 53.6% in the cranial-caudal direction reported by Henderson et al. (2015) on dog fascia lata, as tensile strain at failure. Butler et al. (1984) compared strain measurements techniques on fascia lata samples in tension, they reported 33% strain at failure for grip to grip measurement while it was only 14.5% when measured locally with an optical technique, which is closer to the values observed in this study even though not at failure. Within all the aforementioned results, high variability can be observed. One can wonder, on which part of the stress/strain curves obtained by *ex vivo* tensile testing, the strain states of the fascia lata measured *in situ*, are located. This also depends on the initial strain state of the samples tested *ex vivo*, probably also of fascia location in the body, preservation technique, species and fascia microstructure. These variations may also be related to strain rate and tissue viscosity. Tensile tests by Eng et al. (2014) and Pancheri et al. (2014) were performed at 0.15%/sec, those by Hammer et al. (2012, 2014, 2016) and Zwirner et al. (2019) at around 0.5%/sec while tests by Stecco et al. (2014) at 120%/sec. In the present study, strain rates were depending on knee angle, but average maximum values did not exceed 11.2%/sec, considering all tests and both E_1 and E_2 . If we consider that the applied knee angular velocity was lower than physiological maximal velocity measured

during gait, which can vary between 200 deg/sec to 400 deg/sec for healthy people, depending on gait speed (Mentiplay et al., 2018) the expected physiological strain rate of the fascia lata should be greater than the maximal values that we measured.

If we consider the shear strain mechanisms and sometimes the compressive strains larger than tensile strains, observed in this study, we can hypothesize that it is linked to the fascia microstructure. The fibers oriented in two different directions may be reticulated and act as local frames deformed during shear movements. This hypothesis lends itself less well to the explanation of the shear strain mechanism of the iliotibial tract. As it is made up of mostly collagen fibers in the longitudinal direction, we would have expected a major principal strain oriented in the longitudinal direction. But the observations from Otsuka et al. (2018) showing two main directions of fibers on the iliotibial tract (named lateral in Otsuka et al., 2018) seem in line with a shear mechanism explained by the fibers' arrangement. This shear strain mechanism observed *in situ* may also explain why higher tensile strains have been measured in this study compared to the values measured by Eng et al. (2014) in the main fiber directions. Moreover, in most cases on anterior and lateral fascia lata, the minor strain measured on the fascia lata is larger than the major one in absolute value. This behavior has already been observed in an isolated sample of a hepatic capsule submitted to uniaxial tension (Jayyosi et al., 2014).

As previously presented, literature reports mainly tensile tests (Gratz, 1931; Butler et al., 1984; Hammer et al., 2012, 2014, 2016; Steinke et al., 2012; Pancheri et al., 2014; Stecco et al., 2014; Henderson et al., 2015; Ruiz-Alejos et al., 2016; Otsuka et al., 2018; Zwirner et al., 2019) or biaxial tensile tests (Eng et al., 2014; Pancheri et al., 2014) performed on fascia isolated samples while here, tensile but also shear strain mechanisms, especially on ITT, were highlighted during passive knee movement. Further studies on isolated samples, including bias tests or picture frame tests would allow the analysis of the in-plane shear mechanisms of fascia lata as it is usually done for textile composites (Boisse et al., 2017; Wang et al., 2020). Moreover, as it has been already performed on various fibrous connective membranes (Jayyosi et al., 2016; Lynch et al., 2017; Krasny et al., 2018), the detailed analysis of fascia lata fiber kinematics during such loading would also help in understanding the fiber links and tissue mechanical response. Different strain rates may also be applied to analyze the role of the microstructure in viscous phenomena.

The choice of the reference strain state is of great importance for the data analysis as it conditions the strain levels reached during the knee flexion-extension. But in many cases presented in this study, various strain mechanisms have been observed for two phases of the knee movement delimited by the reference posture of the knee (zero-gravity posture of the knee), which is used as the zero-strain state of fascia lata. This reference position of the knee was chosen as the same for the three subjects, but it may be subjected to inter-subject variability. Further analysis of the strain mechanisms obtained using various reference strain states could help in defining an optimum reference strain state of the fascia lata for each subject and then to identify maximum strain levels during knee movement in a more personalized manner. It is therefore difficult at present to decide on a position of the knee

and hip that will result in a state of minimum strain of the fascia. Further *in situ* studies with more subjects would help to check if the changes in strain mechanisms correspond to a reference posture of the leg regarding the fascia lata strain-state.

For future *in situ* studies, inclusion criteria such as age, gender or body mass index could also be considered to perform an in-depth analysis of strain field based on the proposed methodology. Groups based on knee range of motion, or varus-valgus could also be studied, and the focus on a specific leg pathology or surgical practice could be considered. For instance, a surgical technique, at the knee level, that could benefit this work is the "pie-crusting" technique (Clarke et al., 2005; Nikolopoulos et al., 2015). Patients with varus or valgus knee may need this technique that consists of tissue release, and that can be done on ITT. Tissue release is done by inducing damage in the tissue, usually by making holes in it with a scalpel. The clinical question behind this technique is when to stop releasing the tissue. Thanks to our strain maps and optical motion capture system, strain release could be assessed as well as corresponding knee mobility and varus-valgus angle. Correlations observed experimentally could then be evaluated on patients during surgery.

A further example can be taken from hip surgery; the fascia is usually cut to get access to the joint. It is known that fascia lata participates in hip stability (Eng et al., 2014), therefore thanks to our proposed methodology and analysis, knowing the strain map of fascia around the hip may help in defining a hip position for minimal fascia strain, which could guide the surgeon for positioning patients in order to close fascia lata with minimal tension at the end of the procedure. For a defined hip position, we could evaluate the effect of incision on fascia strain release. Thanks to the obtained strain maps, insights on how hip position can affect strain release could be gathered, experiments could also be coupled with a numerical model of the leg that could reproduce fascia pre-strain on muscular tissue and reproduce both passive and active leg movement under physiological loadings, this last aspect will be challenging and require other experiments. To perform such tests related to surgical technique, possible issues regarding reproducibility in induced damage or incisions may occur. To limit this, these induced tears would need to be standardized using references to anatomical landmarks for the definition of scalpel incision location and size, and would need to be performed using the same technique carried out by the same operator for each subject. As done in the present study during knee flexion, the tracking of fascia lata strains before, during and after incisions using digital image correlation, would need to ensure an adequate field of view and good image quality along each step. Video recording could be done continuously, and knee movement performed before and after incision.

The methodology presented here is not an *in vivo* study; thus, both the contribution of the muscle activation and the effect of fat, superficial fascia and skin, on the deep fascia behavior are ignored. *In vivo* mechanical properties of fascia lata obtained using elastography have been reported (Otsuka et al., 2019) but such observations are still limited to a transversal section and small area of interest. Partial strain maps obtained *in situ* could be used as first validation data of passive numerical simulations.

To assess the effect of muscular activation on fascia strain field, which could then be implemented in leg numerical models, different approaches could be investigated. Firstly, using obtained strain maps *in situ*, specific areas of interest could be then studied *in vivo* using elastography measurements as proposed by Otsuka et al. (2019) and other electromyography measurements. We can also think of strain field acquisition on the skin, as proposed here on fascia. Various orientations should be studied, volunteers varying in gender, age groups and so on should be included, and medical imaging of their leg should be acquired in order to have an associated finite element model. Secondly, experiments following the same experimental protocol with the addition of muscular activation could be performed on animals. That kind of data is useful to develop and validate finite element models, but then the transition from animal data to application for human beings could be problematic due to difference in species, anatomy, or microstructures.

As a conclusion, this study presents some limitations but provides a step in understanding the strain mechanism of the fascia lata during knee movement. Further tests are planned to carry out the same analysis for various hip angles. The strain field measurement will also be applied to assess pre-strain and study strain release on different locations within fascia lata for clinical applications and for implementation in numerical models. More generally, the knowledge of the most released strain state of deep fascias could help surgeons when considering fascia closing after surgery or fascia release for surgical rehabilitations.

DATA AVAILABILITY STATEMENT

The datasets generated for this study are available on request to the corresponding author.

REFERENCES

- Barker, P. J., Briggs, C. A., and Bogeski, G. (2004). Tensile transmission across the lumbar fasciae in unembalmed cadavers: effects of tension to various muscular attachments. *Spine* 29, 129–138. doi: 10.1097/01.BRS.0000107005.62513.32
- Basser, P. J., Schneiderman, R., Bank, R. A., Wachtel, E., and Maroudas, A. (1998). Mechanical properties of the collagen network in human articular cartilage as measured by osmotic stress technique. *Arch. Biochem. Biophys.* 351, 207–219. doi: 10.1006/abbi.1997.0507
- Bennett, M. B., Ker, R. F., Imery, N. J., and Alexander, R. M. (1986). Mechanical properties of various mammalian tendons. *J. Zool.* 209, 537–548. doi: 10.1111/j.1469-7998.1986.tb03609.x
- Boisse, P., Hamila, N., Guzman-Maldonado, E., Madeo, A., Hivet, G., and dell'isola, F. (2017). The bias-extension test for the analysis of in-plane shear properties of textile composite reinforcements and preregs: a review. *Int. J. Mater. Form* 10, 473–492. doi: 10.1007/s12289-016-1294-7
- Butler, D. L., Grood, E. S., Noyes, F. R., Zernicke, R. F., and Brackett, K. (1984). Effects of structure and strain measurement technique on the material properties of young human tendons and fascia. *J. Biomech.* 17, 579–596. doi: 10.1016/0021-9290(84)90090-3
- Carse, B., Meadows, B., Bowers, R., and Rowe, P. (2013). Affordable clinical gait analysis: an assessment of the marker tracking accuracy of a new low-cost optical 3D motion analysis system. *Physiotherapy* 99, 347–351. doi: 10.1016/j.physio.2013.03.001
- Chèze, L., Moissenet, F., and Dumas, R. (2012). State of the art and current limits of musculo-skeletal models for clinical applications. Edited by Floren Colloud. *Mov. Sport Sci.* 90, 7–17. doi: 10.1051/sm/2012026
- Chimich, D., Shrive, N., Frank, C., Marchuk, L., and Bray, R. (1992). Water content alters viscoelastic behaviour of the normal adolescent rabbit medial collateral ligament. *J. Biomech.* 25, 831–837. doi: 10.1016/0021-9290(92)90223-N
- Clarke, H. D., Fuchs, R., Scuderi, G. R., Scott, W. N., and Insall, J. N. (2005). Clinical results in valgus total knee arthroplasty with the “pie crust” technique of lateral soft t releases. *J. Arthroplasty* 20, 1010–1014. doi: 10.1016/j.arth.2005.03.036
- Couppé, C., Hansen, P., Kongsgaard, M., Kovanen, V., Suetta, C., Aagaard, P., et al. (2009). Mechanical properties and collagen cross-linking of the patellar tendon in old and young men. *J. Appl. Physiol.* 107, 880–886. doi: 10.1152/jappphysiol.00291.2009
- Eichelberger, P., Ferraro, M., Minder, U., Denton, T., Blasimann, A., Krause, F., et al. (2016). Analysis of accuracy in optical motion capture – A protocol for laboratory setup evaluation. *J. Biomech.* 49, 2085–2088. doi: 10.1016/j.jbiomech.2016.05.007
- Eng, C. M., Pancheri, F. Q., Lieberman, D. E., Biewener, A. A., and Dorfmann, L. (2014). Directional differences in the biaxial material properties of fascia lata and the implications for fascia function. *Ann. Biomed. Eng.* 42, 1224–1237. doi: 10.1007/s10439-014-0999-993
- Eng, C. M., and Roberts, T. J. (2018). Aponeurosis influences the relationship between muscle gearing and force. *J. Appl. Physiol.* 125, 513–519. doi: 10.1152/jappphysiol.00151.2018

ETHICS STATEMENT

Ethics approval was not required for this study since it is not required by French law. Mortal remains were obtained after the deceased gave their informed consent to donate them to science during their lifetime (law article R2213-13). The authors ensure that these experiments were performed with respect for these remains, and in proper health and safety conditions.

AUTHOR CONTRIBUTIONS

All authors contributed to the conception and design of the study, manuscript revision, read, and approved the submitted version. YS, AN, and KB-G performed the experiments and collected and treated raw data (digital image correlation and motion analysis). YS, AV, KB-G, and L-LG analyzed and discussed the data. YS, KB-G, and L-LG wrote the first draft of the manuscript.

FUNDING

This work was funded by the French institute of science and technology for transport, development and networks and the University Claude Bernard, Lyon.

ACKNOWLEDGMENTS

The authors thank Leïla Ben Boubaker for her precious help in carrying out the tests and Richard Roussillon and Stéphane Ardizzone for their technical support. They also thank Julia Greenfield for her careful proofreading of this manuscript.

- Fairclough, J., Hayashi, K., Toumi, H., Lyons, K., Bydder, G., Phillips, N., et al. (2006). The functional anatomy of the iliotibial band during flexion and extension of the knee: implications for understanding iliotibial band syndrome. *J. Anat.* 208, 309–316. doi: 10.1111/j.1469-7580.2006.00531.x
- Findley, T., Chaudhry, H., and Dhar, S. (2015). Transmission of muscle force to fascia during exercise. *J. Bodywork Mov. Ther.* 19, 119–123. doi: 10.1016/j.jbmt.2014.08.010
- Garfin, S. R., Tipton, C. M., Mubarak, S. J., Woo, S. L., Hargens, A. R., and Akeson, W. H. (1981). Role of fascia in maintenance of muscle tension and pressure. *J. Appl. Physiol.* 51, 317–320. doi: 10.1152/jap.1981.51.2.317
- Gratz, C. (1931). Tensile strength and elasticity tests on human fascia lata. *J. Bone Joint Surg.* 13, 334–340.
- Guilbert, M., Roig, B., Terryn, C., Garnotel, R., Jeannesson, P., Sockalingum, G. D., et al. (2016). Highlighting the impact of aging on type I collagen: label-free investigation using confocal reflectance microscopy and diffuse reflectance spectroscopy in 3D matrix model. *Oncotarget* 7, 8546–8555. doi: 10.18632/oncotarget.7385
- Hammer, N., Huster, D., Boldt, A., Hädrich, C., Koch, H., Möbius, R., et al. (2016). A preliminary technical study on sodium dodecyl sulfate-induced changes of the nano-structural and macro-mechanical properties in human iliotibial tract specimens. *J. Mech. Behav. Biomed. Mater.* 61, 164–173. doi: 10.1016/j.jmbmb.2016.01.018
- Hammer, N., Huster, D., Fritsch, S., Hädrich, C., Koch, H., Schmidt, P., et al. (2014). Do cells contribute to tendon and ligament biomechanics? *PLoS One* 9:e105037. doi: 10.1371/journal.pone.0105037
- Hammer, N., Lingslebe, U., Aust, G., Milani, T., Hädrich, C., and Steinke, H. (2012). Ultimate stress and age-dependent deformation characteristics of the iliotibial tract. *J. Mech. Behav. Biomed. Mater.* 16, 81–86. doi: 10.1016/j.jmbmb.2012.04.025
- Henderson, E. R., Friend, E. J., Toscano, M. J., Parsons, K. J., and Tarlton, J. F. (2015). Biomechanical comparison of canine fascia lata and thoracolumbar fascia: an in vitro evaluation of replacement ts for body wall reconstruction. *Vet. Surg.* 44, 126–134. doi: 10.1111/j.1532-950X.2014.12247.x
- Huang, B. K., Campos, J. C., Peschka, P. G. M., Pretterklieber, M. L., Skaf, A. Y., Chung, C. B., et al. (2013). Injury of the gluteal aponeurotic fascia and proximal iliotibial band: anatomy, pathologic conditions, and MR imaging. *Radiographics* 33, 1437–1452. doi: 10.1148/rg.335125171
- Huijing, P. A. (2009). Epimuscular myofascial force transmission: a historical review and implications for new research. International society of biomechanics mybridge award lecture, Taipei, 2007. *J. Biomech.* 42, 9–21. doi: 10.1016/j.jbiomech.2008.09.027
- Jayyosi, C., Coret, M., and Bruyère-Garnier, K. (2016). Characterizing liver capsule microstructure via in situ bulge test coupled with multiphoton imaging. *J. Mech. Behav. Biomed. Mater.* 54, 229–243. doi: 10.1016/j.jmbmb.2015.09.031
- Jayyosi, C., Fargier, G., Coret, M., and Bruyère-Garnier, K. (2014). Photobleaching as a tool to measure the local strain field in fibrous membranes of connective ts. *Acta Biomater.* 10, 2591–2601. doi: 10.1016/j.actbio.2014.02.031
- Krasny, W., Magoarić, H., Morin, C., and Avril, S. (2018). Kinematics of collagen fibers in carotid arteries under tension-inflation loading. *J. Mech. Behav. Biomed. Mater.* 77, 718–726. doi: 10.1016/j.jmbmb.2017.08.014
- Lynch, B., Bonod-Bidaud, C., Ducourthial, G., Affagard, J.-S., Bancelin, S., Psilodimitrakopoulos, S., et al. (2017). How aging impacts skin biomechanics: a multiscale study in mice. *Sci. Rep.* 7, 1–10. doi: 10.1038/s41598-017-13150-13154
- Masic, A., Bertinetti, L., Schuetz, R., Chang, S. W., Metzger, T. H., Buehler, M. J., et al. (2015). Osmotic pressure induced tensile forces in tendon collagen. *Nat. Commun.* 6:5942. doi: 10.1038/ncomms6942
- Mentiplay, B. F., Banky, M., Clark, R. A., Kahn, M. B., and Williams, G. (2018). Lower limb angular velocity during walking at various speeds. *Gait Posture* 65, 190–96. doi: 10.1016/j.gaitpost.2018.06.162
- Moissenet, F., Chêze, L., and Dmas, R. (2014). A 3D lower limb musculoskeletal model for simultaneous estimation of musculo-tendon, joint contact, ligament and bone forces during gait. *J. Biomech.* 47, 50–58. doi: 10.1016/j.jbiomech.2013.10.015
- Mount, F. E., Whitmore, M., and Stealey, S. L. (2003). *Evaluation of Neutral Body Posture on Shuttle Mission STS-57 (SPACEHAB-1)*. Available online at: <https://ntrs.nasa.gov/search.jsp?R=20040200967> (accessed May 20, 2020).
- Muscaritoli, M., Anker, S. D., Argilès, J., Aversa, Z., Bauer, J. M., Biolo, G., et al. (2010). Consensus definition of sarcopenia, cachexia and pre-cachexia: joint document elaborated by Special Interest Groups (SIG) “cachexia-anorexia in chronic wasting diseases” and “nutrition in geriatrics”. *Clin. Nutr.* 29, 154–159. doi: 10.1016/j.clnu.2009.12.004
- Nau, T., Menth-Chiari, W. A., Seitz, H., and Vécsei, V. (2000). Acute compartment syndrome of the thigh associated with exercise. *Am. J. Sports Med.* 28, 120–122. doi: 10.1177/03635465000280010601
- Nikolopoulos, D., Michos, I., Safos, G., and Safos, P. (2015). Current surgical strategies for total arthroplasty in valgus knee. *World J. Orthop.* 6:469. doi: 10.5312/wjo.v6.i6.469
- Nishimura, T., Hattori, A., and Takahashi, K. (1996). Relationship between degradation of proteoglycans and weakening of the intramuscular connective t during post-mortem ageing of beef. *Meat Sci.* 42, 251–260. doi: 10.1016/0309-1740(95)00051-8
- Osakabe, T., Hayashi, M., Hasegawa, K., Okuaki, T., Ritty, T. M., Mecham, R. P., et al. (2001). Age- and gender-related changes in ligament components. *Ann. Clin. Biochem.* 38, 527–532. doi: 10.1177/000456320103800510
- Otsuka, S., Shan, X., and Kawakami, Y. (2019). Dependence of muscle and deep fascia stiffness on the contraction levels of the quadriceps: an in vivo supersonic shear-imaging study. *J. Electromyogr. Kinesiol.* 45, 33–40. doi: 10.1016/j.jelekin.2019.02.003
- Otsuka, S., Yakura, T., Ohmichi, Y., Ohmichi, M., Naito, M., Nakano, T., et al. (2018). Site specificity of mechanical and structural properties of human fascia lata and their gender differences: a cadaveric study. *J. Biomech.* 77, 69–75. doi: 10.1016/j.jbiomech.2018.06.018
- Pancheri, F. Q., Eng, C. M., Lieberman, D. E., Biewener, A. A., and Dorfmann, L. (2014). A constitutive description of the anisotropic response of the fascia lata. *J. Mech. Behav. Biomed. Mater.* 30, 306–323. doi: 10.1016/j.jmbmb.2013.12.002
- Pavan, P. G., Pachera, P., Stecco, C., and Natali, A. N. (2015). Biomechanical behavior of human crural fascia in anterior and posterior regions of the lower limb. *Med. Biol. Eng. Comput.* 53, 951–959. doi: 10.1007/s11517-015-1308-1305
- Podwojewski, F., Otténio, M., Beillas, P., Guérin, G., Turquier, F., and Mitton, D. (2013). Mechanical response of animal abdominal walls in vitro: evaluation of the influence of a hernia defect and a repair with a mesh implanted intraperitoneally. *J. Biomech.* 46, 561–566. doi: 10.1016/j.jbiomech.2012.09.014
- Podwojewski, F., Otténio, M., Beillas, P., Guérin, G., Turquier, F., and Mitton, D. (2014). Mechanical response of human abdominal walls ex vivo: effect of an incisional hernia and a mesh repair. *J. Mech. Behav. Biomed. Mater.* 38, 126–133. doi: 10.1016/j.jmbmb.2014.07.002
- Ruiz-Alejos, D., Peña, J. A., Pérez, M. M., and Peña, E. (2016). experiments and constitutive model for deep and superficial fascia. Digital image correlation and finite element validation: experiments and constitutive model for deep and superficial fascia. *Strain* 52, 436–445. doi: 10.1111/str.12198
- Schleip, R., Duerksen, L., Vleeming, A., Naylor, I. L., Lehmann-Horn, F., Zorn, A., et al. (2012). Strain hardening of fascia: static stretching of dense fibrous connective ts can induce a temporary stiffness increase accompanied by enhanced matrix hydration. *J. Bodywork Mov. Ther.* 16, 94–100. doi: 10.1016/j.jbmt.2011.09.003
- Snoeck, O., Beyer, B., Feipel, V., Salvia, P., Sterckx, J.-L., Rooze, M., et al. (2014). Tendon and fascial structure contributions to knee muscle excursions and knee joint displacement. *Clin. Biomech.* 29, 1070–1076. doi: 10.1016/j.clinbiomech.2014.08.003
- Stahl, V. A. (2010). *A Biomechanical Analysis of the Role of the Crural Fascia in the Cat Hindlimb*. Available online at: <https://smartech.gatech.edu/handle/1853/34701> (accessed May 20, 2020).
- Stecco, C., Macchi, V., Porzionato, A., Duparc, F., and De Caro, R. (2011). The fascia: the forgotten structure. *Ital. J. Anat. Embryol.* 116, 127–138. doi: 10.13128/IJAE-10683
- Stecco, C., Pavan, P., Pachera, P., De Caro, R., and Natali, A. (2014). Investigation of the mechanical properties of the human crural fascia and their possible clinical implications. *Surg. Radiol. Anat.* 36, 25–32. doi: 10.1007/s00276-013-1152-y
- Steinke, H., Lingslebe, U., Böhme, J., Slowik, V., Shim, V., Hädrich, C., et al. (2012). Deformation behavior of the iliotibial tract under different states of fixation. *Med. Eng. Phys.* 34, 1221–1227. doi: 10.1016/j.medengphys.2011.12.009

- Stelletta, J., Dumas, R., and Lafon, Y. (2016). "Muscle interactions influence the muscular forces," in *Proceedings of the 22nd Congress of the European Society of Biomechanics*, Lyon.
- Stelletta, J., Dumas, R., and Lafon, Y. (2017). "Chapter 23: modeling of the thigh: a 3d deformable approach considering muscle interactions," in *Biomechanics of Living Organs: Hyperelastic Constitutive Laws for Finite Element Modeling*, eds Y. Payan and J. Ohayon (Cambridge, MA: Academic Press). Available online at: <https://www.sciencedirect.com/book/9780128040096/biomechanics-of-living-organs#book-description>
- Thornton, G. M., Shrive, N. G., and Frank, C. B. (2001). Altering ligament water content affects ligament pre-stress and creep behaviour. *J. Orthop. Res.* 19, 845–851. doi: 10.1016/S0736-0266(01)00005-5
- Tournadre, A., Vial, G., Capel, F., Soubrier, M., and Boirie, Y. (2019). Sarcopenia. *Joint Bone Spine* 86, 309–314. doi: 10.1016/j.jbspin.2018.08.001
- Tuttle, L. J., Alperin, M., and Lieber, R. L. (2014). Post-mortem timing of skeletal muscle biochemical and mechanical degradation. *J. Biomech.* 47, 1506–1509. doi: 10.1016/j.jbiomech.2014.02.019
- Vieira, E. L., Vieira, E. A., da Silva, R. T., Berlfein, P. A., Abdalla, R. J., and Cohen, M. (2007). An anatomic study of the iliotibial tract. *Arthroscopy* 23, 269–274. doi: 10.1016/j.arthro.2006.11.019
- Wang, C., Shankar, K., Morozov, E., Ramakrishnan, K. R., and Fien, A. (2020). Characterization of shear behavior in stainless steel wire mesh using bias-extension and picture frame tests. *J. Eng. Mech.* 146:2.
- Westman, A. M., Dyer, S. E., Remer, J. D., Hu, X., Christ, G. J., and Blemker, S. S. (2019). A coupled framework of in situ and in silico analysis reveals the role of lateral force transmission in force production in tricep muscle loss injuries. *J. Biomech.* 85, 118–125. doi: 10.1016/j.jbiomech.2019.01.025
- Wilke, J., Macchi, V., De Caro, R., and Stecco, C. (2019). Fascia thickness, aging and flexibility: is there an association? *J. Anat.* 234, 43–49. doi: 10.1111/joa.12902
- Wu, G., Siegler, S., Allard, P., Kirtley, C., Leardini, A., Rosenbaum, D., et al. (2002). ISB recommendation on definitions of joint coordinate system of various joints for the reporting of human joint motion—part I: ankle, hip, and spine. *J. Biomech.* 35, 543–548. doi: 10.1016/S0021-9290(01)00222-226
- Zwirner, J., Babian, C., Ondruschka, B., Schleifenbaum, S., Scholze, M., Waddell, N. J., et al. (2019). Tensile properties of the human iliotibial tract depend on height and weight. *Med. Eng. Phys.* 69, 85–91. doi: 10.1016/j.medengphy.2019.05.001

Conflict of Interest: The authors declare that the research was conducted in the absence of any commercial or financial relationships that could be construed as a potential conflict of interest.

Copyright © 2020 Sedniewa, Viste, Naaim, Bruyère-Garnier and Gras. This is an open-access article distributed under the terms of the Creative Commons Attribution License (CC BY). The use, distribution or reproduction in other forums is permitted, provided the original author(s) and the copyright owner(s) are credited and that the original publication in this journal is cited, in accordance with accepted academic practice. No use, distribution or reproduction is permitted which does not comply with these terms.

CHAPTER III

MECHANICAL PROPERTIES OF FASCIA DURING A SHEAR LOADING

3.1. Introduction

As for other fibrous soft connective tissues, fascia is composed of elastin and collagen fibers. Collagen is the main component that resists tension. Elastin recoils after the stretching as soon as the force is removed. The combination of fiber networks is responsible for the non-linear and anisotropic behavior of the fascia. Therefore, the structure of fibrous tissue determines its response to the mechanical stress.

The tests available in the literature (uniaxial and bi-axial tensile tests) are not covering the shear loadings affecting the fascia lata; however, they are present *in vivo*, as fascia lata is connected to the surrounding tissues and structures (Otsuka et al. 2021). We also identified this strain mechanism in the *in situ* study, where principal strains were almost equal in absolute value and directed along the bisector of the collagen networks during knee flexion-extension. Yet, the characterization of fascia mechanical properties on samples is mainly done under uniaxial tension. To the best of our knowledge, the only attempt to propose the characterization of fascia lata during shear loading was made by Ruiz-Alejos et al. (2016), where they performed pure shear tests (large band tests) on sheep fascia lata. This consists in performing a uniaxial tensile test but on a large band of tissue to obtain a shear mechanism in the middle of the sample. However, tension was applied along the longitudinal and transverse fibers directions, but not along the bisector of fiber networks.

Therefore, the objective of this chapter is to present shear tests to characterize fascia mechanical properties as this is the strain mechanism highlighted with *in situ* tests. Two types of planar shear tests were performed: bias extension and large band tests, with the stretch applied along the bisector of two main fibers networks (longitudinal and transverse) in agreement with the results obtained during the *in situ* study from Sednieva et al. (2020). Bias extension test was inspired by the usual characterization methodology applied on fabrics used for composite materials (Boisse et al. 2017), and one aim was to check the bias extension tests hypotheses: about the sliding of two main fiber networks that are on two specific layers and about the extension of the fibers during the test. For both types of tests, a specific attention was also paid to the fibers' kinematics during the loading.

3.2. Materials and Methods

3.2.1. Specimen Preparation

The samples of fascia lata were taken from four female post mortem human subjects (PMHS) (numbers: 2017_124, 2019_308, 2021_107, 2021_133), obtained from the Department of Anatomy of the University of Rockefeller (DAUR), Lyon, France. After the dissection of fascia lata (anterior, lateral, and posterior sides of the thigh), identification of anterior, posterior, distal

and proximal sites as well as external and internal sides of fascia lata were made with a ligature at the anterior-proximal site. The samples of whole fascia were wrapped with a tissue soaked in saline solution, and kept at $-20\text{ }^{\circ}\text{C}$. A day before the preparation of testing, samples were kept in the fridge at a temperature of $4\text{ }^{\circ}\text{C}$.

Before cutting the fascia lata into samples, it was cleaned from remaining adipose and muscle tissue. The testing samples were located in accordance with the directions of the major principal strain measured during the first study (Sednieva et al. 2020) and fibers directions, so the load was applied along the bisector between the two fiber's networks (*Figure 3.2-1*).

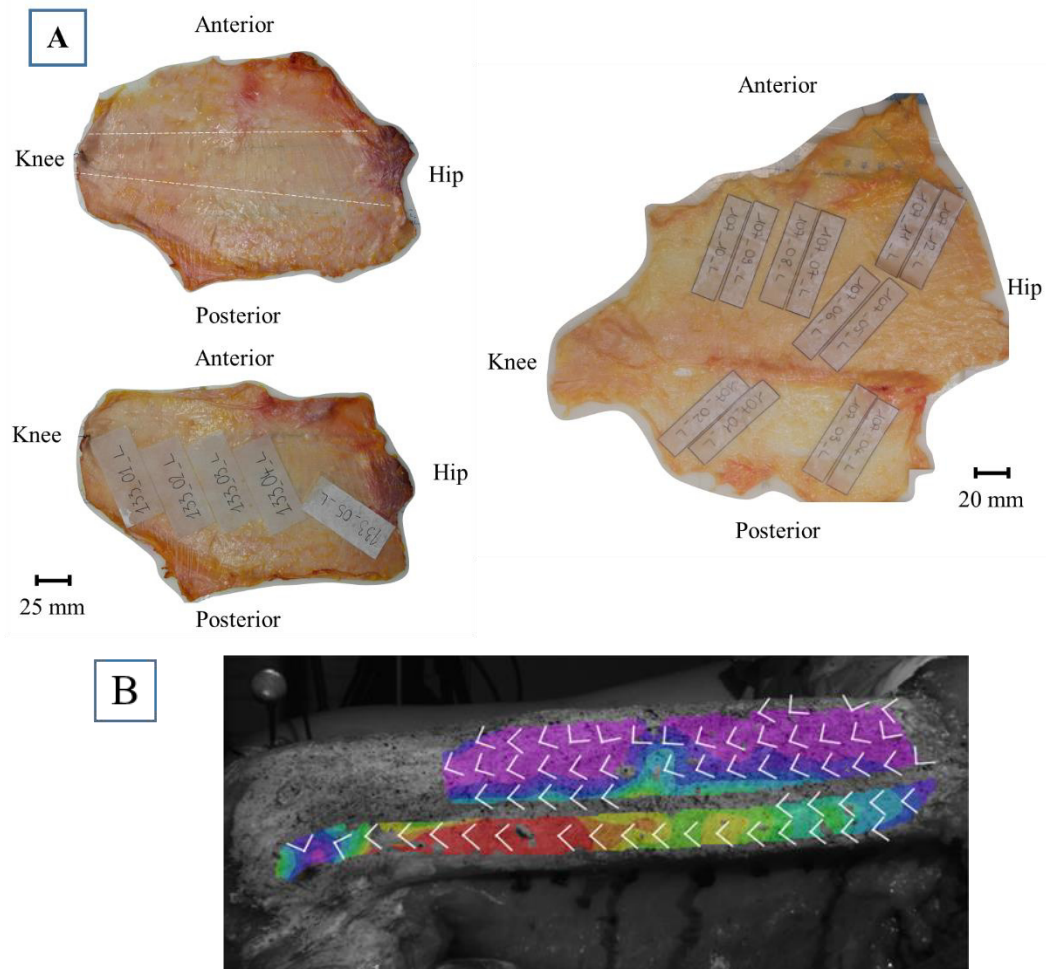


Figure 3.2-1. (A) Example of samples location for large band (on the left) and bias tests (on the right) respectively on internal and external sides of the fascia lata harvested from the corresponding left leg of subjects 2021_133 and 2021_107. (B) Minor and major principal strain directions on the external surface of fascia lata measured in Sednieva et al. (2020).

As the experiment was carried out the next day after samples preparation, they were kept with tissue soaked with saline solution in the fridge at 4°C during the night, and were removed in the morning in order to be at ambient temperature for the testing.

The thickness of each sample was measured with a caliper, when placed between two glasses of known thickness. The cross-sectional area of each sample was assumed constant along the sample length. Width of the sample was considered as equal to the width of the cut.

3.2.1.1. Bias test specimen preparation

For the bias tests, twelve rectangular samples were cut with a scalpel from each fascia lata (*Figure 3.2-1*). There were several sizes of samples depending on their location on the fascia lata and the visibility of the fibers network: 20 x 80 mm and 15 x 60 mm (*Figure 3.2-2*). Larger size was chosen for the thin fascia (anterior, posterior sites), and smaller for the thicker samples (ITT), although, some thick samples were taken with dimensions for thin samples. These twelve samples were cut into pairs to have two contiguous samples, one of which will be tested for the analysis of the kinematics of the fibers and the other one for the strain fields' measurements.

These sample sizes were chosen to ensure the area of interest was at least twice as long as wide, and thus avoid fibers to be attached in both grips, as this would no longer comply with the bias test framework. The useful length of the samples once placed in the jaws is reduced on average to 40-50 mm (*Figure 3.2-2*), which always verifies the condition of the bias test.

On each sample, a mark was made with a red pen to identify the external and distal site of the fascia lata in order to place all the samples the same way for the test.

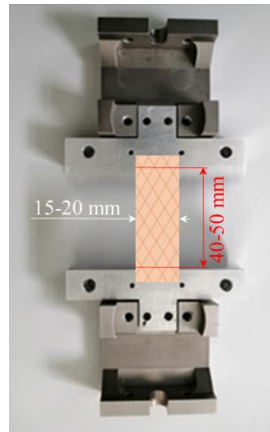


Figure 3.2-2. Representation of the testing sample of fascia lata for a bias test with the identification of its dimensions.

3.2.1.2. Large band specimen preparation

Five samples were taken from each fascia lata including the area of the ITT numbered from 01 to 05 (*Figure 3.2-1*) with at least two pairs of contiguous samples, one of which will be tested for fiber kinematics analysis and the other one for strain field measurement. The large band assembly makes possible to test a sample whose width is very large compared to the length. Therefore, the size of each sample was 30 mm x 70 mm (*Figure 3.2-3*). Nevertheless, after specimen placement into the jaws, the initial width of the sample reduced by around 15 mm.

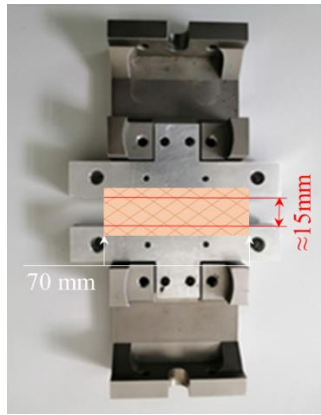


Figure 3.2-3. Representation of the testing sample of fascia lata for a large band test with the identification of its dimensions.

3.2.1.3. Specimen preparation for a bi-photon microscopy

In view of connecting the microstructure of the tissue to the strain results and fiber kinematics from the sample tests, in further work, first observation using bi-photon microscopy were planned. The sample for the microscopy was taken as a band of 5 mm width between the samples (from the right leg of the subject 2021_107) taken on the ITT for the bias test. The measured thickness was 0.8 mm. It was kept at -20°C . On testing day, it was thawed at the room temperature and was kept hydrated in saline solution. Because of the availability of the microscope, only preliminary results will be presented at this stage.

3.2.2. Testing procedures

3.2.2.1. Mechanical test setup

All the tests were carried out on an INSTRON 8802 traction machine (High Wycombe, England), and using a static force S-shape sensor with a capacity of 250 N and 50 N for the large band and bias tests respectively, placed directly on the machine base to avoid the dynamic effects due to the movements of the upper jaw (Figure 3.2-4). The acquisition frequency of the machine was 1000 Hz. The INSTRON machine directly recorded the uniaxial force and the actuator displacement.



Figure 3.2-4. The configurations of the loading cell on the INSTRON machine (on the left) and the fixture (on the right) for the bias and large band tests.

The fixtures for holding the sample were manufactured for the LBMC (*Figure 3.2-4*). All the jaws were covered with emery cloth to prevent the sample from slipping during testing.

For both types of tensile tests, the sample was placed into the upper jaw keeping attention to the position of each sample regarding of the fascia site, so it was always positioned the same way. Then, loading cell was tared when the sample was hanging in the superior jaw. The sample was then fixed in the lower jaw in a vertical position (with the gravity applied to the sample in the opposite direction of pulling). At this stage an image of the sample was taken as the reference image for strain field measurement (see strain field measurement paragraph). After clamping in the lower grip, the initial length between the jaws was measured with a caliper.

3.2.2.2. *Video setup*

To observe the samples surfaces in view of measuring displacement and strain fields by Digital Image Correlation (DIC) or stereo-digital image correlation, or to observe the fibers directions by transparency, Photron SA3 black and white cameras (Tokyo, Japan) with Sigma Macro f/2.8 105 mm objective were used. To synchronize the measurements of load and actuator displacement with the data computed from images, a TTL signal with 5 V magnitude was sent to start video recordings and recorded with other measurements. LED spots provided the lighting.

3.2.2.3. *Loading conditions*

Bias tests were carried out until the rupture of the sample at 25 mm/min speed, i.e. a strain rate of around 0.08 s^{-1} . For the large band tests, 10 tensile cycles were carried out up to an imposed machine strain of 20 % with a displacement speed of 100 mm/min, i.e. an apparent strain rate of around 0.11 s^{-1} .

3.2.3. Strain field measurements

3.2.3.1. *Bias test*

In order to check the layers gliding theory of observed fascia lata's layers, the images of the tests were recorded for both internal and external sides of the fascia lata samples in 2D as the deformations of the fascia remain in the same plane.

White clown makeup with a black speckle was applied on both (external and internal) surfaces of the specimen in order to make simultaneous records from both sides. The white makeup was created to even out the background, and a random black dot pattern (speckles) was created using black spray paint (*Figure 3.2-5*). The speckle must be non-periodic, isotropic and well contrasted.

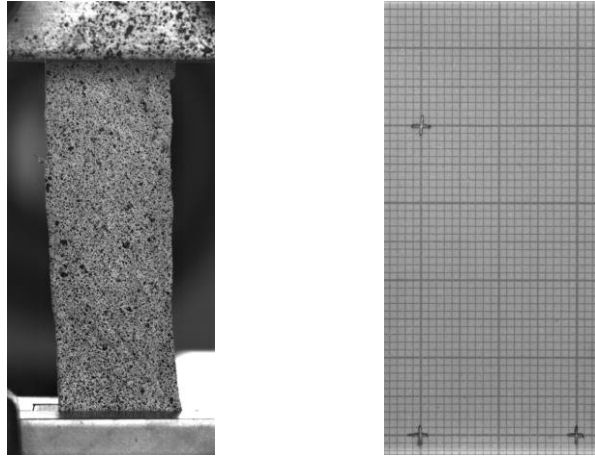


Figure 3.2-5. Example of speckle applied on the surface of fascia lata sample for the bias test (on the left) and the calibration grid for a 2D calibration (on the right).

After, the sample was placed into the upper jaw, the setup was mounted on the testing machine and we took a reference image (zero strain state). The taring was made and the lower part of the sample was clamped to the lower jaws.

The 2D surfacic strains measurement was made using digital image correlation (DIC) VIC-2D 6 software (Correlated Solution ®). Calibration was made by taking images of a graph paper sheet, an example of which is given on the *Figure 3.2-5*.

The images recorded with Photron FASTCAM Viewer Software were post processed with the VIC-2D software in the selected areas of interest (AOI). Fields of displacements and deformations were then obtained on the correlated zones. We were particularly interested in the principal deformations of Green-Lagrange E_1 (major principal strain), E_2 (minor principal strain), and the maximum shear strain calculated as a half of the difference between major and minor strains. Further post processing and representation of the results were done using custom-made Python scripts.

3.2.3.2. Large band test

The images of the tests were recorded for one (internal) side of the fascia lata samples lightened by square spots on tripods. The same two fast-speed cameras with described objectives were recording the changes on the fascia lata surface, but this time in 3D.

Speckles were applied only on the recorded surface (*Figure 3.2-6*) using the same technique as described in the section 3.2.3.1. The mounting of the sample was also the same as during bias test. The reference image is then an image for which the sample is in a state of deformation considered to be zero. 3D correlation of the images was made using VIC-3D 8.

Before assembling the setup with the sample, calibration of cameras was made, where the calibration grid was chosen due to the size of the area of interest: 14 x 10 – 5 mm.

All the following steps were the same as for the bias tests.

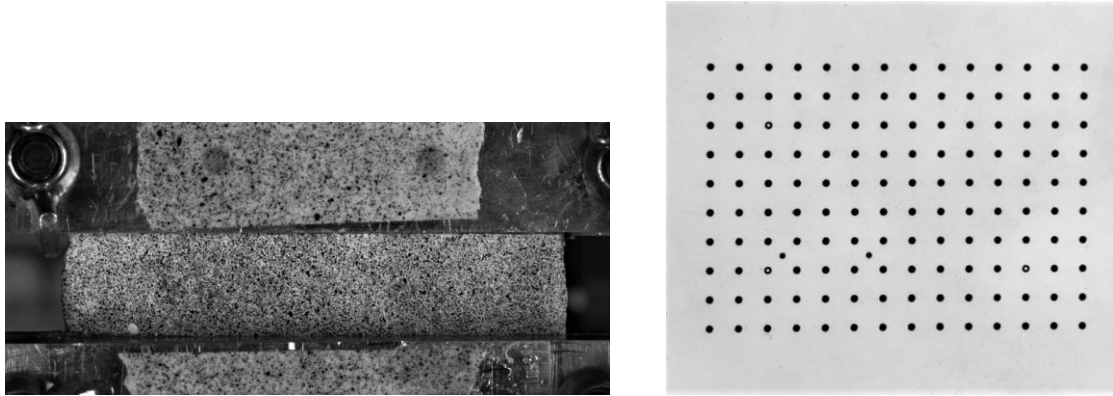


Figure 3.2-6. Example of speckle applied on the surface of fascia lata sample for the large band test (on the left) and the calibration grid for a 3D calibration (on the right).

3.2.4. Fibers kinematics

For the part of the samples dedicated to the fiber kinematics analysis, the orientations of fibers were recorded at 25 Hz using the transparency of the sample, with LED lights placed behind the sample (Figure 3.2-7). The position of the light, the diaphragm aperture of the cameras and the shutter time of the cameras were chosen to obtain clear and contrasted images over its entire surface, with the smallest possible field of view to optimize the resolution (1024 x 1024 px) while ensuring that the sample is fully visible during the entire test.



Figure 3.2-7. Example of an image (0% strain) obtained for the observation of fibers for the large band test (left) (sample 133_L_03) and bias test (right) (front face of sample 107_L_07).

The images were post processed with the Fiji image processing software (National Institutes of Health) and in particular via the Directionality plug-in to identify the fibers orientations and their angles during the loadings. This plug-in allows detecting fibers and plotting the histogram of fiber amounts against chosen orientations.

Only the images corresponding to the tensile strain states of 0% and 10%, which corresponds to the minimum and maximum locally measured strains, for the first three cycles were analyzed.

Due to the contrast of the obtained images, the simultaneous detection of both fiber directions by the Directionality plug-in was not always possible. Therefore, we used shading, perpendicularly to the fibers in order to enhance them (*Figure 3.2-8*).

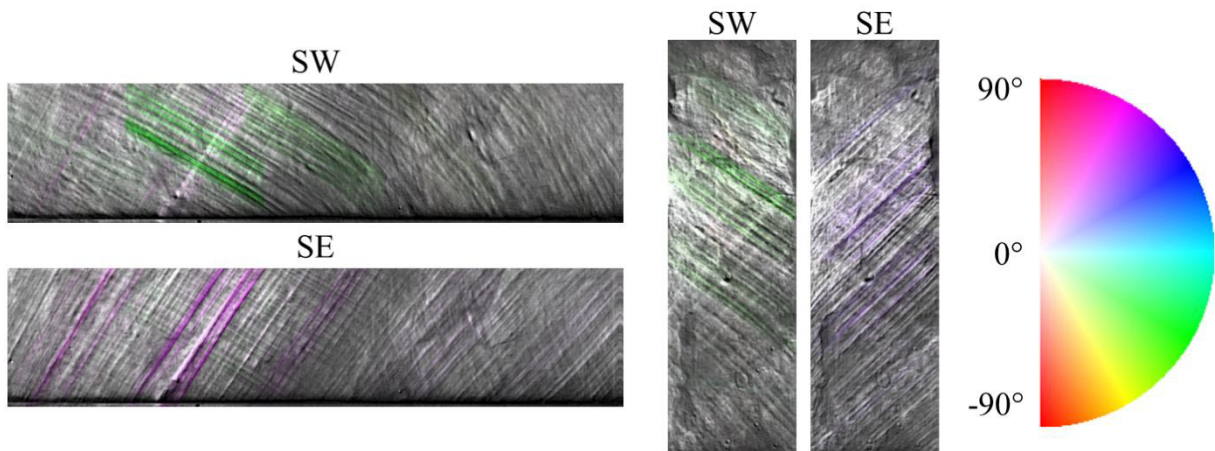


Figure 3.2-8. Examples of the colored detected fibers perpendicular to the shading (SW – South-West, SE – South-East) for the large band test (on the left) (sample 133_L_03) and bias test (on the right) (front face of sample 107_L_07) with color gradient scale for fiber detection.

Directionality plug-in gives the angular distribution of fibers detected on each image. The distribution from the two differently shaded images were combined by keeping the maximum value between them and then the two peaks of the combined distribution were corresponding to the two preferred orientations (*Figure 3.2-9*).

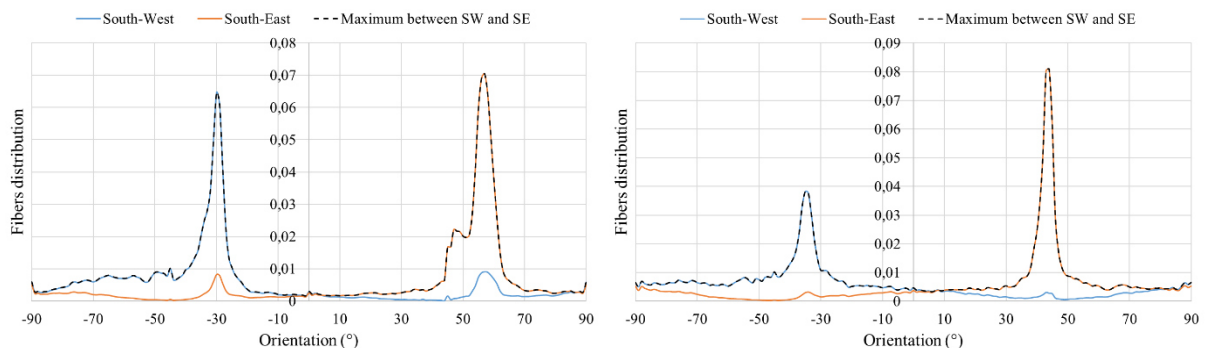


Figure 3.2-9. Example of the histograms for the two types of shading (South-West and South-East) associated with longitudinal and transverse fiber directions with the curve of the maximum values between the two shadows. The results of the left are from the large band test (sample 133_L_03) and on the right – from the bias test (front face of sample 107_L_07) at 0% stretch.

Further, the identification of the shadows will be omitted, and instead, the fiber networks, longitudinal and transverse, will be mentioned. For some samples, we were not able to determine the both fiber networks, and thus direction for only one of them will be presented.

3.2.5. Bi-photon microscopy

In order to obtain some three-dimensional images of the fascia lata's microstructure showing both elastin and collagen, we used Zeiss LSM 880 laser scanning two-photon confocal microscope at the CIQLE ("Centre d'Imagerie Quantitative Lyon-Est") at Rockefeller site,

Lyon. The sample was placed into Nunc® Lab-Tek® Chamber Slide™ system 2-well format, and then all the set up was put under the microscope. Excitation wave length was set to 890 nm and light from elastin fluorescence and collagen SHG signals was collected via filters of 583 nm and 445 nm wavelengths, respectively.

The images obtained by this microscopy are in the form of a stack of 360 μm consisting of 214 layers, with a Z-step of 1.68 μm . Image located at the level #156 found to be closest to the outer surface of the fascia lata. The size of the image was 354 x 354 μm^2 for one recorded zone and scan speed was set to 5 seconds per image with a resolution of 0.35 μm per pixel.

3.3. Results

3.3.1. Mechanical behavior

The nominal stress $\sigma_{nominal}$ is calculated from the data recorded by the tensile machine as:

$$\sigma_{nominal} = \frac{F [N]}{w [mm] \cdot L_0 [mm]},$$

where F is a force, w and L are respectively the thickness and the initial length of the sample. The global strain is given by:

$$\varepsilon = \frac{\Delta L [mm]}{L_0 [mm]},$$

where ΔL is the change in length.

For both tests, the global deformation (or machine strain) of the sample computed using the actuator displacement is almost twice greater than the calculated local strains computed by DIC, due to the set-up low stiffness and possible sliding of the sample (*Figure 3.3-1* and *Figure 3.3-4*).

3.3.1.1. Bias test

The non-linear curve is representing the behavior of the sample before the rupture, occurring around 10% local strain (*Figure 3.3-1*). This strain will be considered as the maximum deformation state for further presentation of the results.

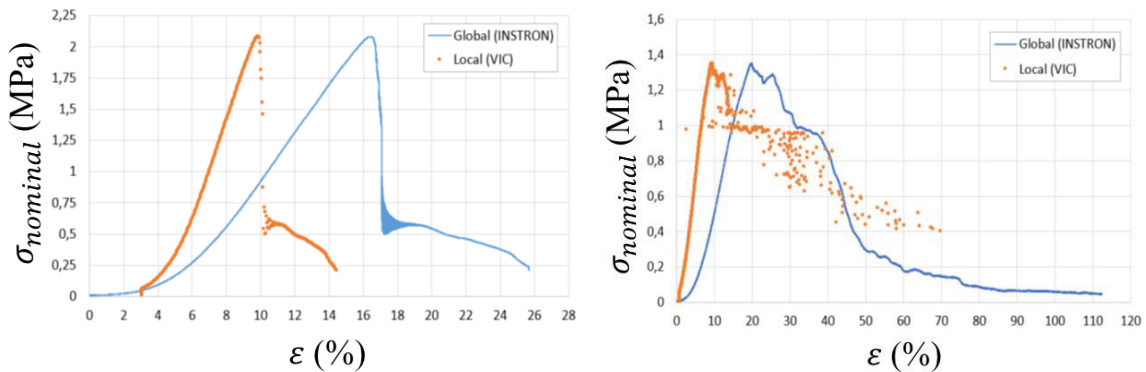


Figure 3.3-1. Nominal stress versus global and local strain curves for samples 107_L_06 (left) and 107_L_08 (right).

The images of the correlations for samples 107_L_06 and 107_L_07 for both, internal and external surfaces, on the *Figure 3.3-2* are corresponding to 10% local strain. On the principal strain distribution surfaces, the orientation of corresponding strain is shown with white arrows, on the maximum shear maps, both directions are plotted. For both samples the direction of the E_1 strain is aligned with the direction of traction and thus with the bisector of the two fiber networks. A square area R0 in the center of the sample was created in order to show an average value of each strain for both faces of the sample. For example, at 10% stretch, measured maximal and minimal strains in the R0 area of the sample 107_L_06 are respectively 10.1% and -25% on the front face, and 11.8% and -24.5% on the back face; for sample 107_L_08, they are 11.8% and -28.9% on the front face, and 13.2% and -31.8% on the back face. The maximum shear strain $maxE_{xy}$ shows a maximal value (in red) in a central zone for all samples.

When comparing the faces within the same sample, we observe strain distributions and strain values are not identical, even if quite close. Therefore, we can think that the layers of fascia lata are gliding in-between themselves or that the strain difference is related to the rotation of the fibers under shear. The strain values and even their distribution may be also explained by different thicknesses of the layers; however, they were not measured during this study.

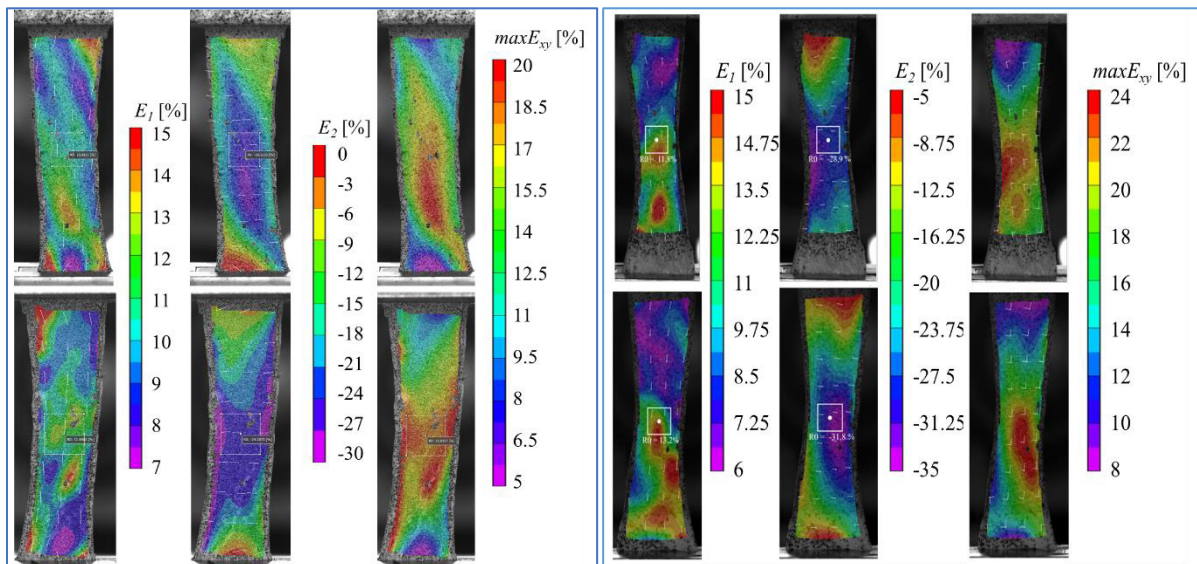


Figure 3.3-2. Strain field on the front (top) and back faces (bottom) of 107_L_06 (left) and 107_L_08 (right) samples at 10% deformation. The white arrows represent the main deformation directions. Square area in the middle of the sample named R0 shows the average value of corresponding strain.

Sample 308_L_03 strains distributions (*Figure 3.3-3*) show same mechanisms of strain, but the distribution of maximal shear strain on the front face of the sample can be fitted into a ‘diamond shape’, which is observed when testing a woven composite (Boisse et al. 2017). However, on the back face this shape is distorted. This sample was taken from a posterior site of the fascia lata, which has the particularity of having two networks of collagen fibers in almost identical proportions (Otsuka et al. 2018). However, this is very particular case, as the samples taken from other sites (anterior, lateral) show the longitudinally oriented fibers outnumber transversally oriented fibers.

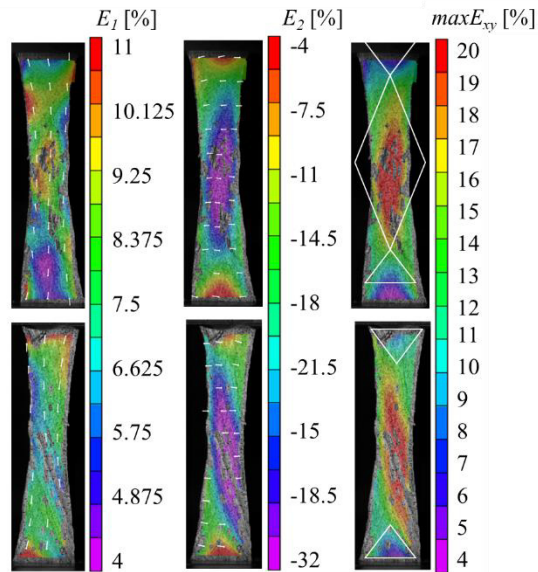


Figure 3.3-3. Correlation results on the front (top) and back faces (bottom) of 308_L_03 sample at 10% deformation. The white arrows represent the main deformation directions.

3.3.1.2. Large band test

For the large band tests, 10 loading-unloading cycles are presented with the curves of the nominal stress as a function of global and local deformations (Figure 3.3-4), calculated the same way as described for the bias tests. Same as before, local and global strains values are different, 15% global strain as set point leads to 8% of local strain. This difference may be caused by the possible deformation of the jaws during traction. On both local and global curves, the first cycle is different from the followings. Each following cycle shows smaller nominal stress value and the presence of irreversible deformation states.

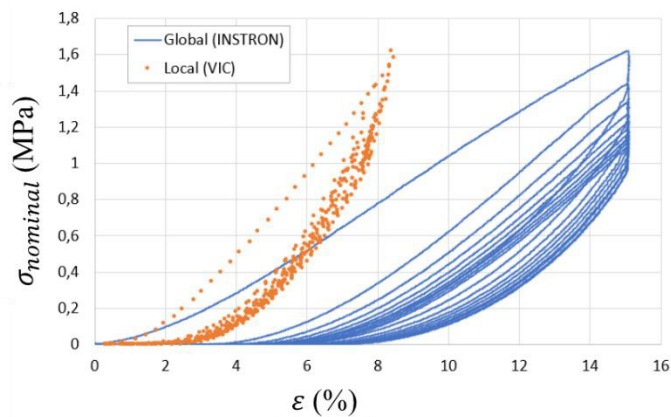


Figure 3.3-4. Nominal stress versus global and local strain curves for 133_R_02 sample.

Examples of strains distributions on the internal surfaces of 133_R_02 and 133_L_04 samples are illustrated on the Figure 3.3-5. As expected for such “pure shear” test, E_2 strain is close to zero at the center of the sample where the edge effects are minimal. The average E_1 and E_2 strains at the central area of the sample R0 are respectively 11.9% and -1.3% for the 133_R_02 sample, 9.42% and -1.06% for the 133_L_04 sample.

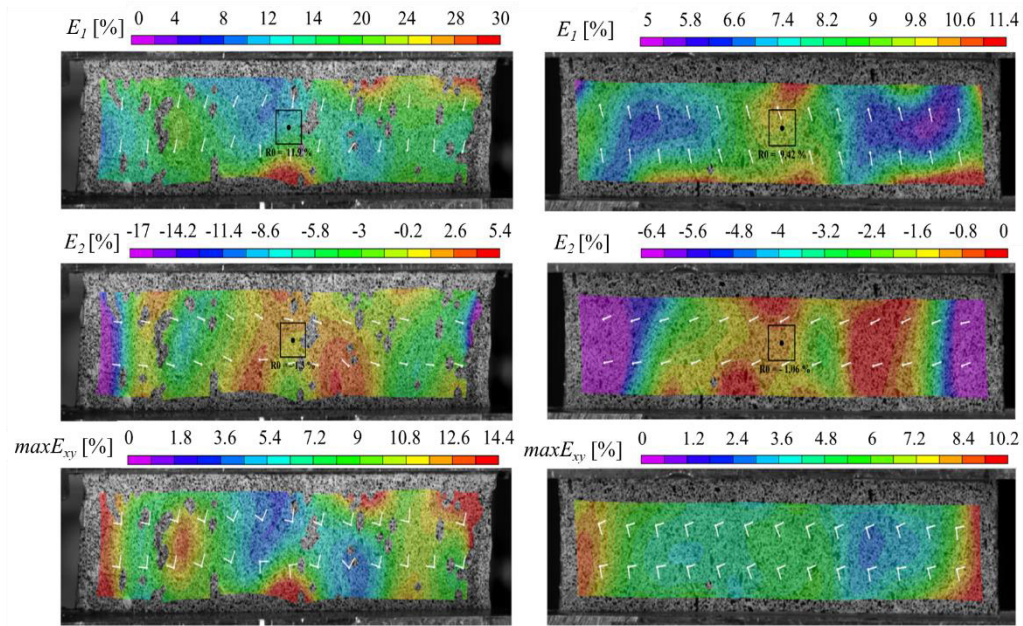


Figure 3.3-5. Strain field on the front (internal) faces of 133_R_02 (left) and 133_L_04 (right) samples for a 9% local deformation. The white arrows represent the main deformation directions. Square area in the middle of the sample named R0 shows the average value of corresponding strain.

3.3.2. Fiber Distribution

3.3.2.1. Bias test

An example of the images obtained with fibers detection identification on 107_L_05 and 107_L_07 samples is presented on the *Figure 3.3-6*. Despite the enhancement by shadowing, the recognition of fibers was complicated for the bias test sample during stretching. For example, on the sample 107_L_05 the software recognized only longitudinal fibers (*Figure 3.3-7*). However, for one sample (107_L_07) taken from the ITT, the orientations of the two fiber networks were identified.

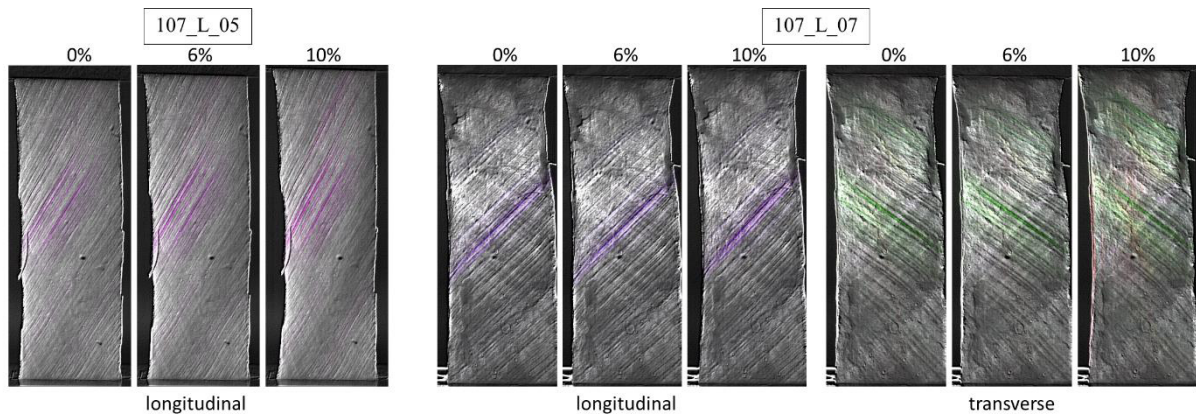


Figure 3.3-6. Longitudinal and transverse fibers detection on the samples during bias test at 0%, 6%, and 10% displacements. Colors of detected fibers correspond to the angles from the gradient scale for fiber detection (*Figure 3.2-8*).

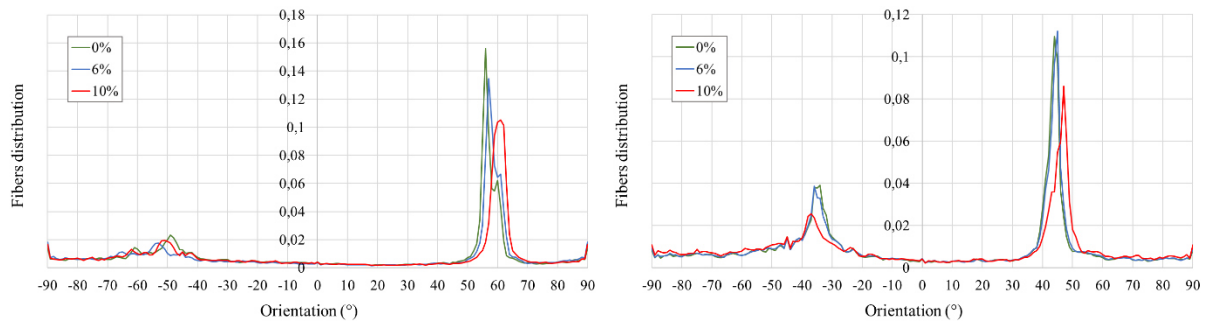


Figure 3.3-7. The amount of fibers corresponding to a given angle for 0%, 6%, and 10% global deformation detected on the 107_L_05 (left) and 107_L_07 (right) samples during bias test.

The main fibers are changing their orientation with the stretch (Figure 3.3-8). Longitudinal fibers angle was around $48.9^\circ \pm 7.6^\circ$, the transverse fibers angle was around $47.0^\circ \pm 16.9^\circ$ in the beginning of the bias test.

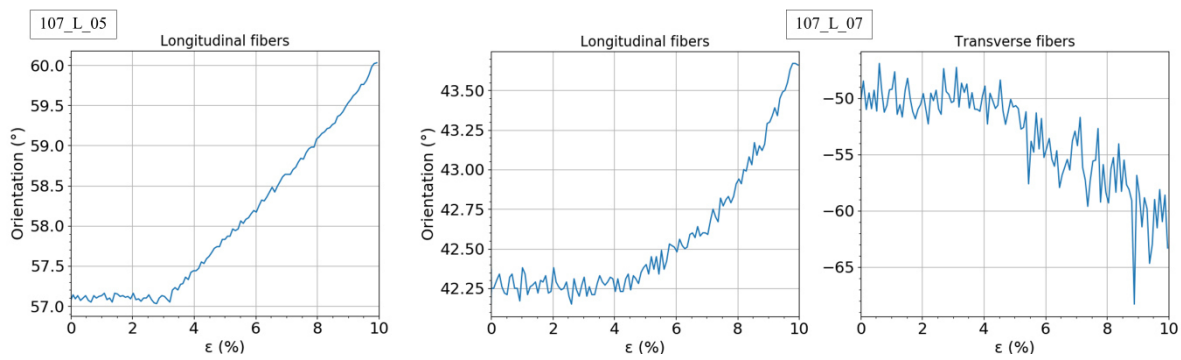


Figure 3.3-8. Reorientation of the main collagen fibers networks along the sample global stretch of 107_L_05 (only longitudinal fibers detected) and 107_L_07 samples (both longitudinal and transverse fibers detected).

The orientation of main fibers for the rest of the samples tested during bias test are presented at APPENDIX II.

3.3.2.2. Large band test

For large band samples, the detection of both fiber networks was easier. The examples of fibers orientations on the 133_R_01 and 133_L_03 samples' surfaces at 0% and 8% local deformations (Figure 3.3-9) show the detected fibers. As the sample is large, the network of transverse fibers may show various main directions. Nevertheless, the Fiji J software does not detect fibers all over the sample. This may be linked to high or low fibers density but considering this bias, the quantity of detected fibers was not considered but only their main orientation, as described below.

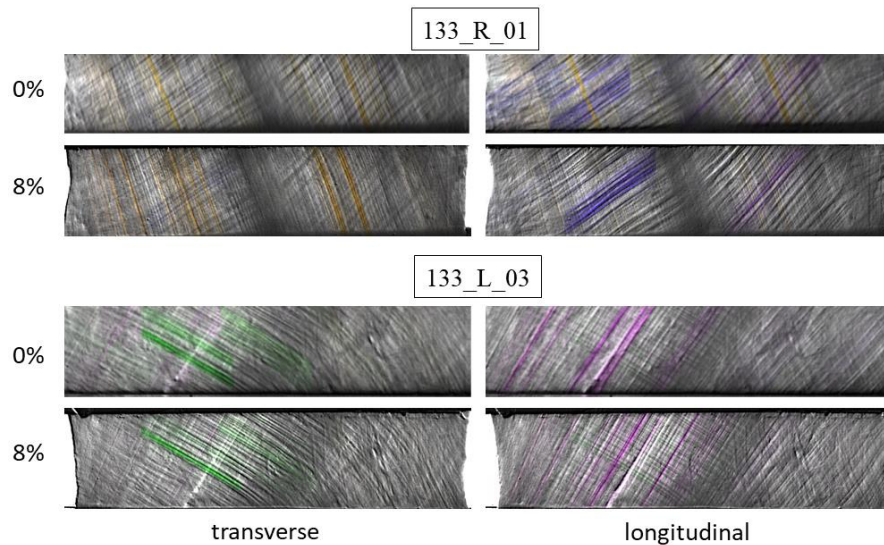


Figure 3.3-9. Longitudinal and transverse fibers detection on the samples during large band test at 0% and 8% displacements. Colors of detected fibers correspond to the angles from the gradient scale for fiber detection (Figure 3.2-8).

The graphs on the *Figure 3.3-10* show the quantification of the fibers amount found according to various shading directions. Six curves represent the distribution of fibers at 0% and 8% local deformations, in dashed and bold lines respectively, during three first loading-unloading cycles. Each of the curves contains two or three peaks highlighting the main fiber orientations. These orientations are changing with the displacement, what is visible as a shift in angles between the results at 0% and 8% strains. This phenomenon reflects a reorientation of the fibers, which tend to align with the direction of the traction.

At 8% deformation of the sample 133_R_01, the peaks of all three cycles converged at 35° , 51° , and -71° angles, decreasing from the first cycle for the positive angles, and increasing from the first cycle for the negative angle. For the sample 133_L_03 at 8%, deformation all curves peaks converged at 60° and at -32° .

The large band test shows the presence of irreversible deformations generated from the first cycle showing that the fibrous structure of the fascia lata deteriorates with the deformation and does not return to its initial state. The fiber kinematics does not clearly explain this non-reversible deformation of the sample after the first cycle. The angle between the main fibers before applying the stretch is $93.7^\circ \pm 11.9^\circ$.

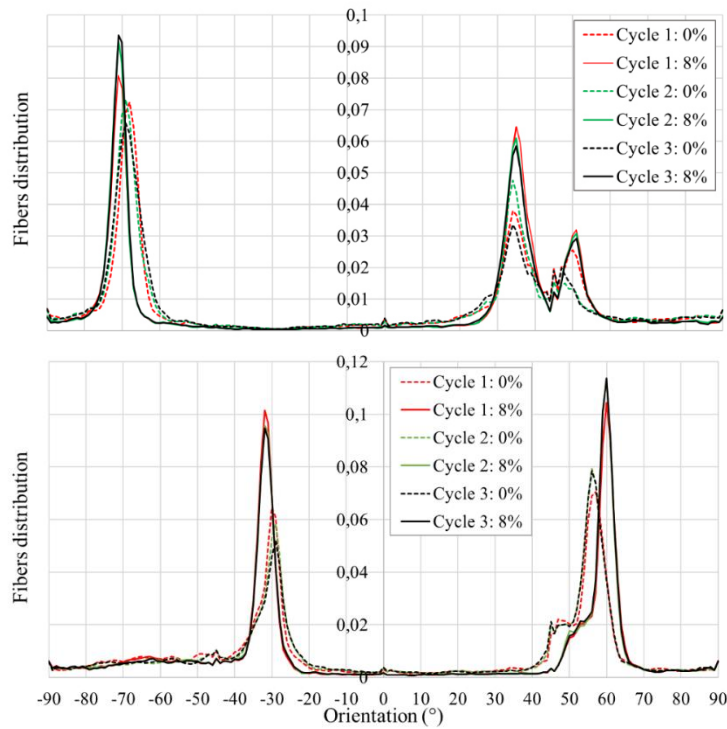


Figure 3.3-10. The amount of fibers corresponding to a given angle for first three cycles at 0% and 8% local deformation detected on the 133_R_01 (top) and 133_L_03 (bottom) samples.

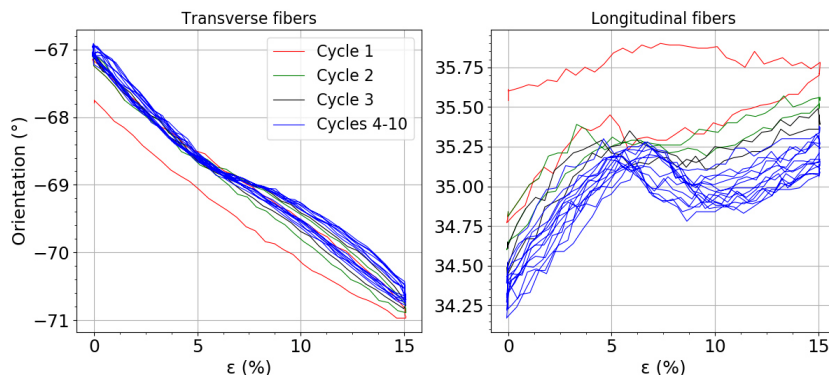


Figure 3.3-11. The transverse and longitudinal fibers orientation along the global strain of the 133_R_01 sample. First three cycles are in red, green and black colors respectively and the rest 6 cycles are in blue color.

3.3.3. Bi-photon microscopy

Presented images (Figure 3.3-12) at levels 262 μm and 291 μm , located respectively closer to the outer surface of the fascia lata sample and deeper inside the sample. The images we got using the bi-photon microscopy are showing elastin and collagen fibers. From the observed results, we suppose that on the top image, collagen fiber shown with white arrow is transversally oriented, and on the bottom image, it is oriented longitudinally. This would mean that transverse layer is the outer layer, and inner layer is consisting of longitudinal fibers.

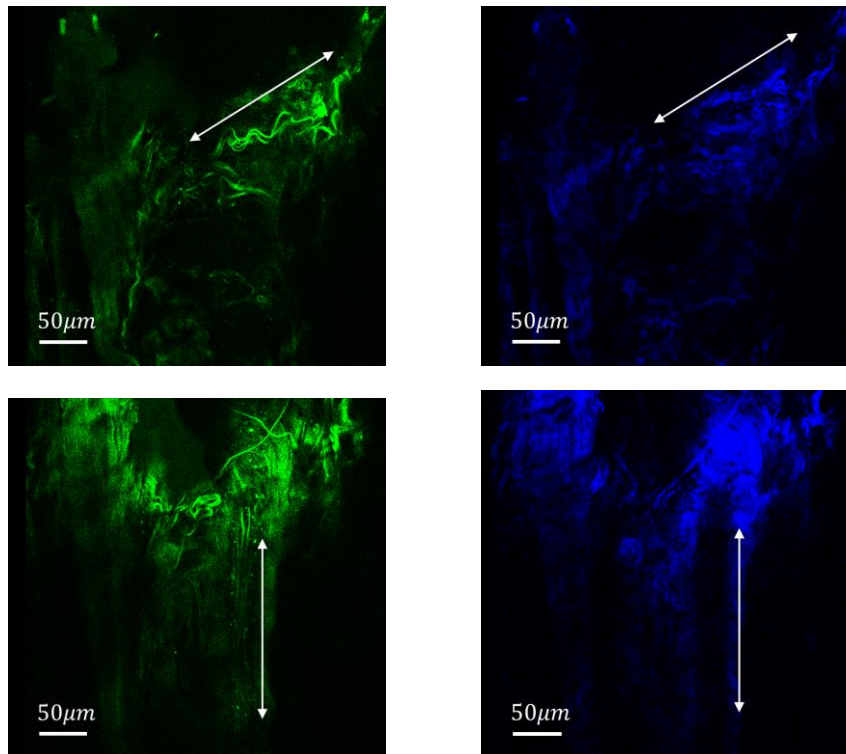


Figure 3.3-12. Human ITT (107_R_05 sample) observation with bi-photon microscopy. Green color corresponds to the elastin fibers (on the left) and blue color to the collagen fibers (on the right). Size of the bar is 50 μm . White arrow is showing the direction of the corresponding fiber.

3.4. Discussion

During the tests, tissue hydration was secured by the saline solution, but during the tensile tests, the hydration of the samples is always difficult to maintain. The dehydration will lead to the loss of water in the ground substance, especially with the stretch of the tissue. Therefore, it can be one of the possible reasons for a different first loading-unloading cycle from the others when looking at the results. To avoid this problem, we propose to redo the tests with samples placed in a bath of saline solution. The effect of temperature on the mechanical properties of the tissue could also be evaluated in this new configuration. However, performing digital image correlation on both faces or stereo digital image correlation in water is much more difficult than doing it in the air.

The strain results we obtained for the samples taken from the different sites of fascia lata differs. As the ITT is the thickest part of the fascia lata, here we obtained the highest values of the strains. For example, during bias test, at the same level of strain sample from the ITT had higher E_2 strain than the sample from the anterior fascia, the difference in absolute value was around 5%, when the E_1 strain was close between samples. In addition, stress value at the same level of strain was also higher for the sample harvested from the ITT with the difference of around 0.8 MPa. For the large band tests, the samples harvested along the ITT from the areas, closer to the knee and closer to the hip, had different E_1 strain and stress values. For the samples from knee area, a maximum measured value of E_1 stress was twice higher than for the samples from the close to hip area. However, the stress value is much higher on the samples from the proximal area of the ITT (1.6 MPa against 7.7 MPa at the maximum tested strain level).

The site dependency of the fascia lata samples has already been shown *in vivo* by Otsuka et al. (2018) and later the mechanical differences of the areas along the ITT (2020). They showed that the specimens taken from the lateral site had significantly higher Young's modulus in the longitudinal direction than those from the medial or posterior sites. The ITT was stiffer at the knee area and most compliant close to the knee, what is also supported by the cadaveric study (Wilhelm et al. 2017). Although we did not measure the stiffness of the specimens in this study, higher values of the stresses on the ITT (lateral site) than other sites, and on the proximal portion compare to all others, converge with the obtained results.

Results for both bias test and large band tests are presented in terms of nominal stress against strain. However, it should be noticed that because of tissue preparation it was difficult to have a sample with a homogenous cross-sectional area, which may impact the stress calculation. Moreover, especially for the bias test, the strain is non-homogeneous in the entire sample, therefore looking at load displacement curve might also give interesting data.

The samples were broken at the strain levels around 10 % what is in the range of 9.84 – 11.15% strain reported by Gratz (1931) and 9.7 – 10.3 % reported by Hammer et al. (2012), nevertheless, it is smaller than 27 ± 1.1 % reported by Butler (1984) or Zwirner et al. (2019). The difference of the strain levels at failure can be related to the site of the tested sample, and the fibers orientations when the load is applied, as listed results from the literature are observed for the uniaxial tests.

As for tests in this study we decided to apply the load along the bisector of the main fibers network, the main difficulty was to define properly the bisector of these two fibers networks. It was possible to distinguish these two layers with the eye only, but since these angles could vary with location, and since the templates used to cut the samples were not transparent, an error could occur when defining the bisector of fibers.

When analyzing the orientations of the fibers with the stretch, we noticed that on the ITT, transverse fibers were hard to identify due to the high density of the longitudinally oriented fibers, what is supported by fibers distribution study by Otsuka et al. (2018). They measured at the lateral site the proportion of longitudinally oriented fibers were 1.5 higher than the longitudinally oriented fibers. Less difference between the main fibers distribution was found for other sites, where on the anterior and medial sites was present the dominance of the longitudinal fibers, and on the posterior site, the dominance of transverse fibers.

For the bias test, it is necessary to check if the hypotheses used for fabrics can be used for fascia. These hypotheses are fibers inextensibility, no sliding between layers, and an angle of 90° between fiber networks. For sure, this last hypothesis is not always verified for fascia samples, as the fibers orientation has been reported to be between 67° and 80° (Pancheri et al. 2014). Nevertheless, it seems that from our results, especially on ITT samples, the total angle between the fibers networks in the beginning of the tests is sometimes close to 90° .

Regarding fibers inextensibility, we can assume this hypothesis is verified as collagen fibers are rigid (Svensson et al. 2010) but they are less stiff than Kevlar fibers used for instance in composite materials. Therefore, their inextensibility has to be checked by looking at the elongation of different specific fibers during the test. The hypothesis will be verified if the fiber rotates only. In the same way, for the sliding between layers, displacements between layers has to be calculated and compared to see if layers move in the same way.

A thorough analysis of fiber kinematics and the calculation of shear angle with the fibers rotation data could help understanding the occurring shear mechanisms, and compare what happens on the different layers. An automated analysis of fibers orientation should be developed to calculate these angles. Hence, high quality of samples images, and samples themselves, will help in this analysis.

Nevertheless, even if the shear bias tests conditions are not fulfilled, the obtained experimental results could still be used for a further analysis and especially using a modeling of its behavior. Constitutive models that include shear mechanisms and that are designed for fibrous materials in the field of composite materials could be applied to our current work. This would contribute to a better understanding of occurring shear mechanisms.

All above discussion and suggestions can be applied for the large band tests. Indeed, we couldn't obtain a minor principal strain within the middle of the sample equal to zero as a criteria for a pure shear test described in Ruiz-Alejos et al. (2016). However, this behavior with a minor strain of about -1% should be analyzed more deeply to understand what phenomenon is occurring during the test, and especially the first cycle.

Regarding the microscopic analysis, we unfortunately could not obtain more images. Unfortunately, despite the quality of the images, it is difficult to conclude on the organization of fibers and networks because the studied area is very small. It seems, however, that the fibers organize and orient themselves in a privileged direction that is changing from layer to layer. It is also noted that the elastin fibers are distributed more randomly than the collagen fibers, which had already been observed by Astruc (2019). In addition, the observation of transverse and longitudinal fibers in the outer and inner layers respectively is consistent with the microscopic observations done on the goat fascia lata (Pancheri et al. 2014).

Nevertheless, we can hypothesize that when looking at the microstructure we will be able to understand macroscopic phenomenon. For instance, to understand fibers kinematics, it might be interesting to see how the fibers networks are connected to each other, probably with specific proteins that might be placed at specific points. The way fibers are arranged would be also useful to study.

As a conclusion on this part, we proposed shear tests on fascia samples, to recover and understand the shear mechanisms observed *in situ*. These results are promising for a thorough analysis of fascia lata mechanical response. The next step is to propose a first finite element analysis of the tissue response to tension and shear loadings.

CHAPTER IV

FINITE ELEMENT (FE) MODELING OF FASCIA SAMPLE'S MECHANICAL BEHAVIOR

4.1. Introduction

The fascia lata is covering many leg muscles, connecting upper part of the leg to the lower one, and at the iliac crest, thereby connecting the muscles of the pelvis with the knee. All these connections are determining the roles of the fascia lata. For example, on the medial side, fascia lata is covering the adductor group of the muscles, therefore it acts as a displacement layer during muscular activity (Zaghloul 2018). The ITT has significant contribution to pelvic and lower extremity stabilities (Merican and Amis 2009; Birnbaum et al. 2004; Kwak et al. 2000) and it participates in the force transmission (Stecco et al. 2013), which can be explained by the tensor fasciae latae and the gluteus maximus insertions on the ITT (Birnbaum et al. 2004).

As mentioned in CHAPTER I, despite of all the functions and importance of the fascia lata in the lower extremity and its two joints, it is not added to any of the existing finite element models (Al-Dirini et al. 2016; Savonnet, Wang, and Duprey 2018; Stelletta, Dumas, and Lafon 2017; Mo et al. 2019). One of the main reasons can be the lack of the fascia lata description in the literature in order to be used for the material model creation.

There is one study presented in the literature, where the finite element simulation was made and validated for the uniaxial and pure shear tests (Ruiz-Alejos et al. 2016). However, due to the connections of the fascia lata to surrounding bones, tissues, and ligaments (Zaghloul 2018), having a high degree of elasticity and movability (Schwind 2006), it must be studied as a three-dimensional network, which allows compensatory changes in all spatial directions. Therefore, we propose a first finite element simulation of fascia lata samples during uniaxial tensile tests and during bias and large band tests (with the load applied along the bisector of two fibers networks, as in the previous tests) to analyze its shear response. The behavior of the material was modeled with the Mooney-Rivlin model reinforced by fibers (Quapp and Weiss 1998).

4.2. Materials and Methods

4.2.1. Geometry, meshing, and boundary conditions

Three models were created to reproduce uniaxial, bias, and large band tests of fascia lata samples. The parameters for the models can be found in the *Table 4.2-1*. For the model used in the longitudinal and transverse tensile tests, the dimensions and boundary conditions were taken from the paper of Ruiz-Alejos et al. (2016) where the samples were harvested from the sheep's hindlimbs. The thickness of the sample was taken from the fascia lata of the goat as 341 μm (Eng et al. 2014b; Pancheri et al. 2014). For the bias and large band tests the geometry and boundary conditions were taken from corresponding 2021_107_L_06 and 2021_133_L_04 samples (CHAPTER III). As the thickness for each of the samples was 800 μm , the layer named "longitudinal layer" represents the layer of the longitudinal fibers and has a thickness of 500 μm ; and the layer, named "transverse layer", represents the layer of the transversal fibers and has a thickness of 300 μm (C. Stecco et al. 2011b).

Meshes created using LS-PrePost software for the uniaxial, bias, and large band models were made of 5 x 30 elements with one element in thickness, 44 x 15 elements with 2 elements in thickness, and 15 x 70 elements with 2 elements in thickness, respectively. Each layer of deep fascia was made of one solid layer of 8-node brick elements. The element formulation was chosen to be a constant stress solid hexahedral element. Hourglass stabilization was added with a number 4 formulation and a coefficient of 0.03. This formulation is using Flanagan-Belytschko algorithm (Flanagan and Belytschko 1981) which is generally more effective than viscous hourglass control for structural parts. A care was always taken to ensure that hourglass energy stays less than 10% of internal energy of all the system.

Table 4.2-1. The parameters for the models.

Model	Material	Test type	Sample size (mm)	Mesh	Loading direction	Speed (mm/min)
One layer with main fibers direction	transversely isotropic hyperplastic model	Uniaxial tension	30 x 5	5 x 30 8-node brick elements	Longitudinal	5
					Transverse	
Two layers with corresponding longitudinal and transverse fiber directions	presented by isotropic Mooney-Rivlin matrix reinforced by collagen fibers (Quapp and Weiss 1998)	Bias	43.8 x 15	44 x 15 x 2 8-node brick elements	Along bisector of two fiber networks	25
		Large band (pure shear)	14.6 x 70	70 x 15 x 2 8-node brick elements		100

For all the tensile models, the boundary conditions were applied by attaching one of the ends of the model, and pulling with the opposite end forward along x -axis for the uniaxial and bias tests, and along y -axis for the large band test (*Figure 4.2-1*). For the uniaxial tensile model, it coincides with the corresponding main fiber direction (longitudinal or transverse), and for the other models it is aligned with the bisector of fibers network. The tissue fibers are defined with the material direction (*Figure 4.2-1*), which is dependent on the layer (transverse or longitudinal) of the fascia sample. Each element has a local coordinate system, where the red arrow shows the material principal direction. Therefore, the material direction in two-layer model was rotated correspondingly to the layer.

For the uniaxial tensile tests, the applied displacement rate was 5 mm/min in order to reproduce quasi-static testing conditions (Ruiz-Alejos et al. 2016). For the bias test, the applied displacement was calculated in order to obtain 10 % strain at 25 mm/min speed and for the large band test in order to obtain 20 % strain at 100 mm/min speed.

The explicit simulation was done using LS-Dyna (R11.1) software (LSTC, Livermore, CA), which is faster as it does not need to recalculate the stiffness matrix but is conditionally stable. Custom made Python codes were created for the extraction of data (forces, cross-section values, strains) in order to calculate the stresses and represent the results.

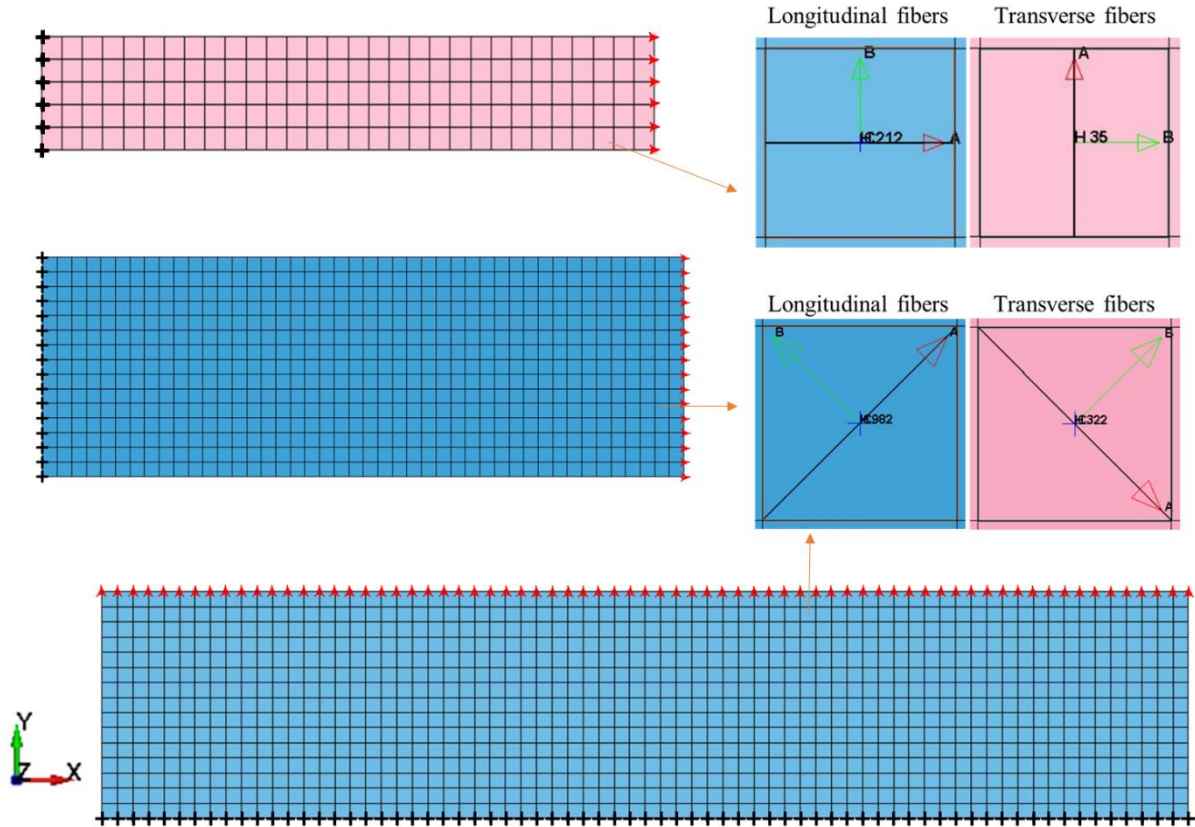


Figure 4.2-1. Boundary conditions of uniaxial tensile (top), bias (middle) and large band (bottom) models of fascia lata samples with corresponding longitudinal (blue) and transverse (pink) material directions. Black crosses highlight fixed nodes and by red triangles indicate translational nodes. On the fibers' identifications, red arrow shows the material principal direction.

4.2.2. Material model: constitutive law

The soft tissue material (91) from LS-Dyna material models is used to describe the behavior of the fascia lata. This material model is a transversely isotropic hyperplastic model, which is presented by isotropic Mooney-Rivlin matrix reinforced by collagen fibers. The strain energy function of the material is composed of ground substance matrix (F_1), collagen fibers (F_2), their interaction (F_3) (Quapp and Weiss 1998), and a bulk term:

$$W = F_1(I_1, I_2) + F_2(\lambda) + F_3(I_1, I_2, \lambda) + F_{bulk} \quad (1)$$

where I_1 and I_2 are the invariants of the right Cauchy stretch tensor, and λ is a stretch along the collagen fiber direction. The ground matrix behavior is described by the Mooney-Rivlin material model (two-coefficient model):

$$F_1 = \frac{c_1}{2}(I_1 - 3) + \frac{c_2}{2}(I_2 - 3) \quad (2)$$

where C_1 [MPa] and C_2 [MPa] are the ground matrix coefficients, the first and the second Mooney-Rivlin constants.

The bulk term is described by:

$$F_{bulk} = \frac{1}{2} K [\ln(J)]^2$$

Where the volume ratio is $J = \det F$. The effective bulk modulus K was calculated using the stiffness from the literature (Hammer et al. 2012). The stretch ratio λ^* at which fibers are straightened was chosen equal to 1.05. This parameter is useful as from a numerical point of view, incompressibility is difficult to manage.

To better understand the role of the different elements of the constitutive law, we here propose to use an analytical approach using the same law but considering that the material is incompressible.

First, we defined the analytical relationships for longitudinal (*Figure 4.2-2*) tensile traction test (the loading is applied parallel to the longitudinal fibers directions):

$$\sigma = \begin{bmatrix} \sigma_{11} & 0 & 0 \\ 0 & 0 & 0 \\ 0 & 0 & 0 \end{bmatrix}$$

For the transverse (*Figure 4.2-2*) tensile test, the σ_{22} will be present instead.

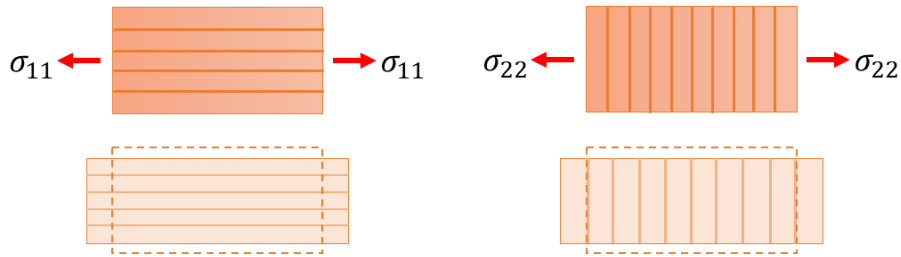


Figure 4.2-2. Representation of longitudinal (on the left) and transverse (on the right) uniaxial tensile tests.

The strain gradient tensor is:

$$F = \begin{bmatrix} \lambda_1 & 0 & 0 \\ 0 & \lambda_2 & 0 \\ 0 & 0 & \lambda_3 \end{bmatrix}$$

We assume that fascia lata is an incompressible material, then $\det F = 1$ and $\lambda_1 \lambda_2 \lambda_3 = 1$.

The Cauchy stress with strain energy from (1) was defined by (Quapp and Weiss 1998) as:

$$\sigma = 2((W_1 + I_1 W_2)B - W_2 B^2) + \lambda W_\lambda a \otimes a + pI, \quad (3)$$

$$B = FF^T,$$

where B is the left Cauchy-Green deformation tensor (Eulerian tensor), a is a unit vector representing the direction of fibers in the current configuration, W_1 , W_2 , and W_λ are strain energy derivatives with respect to the invariants (I_1, I_2, λ) , and p is a hydrostatic pressure. Moreover, $\lambda W_\lambda a \otimes a + pI$ is representing Lanir model. The model describes the stress in ligament as a function of the tensile stretch in the collagen fibers and a hydrostatic pressure from the water in the ground matrix (Lanir 1983).

By derivation of the equations (1) and (2) for a two-coefficient model, we obtain strain energy derivatives:

$$W_1 = \frac{\partial F_1}{\partial I_1} = \frac{C_1}{2}, \quad W_2 = \frac{\partial F_1}{\partial I_2} = \frac{C_2}{2}, \quad W_\lambda = \frac{\partial F_2}{\partial \lambda} + \frac{\partial F_3}{\partial \lambda}$$

In order to describe the behavior of the fibers in the longitudinal direction, the equation (3) was derived by inserting the strain energy derivatives. The stress function for the longitudinal tensile test became:

$$\sigma = (C_1 + I_1 C_2) \begin{bmatrix} \lambda_1^2 & 0 & 0 \\ 0 & \lambda_2^2 & 0 \\ 0 & 0 & \lambda_3^2 \end{bmatrix} - C_2 \begin{bmatrix} \lambda_1^4 & 0 & 0 \\ 0 & \lambda_2^4 & 0 \\ 0 & 0 & \lambda_3^4 \end{bmatrix} + \lambda W_\lambda \begin{bmatrix} 1 & 0 & 0 \\ 0 & 0 & 0 \\ 0 & 0 & 0 \end{bmatrix} + p \begin{bmatrix} 1 & 0 & 0 \\ 0 & 1 & 0 \\ 0 & 0 & 1 \end{bmatrix} \quad (4)$$

As this is an isotropic part of the model, the strain energy density function only depends on the invariants of C . Therefore, I_1 is calculated from the right Cauchy-Green deformation tensor (Lagrangian tensor) as:

$$I_1 = \text{tr}(C) = \text{tr}(F^T F) = \lambda_1^2 + \lambda_2^2 + \lambda_3^2$$

Therefore, Cauchy stresses will be written as following:

$$\begin{cases} \sigma_{11} = (C_1 + C_2(\lambda_1^2 + \lambda_2^2 + \lambda_3^2))\lambda_1^2 - C_2\lambda_1^4 + \lambda W_\lambda + p \\ \sigma_{22} = (C_1 + C_2(\lambda_1^2 + \lambda_2^2 + \lambda_3^2))\lambda_2^2 - C_2\lambda_2^4 + p \\ \sigma_{33} = (C_1 + C_2(\lambda_1^2 + \lambda_2^2 + \lambda_3^2))\lambda_3^2 - C_2\lambda_3^4 + p \end{cases} \quad (5)$$

For a longitudinal stretch from (5b) and (5c), knowing that $\sigma_{22} = \sigma_{33} = 0$ and due to the incompressibility condition ($\lambda_2 = \lambda_3 = \lambda_1^{-\frac{1}{2}}$), the value of the hydrostatic pressure is:

$$p = -C_1\lambda_1^{-1} - C_2\lambda_1^{-2} + C_2\lambda_1 \quad (6)$$

From here we assume $\lambda_1 = \lambda$, and substituting (6) to (5a) the formula for a Cauchy stress under longitudinal loading will be written as:

$$\sigma_{11} = C_1(\lambda^2 - \lambda^{-1}) + C_2(\lambda - \lambda^{-2}) + \lambda W_\lambda \quad (7)$$

For the transverse tensile test, we have to assume $\lambda_1 = \lambda_3 = \lambda_2^{-\frac{1}{2}}$ and $\sigma_{11} = \sigma_{33} = 0$. Nevertheless, the stretch λ is always less than one, and therefore, does not contribute to the strain energy. Then the Cauchy stress under transverse loading takes the form:

$$\sigma_{22} = C_1(\lambda^2 - \lambda^{-1}) + C_2(\lambda - \lambda^{-2}) \quad (8)$$

Fibers behavior and their interaction (F_2 and F_3) were presented by Quapp and Weiss (1998) with the fibers coefficients C_3, C_4, C_5 , which are responsible for certain part of the stress-strain curve. With the assumptions for the collagen fibers incorporated into F_2 , collagen fibers do not support a compressive load, their response is modeled as an exponential approximation of tensile stretch-strain collagen relationship for the toe region and a straight line in the linear region. The strain energy for the collagen fibers became:

$$\begin{cases} \lambda W_\lambda = 0, & \lambda < 0 \\ \lambda W_\lambda = C_3(e^{C_4(\lambda-1)} - 1), & \lambda < \lambda^* \\ \lambda W_\lambda = C_5\lambda + C_6, & \lambda \geq \lambda^* \end{cases} \quad (9)$$

The coefficients C_3 [MPa] and C_4 are representing the toe region (below the stretch value λ^* where the fibers are straightened), correspondingly scaling the exponential stresses. The coefficient C_5 [MPa] is the modulus of straightened collagen (linear region coefficient above λ^*). Coefficient C_6 was determined from the condition that exponential and linear regions are continuous at λ^*):

$$C_6 = C_3(e^{C_4(\lambda^*-1)} - 1) - C_5\lambda^*$$

4.2.3. Data fitting

Parameters estimation for the material model was done using custom made Python code using the described equations (7), (8), and (9) and least-square fitting. The experimental data was taken from the longitudinal tensile test presented by Ruiz-Alejos et al. (2016). The coefficients that fitted this test results were used in the 91_Soft_tissue material model for the transverse tensile test, bias and large band tests.

4.3. Results

4.3.1. Stress-strain distribution during the uniaxial tensile simulations

The coefficients found using the analytical model which were fitted on the Ruiz-Alejos et al. (2016) experimental results for the longitudinal tensile test are listed in the *Table 4.3-1*.

Table 4.3-1. Material coefficients for the longitudinal Cauchy stress-strain curve, describing the fascia lata's behavior.

C_1 [MPa]	C_2 [MPa]	C_3 [MPa]	C_4	C_5 [MPa]
0.03	0.25	0.05	74	120

The material model fits well the experimental data when the stretch was applied along the longitudinal fibers (*Figure 4.3-1*). Nevertheless, the strains of the longitudinal tensile model are located a little bit higher than the other curves. For the transverse tensile model, it is assumed that the transverse fibers do not support a compressive load ($C_3 = C_4 = C_5 = 0$). Therefore, the curves of the analytical model and FE model are different from the experimental curve from Ruis-Alejos et al. (2016) transversally loaded sample. We can clearly see that fibers are not participating in the material behavior for this case, for the FE and analytical curves, what was expectable, as transversal fibers are not modelled in this one fiber network model. The stress value of the experimental data loaded along transversal fiber network is 1.07 MPa for the 6% elongation (Ruis-Alejos et al. (2016)), when for the FE transverse loading simulation with 1 fiber network, it is 0.13 MPa.

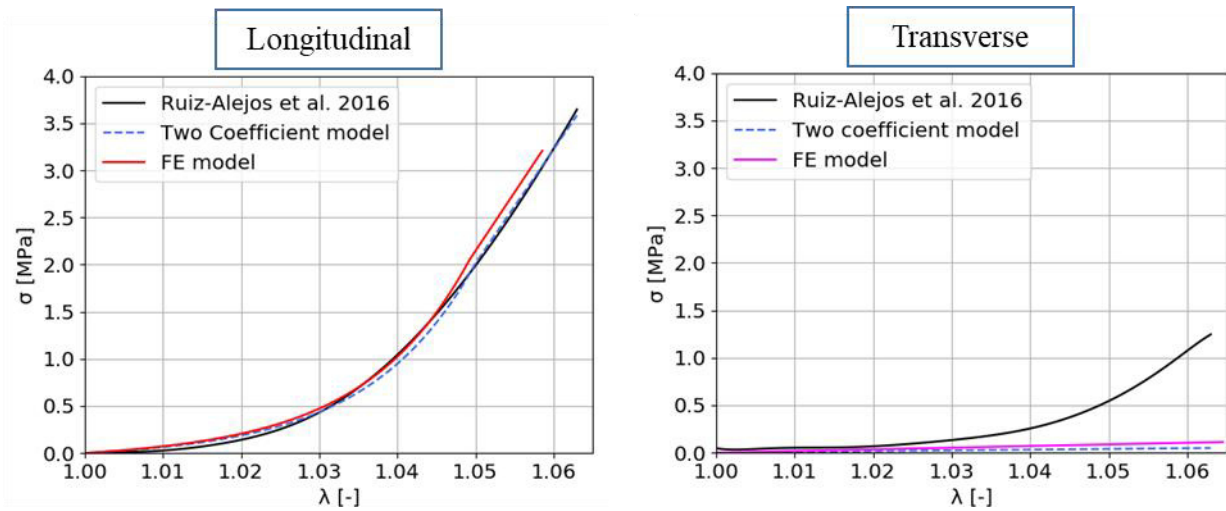


Figure 4.3-1. Stress-strain curves for longitudinally (left) and transversally (right) loaded one-fiber network model from: the experimental data (Ruiz-Alejos et al. 2016), analytically fitted Two Coefficient model, and FE model.

4.3.2. Stress-strain distribution during the bias test simulation

Figure 4.3-2 and Figure 4.3-3 illustrate the contour plots of the strain distributions along x -axis for both layers of the sample observed with the experimental testing and with FE modeling respectively, obtained at the 10% stretch along the bisector of two fibers directions. The stress distribution is available only for the FE model.

As the results obtained with FE simulation were determined by the material model from the longitudinal biaxial testing, the only possibility at this stage is to compare the results qualitatively. With the obtained distributions from the experimental and simulated bias tests we see different strain levels on both sides of the samples. On the front face of the experimental sample, the maximum concentration of the strain is focused in the middle, as for the simulated model (both sides), it is shifted to the left attached side of the back side of the experimental sample.

The Green-Lagrangian strains from the experimental data (Figure 4.3-2) and FE simulation (Figure 4.3-3) of the bias test with the loading direction aligned with the bisector of two fibers directions show similar shapes of the E_2 strain distribution, however, it looks mirrored relatively to x -axis between front face and longitudinal layer, back face and transverse layer. The E_1 strain is different between experimental and simulated results, and for the maximal shear strain although the shapes of the distributions are different, the maximum value is concentrated in the middle of both assets.

Contours of the X -stress from the simulation (Figure 4.3-3) are similar to $\max E_{xy}$ strains distributions observed during the experiment (Figure 4.3-2).

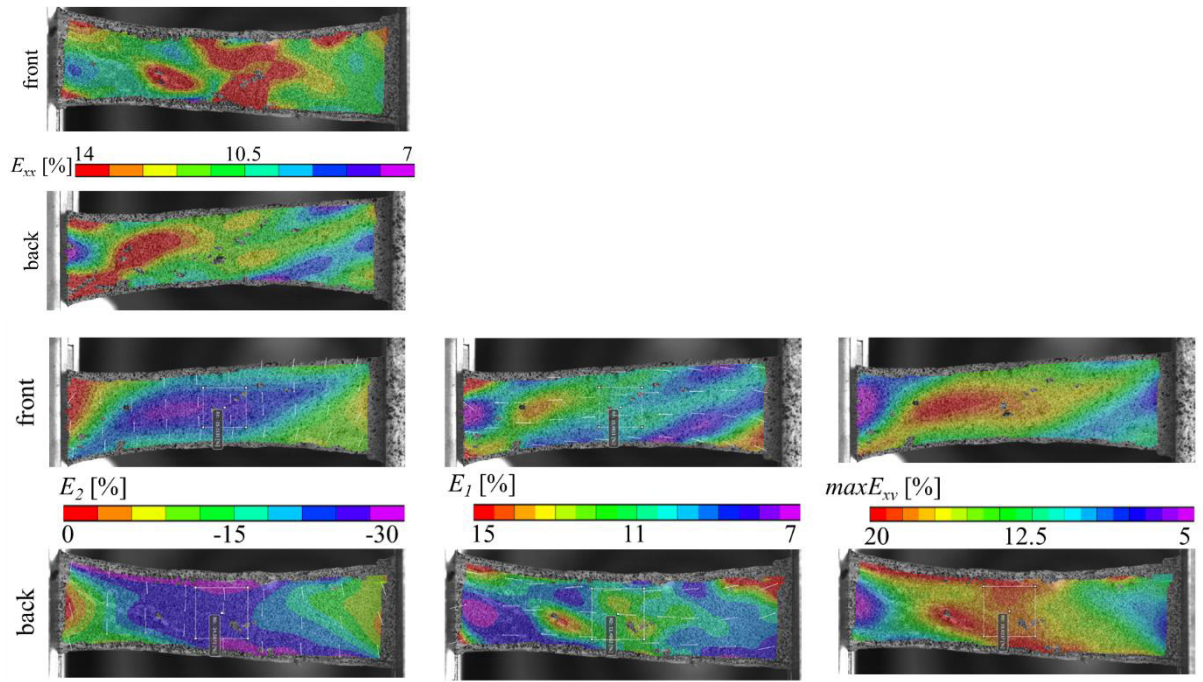


Figure 4.3-2. Contour plots of the E_{xx} , principal (E_1 and E_2) and maximal shear ($maxE_{xy}$) strains distributions on the front and back faces of the experimental sample obtained at 10% stretch during bias test.

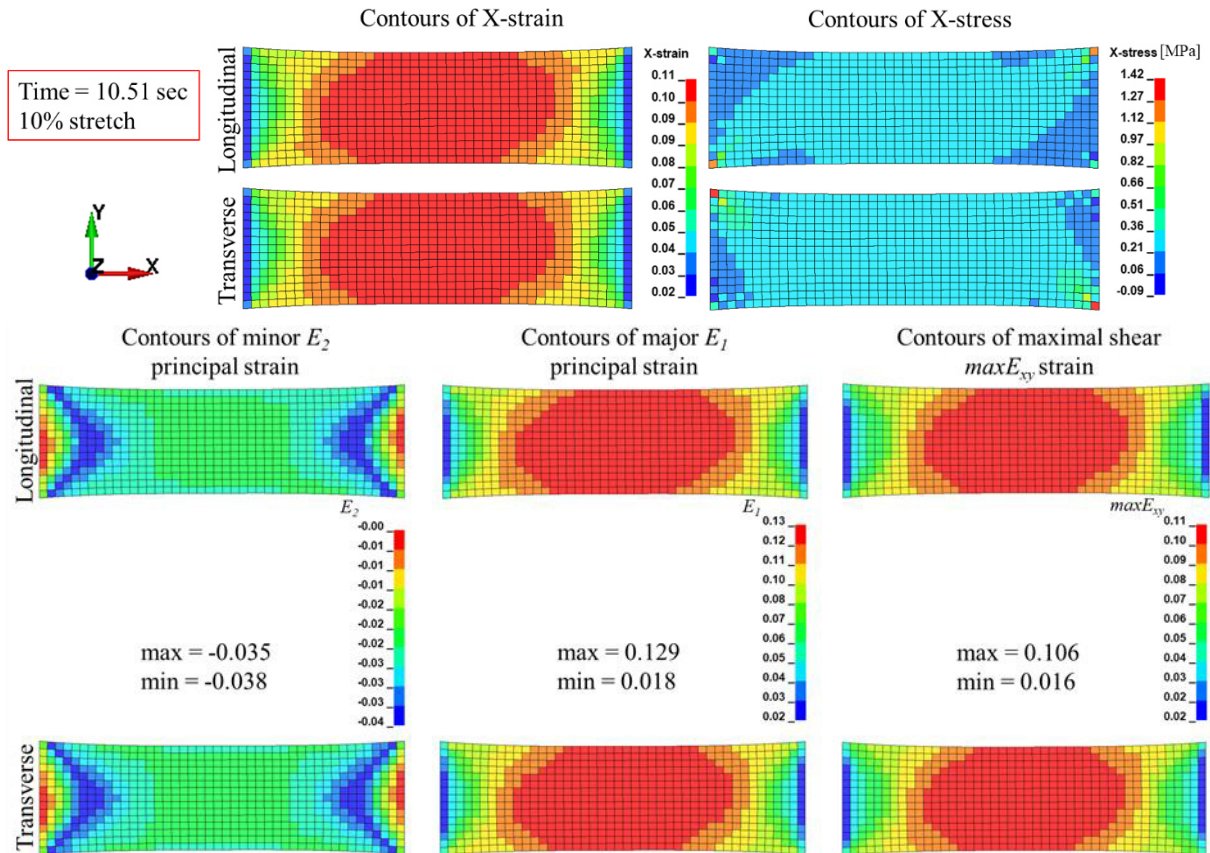


Figure 4.3-3. Contour plots of the strains distributions in the longitudinal and transverse layers along the loading direction (which is chosen to be the bisector of two fibers directions) during bias test simulation obtained at the 10% strain.

The maximum stress value of the FE model at 10% strain is 0.22 MPa (Figure 4.3-4), which is much lower compared to the experimental stress we observed for this sample during the test (0.97 MPa). At 6% stretch the nominal stress is 0.12 MPa, what is close to the nominal stress of the transverse model (0.13 MPa).

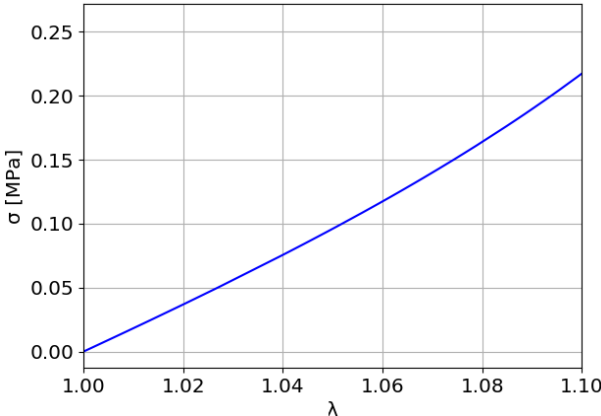


Figure 4.3-4. Nominal stress-stretch curve of the bias test simulation.

4.3.3. Stress-strain distribution during the large band test simulation

The Y-strain distribution during the simulation of the large band test is reminding the one during experimental test (Figure 4.3-5 and Figure 4.3-6). What is interesting to notice, during the simulation, the distribution of Y-stress is concentrated in the diagonally opposite corners of longitudinal and transverse layers, parallel to the corresponding fibers directions. However, the same tendency is visible for the bias test simulations.

As we can see from the strains contour plots (Figure 4.3-5 and Figure 4.3-6), the E_2 strain distribution is just a little bit similar between experimental and simulated results, having a defined transverse area on the left and the right sides of the sample. The rest of the strain distributions are very different.

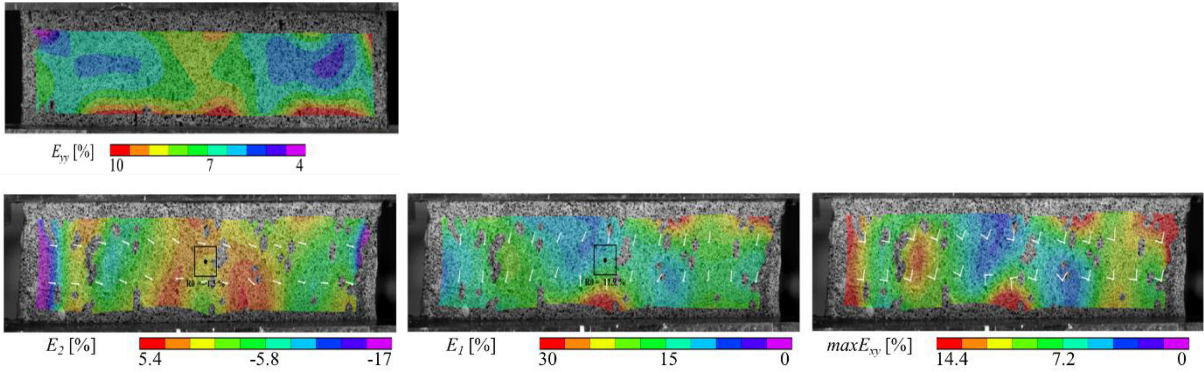


Figure 4.3-5. Contour plots of the E_{yy} , principal (E_1 and E_2) and maximal shear ($maxE_{xy}$) strains distributions for the experimental sample (front face only) during the large band test at the 6% strain.

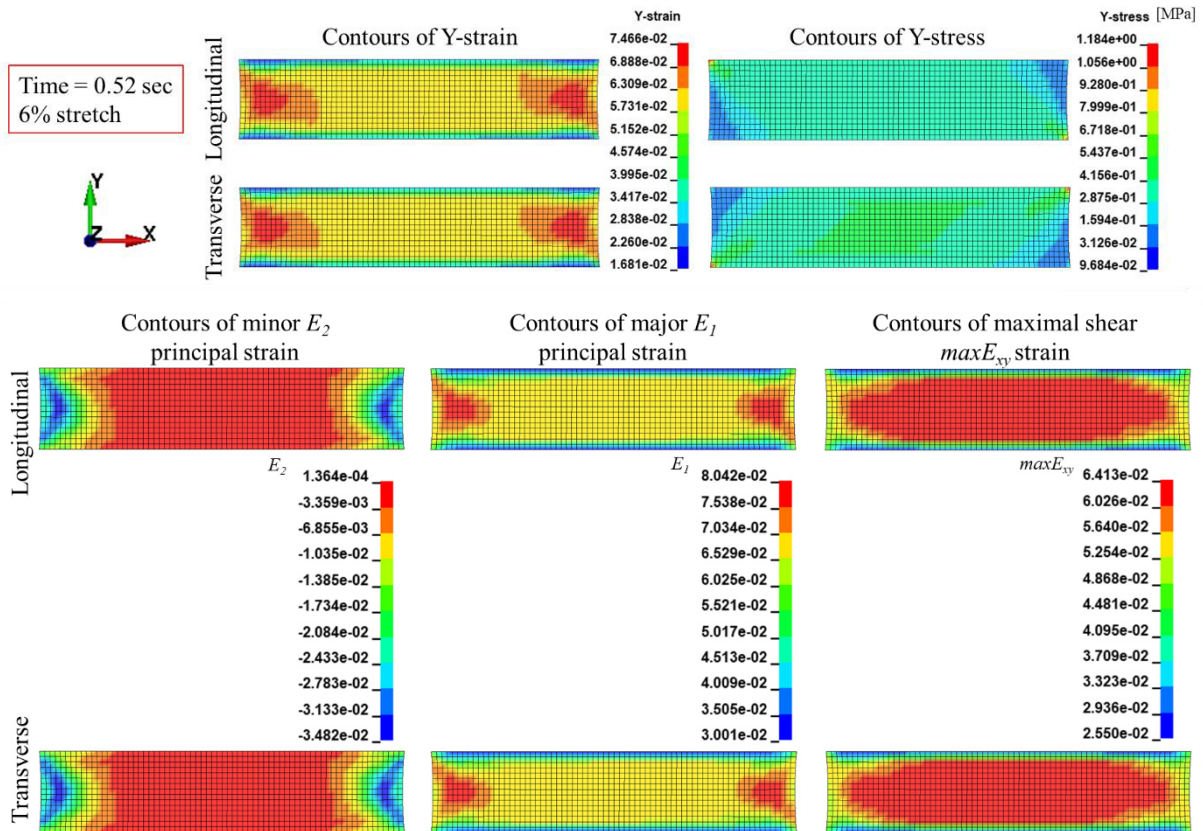


Figure 4.3-6. Contour plots of the Y -stress, E_{yy} , principal (E_1 and E_2) and maximal shear ($maxE_{xy}$) strains distributions in longitudinal and transverse layers along the loading direction (which is chosen to be aligned with the bisector of two fibers directions) during large band simulation, obtained at the 6% strain.

Nevertheless, the nominal stress value computed for the experiment at 6% strain was 1.6 MPa during first loading, and for the simulation we got 1.9 MPa (Figure 4.3-7), what is quite close.

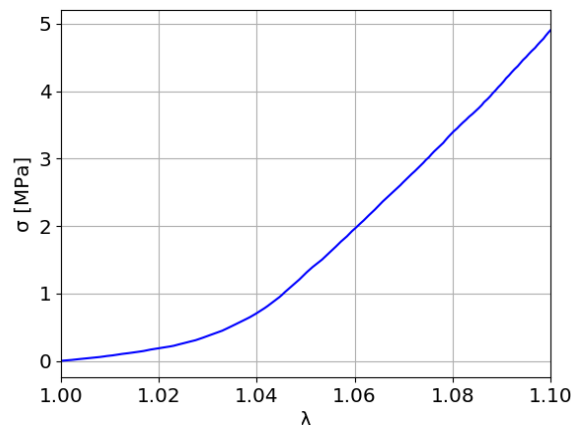


Figure 4.3-7. Nominal stress-strain curve of the large band test simulation.

4.4. Discussion and Perspectives

The parameters for the material model were fitted only to the longitudinally loaded sheep's fascia sample from the paper of Ruiz-Alejos et al. (2016), and used after for all the models, including bias and large band tests models. Therefore, Cauchy stress values of transversal

tensile FE simulation with one fiber network model (*Figure 4.3-1*) are much smaller compared to the experimental data, because of the lack of transverse fibers network. In this case, longitudinal fibers did not contribute to the resulting behavior of the sample, but only the ground substance matrix. Moreover, when sample is subjected to the transverse loading, longitudinal fibers may also be loaded, as they are forming a certain angle relatively to the adjacent layer of transverse fibers (67-80° (Pancheri et al. 2014)).

Since the material properties were not changed for the models used to simulate bias and large band tests, we cannot provide a quantitative comparison of stress levels measured experimentally and calculated numerically. Indeed, stress levels were very different (*Figure 4.3-4*), and thus material parameters have to be fitted on experimental data. Nevertheless, for the bias tests, the contour plot of the maximum shear shows a strain distribution which is getting close to what is expected for bias extension tests: a central area of maximum shear strain, two areas with half shear strain and an undeformed area (Boisse et al. 2017), even though the undeformed area is not so clear in our simulation results; and also to what we observed experimentally. However, further developments are required before coming to a conclusion.

For the bias and large band tests, within the two layers models, the angle between fiber networks is 90° (which also corresponds to the expected angle between fibers of fabrics when tested in bias), however it is higher than reported in the literature, 67° – 80° (Pancheri et al. 2014). Nevertheless, this is close to what we observed during the tests on isolated samples (CHAPTER III) where the angle between collagen networks was a bit larger around 93°, especially for the ITT samples. One way to compare the results from the modeling with the experimental data, especially when dealing with fiber angles could be to track fibers orientations within the simulation, thanks to the calculation of deformation gradient, and compare it with the kinematics analysis of fibers done experimentally. The influence of fibers orientation and of fibers proportion or mechanical properties within each tissue layer could be assessed numerically with for instance a numerical design of experiments.

This part presents the preliminary results obtained to get familiar with simulations. The identification of the material parameters using tensile data from bias and large band tests should be performed, considering the measured angles between the layers, and even new constitutive laws can be created to address the issues with the existing one used here. It is also possible to calculate the change of the material direction (i.e. fibers) with the stretch, by multiplying the initial vector of the direction by the deformation tensor. The size and formulation of the elements have also to be considered when meshing the model. Here, we have used solid elements, but as fascia lata is quite thin, another interest may be to use shell or membrane elements. However, restricted number of possible constitutive laws may cause the difficulty to represent fascia mechanical response, while the existing constitutive laws for shell and membranes might not describe properly the behavior of fibrous tissues. The development of an appropriate constitutive law could then be performed to be implemented to the model of the leg. After validation, the model would be useful for different applications, as simulations of surgical and manual therapies.

CHAPTER V

ITT STRAIN RELEASE AND KNEE MOBILITY

5.1. Introduction

Lateral soft tissues release at the knee level (ITT, anterolateral capsule, lateral collateral ligament, and popliteus tendon) is a technique used for the correction of valgus deformity (Buechel 1990; Matsuda, Lustig, and van der Merwe 2017). In general, the release starts with the posterolateral capsule, which is cut at the level of the tibial osteotomy between the posterior border of the ITT and the popliteal tendon, followed by pie-crusting of the capsule above the initial cut. If the extension gap is still unbalanced, the ITT is elongated with the pie-crusting technique (intra-articular release) (Elkus et al. 2004; Ranawat et al. 2005; Whiteside and Roy 2009) or liberated from Gerdy's tubercle (extra-articular release) (Matsuda, Lustig, and van der Merwe 2017). The pie-crusting technique consists in performing multiple small incisions across the ITT (Bruzzone et al. 2010; Sangkaew 2007). The surgeon decides the number of incisions to reach the tissue balance.

The pie-crusting is also used to release the pressure on the lateral femoral epicondyle in patients with iliotibial band syndrome, exhibiting a tight ITT (Lavine 2010). The technique is applied when the knee is flexed at around 30° corresponding to the position in which the ITT is compressed against the lateral condyle (Fairclough et al. 2006; Noble 1979). The incisions are made on the ITT covering the lateral femoral epicondyle (Sangkaew 2007).

However, some complications may occur after using this technique, such as unstable knee due to over-release, elevation of joint line, which may affect track of patella and hemarthrosis caused by periarticular arterial injuries (Del gaizo and Della Valle 2011; Dragosloveanu et al. 2014; Schwarzkopf et al. 2013).

Therefore, to objectify the empiric know-how of surgeons for such surgical technique could allow a better understanding of the associated strain mechanisms and contribute to limit complications. The aim of this study was thus to measure the impact of the pie-crusting technique on the ITT, on its surfacic strain state, and also on the knee mobility during flexion-extension.

5.2. Materials and Methods

5.2.1. Specimen Preparation

Three fresh female post mortem human subjects (PMHS) were obtained from the Department of Anatomy of the University of Rockefeller (DAUR), Lyon, France. The anthropometry parameters in average were: 91.5 (\pm 3.5), years-old, 61.5 (\pm 13.5) kg, 156.5 (\pm 11.5) cm. Subjects had a BMI of 18.5, 35.2, and 19.4 kg/m² respectively.

Bodies were kept at 4°C, during 4.7 days in average until the beginning of the tests. Prior to the experiments, each body was instrumented with six tripods used for motion capture (*Figure 5.2-1A*). The tripods were screwed into the bones of both legs: on anterior superior iliac spine

of pelvis, medial condyle of femur, and medial surface of tibia (*Figure 5.2-1A*). Each tripod represents four spherical reflective passive markers (10 mm in the diameter) fixed to a rod. This was done in order to avoid the soft tissue artifact ('soft tissue shifting' effect) (Leardini et al. 2005). Moreover, square brackets were used to fix the ankle at 90°.

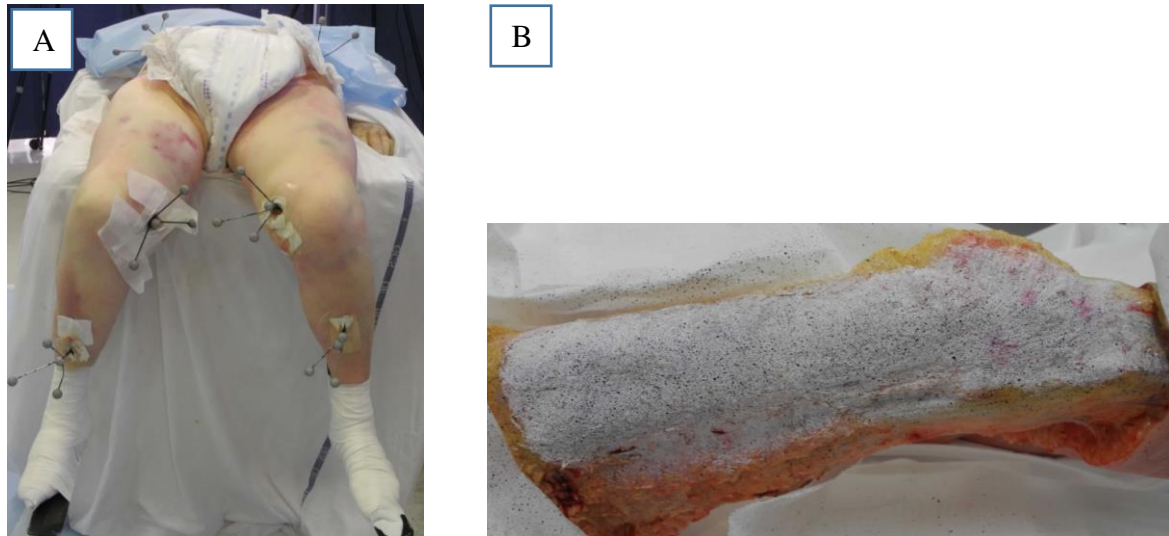


Figure 5.2-1. Body preparation: (A) tripods drilled into the major anatomical points for motion analysis (subject 2021_073), (B) speckles pattern for digital image correlation (DIC) (subject 2021_098).

To perform digital image correlation (DIC) and calculate surfacic strains on the ITT during movements and before and after pie-crusting technique, skin, adipose tissues and vessels were dissected from the legs. In order to keep ITT and fascia lata hydrated, dissection was done on the left leg first, and just before tests on the right leg. The same procedure was repeated on each leg. Dissection was performed with an attention to avoid damaging of the ITT and fascia lata. To create the speckle necessary for DIC, a thin layer of white clown mask was applied on the area of interest (lateral side of fascia lata, which includes ITT) and sprayed with black paint using a toothbrush to create a black dots pattern (Podwojewski et al. 2014) (*Figure 5.2-1B*). This technique allows standardizing the background and obtaining good black and white contrast. Moreover, the white mask can be easily removed with water, what makes possible to redo the speckles until the needed quality (density, size, etc.) to perform image correlation is reached. When the time between tests was long, fascia lata was hydrated by application of a paper towel soaked with saline solution.

During the experiments, the body was placed on the table in a lying position (*Figure 5.2-1A*). Subject's buttock was placed at the edge of the table so that legs were suspended allowing a movement of the knee.

5.2.2. Anatomical Frames Acquisition and Motion Analysis

In order to compute leg movements during all experiments, we used motion capture and 3D tracking system OptiTrack™ with ten high-speed tracking cameras placed around the body (*Figure 5.2-2*) to cover the area of the experiment. Image sensor's resolution and recording frame rate were 1280 × 1024 and 100 Hz, respectively.

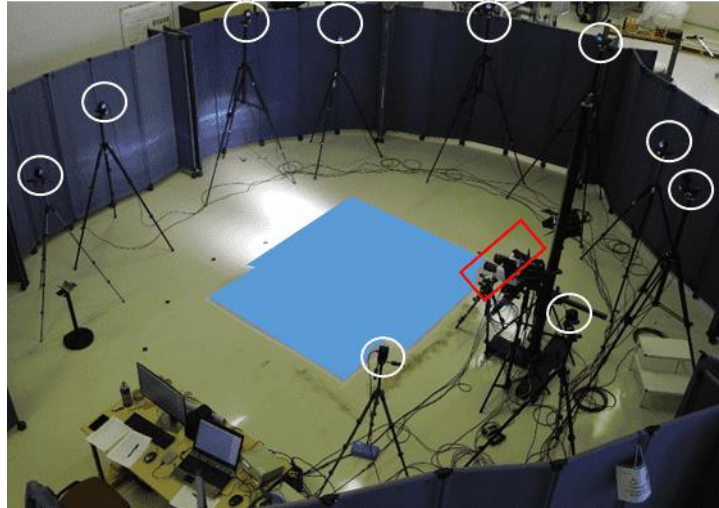


Figure 5.2-2. Experimentation area: motion analysis cameras (white) and Photron cameras for the DIC (red).

Technical frames for the leg movements were defined from the tripods screwed earlier into the legs and pelvis. Anatomical frames, in turn, were created by palpating all the anatomical points with an additional tripod (with four reflecting markers fixed to a rod with a tip on the end) when body was in lying position (Figure 5.2-3). All the palpated anatomical points are listed on the Figure 5.2-3. In order to reconstruct a position of a posterior superior iliac spine, it was assumed that the mid sacrum marker was positioned vertically relative to the middle of the left and right anterior superior iliac spine on the table plane.

Before any acquisitions, the system was calibrated, including the tip of the tripod used for the palpation by pointing three known positions on the floor. Therefore, it was possible to know the position of the tip relatively to its technical frame, and therefore, the coordinates of the corresponding anatomical landmark (Figure 5.2-3). This information was after used for the reconstruction of the anatomical frames.

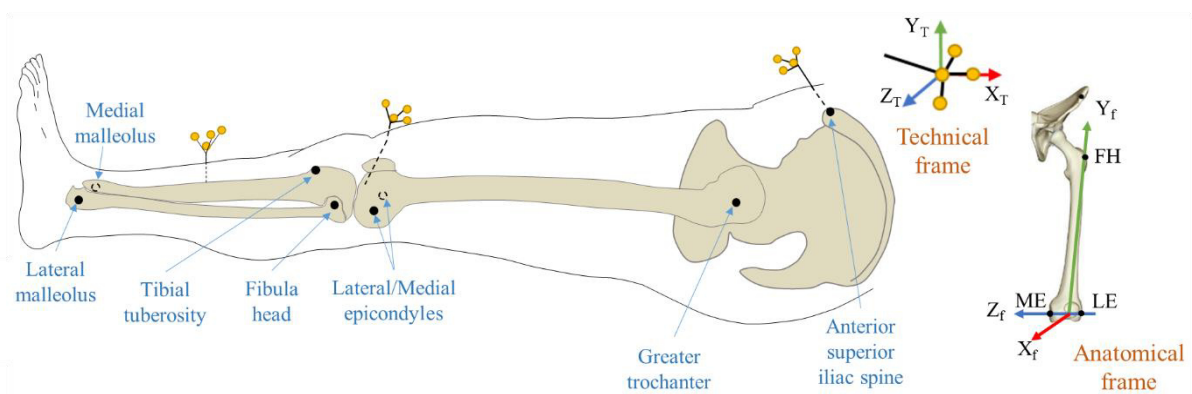


Figure 5.2-3. Diagram showing locations of the anatomical landmarks (black circles), and the reflective markers (yellow circles) on the left leg, and an example of the orientation of the anatomical reference frame for the femur. ME, LE, and FH corresponds to medial malleolus, lateral malleolus, and fibula head, respectively.

Finally, joint kinematics was calculated using an anatomical frame and Euler sequences recommended by the International Society of Biomechanics (Wu et al. 2002) using MATLAB®.

5.2.3. Passive leg movements

The studied movements were: knee flexion-extension, knee rotation performed at three knee flexion angles (0° , 20° and 50°), knee abduction-adduction performed at three knee flexion angles (0° , 20° and 50°). These movements were chosen in order to cover the possible positions of the leg during daily life activities (walking, step climbing, etc.) and stretching. All movements were applied to the leg manually.

Flexion-extension movements (*Figure 5.2-4*) were applied to cover maximal range of the angles, approximately from 0° to 120° , where 0° is dedicated to the extension and 120° to the maximal flexion of the leg.

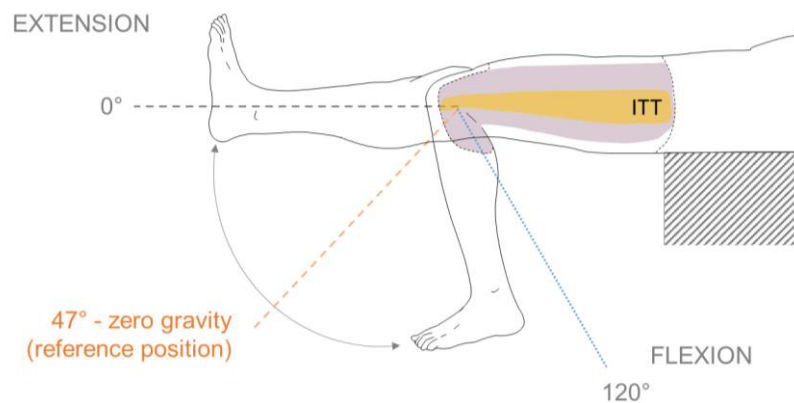


Figure 5.2-4. Lateral view of the flexion-extension movement of the left leg with identification of the iliotibial tract (ITT) and reference image of 47° , which is defining the zero-strain position.

Varus-valgus and rotation movements were applied manually at certain knee flexion angle (*Figure 5.2-5A*), correspondingly 0° , 20° , and 50° , which are approximate angles we defined and tried to keep stable during each of the movements record. Varus-valgus movements were performed by moving the tibia laterally away from the midline of the body (abduction, i.e. varus) and bringing it toward the body or across the midline (adduction, i.e. valgus). (*Figure 5.2-5B*). Rotation movements (*Figure 5.2-5C*) were made by rotating the ankle internally (medial rotation) and externally (lateral rotation) relatively to the tibia axes.

In the following, the movement will be named as varus-valgus, but the knee angles will be called adduction and abduction angles for easier understanding of the results interpretations.

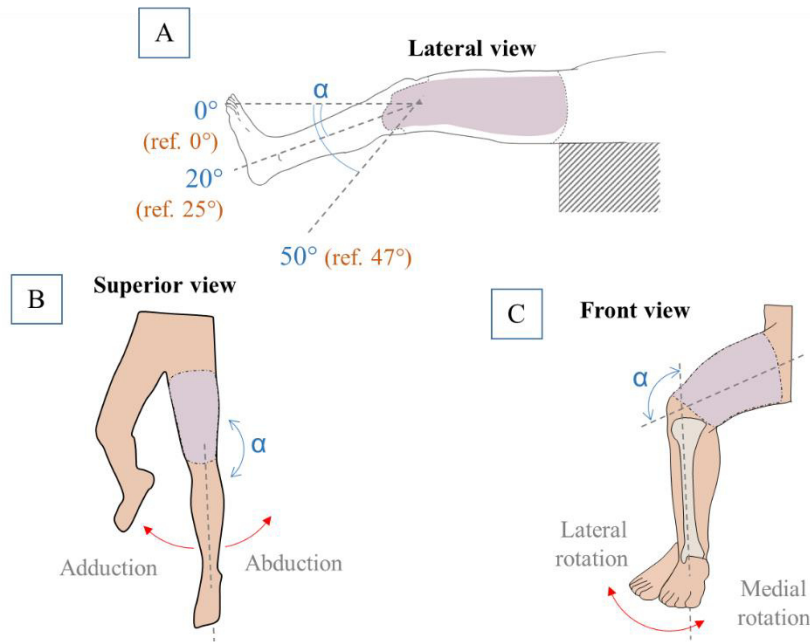


Figure 5.2-5. Schematically illustrated leg movements: (A) common lateral view with knee flexion angles identifications for both movements, (B) varus-valgus (adduction-abduction) and (C) rotation. Reference knee flexion angles are indicated in orange font.

5.2.4. Strain field measurements by DIC

DIC set-up was used to get 3D surfacic strain maps of fascia lata. This method employs stereovision and image correlation for the computations of displacement and strain fields. Thus, two Photron FASTCAM SA3 black and white cameras (Tokyo, Japan) were placed in order to capture the pie-crust area and the ITT release, what means the area approximately between the ITT tibial insertion and the middle of the thigh on the lateral side (Figure 5.2-6). For the area of interest, Sigma Macro f/2.8 objectives with lenses of 70 mm were sufficient to have good quality images with a size of 1024 px \times 1024 px.

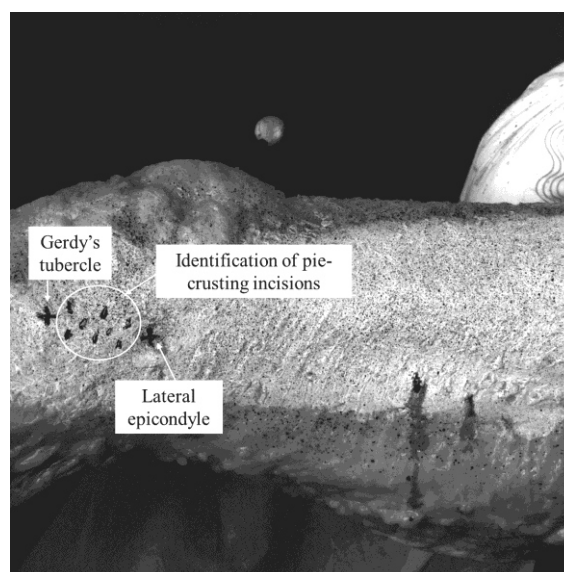


Figure 5.2-6. Example of the image recorded by Photron camera with identifications of ITT insertions and area for the pie-crusting (subject 073_L).

The frame rate for the images acquisition was chosen twice smaller than for the motion analysis, 50 Hz. This frame rate was enough for the passive movement of the leg. With a maximum closure of an aperture (f/16), the depth of field was deep and images were not blurry. The light was adjusted to optimize images quality and contrast. Cameras' views were centered on the area of interest (*Figure 5.2-6*). Calibration of cameras was made with a calibration grid adapted to the field of view with a frame rate of 5 Hz.

Data processing was made on VIC-3D 8 System software. Depending on the movement of the knee, the subset and a step for the maps' calculations were chosen to obtain the best possible strain calculations.

A specific reference image, considered as the zero strain state, was chosen for each movement analysis. For the static analysis, the reference image was the one with an extended leg (0°). For the rotation and adduction-abduction movements, when the knee was flexed at around 20° or 50° , the reference image was corresponding to the knee angle of 25° or 47° respectively (*Figure 5.2-5A*). During the flexion-extension leg's movement, the image was chosen with the knee flexed at 47° (*Figure 5.2-4*).

The angle of 47° for the knee was chosen due to the position of the body with zero gravity (Mount 2003). All reference images were taken when fascia lata was intact and the pie-crusting technique has not been applied yet.

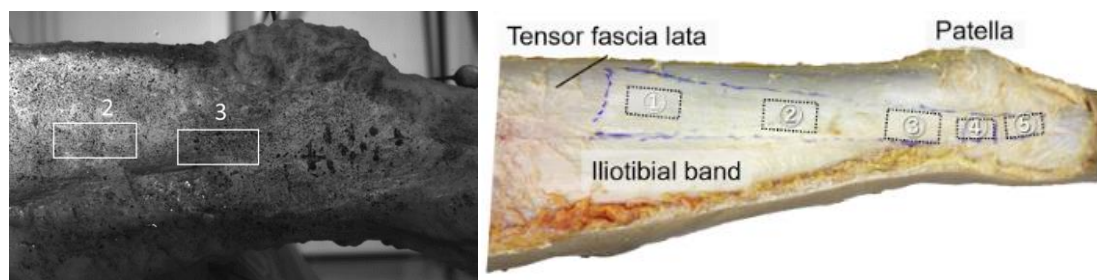


Figure 5.2-7. Lateral view of the right extended leg (subject 073) with identification of defined areas 2 and 3 on the iliotibial tract (ITT) (on the left) from the areas corresponding to those from Otsuka et al. (2020) (on the right).

In order to compare the strains locally, we defined two areas of interest on the ITT. These two areas are the areas 2 and 3, as defined by Otsuka et al. (2020) and illustrated on the *Figure 5.2-7*. Area 2 is close to the middle of the thigh, while area 3 is close to the knee and the area where pie-crusting technique was applied. The dimensions of the areas 2 and 3 are $2.5 \times 5 \text{ cm}^2$ and $2.5 \times 3.5 \text{ cm}^2$ respectively.

5.2.5. Pie-crusting Technique

On each subject and on each leg, the movement and the strain changes on fascia lata were computed for three cases studied in the following order: the initial case where no actions have been done on the ITT (case I), the second case where pie-crusting is performed on the ITT (case A), the third case where the ITT dissection from the tibial insertion was performed (case B).

Pie-crusting cuts were done with an 11-blade scalpel and located between the lateral condyle of the tibia and the lateral epicondyle of the femur as schematically illustrated on the *Figure 5.2-8A*, and as an example shown on *Figure 5.2-6* for subject 073. Number of the incisions was

varying from 8 to 9 depending on the distance between Gerdy's tubercle and lateral epicondyle, due to the variability of the height and legs anatomy.

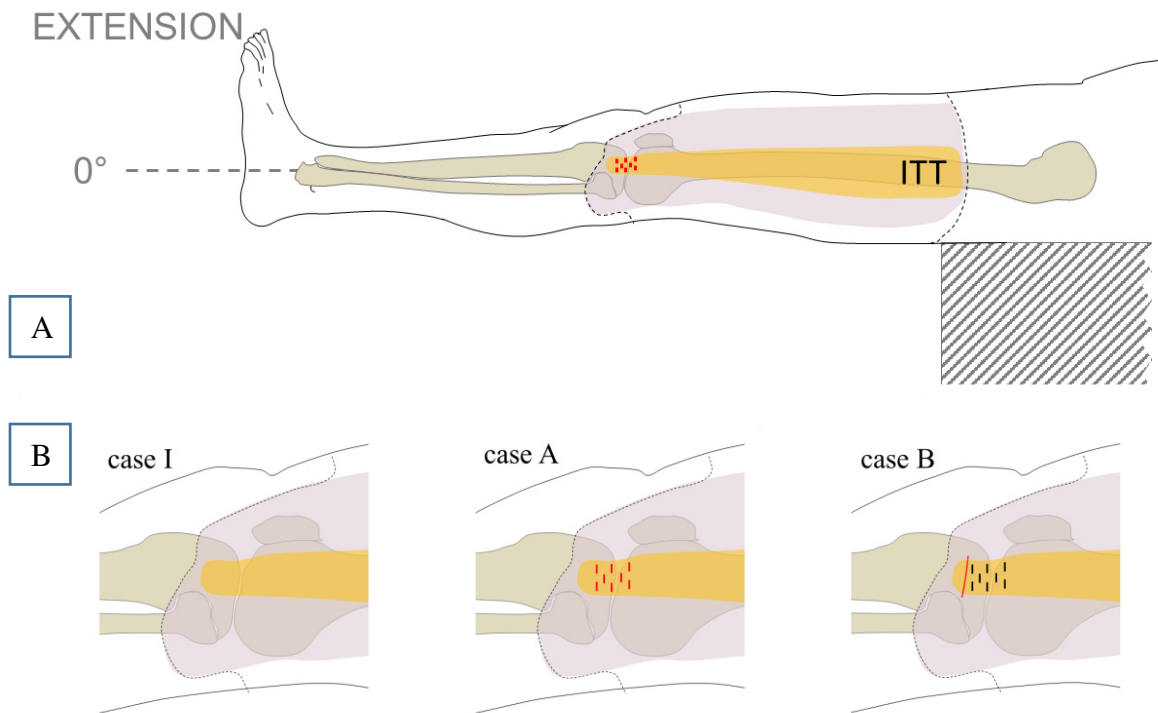


Figure 5.2-8. Illustrations of: A – leg position with identification of ITT and cuts for a pie-crusting technique in lateral view; B – identifications of: initial (case I), after pie-crusting state (case A), after ITT dissection from tibial insertion (case B).

5.3. Test Conduction

For each case, and thus after each case, a sequence of three passive knee movements was applied and recorded: knee flexion-extension, knee rotation, and knee varus-valgus, followed by static recordings of the leg after each test in a same reference position for the hip and knee angles.

The static analysis consisted in comparing the ITT strain state, from its reference strain state defined as the initial (case I) strain state before any strain release, to its average strain release after pie-crusting cuts (case A) and after a full ITT dissection of the tibia insertion (case B) (Figure 5.2-8B).

Therefore, after each strain release, a set of knee movements as described above was performed.

During each leg movements, care was taken to avoid subject contact with the experimental setup, keeping the femur parallel to the DIC system to stay in the field of the view, keeping attention to keep the same speed of the passive movements. Movements were recorded with the lateral area of the fascia lata (the region of interest is ITT and its insertion into the tibia).

The order of the leg movements performed for each subject's leg is listed in the Table 5.2-1. In total, three tests consisting of five cycles of knee flexion-extension; nine tests of 8-10 cycles of knee rotation, nine tests of 8-10 cycles of knee varus-valgus; and 22 static records, including pie-crusting and ITT dissection were performed. Cycles were applied continuously. Between

each cycle, a waiting time up to 4 minutes was observed to record the same static position of the leg. Static records were made in order to reproduce the movement with the respect to the position of the leg in the space and the distance to the recording cameras. Therefore, 86 records per subject were made and post processed for each, strain and motion, analyses. For motion analysis, and for each knee movement, the three knee angles were studied: flexion-extension angle, rotation angle, and abduction-adduction angle.

Table 5.2-1. List of the recordings corresponding to leg movements performed on each leg during the experiment.

Leg	Case	Knee movement	Knee flexion angle, °	Cycles
Left / Right	Case I	Static	0	5
		Flexion-Extension (F-E)		
		Static		
		Varus-Valgus		
		Static		
		Varus-Valgus		
		Static		
		Varus-Valgus		
		Static		
		Rotation		
		Static		
		Rotation		
		Static		
		Rotation		
Pie-crusting				
Case A	Same movements with the corresponding number of the cycles, as listed in the case I			
ITT dissection from the tibial insertion				
Case B	Same movements with the corresponding number of the cycles, as listed in the case I			
Total number of recordings for one subject per leg		Static (+ pie-crusting, ITT dissection)	22	Total: 43x2
		Flexion-Extension (F-E)	3	
		Varus-Valgus	9	
		Rotation	9	

Motion analysis and digital image correlation acquisitions were synchronized using a common trigger box sending a rising edge square signal to both systems. All the data extracted from motion analysis and digital image correlation were processed using custom-made scripts in Python.

5.4. Results

5.4.1. Static strain analysis

Strain release along the x -axis, corresponding to the thigh longitudinal axis (average E_{xx}) during pie-crusting and ITT dissection is illustrated on the *Figure 5.4-1* for the two areas of interest, defined previously as area 3 and area 2. The strains were filtered with simple moving average method with window size 7, due to a big amount of noise, especially on the area close to the knee (area 3), close to where the surgical intervention took place.

The initial zero strain corresponds to the strain state before any passive movement of the leg and the next value is the one observed after the passive movements were applied, just before any cutting action. Then, the x -axis strain was increasing each time when an incision was made, especially on the area 3, which is closer to the cutting zone. These increases may differ due to the more or less great stiffness of contact between the ITT and the blade.

After each cut during pie-crusting and dissection, the shortening along the x -axis is clearly observed on the both area 2 and 3, even if it is more evident on area 3 which is closer to the cutting zone. On the presented graphs, for the subject 219_L, the strain release along x -axis for areas 2 and 3 is respectively -0.022% and -0.034% after pie-crusting, -0.02% and -0.005% after dissection; for the subject 073_R, it is respectively 0.075% and 0% after pie-crusting, -0.02% and -0.03% after dissection.

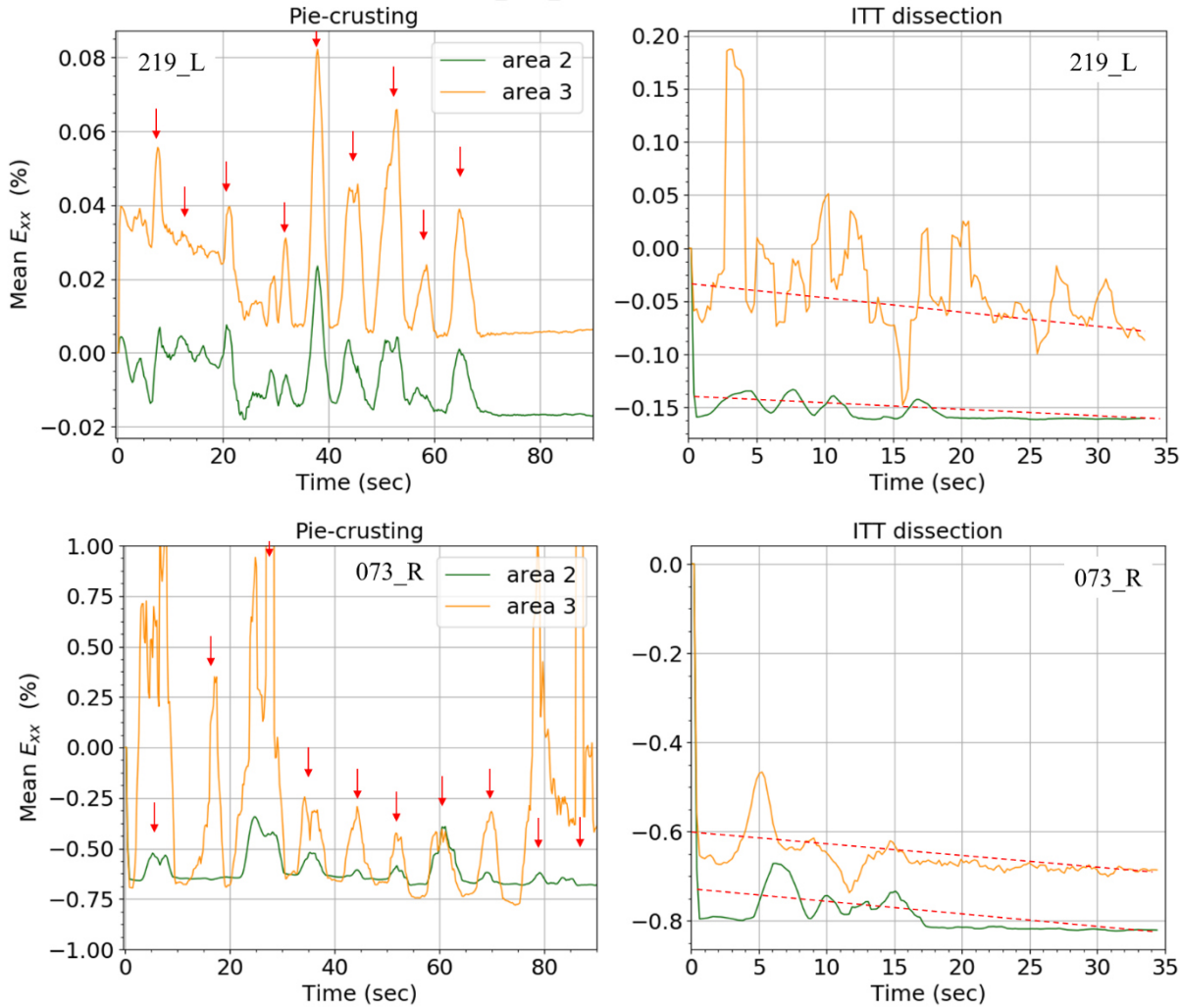


Figure 5.4-1. Subjects 219_L and 073_R x -axis strains evolutions along the time during the pie-crusting technique and ITT dissection on areas 2 (green) and 3 (orange). Scale range is the same for pie-crusting (on the left) and ITT dissection (on the right) plots.

* Red arrows indicate when the cuts were made; Red dashed lines show the behavior of the strain when the ITT is cut from its insertion on tibia.

It can also be noticed that strain values after pie-crusting were not the same as the ones just before ITT dissection, as passive movements were applied to the leg between these two cases. One may wonder what the effect of the applied movements on the ITT strain state is. We thus

looked at corresponding strain values for the case after the pie-crusting and before the beginning of the ITT’s dissection for each subjects’ leg (*Figure 5.4-2*). Hence, the E_{xx} strain on the area 2 is decreasing, suggesting that ITT is shortening, except for a subject 219_R, for which the strain is increasing. On the area 3, which is closer to the pie-crusting area, the strain is decreasing also suggesting shortening of the ITT, except for a subject 073 (both legs) and 219_R, meaning the elongation of the ITT.

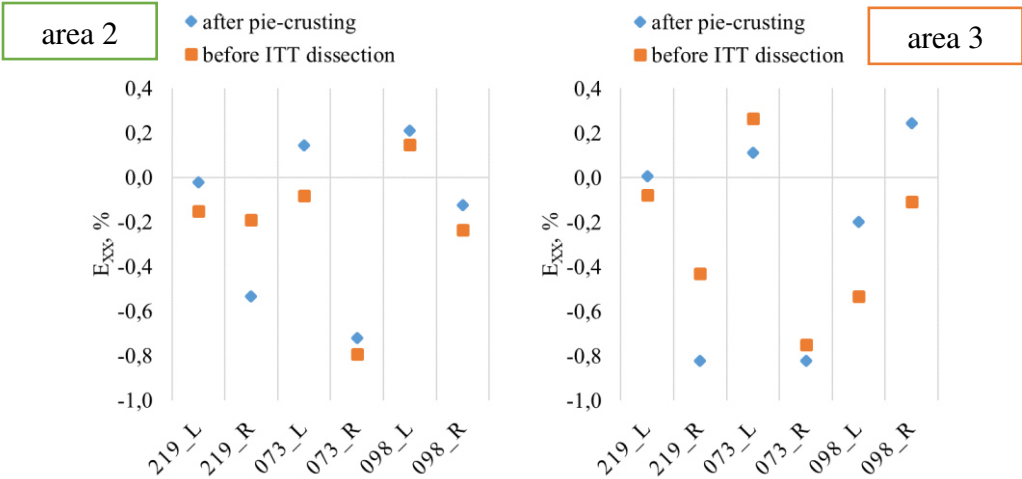


Figure 5.4-2. E_{xx} after the pie-crusting and before the ITT dissection on the areas 2 and 3 for each leg of all subjects.

On the *Figure 5.4-3A* is presented the location of three extensometers, which are used to measure a global strain of the ITT (E0 – longitudinal, E1 and E2 – transverse). This global strain is calculated as $\Delta L/L_0$, where L_0 is the initial length measured on the reference image, and ΔL is the difference between new length (L_1 – after pie-crusting, L_2 – before ITT dissection) and L_0 . For all subjects, we can see a small shortening of the ITT in the longitudinal direction and lengthening of the ITT in the transverse direction (*Figure 5.4-3B*), except for 219_R with opposite changes in the length.

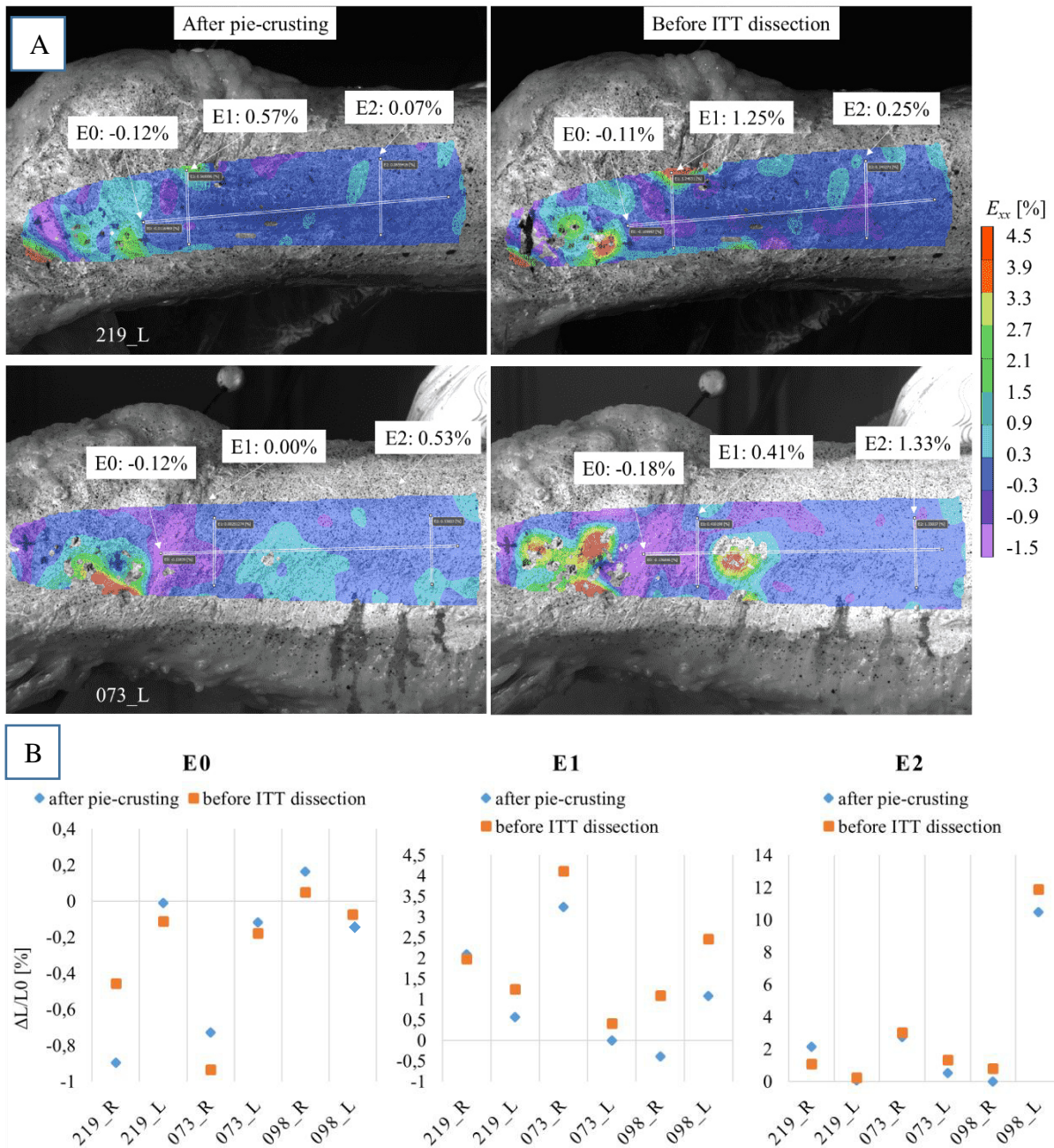


Figure 5.4-3. (A) Distribution maps of the E_{xx} strain after pie-crusting (left) and before ITT dissection (right) on the ITT from subjects 219_L (top) and 073_L (bottom) with three extensometers (white lines): E0 in the longitudinal direction of the ITT, E1 and E2 in the transverse direction of the ITT. (B) Displacement measured with the corresponding extensometer (E0, E1, and E2) for all subjects.

The average ($n=6$) values of the ratio $\Delta L/L_0$ for E0, E1, and E2 extensometers are listed in the Table 5.4-1. The ratio measured with the longitudinal extensometer E0 before the ITT dissection remained almost the same or shortened a little bit after the pie-crusting. This shortening was observed earlier with the E_{xx} strain on the local areas (Figure 5.4-2). For the transversal E1 and E2 extensometers, corresponding lengthening was around 0.79% and 0.41%, respectively. These changes of lengths are not big. Nevertheless, we see that there is an impact of the movements made between the pie-crusting and before the ITT dissection, which shorten or elongate the fascia lata. Moreover, the shortening of the ITT in the longitudinal direction and

lengthening in the transverse direction after the pie-crusting are well visible comparing the initial lengths of the reference image and the image after pie-crusting.

Table 5.4-1. Average values of the ratio $\Delta L/L_0$ measured from three extensometers with standard deviation (std), averaged for all subjects.

Extensometer	E0		E1		E2	
	average	std	average	std	average	std
after pie-crusting	-0.28	0.43	1.10	1.36	2.66	3.99
before ITT dissection	-0.28	0.36	1.89	1.31	3.07	4.43

5.4.2. Ranges of motion

5.4.2.1. Flexion-extension leg movements

It was expected that both the pie-crusting and dissection of the ITT, affect the range of the knee motion and its stability. For flexion-extension movements of the leg, an example of knee angles (flexion, rotation, and abduction angles) are presented on the *Figure 5.4-4*. The ranges were calculated as the differences between the maximum and minimum angle values, and they are illustrated on the *Figure 5.4-5*. During this movement, the flexion angle range does not seem affected by any procedure, but rotation and abduction angles are shifted and increased, which may demonstrate a lack of the knee stability.

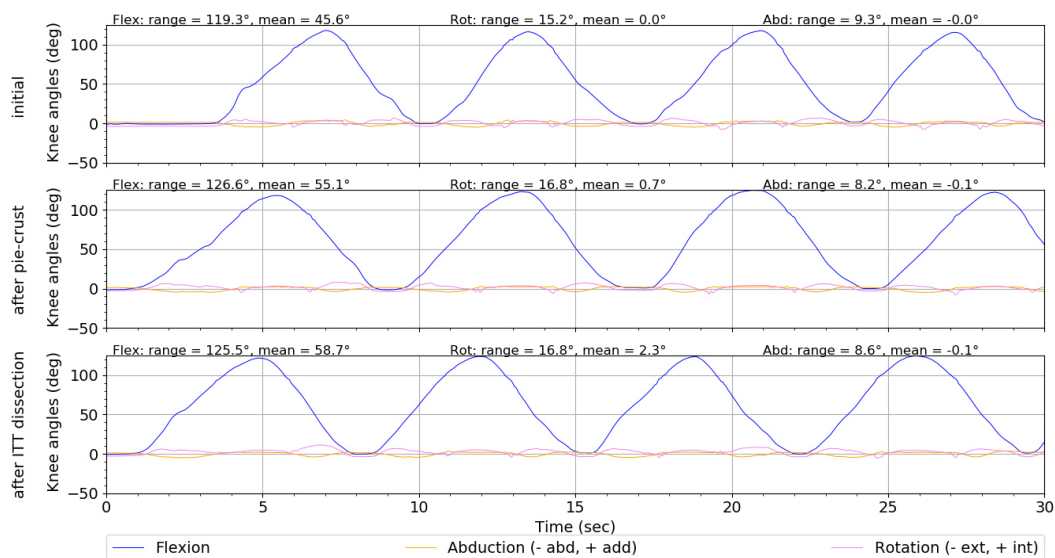


Figure 5.4-4. Subject 098_R flexion-extension movements knee joint angles with statistical data (range, mean values) during the initial, after pie-crusting, after ITT dissection cases.

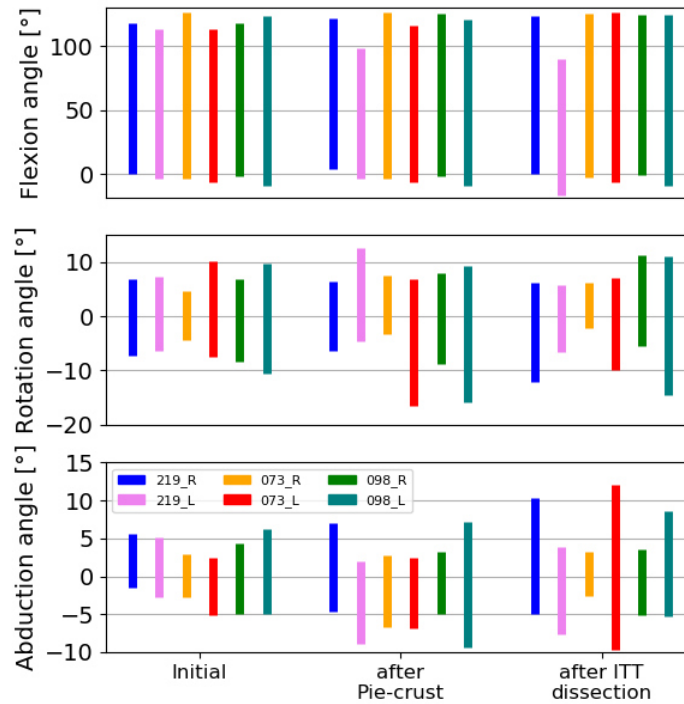


Figure 5.4-5. Flexion-extension movements knee joint angles' ranges (from the minimum to the maximum angle) for all subjects and all cases (initial, after pie-crusting, after ITT dissection from tibial insertion).

* R and L in the subject number legend identifies the right and the left leg, respectively.

5.4.2.2. Rotation leg movements

For rotation movements, an example of the knee joint angles during the movement is given on the *Figure 5.4-6*. This illustrates the range and the mean values of these angles for all subjects. Flexion angle range is a little bit varying between the subjects through the cases, due to the human factor in the passive movements, but an average mean value of flexion angle is approximately the same, meaning a good repeatability between the subjects in terms of the leg position during each acquisitions. As expected, rotation angles when the knee is flexed at 20° and 50° are higher compared to those at 0° flexion. However, abduction angles are roughly the same. This is also noticeable on the *Figure 5.4-7*.

Due to the values of the joints' angles ranges averaged for all subjects during rotation movements (*Table 5.4-2*), rotation angles after pie-crusting increased or remained the same for all the rotations. When the corresponding leg was flexed at approximately 0° and 50° the range increased from $20.8 \pm 11.5^\circ$ to $25.7 \pm 9.0^\circ$ and from 35.9 ± 8.8 to 36.5 ± 7.4 , respectively; for 20° leg flexion, the range remained almost the same, around 32°. During this movement of rotation, ranges of the abduction angle decreased after the pie-crusting by 15-25% from the average range value. This may illustrate the loose of coupling between the knee rotation and abduction due to the ITT pie-crusting.

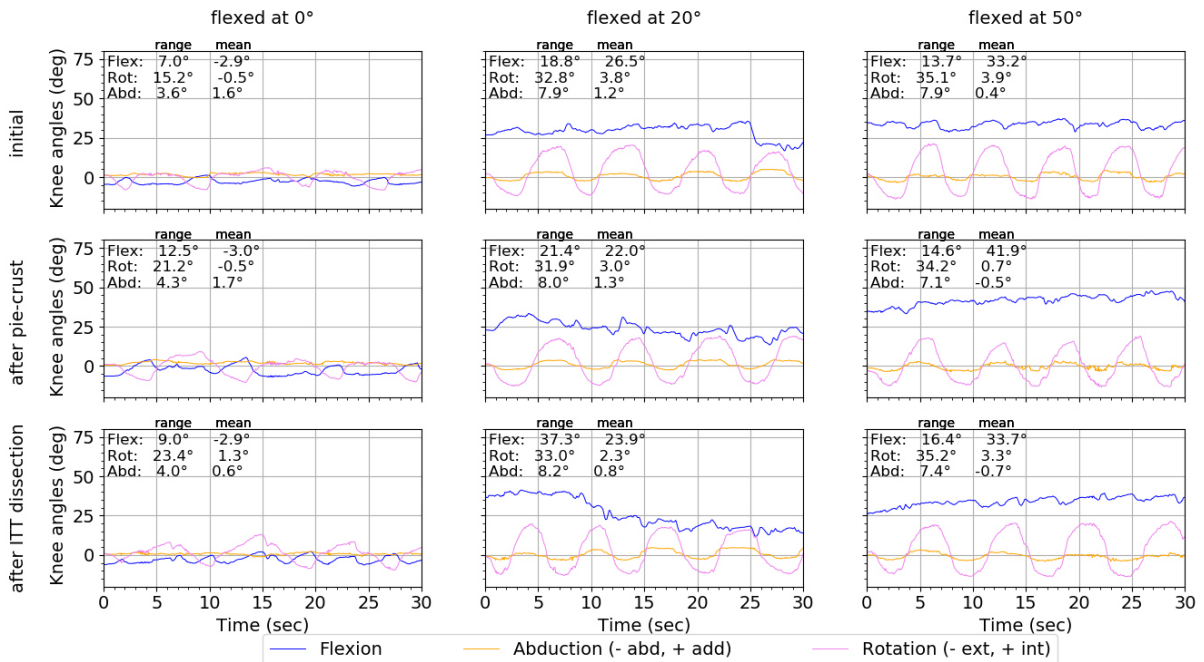


Figure 5.4-6. Subject 098_R rotation movements knee joint angles' with statistical data (range and mean values) when the leg was flexed at approximately 0°, 20°, and 50° during the initial, after pie-crusting, and after ITT dissection cases.

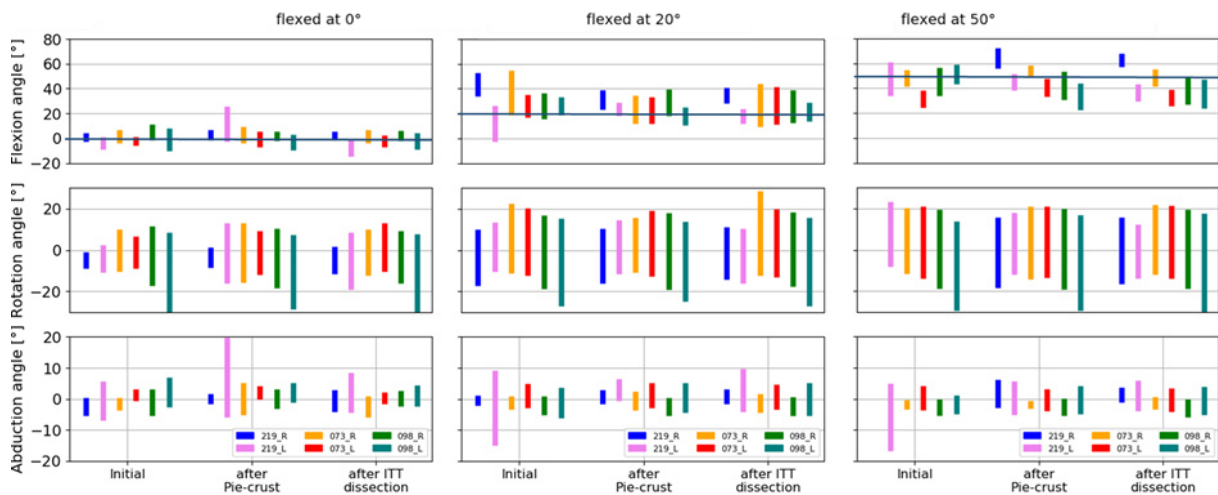


Figure 5.4-7. Rotation movements knee joint angles' ranges (from the minimum to the maximum angle) for all subjects and all cases (initial, after pie-crusting, after ITT dissection from tibial insertion) when the leg was flexed at approximately 0°, 20°, and 50°. R and L in the subject number legend identifies the right and the left leg, respectively.

5.4.2.3. Varus-valgus leg movements (abduction-adduction)

An example illustrated on the Figure 5.4-8 shows knee joint angles during varus-valgus movements for a subject 098_R. Like for the rotation movements, ranges and mean values are proposed to compare the different cases and subjects on Figure 5.4-9.

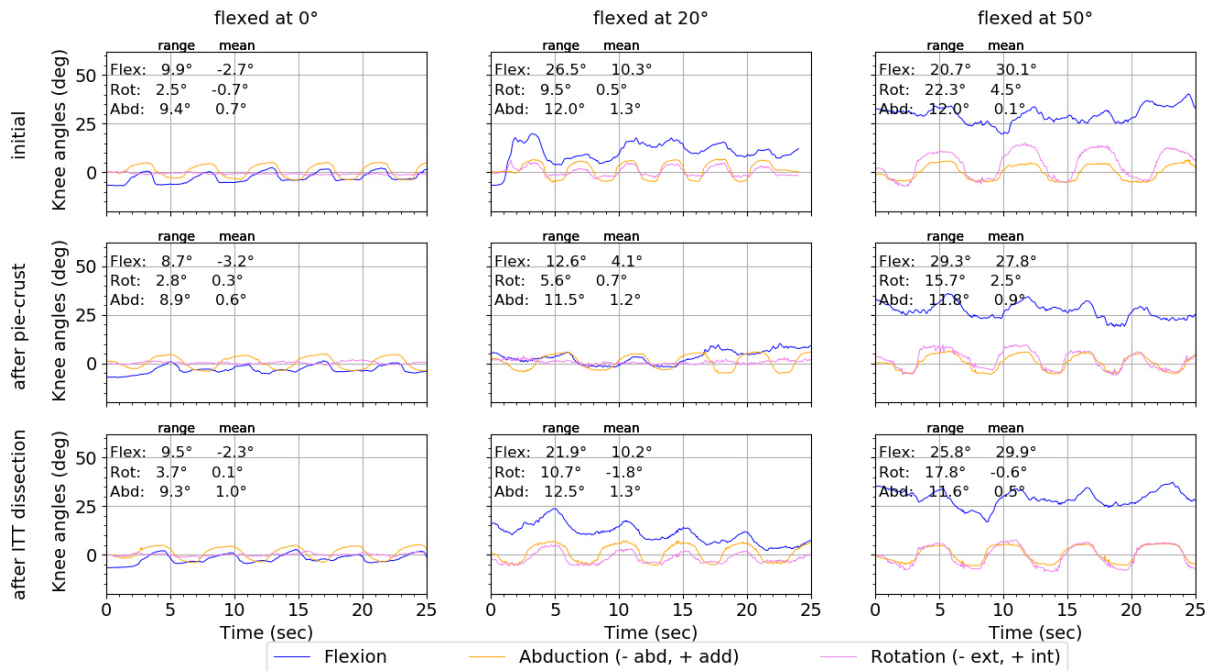


Figure 5.4-8. Subject 098_R varus-valgus movements' knee joint angles with statistical data (range, mean values) when the leg was flexed at approximately 0°, 20°, and 50° during the initial, after pie-crusting, and after ITT dissection cases.

The ranges illustrated on the Figure 5.4-9 for the varus-valgus movements during various knee flexion angles (0°, 20°, and 50°) show that, as during the rotation movements, the flexion of the knee at 20° and 50° are not reached and maintained. In average, we reach around 10° instead of 20° and around 30° instead of 50°. However, even if the expected flexion angle was not reached, the unlocking of the varus-valgus movement by flexing the knee is obtained and illustrated by large both rotation and adduction-abduction ranges for the flexed knee.

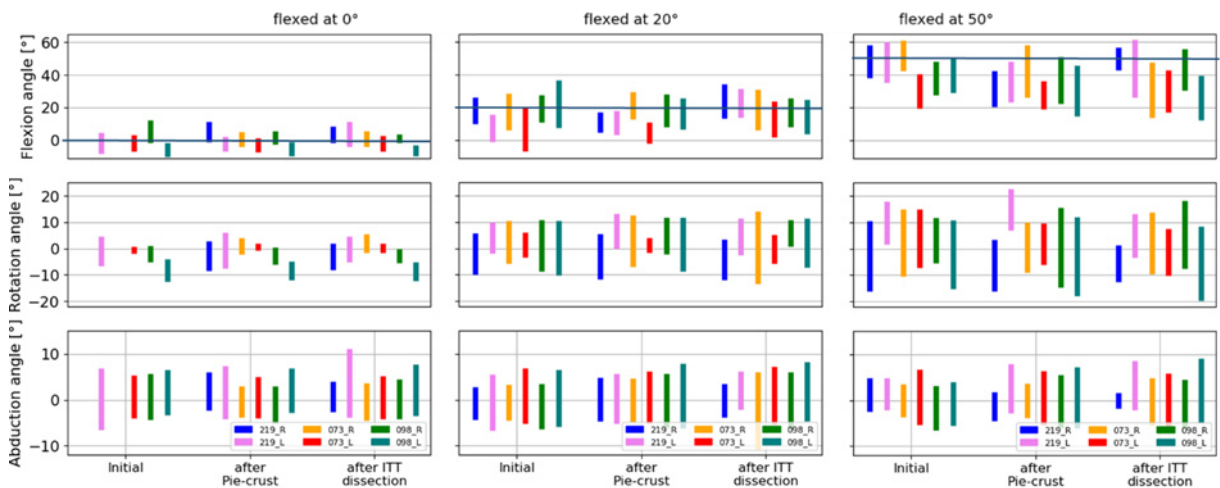


Figure 5.4-9. Varus-valgus movements' knee joint angles' ranges (from the minimum to the maximum angle) for all subjects and all cases (initial, after pie-crusting, after ITT dissection from tibial insertion) when the leg was flexed at approximately 0°, 20°, and 50°. R and L in the subject number legend identifies the right and the left leg, respectively.

During all the records, the average range of rotation and adduction-abduction angles was the same as in the initial state or close to the values after the pie-crusting, what suggests, the ITT

dissection did not have any bigger effect on the motion of the knee than the pie-crusting (Table 5.4-2).

Table 5.4-2. Ranges of joints' angles (rotation and abduction) averaged from all the subjects corresponding to rotation and varus-valgus movements when the knee was flexed at approximately 0°, 20°, and 50°.

* Cases I, A, and B corresponds to the initial, after pie-crusting, and after ITT dissection from the tibial insertion, respectively.

Case	Joint angle	Rotation			Varus-valgus		
		0°	20°	50°	0°	20°	50°
I	Rotation	20.8	32.6	35.9	7.2	15.6	22.4
	Abduction	7.4	9.2	8.8	10.8	10.2	8.8
A	Rotation	25.7	31.1	36.4	7.9	15.1	21.7
	Abduction	9.4	6.8	7.4	8.9	11.2	10.2
B	Rotation	25.1	34.1	35.5	7.2	16.1	20.9
	Abduction	7.1	8.2	6.8	9.8	11.7	10.1

5.4.3. Strains after movements

To evaluate the evolution of the strain release on the ITT after different movements and surgical interventions, the graphs with the average values of E_{xx} on area 2 and 3, for every static record after the leg movement are plotted on the *Figure 5.4-10*. Two vertical dashed red lines indicate the static position of the leg respectively after pie-crusting procedure and before the ITT dissection on the areas 2 and 3. Some static records for the subject 219 for both legs are missing; nevertheless, we still can see the overall picture of all the strains during the performed movements.

First, a difference of the strains between the subjects and even between the legs within one subject is visually noticeable (*Figure 5.4-10*). Each time after the flexion-extension movement the E_{xx} strain on both areas decreased (except for the leg 098_L on area 2).

From these results, it is difficult to highlight clear trends. The pie-crusting technique, the ITT dissection and the movements are modifying the strain states on the measured areas 2 and 3, but these changes are small and difficult to interpret.

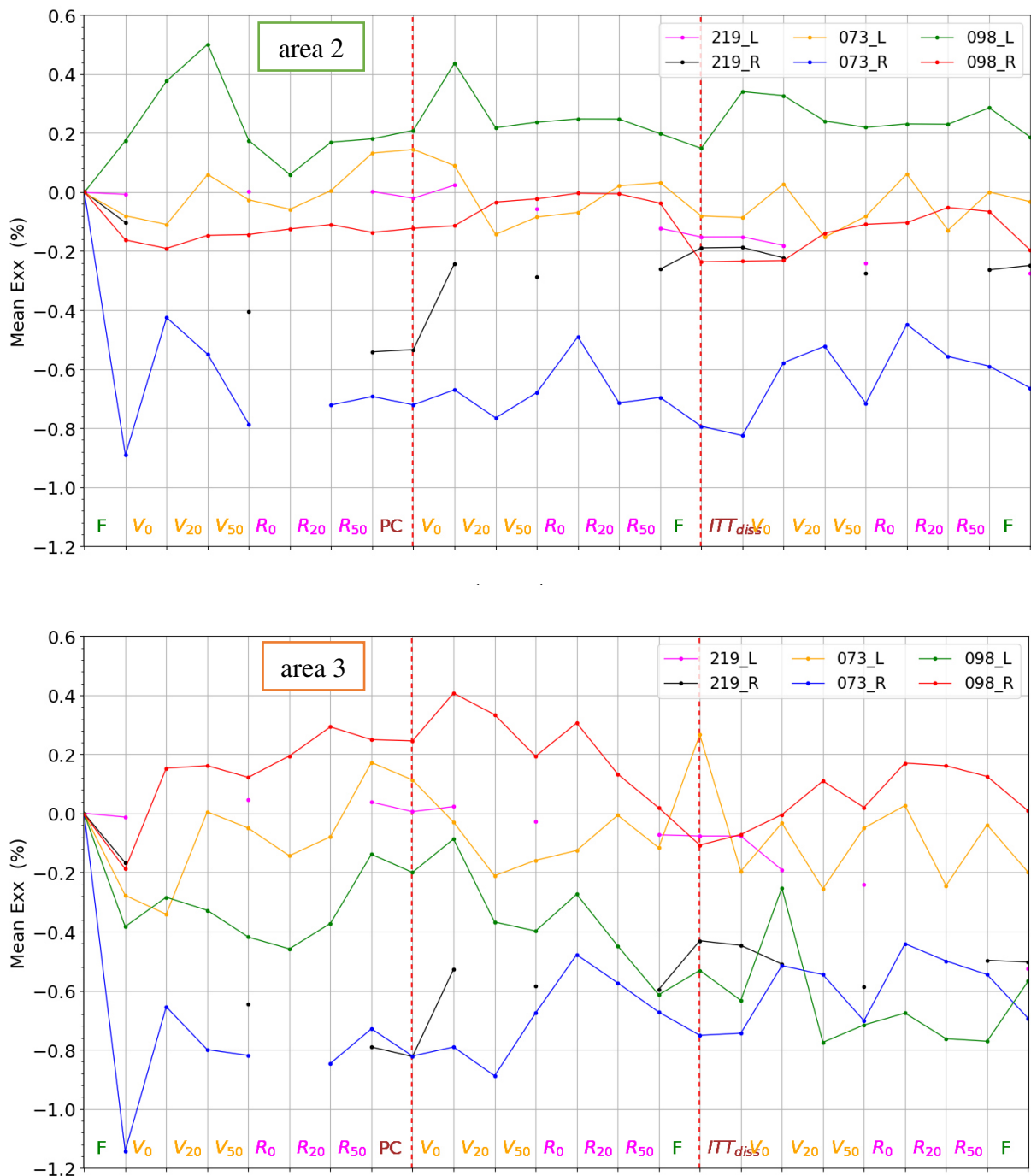


Figure 5.4-10. Comparison of the average Exx along the static extended positions of the leg between subjects on the areas 2 (top) and 3 (bottom). Dashed red vertical lines indicate the strains after pie-crusting (PC) and before the ITT dissection (ITT diss). F – flexion, V₀/R₀, V₂₀/R₂₀, V₅₀/R₅₀, correspondingly, varus valgus/rotation when knee is extended (0°), flexed at 20° and 50°.

5.4.4. Strain mechanisms during movements

5.4.4.1. Strain along the thigh

5.4.4.1.1. Leg flexion movement

For the flexion-extension movement, an example of the x -axis strain (E_{xx}) along time and along flexion angle is illustrated on the *Figure 5.4-11*, for both areas 2 and 3. The strain level is decreasing on both areas after the pie-crusting, remaining higher on the area 3 than on the area 2. After the ITT dissection it continues to decrease on the area 2. As expected, with the maximum flexion, the strain is increasing in absolute value, however, not clear is its negative sign, as it means that the fascia lata is shortening on the measured area.

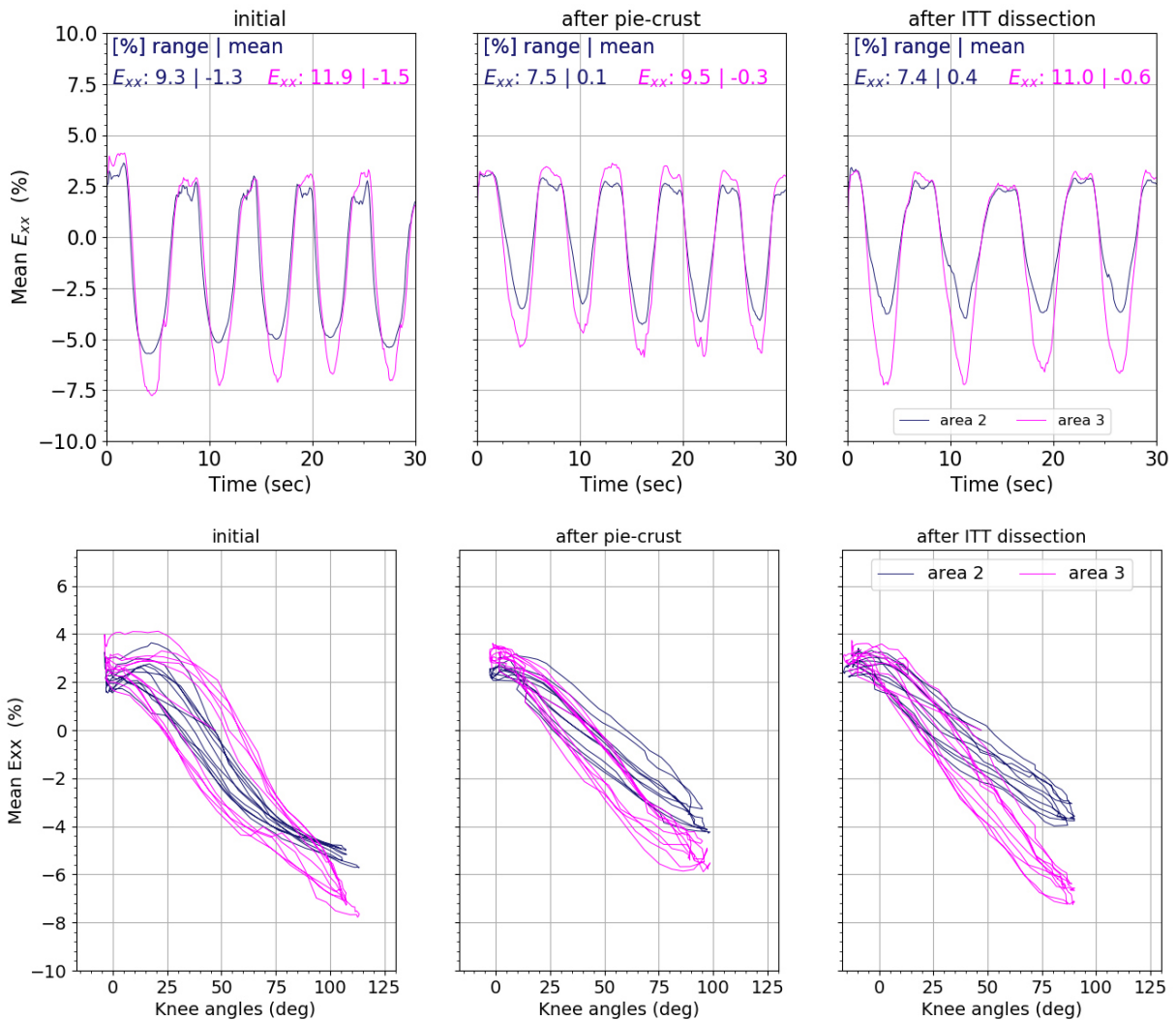


Figure 5.4-11. Subject 219_L mean E_{xx} strain along time (top) and along flexion knee angle (bottom) during leg flexion movements on both areas. The curves in blue color are representing the results on the area 2, and the curves in magenta color are representing the results on the area 3.

Averaged ($n=6$) maximum and minimum values of the E_{xx} strain on the areas 2 and 3 are listed in the *Table 5.4-3*. The changes in minimum and maximum values are not big, however, we

can conclude, that maximum strain corresponds to the extended leg, and minimum to the flexed leg.

Table 5.4-3. Average and standard deviation (std) of maximum (max) and minimum (min) values of the E_{xx} strain from all subjects during flexion-extension movements for all cases.

* Cases I, A, and B corresponds to the initial, after pie-crusting, and after ITT dissection from the tibial insertion, respectively.

E _{xx} [%]	area 2				area 3			
	average max	std max	average min	std min	average max	std max	average min	std min
I	2.7	2.9	-5.5	1.0	4.5	4.5	-7.5	3.2
A	2.5	2.9	-5.0	0.9	4.5	4.8	-8.5	4.1
B	3.2	2.8	-4.5	1.7	4.4	4.1	-8.1	3.4

5.4.4.1.2. Leg rotation and varus-valgus movements

Figure 5.4-12 illustrates an example of the evolution of the average strain E_{xx} , the strain along the x -axis of the image, corresponding to the leg longitudinal axis, during all leg rotation movement on the two areas of interest. For these rotation movements of the leg, the fascia lata is stretching or shortening, showing respectively positive or negative value of the strain along x -axis. As area 3 is located closer to the knee and to area of the pie-crusting, the strain reaches higher values compared to strain on area 2.

The average range and mean values of E_{xx} strain on the two areas of interest were calculated as the average from the corresponding test and area of each subject (Table 5.4-4).

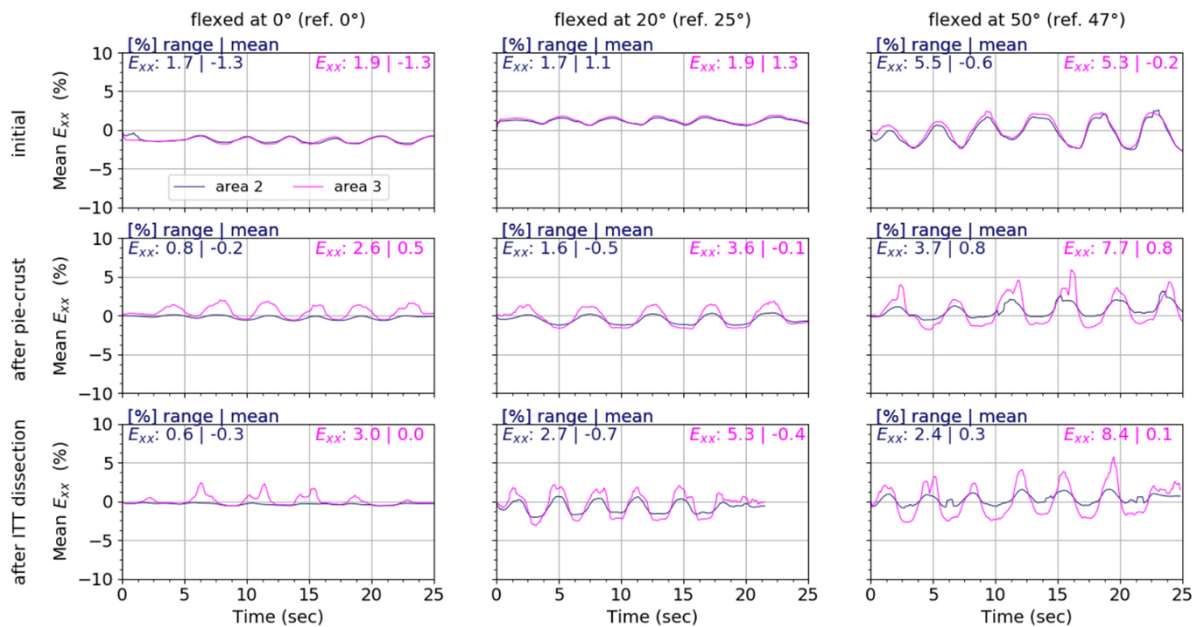


Figure 5.4-12. Knee rotation movements for leg 2019_L : mean value of x -axis– strain (E_{xx}) along the time on the area 2 (mid-thigh) and area 3 (closer to the pie-crust zone)s that are closer and further from the pie-crusting and ITT dissection, corresponding to area 3 (magenta) and area 2 (blue).

The biggest noticeable difference in the E_{xx} strain range after the pie-crusting we observe during rotation and varus-valgus movements with 50° flexion, correspondingly 1.28% – 1.86% and 0.45% – 0.84% (Table 5.4-4). After the ITT dissection, strain range is close to the one observed after the pie-crusting for all the movements configurations. The average mean value of the strain E_{xx} changed, either it gets higher, either smaller, but the difference in value did not exceed more than $0.83 \pm 0.59\%$ of the initial strain (strain during case I).

Table 5.4-4. Average of the E_{xx} strain range and mean values from all subjects during rotations and varus-valgus movements with varying knee flexion angles for all cases.

* Cases I, A, and B corresponds to the initial, after pie-crusting, and after ITT dissection from the tibial insertion, respectively.

Case	Knee flexion angle [°]	Rotation				Varus-valgus			
		area 2		area 3		area 2		area 3	
		range [%]	mean [%]	range [%]	mean [%]	range [%]	mean [%]	range [%]	mean [%]
I	0	2.26	-0.51	2.74	-0.65	2.37	-0.61	2.65	-0.68
A		1.93	-0.38	2.65	-0.42	2.27	-0.22	2.53	-0.34
B		2.00	-0.59	3.03	-0.71	2.50	-0.09	3.65	-0.30
I	20	3.19	0.06	5.85	-0.04	3.46	0.35	3.80	1.04
A		3.03	-0.27	5.42	-0.11	3.71	0.49	4.27	0.75
B		3.44	-0.40	6.42	-0.47	3.43	0.05	4.62	0.48
I	50	4.82	-0.29	7.04	-0.16	4.95	0.60	5.20	0.95
A		6.10	-0.60	8.90	-0.93	5.40	0.65	6.04	1.22
B		6.61	0.60	9.14	-0.21	5.68	0.00	7.24	0.28

5.4.4.2. Principal strains

5.4.4.2.1. Leg flexion movement

Principal strains distribution during flexion-extension movements are illustrated on the Figure 5.4-13 for area 2 and 3 for the subject 219_L, for the different cases. As for the E_{xx} strain, the principal strains on the area 3 are higher than on area 2. The E_1 strain is increasing and the E_2 strain in absolute value is decreasing after pie-crusting technique was applied on the area 3 with the difference around 3% and 2%, respectively. There is almost no change in strain values after the ITT dissection. Comparing the shear maximal strain from the areas to the same strain on the whole ITT (CHAPTER II), there is also a strain mechanism close to pure shear strain situation for the area 2, which is further from the area of the incisions.

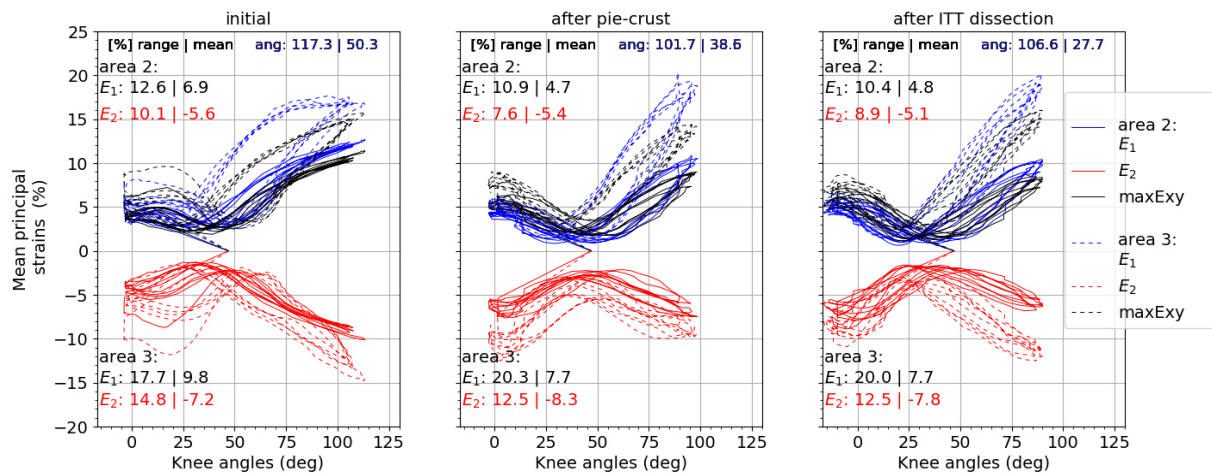


Figure 5.4-13. Subject 219_L principal strains and maximal shear strain distributions with the knee flexion angles during flexion-extension movement for areas 2 and 3. Bold and dashed lines are corresponding to the strains from the area 2 and 3, respectively. In blue – minor principal strain E_1 , in red – major principal strain E_2 , in black - maximal shear strain $maxE_{xy}$. The range and mean values of corresponding strain and of angles is on the top of the graphs.

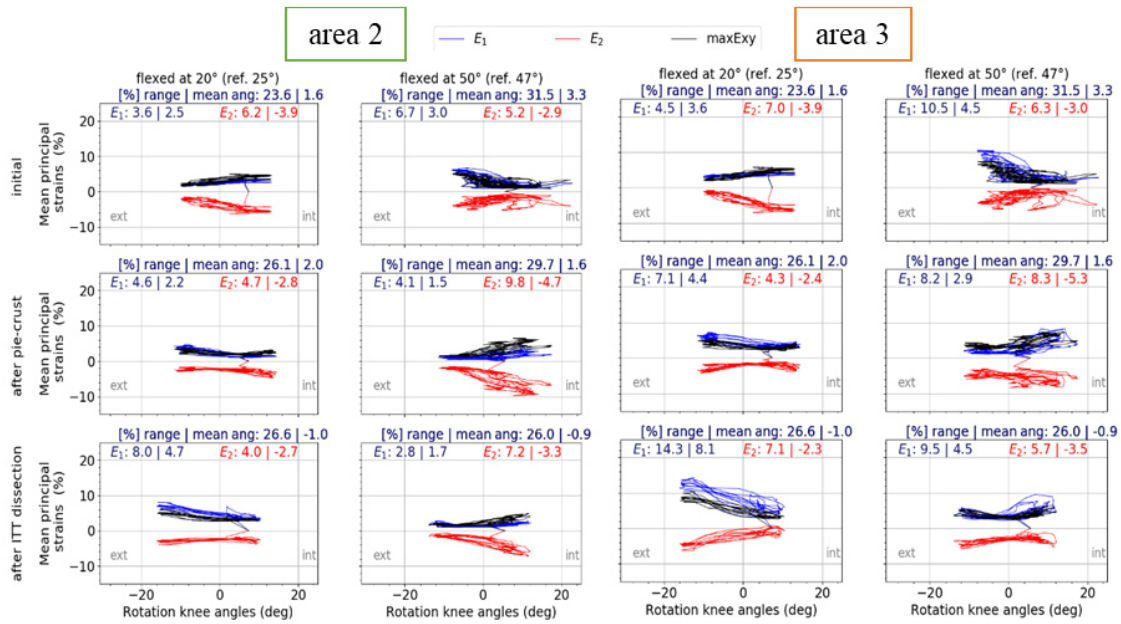
5.4.4.2.2. Leg rotation and varus-valgus movements

Because rotation and varus-valgus movements at 0° knee flexion were hard to perform, the corresponding rotation and abduction angles were not changing that much, we decided to remove the illustrations of the strains for these particular movements.

The examples of principal strain distribution along the rotation and adduction angles, respectively for rotation and varus-valgus movements are presented on Figure 5.4-14. For both movements, maximal shear strain $maxE_{xy}$ is almost overlapping the values of major principal strain E_1 , suggesting similarity of the major and minor strains in absolute values, and presence of shear strain mechanism. Although, the maximal shear strain is decreasing in value with the application of the pie-crusting and ITT dissection, especially, it is visible on area 3 (Figure 5.4-14), meaning that the area close to the knee is under tension in the principal direction and that the associated compression is higher in absolute value.

Nevertheless, the results of principal strains presented in the APPENDIX III suggests that during rotation movements, after both the pie-crusting and the ITT dissection, the minor E_2 strain range has increased from the initial strain level for areas 2 and 3. When the maximum average E_1 strain range did not change significantly neither for case A, either for case B. The only increase was for the rotation movement at 20° knee flexion angle after the ITT dissection for both areas of interest (by up to 30% from the initial value of E_1). As a result, the average on all the subjects mean value of E_2 has increased by 2.5 times for the area 2, and by 3.5 times for the area 3 from the initial value of corresponding initial strain. The highest strains levels were reached for the rotations with 20° flexed knee.

Rotation



Varus-valgus

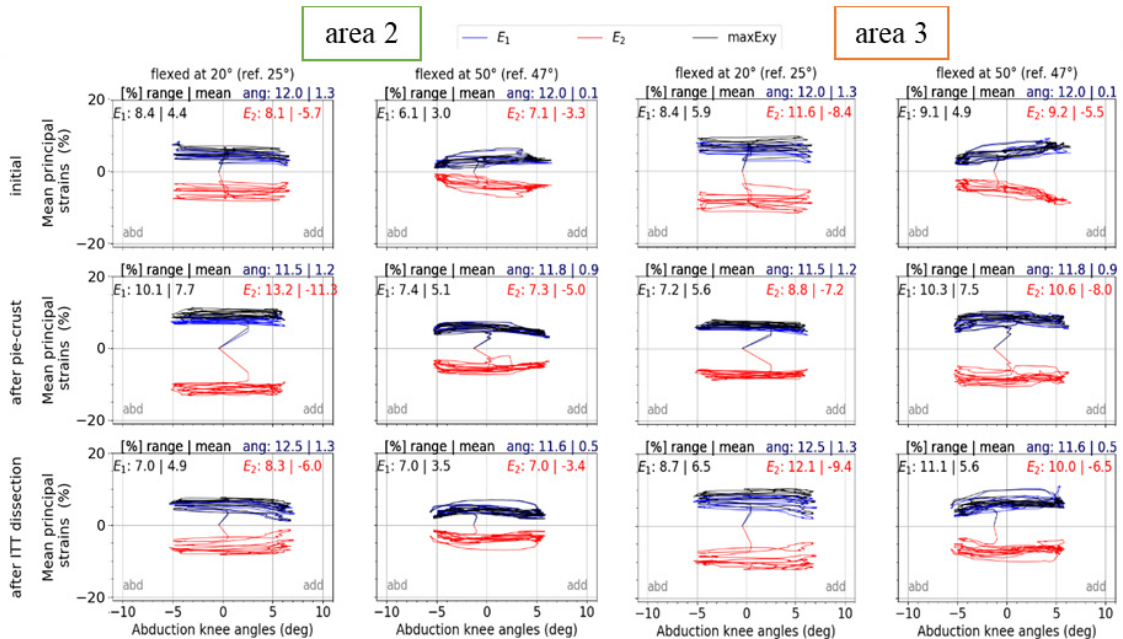


Figure 5.4-14. Average maximal shear $maxE_{xy}$, principal major E_1 and minor E_2 strains change with the rotation and adduction-abduction knee angle during subject 219_L rotation and subject 073_L varus-valgus movements, respectively. Rotations and varus-valgus movements with different knee flexion angles (0° , 20° , and 50°) for initial, after pie-crusting, and after ITT dissection cases on the areas 2 and 3 along the ITT.

* E_1 – maximum principal strain (blue), E_2 – minimum principal strain (red), $maxE_{xy}$ – maximal shear strain (black).

Even if the value of the minor strain increased after the pie-crusting and after the ITT dissection, its absolute value is remaining lower than the value of major strain. However, the E_2 strain in absolute value is almost equal to the E_1 strain during rotations with 50° flexed knee and after ITT dissection, what suggests that fascia lata is close to pure shear state at this case. This also

may be visible on the *Figure 5.4-15*, where the E_1 strain is superior to the E_2 strain in absolute value.

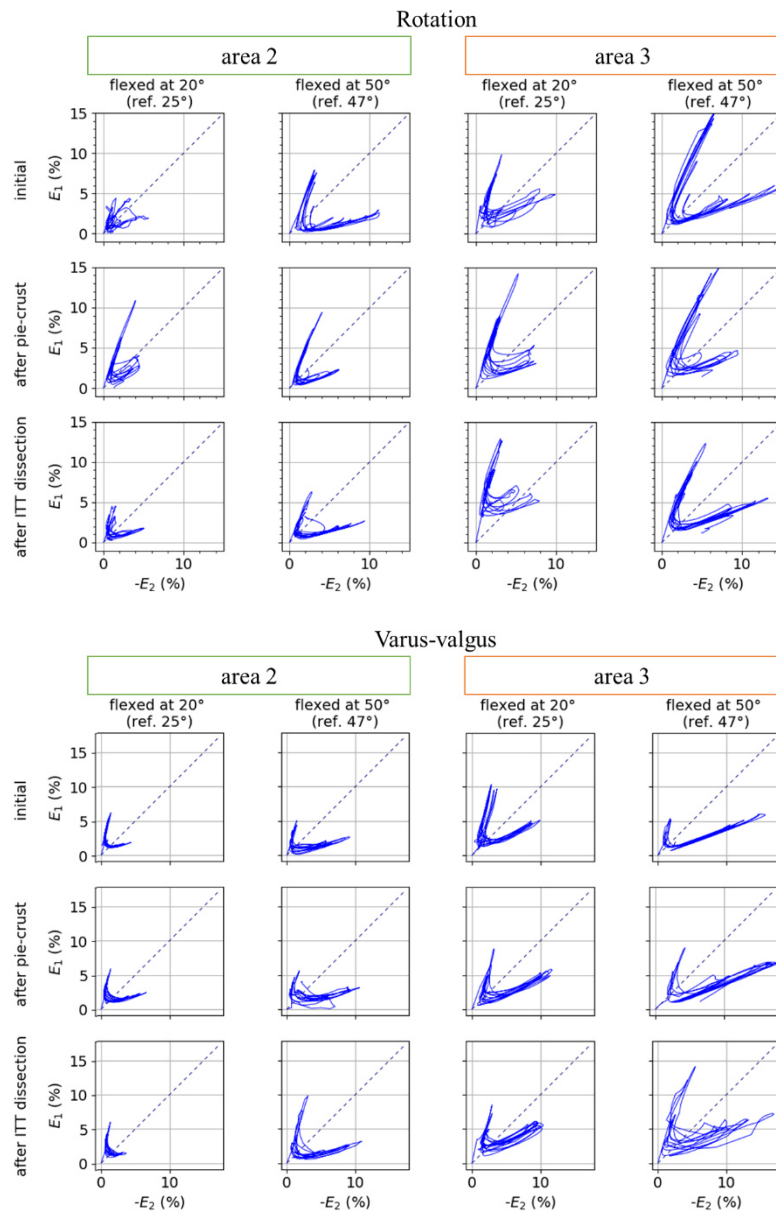


Figure 5.4-15. Subject 098_R E_1 strain against E_2 strain in absolute value during rotation and varus-valgus movements with flexed knee at 0° , 20° , and 50° along the areas 2 and 3 on the ITT.

During varus-valgus movements, the same behavior of minor and major strains as during rotation movements can be observed (APPENDIX III). The average range of the E_2 strain is increasing after the pie-crusting by 3.5 times and by 4 times from the initial range for area 2 and area 3 respectively. After the ITT dissection, strains continue to increase, accordingly, by 4.3 times and by 3.8 times. The E_1 strain decreased in some cases of the varus-valgus acquisitions on maximum of 10% from the initial range value and in the others, increased maximum by 1.5 times.

The pie-crusting and the ITT dissection increased the values of E_2 strain making it superior to the E_1 strain during varus-valgus movements (*Figure 5.4-15*). The maximal shear strain, like

for the rotation movements, shows close to pure shear strain state after both the pie-crusting and the ITT dissection.

5.5. Discussion

We conducted an *in situ* experiment on three subjects to highlight the effect of the pie-crusting technique on the ITT and of the ITT dissection on the knee movements, and on the strain states on the ITT in two specific areas. The main results are discussed afterwards.

The long experimental protocol may lead to the dryness of the tissue, what will make it more difficult to see and measure strain release. Even if we do not evaluate the mechanical parameters, such as Young's modulus, the loss of water may change the properties of the fascia lata, and thus its strain release mechanisms. In addition, in order to measure the strains on the fascia lata surface, we used the black dot pattern, which is created manually, and the measurements will depend on the quality of these speckles and the light that will create minimal reflection from the covered pattern.

Another limitation of this study, as for the one described in the chapter II, is the limited number of subjects, their age, and anthropometry. In the current study, tested subjects were old and therefore, the muscular volume was very poor. Soft tissues are not as elastic as in the younger population. Old subjects are also not representative of what can happen on young patients suffering from ITBS, but can be close to what is experienced by patients who need knee arthroplasty. Although, we did not have any information about the prior diseases or pathologies of subjects that may affect the experimental interest.

Although leg movements were done manually, we got quite good reproducibility between tests and subjects. We detected an effect on strain levels of the pie-crust incisions and ITT dissection, even though these strain values were very small. These values are smaller than expected and may be difficult to interpret, but to the best of our knowledge, this is the first study that investigates the strain release by applying pie-crusting technique on the fascia lata, and further investigations are required.

We assumed that applied movements after the pie-crusting had an influence on the strain release, and less after the ITT dissection, except for the area close to the knee, where the major principal strain increased. However, it is hard to highlight the movement that induced the most strain release by analyzing the strain during movements.

Strain mechanisms observed in chapter II on the whole ITT, were also observed in this study on smaller areas. Pure shear was also observed for rotation and varus-valgus (i.e. abduction-adduction) movements. Pie-crusting and ITT dissection didn't change these mechanisms except strain levels were higher than before performing these surgical techniques.

Changes in range of motion after pie-crusting or after ITT dissection couldn't be interpreted due to small values, as well as overall changes in measured strain levels. Nevertheless, the strain levels on the area closest to the knee were higher compared to those farther along the ITT.

ITT shortening in the area above the knee may suggest that its overall stiffness has decreased, but it was not possible to assess this parameter. In order to evaluate the changes in the knee stiffness it is necessary to evaluate the load applied to move the leg. This might be done by performing the test on an ergometer, with controlled applied load on the leg.

In order to evaluate the strains the main issue is to choose the zero strain state. Therefore, reference images were chosen closer to the leg flexion angle during the movement, for example, if the leg was extended, reference image was chosen with knee flexion angle at 0° . For the flexion-extension movement, the reference image was with the knee flexed at 47° , because this angle corresponds to zero gravity position of the human body. Further analysis is needed to compute the strains with several reference images to see, which one can give the best possible interpretation of the results. A good knowledge of the minimal and maximal strain state of the ITT according to the leg posture could also help surgeons to choose the best posture for an efficient pie-crusting during the surgical procedure.

To conclude, the measured strains are very low and the areas of the interest may be small, that may explain the lack of accuracy to observe tendencies. The variabilities of the subjects' fascia lata, applied passive movements, and surgical actions may bias too much the strain measurements.

Nevertheless, further work and improvement of the protocol can help to better interpret the effect of the pie-crusting and caused strain release. It is important to study the strains with connection to the knee movements, as ITT has a role in stabilizing rotation during knee flexion (Matsuda, Lustig, and van der Merwe 2017). It is also responsible for the stability of the lateral compartment of the knee (Kaplan 1958; Evans 1979). Moreover, it was found that the ITT's forces can affect knee kinematics (Kwak et al. 2000), and its tension affects patellofemoral and tibio-femoral kinematics (Merican and Amis 2009).

CONCLUSIONS

The objective of the presented work was to analyze the mechanisms of the fascia lata's deformation during various leg movements and to associate them with the kinematics of the fibers, in order to contribute to a more realistic modeling of the fascia lata in finite element models of the lower limb. Moreover, the problem of natural pre-tension of the fascia lata is particularly important in knee pathologies and corrective surgery. A particular case of surgical correction of ITT pre-tensions by pie-crusting technique was addressed *in situ* by quantifying strain release and analyzing its impact on knee mobility and on the mechanism of ITT deformations.

First, an *in situ* study was carried out to analyze the mechanisms of deformation of the fascia lata during knee flexion-extension movements. We associated the measurements of the knee joint angles during the motion to the measurement of the surfacic strain fields of the fascia lata separated by three regions: anterior, lateral (between anterior and ITT) and ITT. We observed different strain mechanisms depending on the region of the fascia lata. When the leg is extended or flexed with the knee flexion angle between 0° and 47° , the ITT is under a large transversal compression. When the knee flexion angle is higher than 47° , we observe mainly longitudinal tension and also pure shear with principal strains along the bisector of the two collagen fiber networks. For the anterior and lateral fascias, in most cases, we observed a high tissue transversal compression. The maximum average major principal strain values were 3.5%, 10%, and 12% respectively on the anterior fascia, lateral fascia, and ITT. Strain rates were depending on knee angle, but average maximum values did not exceed 11.2%/sec, considering all tests and both strains.

During this study, different strain mechanisms were observed, with a behavior close to pure shear on the ITT with principal strains along the bisector of the two collagen fiber networks, and sometimes a large transversal compressive strain compared to the tensile one. From these findings, we can wonder what are the origins of these mechanisms. One assumption is that it can be explained by the microstructural arrangements of the fascia lata collagen and elastin fibers, and the movements of these fiber networks. Therefore, the pure shear may illustrate the deforming of this kind of fibers frame and the large transversal compression may be due to buckling of transversal fibers. Therefore, when performing tests in isolated samples, the tissue had to be tested by considering the direction of the fibers and the direction of the applied load.

We observed a change in the strain mechanisms when the knee flexion angle was higher than 47° , which was considered as a reference image, i.e. zero strain state. This knee flexion angle corresponds to the zero gravity position of human body. Hence, other knee positions may be used for the definition of the zero strain in order to see if the shear strains will be present and how much similar results we can expect. Probably, the reference image should be personalized, considering the possible injuries and diseases at the knee level that could affect the ITT strains.

This *in situ* approach implies the dissection of the skin and adipose tissues followed by passive leg movements. In these conditions, we are far from the *in vivo* state. Nevertheless, it offers precious data for the first validation of a FE model and, in further work, it could be associated with a methodology applicable *in vivo* before dissection, such as ultrasound elastography.

To complete this first analysis and observe strain mechanisms, an *ex vivo* study was carried out to quantify stress-strain behavior of fascia lata samples and to analyze collagen fibers kinematics under loadings inspired from the *in situ* experiments. We choose to perform large band test, named “pure shear test” in the literature and bias extension test, by applying the load to the bisector of longitudinal and transverse fibers networks. During bias extension tests, we measured strain field and main fibers orientations on both sides of the sample in order to see if the layers are sliding above each other, and how they deform during the loading.

During bias tests, the strains distributions from both sides within the sample were not identical, however with similar strain levels. It can support the hypothesis of sliding layers or can be explained by different kinematics of the two networks of fibers located in different layers. The sample taken from the posterior site of fascia lata showed particular distribution of the strain, such as composite materials during bias test (Boisse et al. 2017), we suppose this is due to almost identical proportions of two networks of collagen fibers on the posterior fascia lata. The nominal stress at 10% stretch during bias test and at 8% stretch during large band test was respectively 1.38 – 2.15 MPa and around 1.6 MPa.

Large band tests or “pure shear test” demonstrated a minor strain close to zero. These loading conditions are different from the shear strain mechanisms observed *in situ*. Therefore, another option could be to perform picture frame tests with the same direction of the load, i.e. along the bisector of the two collagen fiber networks. With such kind of test, the sample would be attached on each side and the shear kinematics would be applied to the fibers’ networks, to better reproduce the conditions of the fascia lata *in situ*, where tissue is keeping the attachments to the surrounding structures.

The angles of the two main fiber directions were approximately -35° and 69° for all the samples, meaning the angle between two main directions was around $93.7^\circ \pm 11.9^\circ$. During bias test, at 10% stretch, the fibers rotated by around 30° . During the large band tests, the angles were varying by approximately $4 - 10^\circ$ with the stretch. These differences are explained by the test conditions where fibers are free to move in the bias test since only one fiber extremity is attached in the jaws, while fibers are attached to their both ends in the large band test. However, it also should be noticed that it was difficult to have a loading direction aligned with the bisector of the fibers’ networks, which should be improved. Indeed, it is not easy to get the fiber orientations at a macroscopic scale. A thorough analysis of fiber kinematics and the calculation of shear strain vs the fibers rotation angles could help understanding the occurrence of shear mechanisms, and compare what happens on the different layers.

Regarding the microscopic analysis, we unfortunately could not obtain many images and therefore, it is difficult to conclude on the organization of fibers and networks because the studied area is very small. It seems, however, that the fibers organize and orient themselves in a privileged direction that is changing from layer to layer. It is also noted that the elastin fibers are distributed more randomly than the collagen fibers, which had already been observed by Astruc (2019) on another connective tissue which was the linea alba (abdominal region). To go further, bi-photon microscopy observations under loading should provide more information about the relationship between fibers kinematics and strain mechanisms.

A first numerical analysis was performed to simulate the *ex vivo* experiments using Mooney-Rivlin material reinforced by collagen fibers. Unfortunately, with the current models and material law, we did not get significant difference of the stress values between the models, and

it is hard to give any quantitative analysis at this stage. There is a need to improve the models and to find another constitutive law which would simulate correctly the behavior of the fascia lata. An appropriate constitutive law could then be implemented to the model of the leg. After validation, such FE model would be useful for different applications, for example, surgeries and manual therapies simulations. Adding fascia lata around the muscles is expected to improve the simulation of the muscle force transmission during contraction and leg stability.

In order to access and measure the strain release on the fascia lata, we studied the impact of a surgical technique named “pie-crusting” on the area of ITT close to the knee. This pie-crusting technique is widely used during knee arthroplasty and during correction of varus/valgus deformity of the knee. The main interest was to quantify the strain release and see its effect on the knee joint motion angles.

Unfortunately, changes in range of motion after pie-crusting or after ITT dissection couldn't be interpreted due to small values, as well as overall changes in measured strain levels. Nevertheless, the strain levels on the area closest to the knee were higher compared to those further along the ITT. As in the first *in situ* study, we observed strains close to pure shear on the ITT during rotation and varus-valgus (i.e. adduction-abduction) movements.

We assume that applied movements after the pie-crusting had an influence on the strain release, but less after the ITT dissection, except for the area close to the knee, where the major principal strain increased. However, we haven't been able to identify which movement induced the most strain release.

ITT shortening in the area above the knee after pie-crusting may suggest that its overall stiffness has decreased, but it was not possible to assess this parameter. In order to evaluate the changes in the knee stiffness, it is necessary to evaluate the load applied to move the leg. This might be done by performing the test on an ergometer, with controlled applied load on the leg.

To conclude, current research brings new elements in the investigation of the mechanical behavior of the fascia lata. It is a first step in understanding its strain mechanisms during knee movements, such as flexion-extension, internal-external rotation and varus-valgus. We performed bias and pure shear tests on isolated samples with main tensile stretch along the bisector of the two main fiber networks, considering the observation made *in situ*. In addition, we looked into the kinematics of the fibers, which are rotating a lot during bias tests.

The different approaches and methodologies developed in this thesis will help to go deeper in the quantification of the fascia lata mechanical behavior with respect of the fibers' distributions, in view of enhancing FE models useful in various applications as comfort assessment, car crash simulations and assessment of joint stability, massage techniques or ITT flaps usage.

BIBLIOGRAPHY

- Al-Dirini, Rami M. A., Matthew P. Reed, Jingwen Hu, and Dominic Thewlis. 2016. 'Development and Validation of a High Anatomical Fidelity FE Model for the Buttock and Thigh of a Seated Individual'. *Annals of Biomedical Engineering* 44 (9): 2805–16. <https://doi.org/10.1007/s10439-016-1560-3>.
- Ali, S Z, S Srinivasan, and W C G Peh. 2014. 'MRI in Necrotizing Fasciitis of the Extremities'. *The British Journal of Radiology* 87 (1033): 20130560. <https://doi.org/10.1259/bjr.20130560>.
- Astruc, Laure. 2019. 'Characterization and Histologically-Based Modeling of the Mechanical Behavior of Connective Tissues Constituting the Human Abdominal Wall'. Phdthesis, Ecole Centrale de Lille. <https://tel.archives-ouvertes.fr/tel-02390785>.
- Baker, Robert L., and Michael Fredericson. 2016. 'Iliotibial Band Syndrome in Runners: Biomechanical Implications and Exercise Interventions'. *Physical Medicine and Rehabilitation Clinics of North America, Running Injuries*, 27 (1): 53–77. <https://doi.org/10.1016/j.pmr.2015.08.001>.
- Barker, Priscilla J., Christopher A. Briggs, and Goce Bogeski. 2004. 'Tensile Transmission across the Lumbar Fasciae in Unembalmed Cadavers: Effects of Tension to Various Muscular Attachments'. *Spine* 29 (2): 129–38. <https://doi.org/10.1097/01.BRS.0000107005.62513.32>.
- Beals, Corey, and David Flanigan. 2013. 'A Review of Treatments for Iliotibial Band Syndrome in the Athletic Population'. *Journal of Sports Medicine* 2013 (October): e367169. <https://doi.org/10.1155/2013/367169>.
- Beck, Jennifer J., Karren Takamura, Jeanne M. Beck, Grace Chang, and Richard E. Bowen. 2020. 'Iliotibial Band Autograft: What Size Is the Graft? A Mathematical and Cadaveric Model: ITB Single and Double Strand Size'. *Archives of Orthopaedic and Trauma Surgery* 140 (1): 19–23. <https://doi.org/10.1007/s00402-019-03208-5>.
- Benetazzo, L., A. Bizzego, R. De Caro, G. Frigo, D. Guidolin, and C. Stecco. 2011. '3D Reconstruction of the Crural and Thoracolumbar Fasciae'. *Surgical and Radiologic Anatomy: SRA* 33 (10): 855–62. <https://doi.org/10.1007/s00276-010-0757-7>.
- Bennett, M. B., R. F. Ker, Nicola J. Imery, and R. McN. Alexander. 1986. 'Mechanical Properties of Various Mammalian Tendons'. *Journal of Zoology* 209 (4): 537–48. <https://doi.org/10.1111/j.1469-7998.1986.tb03609.x>.
- Bhattacharya, Visweswar, ParthaSarathi Barooah, TapasChandra Nag, GaurabRanjan Chaudhuri, and Siddhartha Bhattacharya. 2010. 'Detail Microscopic Analysis of Deep Fascia of Lower Limb and Its Surgical Implication'. *Indian Journal of Plastic Surgery* 43 (2): 135. <https://doi.org/10.4103/0970-0358.73424>.
- Birnbaum, K., C. H. Siebert, T. Pandorf, E. Schopphoff, A. Prescher, and F. U. Niethard. 2004. 'Anatomical and Biomechanical Investigations of the Iliotibial Tract'. *Surgical and Radiologic Anatomy: SRA* 26 (6): 433–46. <https://doi.org/10.1007/s00276-004-0265-8>.
- Boisse, P., N. Hamila, E. Guzman-Maldonado, Angela Madeo, G. Hivet, and F. dell'Isola. 2017. 'The Bias-Extension Test for the Analysis of in-Plane Shear Properties of Textile Composite Reinforcements and Prepregs: A Review'. *International Journal of Material Forming* 10 (4): 473–92. <https://doi.org/10.1007/s12289-016-1294-7>.
- Bordoni, Bruno, and Thomas Myers. 2020. 'A Review of the Theoretical Fascial Models: Biotensegrity, Fascintegrity, and Myofascial Chains'. *Cureus* 12 (2): e7092. <https://doi.org/10.7759/cureus.7092>.
- Bruzzone, Matteo, Amar Ranawat, Filippo Castoldi, Federico Dettoni, Paolo Rossi, and Roberto Rossi. 2010. 'The Risk of Direct Peroneal Nerve Injury Using the Ranawat

- “Inside-Out” Lateral Release Technique in Valgus Total Knee Arthroplasty’. *The Journal of Arthroplasty* 25 (1): 161–65. <https://doi.org/10.1016/j.arth.2008.08.016>.
- Buechel, F. F. 1990. ‘A Sequential Three-Step Lateral Release for Correcting Fixed Valgus Knee Deformities during Total Knee Arthroplasty’. *Clinical Orthopaedics and Related Research*, no. 260 (November): 170–75.
- Butler, David L., Edward S. Groot, Frank R. Noyes, Ronald F. Zernicke, and Kim Brackett. 1984. ‘Effects of Structure and Strain Measurement Technique on the Material Properties of Young Human Tendons and Fascia’. *Journal of Biomechanics* 17 (8): 579–96. [https://doi.org/10.1016/0021-9290\(84\)90090-3](https://doi.org/10.1016/0021-9290(84)90090-3).
- Charles, Derek, and Clay Rodgers. 2020. ‘A LITERATURE REVIEW AND CLINICAL COMMENTARY ON THE DEVELOPMENT OF ILIOTIBIAL BAND SYNDROME IN RUNNERS’. *International Journal of Sports Physical Therapy* 15 (3): 460–70.
- Chaudhry, Hans, Chien-Yueh Huang, Robert Schleip, Zhiming Ji, Bruce Bukiet, and Thomas Findley. 2007. ‘Viscoelastic Behavior of Human Fasciae under Extension in Manual Therapy’. *Journal of Bodywork and Movement Therapies* 11 (2): 159–67. <https://doi.org/10.1016/j.jbmt.2006.08.012>.
- Chaudhry, Hans, Roman Max, Stecco Antonio, and Thomas Findley. 2012. ‘Mathematical Model of Fiber Orientation in Anisotropic Fascia Layers at Large Displacements’. *Journal of Bodywork and Movement Therapies* 16 (2): 158–64. <https://doi.org/10.1016/j.jbmt.2011.04.006>.
- Chaudhry, Hans, Robert Schleip, Zhiming Ji, Bruce Bukiet, Miriam Maney, and Thomas Findley. 2008. ‘Three-Dimensional Mathematical Model for Deformation of Human Fasciae in Manual Therapy’. *Journal of Osteopathic Medicine* 108 (8): 379–90. <https://doi.org/10.7556/jaoa.2008.108.8.379>.
- Chen, Tony Lin-Wei, Duo Wai-Chi Wong, Yan Wang, Jin Lin, and Ming Zhang. 2019. ‘Foot Arch Deformation and Plantar Fascia Loading during Running with Rearfoot Strike and Forefoot Strike: A Dynamic Finite Element Analysis’. *Journal of Biomechanics* 83 (January): 260–72. <https://doi.org/10.1016/j.jbiomech.2018.12.007>.
- Chen, Yen-Nien, Chih-Wei Chang, Chun-Ting Li, Chih-Han Chang, and Cheng-Feng Lin. 2015. ‘Finite Element Analysis of Plantar Fascia During Walking: A Quasi-Static Simulation’. *Foot & Ankle International* 36 (1): 90–97. <https://doi.org/10.1177/1071100714549189>.
- Cheng, Hsin-Yi Kathy, Chun-Li Lin, Hsien-Wen Wang, and Shih-Wei Chou. 2008. ‘Finite Element Analysis of Plantar Fascia under Stretch—The Relative Contribution of Windlass Mechanism and Achilles Tendon Force’. *Journal of Biomechanics* 41 (9): 1937–44. <https://doi.org/10.1016/j.jbiomech.2008.03.028>.
- Chèze, Laurence, Florent Moissenet, and Raphaël Dumas. 2012. ‘State of the Art and Current Limits of Musculo-Skeletal Models for Clinical Applications’. Edited by Floren Colloud. *Movement & Sport Sciences - Science & Motricité*, no. 90: 7–17. <https://doi.org/10.1051/sm/2012026>.
- Couppé, C., P. Hansen, M. Kongsgaard, V. Kovanen, C. Suetta, P. Aagaard, M. Kjær, and S. P. Magnusson. 2009. ‘Mechanical Properties and Collagen Cross-Linking of the Patellar Tendon in Old and Young Men’. *Journal of Applied Physiology* 107 (3): 880–86. <https://doi.org/10.1152/jappphysiol.00291.2009>.
- Cury, Diego, Fernando Dias, Maria Miglino, and Ii-Sei Watanabe. 2016. ‘Structural and Ultrastructural Characteristics of Bone-Tendon Junction of the Calcaneal Tendon of Adult and Elderly Wistar Rats’. *PLoS ONE* 11 (April): e0153568. <https://doi.org/10.1371/journal.pone.0153568>.
- Czekalla, Carolin, Karl-Heinz Schönborn, Nadine Döge, Sora Jung, Maxim E. Darwin, Jürgen Lademann, and Martina C. Meinke. 2017. ‘Impact of Body Site, Age, and Gender on

- the Collagen/Elastin Index by Noninvasive in Vivo Vertical Two-Photon Microscopy'. *Skin Pharmacology and Physiology* 30 (5): 260–67. <https://doi.org/10.1159/000477854>.
- Del gaizo and Della Valle. 2011. 'Instability in Primary Total Knee Arthroplasty'. *Orthopedics* 34 (9): e519–21. <https://doi.org/10.3928/01477447-20110714-46>.
- DellaGrotte, Josef, Renzo Ridi, Monica Landi, and James Stephens. 2008. 'Postural Improvement Using Core Integration to Lengthen Myofascia'. *Journal of Bodywork and Movement Therapies* 12 (3): 231–45. <https://doi.org/10.1016/j.jbmt.2008.04.047>.
- Demiray, Hilmi. 1972. 'A Note on the Elasticity of Soft Biological Tissues'. *Journal of Biomechanics* 5 (3): 309–11. [https://doi.org/10.1016/0021-9290\(72\)90047-4](https://doi.org/10.1016/0021-9290(72)90047-4).
- Dragosloveanu, Serban, Stefan Cristea, Cristian Stoica, and Calin Dragosloveanu. 2014. 'Outcome of Iatrogenic Collateral Ligaments Injuries during Total Knee Arthroplasty'. *European Journal of Orthopaedic Surgery & Traumatology* 24 (8): 1499–1503. <https://doi.org/10.1007/s00590-013-1330-y>.
- Elkus, Mark, Chitranjan S. Ranawat, Vijay J. Rasquinha, Sushrut Babhulkar, Roberto Rossi, and Amar S. Ranawat. 2004. 'Total Knee Arthroplasty for Severe Valgus Deformity. Five to Fourteen-Year Follow-Up'. *The Journal of Bone and Joint Surgery. American Volume* 86 (12): 2671–76. <https://doi.org/10.2106/00004623-200412000-00013>.
- Eng, Carolyn M., Francesco Q. Pancheri, Daniel E. Lieberman, Andrew A. Biewener, and Luis Dorfmann. 2014a. 'Directional Differences in the Biaxial Material Properties of Fascia Lata and the Implications for Fascia Function'. *Annals of Biomedical Engineering* 42 (6): 1224–37. <https://doi.org/10.1007/s10439-014-0999-3>.
- . 2014b. 'Directional Differences in the Biaxial Material Properties of Fascia Lata and the Implications for Fascia Function'. *Annals of Biomedical Engineering* 42 (6): 1224–37. <https://doi.org/10.1007/s10439-014-0999-3>.
- Evans, P. 1979. 'The Postural Function of the Iliotibial Tract.' *Annals of The Royal College of Surgeons of England* 61 (4): 271–80.
- Fairclough, John, Koji Hayashi, Hechmi Toumi, Kathleen Lyons, Graeme Bydder, Nicola Phillips, Thomas M Best, and Mike Benjamin. 2006. 'The BlackwellPublishingLtd Functional Anatomy of the Iliotibial Band during Flexion and Extension of the Knee: Implications for Understanding Iliotibial Band Syndrome', 8.
- Fairclough, John, Koji Hayashi, Hechmi Toumi, Kathleen Lyons, Graeme Bydder, Nicola Phillips, Thomas M. Best, and Mike Benjamin. 2007. 'Is Iliotibial Band Syndrome Really a Friction Syndrome?' *Journal of Science and Medicine in Sport* 10 (2): 74–76. <https://doi.org/10.1016/j.jsams.2006.05.017>.
- Farrell, Kevin C., Kim D. Reisinger, and Mark D. Tillman. 2003. 'Force and Repetition in Cycling: Possible Implications for Iliotibial Band Friction Syndrome'. *The Knee* 10 (1): 103–9. [https://doi.org/10.1016/S0968-0160\(02\)00090-X](https://doi.org/10.1016/S0968-0160(02)00090-X).
- Ferber, Reed, Brian Noehren, Joseph Hamill, and Irene Davis. 2010. 'Competitive Female Runners With a History of Iliotibial Band Syndrome Demonstrate Atypical Hip and Knee Kinematics'. *Journal of Orthopaedic & Sports Physical Therapy* 40 (2): 52–58. <https://doi.org/10.2519/jospt.2010.3028>.
- Findley, Thomas, Hans Chaudhry, Antonio Stecco, and Max Roman. 2012. 'Fascia Research – A Narrative Review'. *Journal of Bodywork and Movement Therapies* 16 (1): 67–75. <https://doi.org/10.1016/j.jbmt.2011.09.004>.
- Fischer, Benjamin, Sascha Kurz, Andreas Höch, and Stefan Schleifenbaum. 2020. 'The Influence of Different Sample Preparation on Mechanical Properties of Human Iliotibial Tract'. *Scientific Reports* 10 (1): 14836. <https://doi.org/10.1038/s41598-020-71790-5>.
- Flanagan, D. P., and T. Belytschko. 1981. 'A Uniform Strain Hexahedron and Quadrilateral with Orthogonal Hourglass Control'. *International Journal for Numerical Methods in Engineering* 17 (5): 679–706. <https://doi.org/10.1002/nme.1620170504>.

- Foch, Eric, Jeffrey A. Reinbolt, Songning Zhang, Eugene C. Fitzhugh, and Clare E. Milner. 2015. 'Associations between Iliotibial Band Injury Status and Running Biomechanics in Women'. *Gait & Posture* 41 (2): 706–10. <https://doi.org/10.1016/j.gaitpost.2015.01.031>.
- Fredericson, M., M. Guillet, and L. DeBenedictis. 2000. 'Innovative Solutions for Iliotibial Band Syndrome'. *The Physician and Sportsmedicine* 28 (2): 53–68. <https://doi.org/10.3810/psm.2000.02.693>.
- Fredericson, Michael, and Adam Weir. 2006. 'Practical Management of Iliotibial Band Friction Syndrome in Runners'. *Clinical Journal of Sport Medicine* 16 (3): 261–68.
- Freed, Alan. 2009. 'Anisotropy in Hypoelastic Soft-Tissue Mechanics, II: Simple Extensional Experiments'. *Journal of Mechanics of Materials and Structures* 4 (6): 1005–25. <https://doi.org/10.2140/jomms.2009.4.1005>.
- Freeman, T Sculco, and R C Todd. 1977. 'Replacement of the Severely Damaged Arthritic Knee by the ICLH (Freeman-Swanson) Arthroplasty'. *The Journal of Bone and Joint Surgery. British Volume* 59 (1): 64–71. <https://doi.org/10.1302/0301-620X.59B1.845230>.
- Fung, Y. C. 1984. *Biodynamics: Circulation*. New York: Springer-Verlag. <https://doi.org/10.1007/978-1-4757-3884-1>.
- García, J. M., M. Doblare, B. Seral, F. Seral, D. Palanca, and L. Gracia. 2000. 'Three-Dimensional Finite Element Analysis of Several Internal and External Pelvis Fixations'. *Journal of Biomechanical Engineering* 122 (5): 516–22. <https://doi.org/10.1115/1.1289995>.
- Gardiner, John C., and Jeffrey A. Weiss. 2000. 'Simple Shear Testing of Parallel-Fibered Planar Soft Tissues'. *Journal of Biomechanical Engineering* 123 (2): 170–75. <https://doi.org/10.1115/1.1351891>.
- Garfin, S. R., C. M. Tipton, S. J. Mubarak, S. L. Woo, A. R. Hargens, and W. H. Akeson. 1981. 'Role of Fascia in Maintenance of Muscle Tension and Pressure'. *Journal of Applied Physiology* 51 (2): 317–20. <https://doi.org/10.1152/jappl.1981.51.2.317>.
- Gratz, Chas Murray. 1931. 'TENSILE STRENGTH AND ELASTICITY TESTS ON HUMAN FASCIA LATA', 8.
- Gu, Y. D., Z. Y. Li, W. W. Shen, and J. B. Ma. 2013. 'Mechanical Analysis of Foot Plantar Fascia During Normal Walking Condition'. In *World Congress on Medical Physics and Biomedical Engineering May 26-31, 2012, Beijing, China*, edited by Mian Long, 39:242–44. Berlin, Heidelberg: Springer Berlin Heidelberg. https://doi.org/10.1007/978-3-642-29305-4_65.
- Guilbert, Marie, Blandine Roig, Christine Terryn, Roselyne Garnotel, Pierre Jeannesson, Ganesh D. Sockalingum, Michel Manfait, et al. 2016. 'Highlighting the Impact of Aging on Type I Collagen: Label-Free Investigation Using Confocal Reflectance Microscopy and Diffuse Reflectance Spectroscopy in 3D Matrix Model'. *Oncotarget* 7 (8): 8546–55. <https://doi.org/10.18632/oncotarget.7385>.
- Gunter, P, M Schweltnus, and P Fuller. 2004. 'Local Corticosteroid Injection in Iliotibial Band Friction Syndrome in Runners: A Randomised Controlled Trial'. *British Journal of Sports Medicine* 38 (3): 269–72. <https://doi.org/10.1136/bjism.2003.000283>.
- Guo, Junchao, Xiaoyu Liu, Xili Ding, Lizhen Wang, and Yubo Fan. 2018. 'Biomechanical and Mechanical Behavior of the Plantar Fascia in Macro and Micro Structures'. *Journal of Biomechanics* 76 (July): 160–66. <https://doi.org/10.1016/j.jbiomech.2018.05.032>.
- Hadeed, Andrew, and David C. Tapscott. 2019. 'Iliotibial Band Friction Syndrome'. In *StatPearls*. Treasure Island (FL): StatPearls Publishing. <http://www.ncbi.nlm.nih.gov/books/NBK542185/>.

- Hamill, Joseph, Ross Miller, Brian Noehren, and Irene Davis. 2008. 'A Prospective Study of Iliotibial Band Strain in Runners'. *Clinical Biomechanics* 23 (8): 1018–25. <https://doi.org/10.1016/j.clinbiomech.2008.04.017>.
- Hammer, Niels, Daniel Huster, Andreas Boldt, Carsten Hädrich, Holger Koch, Robert Möbius, Gundula Schulze-Tanzil, and Holger A Scheidt. 2016. 'A Preliminary Technical Study on Sodium Dodecyl Sulfate-Induced Changes of the Nano-Structural and Macro-Mechanical Properties in Human Iliotibial Tract Specimens'. *Journal of the Mechanical Behavior of Biomedical Materials* 61 (August): 164–73. <https://doi.org/10.1016/j.jmbbm.2016.01.018>.
- Hammer, Niels, Uwe Lingslebe, Gabriela Aust, Thomas L. Milani, Carsten Hädrich, and Hanno Steinke. 2012. 'Ultimate Stress and Age-Dependent Deformation Characteristics of the Iliotibial Tract'. *Journal of the Mechanical Behavior of Biomedical Materials* 16 (December): 81–86. <https://doi.org/10.1016/j.jmbbm.2012.04.025>.
- He, Xuan, Hong Cai, and Ke Zhang. 2018. 'Pie-Crusting Technique Is Effective and Safe to Release Superficial Medial Collateral Ligament for Total Knee Arthroplasty'. *Journal of Orthopaedic Translation* 13 (April): 33–40. <https://doi.org/10.1016/j.jot.2018.01.001>.
- Henderson, Elisabeth R., Ed J. Friend, Michael J. Toscano, Kevin J. Parsons, and John F. Tarlton. 2014. 'Biomechanical Comparison of Canine Fascia Lata and Thoracolumbar Fascia: An *In Vitro* Evaluation of Replacement Tissues for Body Wall Reconstruction: Biomechanical Comparison of Canine Fascia Lata and Thoracolumbar Fascia'. *Veterinary Surgery*, July, n/a-n/a. <https://doi.org/10.1111/j.1532-950X.2014.12247.x>.
- Holmes, James C., Andrew L. Pruitt, and Nina J. Whalen. 1993. 'Iliotibial Band Syndrome in Cyclists'. *The American Journal of Sports Medicine* 21 (3): 419–24. <https://doi.org/10.1177/036354659302100316>.
- Holzappel, Gerhard A. 2002. 'Nonlinear Solid Mechanics: A Continuum Approach for Engineering Science'. *Meccanica* 37 (4): 489–90. <https://doi.org/10.1023/A:1020843529530>.
- Huijing, Peter A. 2009. 'Epimuscular Myofascial Force Transmission: A Historical Review and Implications for New Research. International Society of Biomechanics Muybridge Award Lecture, Taipei, 2007'. *Journal of Biomechanics* 42 (1): 9–21. <https://doi.org/10.1016/j.jbiomech.2008.09.027>.
- Jabalameh, Mahmoud, Abolfazl Bagherifard, Hosseinali Hadi, and Iman Qomashi. 2016. 'Total Knee Arthroplasty in Patients With Valgus Deformity'. *Shafa Orthopedic Journal* In Press (In Press). <https://doi.org/10.17795/soj-4153>.
- Jayyosi, C., J.-S. Affagard, G. Ducourthial, C. Bonod-Bidaud, B. Lynch, S. Bancelin, F. Ruggiero, et al. 2017. 'Affine Kinematics in Planar Fibrous Connective Tissues: An Experimental Investigation'. *Biomechanics and Modeling in Mechanobiology* 16 (4): 1459–73. <https://doi.org/10.1007/s10237-017-0899-1>.
- Jayyosi, C., M. Coret, and K. Bruyère-Garnier. 2016. 'Characterizing Liver Capsule Microstructure via in Situ Bulge Test Coupled with Multiphoton Imaging'. *Journal of the Mechanical Behavior of Biomedical Materials* 54 (February): 229–43. <https://doi.org/10.1016/j.jmbbm.2015.09.031>.
- Kaplan, Emanuel. 1958. 'The Iliotibial Tract: Clinical and Morphological Significance'. *The Journal of Bone & Joint Surgery* 40 (4): 817–32.
- Klein Horsman, M. D., H. F. J. M. Koopman, F. C. T. van der Helm, L. Poliacu Prosé, and H. E. J. Veeger. 2007. 'Morphological Muscle and Joint Parameters for Musculoskeletal Modelling of the Lower Extremity'. *Clinical Biomechanics* 22 (2): 239–47. <https://doi.org/10.1016/j.clinbiomech.2006.10.003>.

- Klingler, W., M. Velders, K. Hoppe, M. Pedro, and R. Schleip. 2014. 'Clinical Relevance of Fascial Tissue and Dysfunctions'. *Current Pain and Headache Reports* 18 (8): 439. <https://doi.org/10.1007/s11916-014-0439-y>.
- Kwak, S. D., C. S. Ahmad, T. R. Gardner, R. P. Grelsamer, J. H. Henry, L. Blankevoort, G. A. Ateshian, and V. C. Mow. 2000. 'Hamstrings and Iliotibial Band Forces Affect Knee Kinematics and Contact Pattern'. *Journal of Orthopaedic Research: Official Publication of the Orthopaedic Research Society* 18 (1): 101–8. <https://doi.org/10.1002/jor.1100180115>.
- Langevin, Helene M, and Peter A Huijing. 2009. 'Communicating About Fascia: History, Pitfalls, and Recommendations'. *International Journal of Therapeutic Massage & Bodywork: Research, Education, & Practice* 2 (4): 3–8. <https://doi.org/10.3822/ijtmb.v2i4.63>.
- Lanir, Y. 1983. 'Constitutive Equations for Fibrous Connective Tissues'. *Journal of Biomechanics* 16 (1): 1–12. [https://doi.org/10.1016/0021-9290\(83\)90041-6](https://doi.org/10.1016/0021-9290(83)90041-6).
- Lavine, Ronald. 2010. 'Iliotibial Band Friction Syndrome'. *Current Reviews in Musculoskeletal Medicine* 3 (1–4): 18–22. <https://doi.org/10.1007/s12178-010-9061-8>.
- Leardini, Alberto, Lorenzo Chiari, Ugo Della Croce, and Aurelio Cappozzo. 2005. 'Human Movement Analysis Using Stereophotogrammetry: Part 3. Soft Tissue Artifact Assessment and Compensation'. *Gait & Posture* 21 (2): 212–25. <https://doi.org/10.1016/j.gaitpost.2004.05.002>.
- Majewski, M., Habelt Susanne, and Steinbrück Klaus. 2006. 'Epidemiology of Athletic Knee Injuries: A 10-Year Study'. *The Knee* 13 (3): 184–88. <https://doi.org/10.1016/j.knee.2006.01.005>.
- Majumder, Santanu, Amit Roychowdhury, and Subrata Pal. 2007. 'Simulation of Hip Fracture in Sideways Fall Using a 3D Finite Element Model of Pelvis–Femur–Soft Tissue Complex with Simplified Representation of Whole Body'. *Medical Engineering & Physics* 29 (10): 1167–78. <https://doi.org/10.1016/j.medengphy.2006.11.001>.
- Mansfield, Jessica C., C. Peter Winlove, Julian Moger, and Steve J. Matcher. 2008. 'Collagen Fiber Arrangement in Normal and Diseased Cartilage Studied by Polarization Sensitive Nonlinear Microscopy'. *Journal of Biomedical Optics* 13 (4): 044020. <https://doi.org/10.1117/1.2950318>.
- Martens, M., P. Libbrecht, and A. Burssens. 1989. 'Surgical Treatment of the Iliotibial Band Friction Syndrome'. *The American Journal of Sports Medicine* 17 (5): 651–54. <https://doi.org/10.1177/036354658901700511>.
- Matsuda, Shuichi, Sébastien Lustig, and Willem van der Merwe, eds. 2017. *Soft Tissue Balancing in Total Knee Arthroplasty*. Berlin, Heidelberg: Springer Berlin Heidelberg. <https://doi.org/10.1007/978-3-662-54082-4>.
- McLean, S. G., A. Su, and A. J. van den Bogert. 2003. 'Development and Validation of a 3-D Model to Predict Knee Joint Loading During Dynamic Movement'. *Journal of Biomechanical Engineering* 125 (6): 864–74. <https://doi.org/10.1115/1.1634282>.
- Merican, Azhar M., and Andrew A. Amis. 2009. 'Iliotibial Band Tension Affects Patellofemoral and Tibiofemoral Kinematics'. *Journal of Biomechanics* 42 (10): 1539–46. <https://doi.org/10.1016/j.jbiomech.2009.03.041>.
- Michels, F., S. Jambou, M. Allard, V. Bousquet, P. Colombet, and C. de Lavigne. 2009. 'An Arthroscopic Technique to Treat the Iliotibial Band Syndrome'. *Knee Surgery, Sports Traumatology, Arthroscopy* 17 (3): 233–36. <https://doi.org/10.1007/s00167-008-0660-5>.
- Mo, Fuhao, Junjie Li, Minchao Dan, Tang Liu, and Michel Behr. 2019. 'Implementation of Controlling Strategy in a Biomechanical Lower Limb Model with Active Muscles for

- Coupling Multibody Dynamics and Finite Element Analysis'. *Journal of Biomechanics* 91 (June): 51–60. <https://doi.org/10.1016/j.jbiomech.2019.05.001>.
- Monaghan, Michael G., Sebastian Kroll, Sara Y. Brucker, and Katja Schenke-Layland. 2016. 'Enabling Multiphoton and Second Harmonic Generation Imaging in Paraffin-Embedded and Histologically Stained Sections'. *Tissue Engineering, Part C, Methods* 22 (6): 517–23. <https://doi.org/10.1089/ten.tec.2016.0071>.
- Mooney, M. 1940. 'A Theory of Large Elastic Deformation'. *Journal of Applied Physics* 11 (9): 582–92. <https://doi.org/10.1063/1.1712836>.
- Mount, Frances E. Whitmore. 2003. 'Evaluation of Neutral Body Posture on Shuttle Mission STS-57 (SPACEHAB-1). Revision'. <https://ntrs.nasa.gov/search.jsp?R=20040200967>.
- Noble, C. A. 1979. 'The Treatment of Iliotibial Band Friction Syndrome.' *British Journal of Sports Medicine* 13 (2): 51–54.
- Ogden, R. W. 1997. *Non-Linear Elastic Deformations*. Courier Corporation.
- Osakabe, T, M Hayashi, K Hasegawa, T Okuaki, T M Ritty, R P Mecham, H Wachi, and Y Seyama. 2001. 'Age- and Gender-Related Changes in Ligament Components', 6.
- Otsuka, Shun, Xiyao Shan, Keisuke Kurumisawa, Shiho Omura, Takaki Yamagishi, Munekazu Naito, and Yasuo Kawakami. 2021. 'Investigation of the Association between Human Fascia Lata Thickness and Its Neighboring Tissues' Morphology and Function Using B-mode Ultrasonography'. *Journal of Anatomy*, July, joa.13505. <https://doi.org/10.1111/joa.13505>.
- Otsuka, Shun, Xiyao Shan, Kyoka Yoshida, Tomiko Yakura, Munekazu Naito, and Yasuo Kawakami. 2020. 'Site Dependent Elastic Property of Human Iliotibial Band and the Effect of Hip and Knee Joint Angle Configuration'. *Journal of Biomechanics* 109 (August): 109919. <https://doi.org/10.1016/j.jbiomech.2020.109919>.
- Otsuka, Shun, Tomiko Yakura, Yusuke Ohmichi, Mika Ohmichi, Munekazu Naito, Takashi Nakano, and Yasuo Kawakami. 2018. 'Site Specificity of Mechanical and Structural Properties of Human Fascia Lata and Their Gender Differences: A Cadaveric Study'. *Journal of Biomechanics* 77 (August): 69–75. <https://doi.org/10.1016/j.jbiomech.2018.06.018>.
- Pancheri, F. Q., C. M. Eng, D. E. Lieberman, A. A. Biewener, and L. Dorfmann. 2014. 'A Constitutive Description of the Anisotropic Response of the Fascia Lata'. *Journal of the Mechanical Behavior of Biomedical Materials* 30 (February): 306–23. <https://doi.org/10.1016/j.jmbbm.2013.12.002>.
- Pandit, Sandeep R., Daniel J. Solomon, Daniel J. Gross, Petar Golijanin, and Matthew T. Provencher. 2014. 'Isolated Iliotibial Band Rupture after Corticosteroid Injection as a Cause of Subjective Instability and Knee Pain in a Military Special Warfare Trainee'. *Military Medicine* 179 (4): e469-472. <https://doi.org/10.7205/MILMED-D-13-00438>.
- Parry, David A. D. 1988. 'The Molecular Fibrillar Structure of Collagen and Its Relationship to the Mechanical Properties of Connective Tissue'. *Biophysical Chemistry* 29 (1): 195–209. [https://doi.org/10.1016/0301-4622\(88\)87039-X](https://doi.org/10.1016/0301-4622(88)87039-X).
- Pavan, Piero G., Paola Pachera, Antonella Forestiero, and Arturo N. Natali. 2017. 'Investigation of Interaction Phenomena between Crural Fascia and Muscles by Using a Three-Dimensional Numerical Model'. *Medical & Biological Engineering & Computing* 55 (9): 1683–91. <https://doi.org/10.1007/s11517-017-1615-0>.
- Piazza, Stephen J., and Scott L. Delp. 2001. 'Three-Dimensional Dynamic Simulation of Total Knee Replacement Motion During a Step-Up Task'. *Journal of Biomechanical Engineering* 123 (6): 599–606. <https://doi.org/10.1115/1.1406950>.
- Podwojewski, F., M. Otténio, P. Beillas, G. Guérin, F. Turquier, and D. Mitton. 2014. 'Mechanical Response of Human Abdominal Walls Ex Vivo: Effect of an Incisional

- Hernia and a Mesh Repair'. *Journal of the Mechanical Behavior of Biomedical Materials* 38 (October): 126–33. <https://doi.org/10.1016/j.jmbbm.2014.07.002>.
- Politi, Joel, and Richard Scott. 2004. 'Balancing Severe Valgus Deformity in Total Knee Arthroplasty Using a Lateral Cruciform Retinacular Release: 1 No Benefits or Funds Were Received in Support of This Study.' *The Journal of Arthroplasty* 19 (5): 553–57. <https://doi.org/10.1016/j.arth.2003.12.083>.
- Quapp, K. M., and J. A. Weiss. 1998. 'Material Characterization of Human Medial Collateral Ligament'. *Journal of Biomechanical Engineering* 120 (6): 757–63. <https://doi.org/10.1115/1.2834890>.
- Rahnemai-Azar, Ata A., R. Matthew Miller, Daniel Guenther, Freddie H. Fu, Bryson P. Lesniak, Volker Musahl, and Richard E. Debski. 2016. 'Structural Properties of the Anterolateral Capsule and Iliotibial Band of the Knee'. *The American Journal of Sports Medicine* 44 (4): 892–97. <https://doi.org/10.1177/0363546515623500>.
- Ranawat, Amar S., Chitranjan S. Ranawat, Mark Elkus, Vijay J. Rasquinha, Roberto Rossi, and Sushrut Babhulkar. 2005. 'Total Knee Arthroplasty for Severe Valgus Deformity'. *JBJS* 87 (1_suppl_2): 271–84. <https://doi.org/10.2106/JBJS.E.00308>.
- Rezakhaniha, R., A. Agianniotis, J. T. C. Schrauwen, A. Griffa, D. Sage, C. V. C. Bouten, F. N. van de Vosse, M. Unser, and N. Stergiopoulos. 2012. 'Experimental Investigation of Collagen Waviness and Orientation in the Arterial Adventitia Using Confocal Laser Scanning Microscopy'. *Biomechanics and Modeling in Mechanobiology* 11 (3–4): 461–73. <https://doi.org/10.1007/s10237-011-0325-z>.
- Richards, David P., F. Alan Barber, and Randal L. Troop. 2003. 'Iliotibial Band Z-Lengthening'. *Arthroscopy: The Journal of Arthroscopic & Related Surgery* 19 (3): 326–29. <https://doi.org/10.1053/jars.2003.50081>.
- Rivard, Maxime, Mathieu Laliberté, Antony Bertrand-Grenier, Catalin Harnagea, Christian P. Pfeffer, Martin Vallières, Yves St-Pierre, Alain Pignolet, My Ali El Khakani, and François Légaré. 2011. 'The Structural Origin of Second Harmonic Generation in Fascia'. *Biomedical Optics Express* 2 (1): 26. <https://doi.org/10.1364/BOE.2.000026>.
- Ruiz-Alejos, D., J. A. Peña, M. M. Pérez, and E. Peña. 2016. 'Experiments and Constitutive Model for Deep and Superficial Fascia. Digital Image Correlation and Finite Element Validation: Experiments and Constitutive Model for Deep and Superficial Fascia'. *Strain* 52 (5): 436–45. <https://doi.org/10.1111/str.12198>.
- Sancheti, P., M. Razi, E. B. S. Ramanathan, and P. Yung. 2010. 'Injuries around the Knee - Symposium'. *British Journal of Sports Medicine* 44 (Suppl_1): i1–i1. <https://doi.org/10.1136/bjism.2010.078725.1>.
- Sangkaew, Chanchit. 2007. 'Surgical Treatment of Iliotibial Band Friction Syndrome with the Mesh Technique'. *Archives of Orthopaedic and Trauma Surgery* 127 (4): 303–6. <https://doi.org/10.1007/s00402-006-0152-3>.
- Savonnet, Léo, Xuguang Wang, and Sonia Duprey. 2018. 'Finite Element Models of the Thigh-Buttock Complex for Assessing Static Sitting Discomfort and Pressure Sore Risk: A Literature Review'. *Computer Methods in Biomechanics and Biomedical Engineering* 21 (4): 379–88. <https://doi.org/10.1080/10255842.2018.1466117>.
- Schwarzkopf, Ran, Scott Hadley, Mohammed Abbasi, and Patrick A. Meere. 2013. 'Computer-Assisted Surgery Patterns of Ligamentous Deformity of the Knee: A Clinical and Cadaveric Study'. *The Journal of Knee Surgery* 26 (4): 233–38. <https://doi.org/10.1055/s-0032-1329716>.
- Schwellnus, M. P., L. Theunissen, T. D. Noakes, and S. G. Reinach. 1991. 'Anti-Inflammatory and Combined Anti-Inflammatory/Analgesic Medication in the Early Management of Iliotibial Band Friction Syndrome. A Clinical Trial'. *South African Medical Journal = Suid-Afrikaanse Tydskrif Vir Geneeskunde* 79 (10): 602–6.

- Schwind, Peter. 2006. 'Chapter 4 - Form-Oriented Treatment Techniques'. In *Fascial and Membrane Technique*, edited by Peter Schwind, 31–133. Edinburgh: Churchill Livingstone. <https://doi.org/10.1016/B978-044310219-6.50007-2>.
- Sednieva, Yuliia, Anthony Viste, Alexandre Naaim, Karine Bruyère-Garnier, and Laure-Lise Gras. 2020. 'Strain Assessment of Deep Fascia of the Thigh during Leg Movement: An in Situ Study'. *Frontiers in Bioengineering and Biotechnology* 8. <https://doi.org/10.3389/fbioe.2020.00750>.
- Snoeck, O., B. Beyer, V. Feipel, P. Salvia, J.-L. Sterckx, M. Rooze, and S. Van Sint Jan. 2014. 'Tendon and Fascial Structure Contributions to Knee Muscle Excursions and Knee Joint Displacement'. *Clinical Biomechanics* 29 (9): 1070–76. <https://doi.org/10.1016/j.clinbiomech.2014.08.003>.
- Stahl, Victoria Ann. 2010. 'A Biomechanical Analysis of the Role of the Crural Fascia in the Cat Hindlimb', July. <https://smartech.gatech.edu/handle/1853/34701>.
- Stecco, A., V. Macchi, S. Masiero, A. Porzionato, C. Tiengo, C. Stecco, V. Delmas, and R. De Caro. 2009a. 'Pectoral and Femoral Fasciae: Common Aspects and Regional Specializations'. *Surgical and Radiologic Anatomy* 31 (1): 35–42. <https://doi.org/10.1007/s00276-008-0395-5>.
- . 2009b. 'Pectoral and Femoral Fasciae: Common Aspects and Regional Specializations'. *Surgical and Radiologic Anatomy* 31 (1): 35–42. <https://doi.org/10.1007/s00276-008-0395-5>.
- Stecco, Carla. 2014. *Functional Atlas of the Human Fascial System E-Book*. Elsevier Health Sciences.
- Stecco, Carla, Piero Pavan, Paola Pachera, Raffaele De Caro, and Arturo Natali. 2014. 'Investigation of the Mechanical Properties of the Human Crural Fascia and Their Possible Clinical Implications'. *Surgical and Radiologic Anatomy: SRA* 36 (1): 25–32. <https://doi.org/10.1007/s00276-013-1152-y>.
- Stecco, Carla, Andrea Porzionato, Luca Lancerotto, Antonio Stecco, Veronica Macchi, Julie Ann Day, and Raffaele De Caro. 2008. 'Histological Study of the Deep Fasciae of the Limbs'. *Journal of Bodywork and Movement Therapies* 12 (3): 225–30. <https://doi.org/10.1016/j.jbmt.2008.04.041>.
- Stecco, Carla, R. Stern, A. Porzionato, V. Macchi, S. Masiero, A. Stecco, and R. De Caro. 2011a. 'Hyaluronan within Fascia in the Etiology of Myofascial Pain'. *Surgical and Radiologic Anatomy* 33 (10): 891–96. <https://doi.org/10.1007/s00276-011-0876-9>.
- . 2011b. 'Hyaluronan within Fascia in the Etiology of Myofascial Pain'. *Surgical and Radiologic Anatomy* 33 (10): 891–96. <https://doi.org/10.1007/s00276-011-0876-9>.
- Stecco, Gilliar Wolfgang, Hill Robert, Brad Fullerton, and Stecco Carla. 2013. 'The Anatomical and Functional Relation between Gluteus Maximus and Fascia Lata'. *Journal of Bodywork and Movement Therapies* 17 (4): 512–17. <https://doi.org/10.1016/j.jbmt.2013.04.004>.
- Steinke, Hanno, Uwe Lingslebe, Jörg Böhme, Volker Slowik, Vickie Shim, Carsten Hädrich, and Niels Hammer. 2012. 'Deformation Behavior of the Iliotibial Tract under Different States of Fixation'. *Medical Engineering & Physics* 34 (9): 1221–27. <https://doi.org/10.1016/j.medengphy.2011.12.009>.
- Stelletta, Julien, Raphaël Dumas, and Yoann Lafon. 2016. 'MUSCLE INTERACTIONS INFLUENCE THE MUSCULAR FORCES'. In *22nd Congress of the European Society of Biomechanics*. Proceedings of the 22nd Congress of the European Society of Biomechanics. Lyon, France. <https://hal.archives-ouvertes.fr/hal-01609529>.
- . 2017. 'Modeling of the Thigh: A 3D Deformable Approach Considering Muscle Interactions'. In *Biomechanics of Living Organs: Hyperelastic Constitutive Laws for Finite Element Modeling*, 497–521. <https://hal.archives-ouvertes.fr/hal-01913274>.

- Stoller, Patrick, Peter M. Celliers, Karen M. Reiser, and Alexander M. Rubenchik. 2003. 'Quantitative Second-Harmonic Generation Microscopy in Collagen'. *Applied Optics* 42 (25): 5209–19. <https://doi.org/10.1364/AO.42.005209>.
- Strauss, Eric J., Suezie Kim, Jacob G. Calcei, and Daniel Park. 2011. 'Iliotibial Band Syndrome: Evaluation and Management'. *JAAOS - Journal of the American Academy of Orthopaedic Surgeons* 19 (12): 728–36.
- Svensson, René B., Tue Hassenkam, Colin A. Grant, and S. Peter Magnusson. 2010. 'Tensile Properties of Human Collagen Fibrils and Fascicles Are Insensitive to Environmental Salts'. *Biophysical Journal* 99 (12): 4020. <https://doi.org/10.1016/j.bpj.2010.11.018>.
- Szotek, Sylwia, Joanna Czogała, Krzysztof Ścigała, Krzysztof Marycz, and Krzysztof Maksymowicz. 2012. 'The Biomechanical and Ultrastructural Properties of Human Fascia Lata'. *Journal of Bodywork and Movement Therapies* 16 (3): 397–98. <https://doi.org/10.1016/j.jbmt.2012.01.036>.
- Taber, Larry A. 2004. *Nonlinear Theory Of Elasticity: Applications In Biomechanics*. World Scientific.
- Takasugi, H., H. Inoue, and O. Akahori. 1976. 'Scanning Electron Microscopy of Repaired Tendon and Pseudosheath'. *The Hand* 8 (3): 228–34. [https://doi.org/10.1016/0072-968x\(76\)90006-1](https://doi.org/10.1016/0072-968x(76)90006-1).
- Tan, Wei, Aylin Sendemir-Urkmez, Lester J. Fahrner, Russell Jamison, Deborah Leckband, and Stephen A. Boppart. 2004. 'Structural and Functional Optical Imaging of Three-Dimensional Engineered Tissue Development'. Research-article. <https://Home.Liebertpub.Com/Ten>. Mary Ann Liebert, Inc. 2 Madison Avenue Larchmont, NY 10538 USA. 2 Madison Avenue Larchmont, NY 10538 USA. 28 December 2004. <https://doi.org/10.1089/ten.2004.10.1747>.
- Taunton, J. E., M. B. Ryan, D. B. Clement, D. C. McKenzie, D. R. Lloyd-Smith, and B. D. Zumbo. 2002. 'A Retrospective Case-Control Analysis of 2002 Running Injuries'. *British Journal of Sports Medicine* 36 (2): 95–101. <https://doi.org/10.1136/bjism.36.2.95>.
- Terry, Glenn C., Jack C. Hughston, and Lyle A. Norwood. 1986. 'The Anatomy of the Iliopatellar Band and Iliotibial Tract'. *The American Journal of Sports Medicine* 14 (1): 39–45. <https://doi.org/10.1177/036354658601400108>.
- Themes, U. F. O. 2016a. 'The Femur'. *Musculoskeletal Key* (blog). 3 September 2016. <https://musculoskeletalkey.com/the-femur/>.
- . 2016b. 'The Hip'. *Musculoskeletal Key* (blog). 3 September 2016. <https://musculoskeletalkey.com/the-hip-5/>.
- Tzanetis, Periklis, Marco A. Marra, René Fluit, Bart Koopman, and Nico Verdonshot. 2021. 'Biomechanical Consequences of Tibial Insert Thickness after Total Knee Arthroplasty: A Musculoskeletal Simulation Study'. *Applied Sciences* 11 (5): 2423. <https://doi.org/10.3390/app11052423>.
- Van der Wal, Jacob C. 2009. 'The Architecture of the Connective Tissue in the Musculoskeletal System - An Often Overlooked Functional Parameter as to Proprioception in the Locomotor Apparatus'. *International Journal of Therapeutic Massage & Bodywork: Research, Education, & Practice* 2 (4): 9–23. <https://doi.org/10.3822/ijtmb.v2i4.62>.
- Wanich, Tony, Christopher Hodgkins, Jean-Allain Columbier, Erika Muraski, and John G. Kennedy. 2007. 'Cycling Injuries of the Lower Extremity'. *JAAOS - Journal of the American Academy of Orthopaedic Surgeons* 15 (12): 748–56.
- Weiss, Jeffrey Arthur. 1994. 'A Constitutive Model and Finite Element Representation for Transversely Isotropic Soft Tissues'. Ann Arbor, Mich: Proquest Information and Learning.

- White, Tim D., Michael T. Black, and Pieter A. Folkens. 2012. 'Chapter 12 - Leg: Femur, Patella, Tibia, and Fibula'. In *Human Osteology (Third Edition)*, edited by Tim D. White, Michael T. Black, and Pieter A. Folkens, 241–70. San Diego: Academic Press. <https://doi.org/10.1016/B978-0-12-374134-9.50012-X>.
- Whiteside, Leo A. 2002. 'Soft Tissue Balancing: The Knee'. *The Journal of Arthroplasty* 17 (4): 23–27. <https://doi.org/10.1054/arth.2002.33264>.
- Whiteside, Leo A., and Marcel E. Roy. 2009. 'Anatomy, Function, and Surgical Access of the Iliotibial Band in Total Knee Arthroplasty'. *JBJS* 91 (Supplement_6): 101–6. <https://doi.org/10.2106/JBJS.I.00532>.
- Wilhelm, Mark, Omer Matthijs, Kevin Browne, Gesine Seeber, Anja Matthijs, Phillip S. Sizer, Jean-Michel Brismée, C. Roger James, and Kerry K. Gilbert. 2017. 'DEFORMATION RESPONSE OF THE ILIOTIBIAL BAND-TENSOR FASCIA LATA COMPLEX TO CLINICAL-GRADE LONGITUDINAL TENSION LOADING IN-VITRO'. *International Journal of Sports Physical Therapy* 12 (1): 16–24.
- Wilke, Jan, Veronica Macchi, Raffaele De Caro, and Carla Stecco. 2019. 'Fascia Thickness, Aging and Flexibility: Is There an Association?' *Journal of Anatomy* 234 (1): 43–49. <https://doi.org/10.1111/joa.12902>.
- Wilke, Jan, Robert Schleip, Can A. Yucesoy, and Winfried Banzer. 2018. 'Not Merely a Protective Packing Organ? A Review of Fascia and Its Force Transmission Capacity'. *Journal of Applied Physiology* 124 (1): 234–44. <https://doi.org/10.1152/jappphysiol.00565.2017>.
- Wu, Ge, Sorin Siegler, Paul Allard, Chris Kirtley, Alberto Leardini, Dieter Rosenbaum, Mike Whittle, et al. 2002. 'ISB Recommendation on Definitions of Joint Coordinate System of Various Joints for the Reporting of Human Joint Motion—Part I: Ankle, Hip, and Spine'. *Journal of Biomechanics* 35 (4): 543–48. [https://doi.org/10.1016/S0021-9290\(01\)00222-6](https://doi.org/10.1016/S0021-9290(01)00222-6).
- Yeh, Alvin T., Marie J. Hammer-Wilson, David C. Van Sickle, Hilary P. Benton, Aikaterini Zoumi, Bruce J. Tromberg, and George M. Peavy. 2005. 'Nonlinear Optical Microscopy of Articular Cartilage'. *Osteoarthritis and Cartilage* 13 (4): 345–52. <https://doi.org/10.1016/j.joca.2004.12.007>.
- Zaghloul, Ahmed. 2018. 'Hip Joint: Embryology, Anatomy and Biomechanics'. *Biomedical Journal of Scientific & Technical Research* 12 (3). <https://doi.org/10.26717/BJSTR.2018.12.002267>.
- Zwirner, Johann, Carsten Babian, Benjamin Ondruschka, Stefan Schleifenbaum, M. Scholze, Neil John Waddell, and Niels Hammer. 2019. 'Tensile Properties of the Human Iliotibial Tract Depend on Height and Weight'. *Medical Engineering & Physics* 69 (July): 85–91. <https://doi.org/10.1016/j.medengphy.2019.05.001>.

Additional results to the Chapter II

Materials and Methods

The anthropometric parameters of three additional fresh female post mortem human subjects were: 91.5 (\pm 3.5) years-old, 61.5 (\pm 13.5) kg, 156.5 (\pm 11.5) cm, with a BMI of 18.5, 35.2, and 19.4 kg/m² respectively. The specimen preparation, anatomical frames acquisition, motion analysis, and digital image correlation were the same as described in the article Material and Methods part. Flexion-extension movement analysis and strain measurement were performed on the lateral surface of fascia lata only. Therefore, only the results from the ITT will be presented.

Results

Knee Angular Velocity

Angular velocity recorded for all flexion-extension movements for all subjects illustrated on the *Figure 1* is showing that the passive movement was applied with similar speed within the five cycles over three tests, and even within the subjects and the legs. Relative standard deviations (RSD) ranged from 18.5 to 28.8% with a mean value of 23.8% for all the tests. The difference between maximum angular velocities for the movements from flexion to extension and from extension to flexion did not exceed 8 deg/sec within subject.

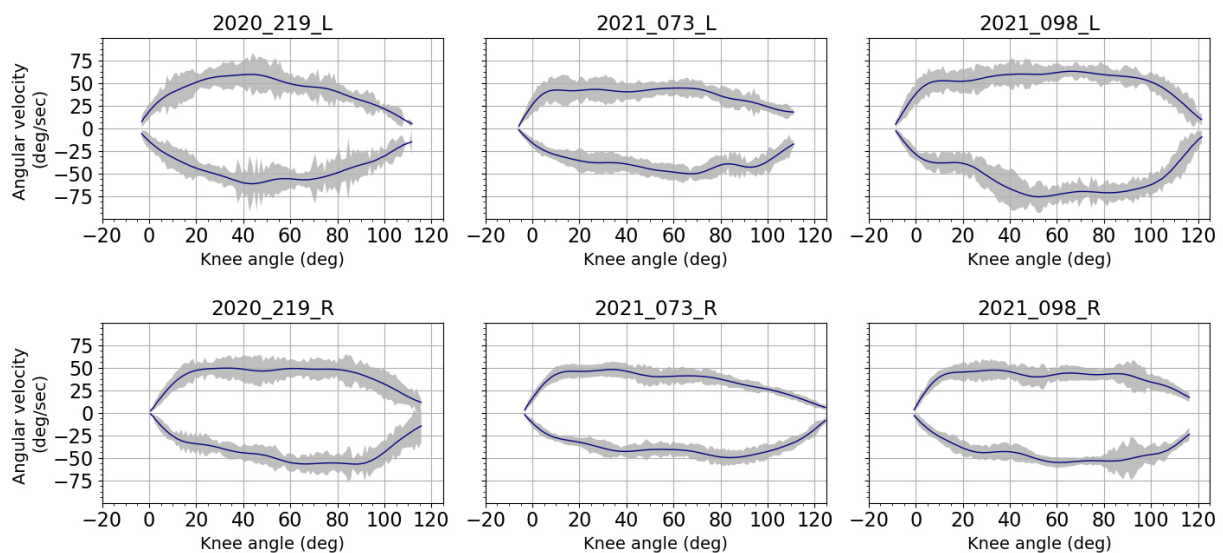


Figure 1. Averaged angular velocities and corresponding standard deviations (grey area) over the knee angles for left L (top) and right R (bottom) legs from all subjects. Data was filtered using a forward-backward linear filter. Filter coefficients were obtained from a low-pass digital Butterworth filter (3rd order, cut off frequency of 2Hz) that was first applied on data. Even though angular velocity was applied manually, results show good reproducibility for each subject. Inter-subject variability can be observed because of subjects' different knee mobility and associated range of motion.

Strain Analysis

Average strains

Shear strain fields with the directions of minor and major principal strains are illustrated for three knee flexion angles (20° , 60° , and 90°) (Figure 2). With higher knee flexion angle, the directions of the principal strains are turning, getting oriented along the bisector of the angle between the two collagen fiber networks (longitudinal and transverse), and showing the maximal strain concentration close to the knee.

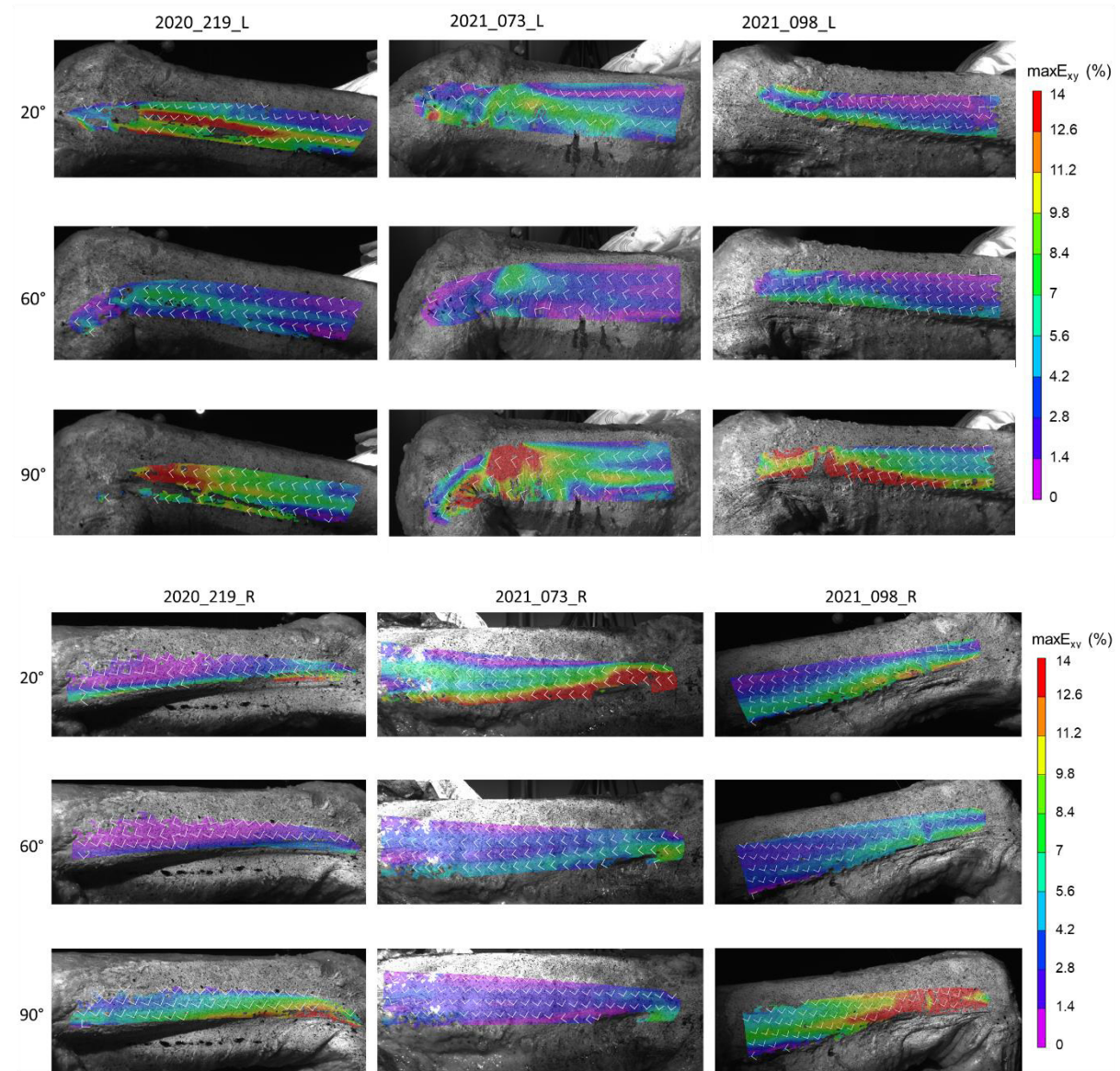


Figure 2. Maximal shear strain distribution $\max E_{xy}$ on the ITT, at knee angles of $20 \pm 0.5^\circ$, $60 \pm 0.5^\circ$, and $90 \pm 0.5^\circ$ for all subjects (Test 1). White arrows show the direction of the major E_1 and minor E_2 principal strains, which are perpendicular to each other.

The evolution of the average strains during knee flexion (extension) angles (Figure 3) shows a good reproducibility between the tests. However, for the subject 2020_219 left leg, the range of the angles decreased, because we did not keep the same maximum flexion angle, although,

it has no impact on the strain levels measured at the corresponding flexion angle between three tests.

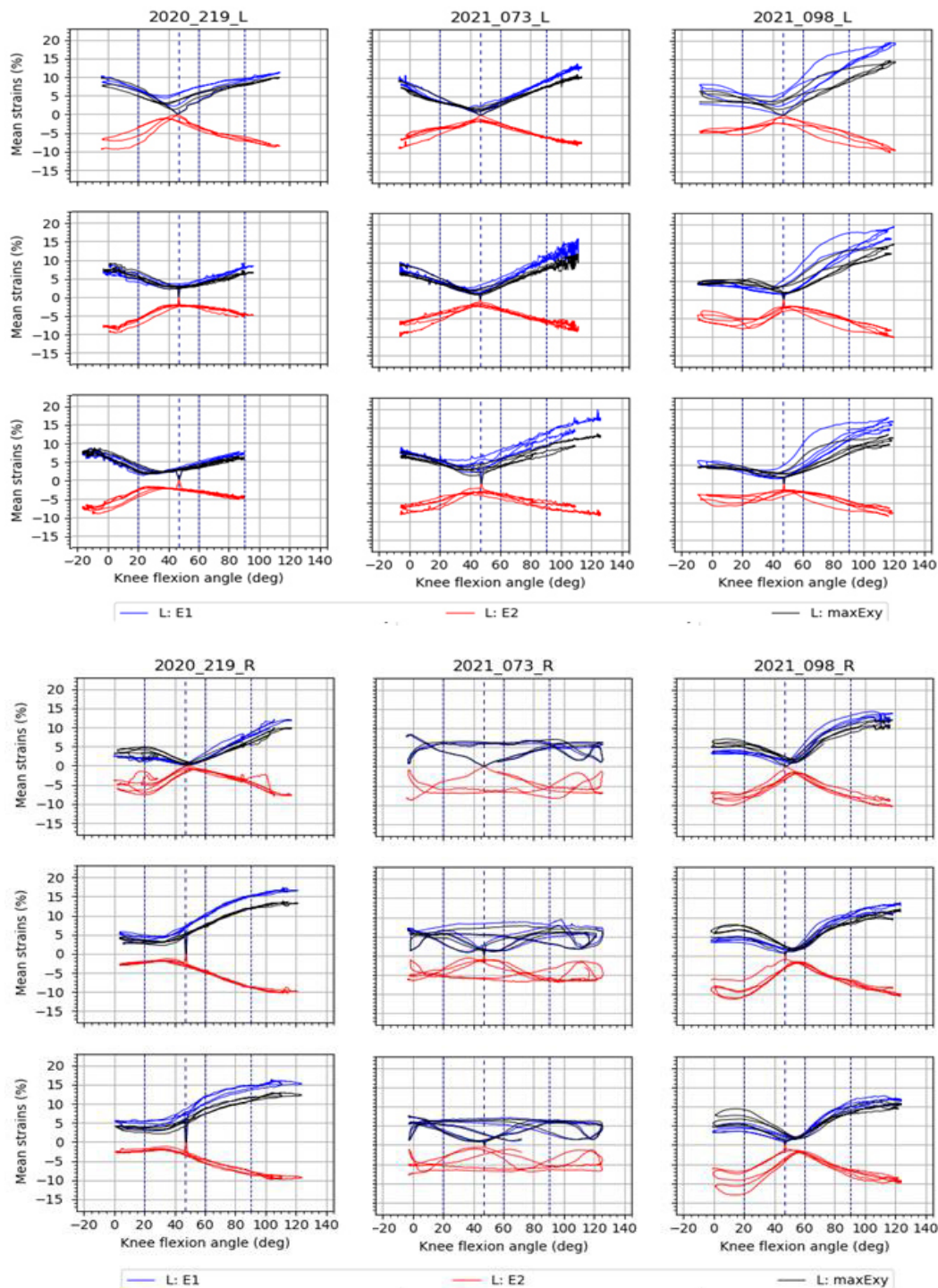


Figure 3. Mean strain distributions over the knee angles for the ITT. In blue, mean major principal strain E_1 , in red, minor principal strain E_2 , and in black maximal shear strain $\max E_{xy}$. For each test, all cycles are plotted. Vertical dashed line represents the knee position chosen as reference: 47° . Three other vertical lines locate knee angles of 20° , 60° , and 90° .

Most of the time, the E_1 strain levels are higher when the knee is flexed, and the E_2 strains are similar between the extension and maximal knee flexion angles. For subject 219_L, the E_1 strain

levels are similar at the extension and maximum flexion, as the maximum flexion angle is smaller compared to other subjects (90 – 100° instead of 120°). For the right leg of subject 2021_073, the curves are different from those illustrated for the other subjects; they are flat. This might be explained by the difficulty to post process the images by the digital image correlation. For all the subjects and tests, the strain levels are similar, with the maximum value of E_1 varying from 7 to 20%, if we include the results of the subject 2020_219_L that were obtained for a lower range of flexion angles.

Standard deviation values for E_1 and E_2 strains are listed in *Table 1*. They are in average from 8 to 37%. For all the curves, maximum RSD was obtained for knee angles around the reference position of 47°.

Table 1. Mean, standard deviation (SD) and maximum relative standard deviations (RSD) for the ITT, for each subject, both legs, and for both major E_1 and minor E_2 strains. RSD were calculated considering the five cycles and the three performed tests. Italicized values are mean values for the three subjects and both legs.

Subject #	mean RSD for E_1 (%)	SD RSD for E_1 (%)	max RSD for E_1 (%)	mean RSD for E_2 (%)	SD RSD for E_2 (%)	max RSD for E_2 (%)
2020_219_L	9	4	35	12	3	31
2021_073_L	10	5	35	14	3	34
2021_098_L	17	10	48	20	5	50
2020_219_R	8	4	34	11	3	22
2021_073_R	35	11	25	37	10	46
2021_098_R	12	5	46	16	6	56
<i>mean</i>	<i>15</i>			<i>18.2</i>		

For each subject, average curves obtained for the different areas of the ITT are illustrated on *Figure 4*. All the subjects produce similar results, except the right leg of the subject 2021_073, what is linked to the post processing, but not to the physical conditions of the leg.

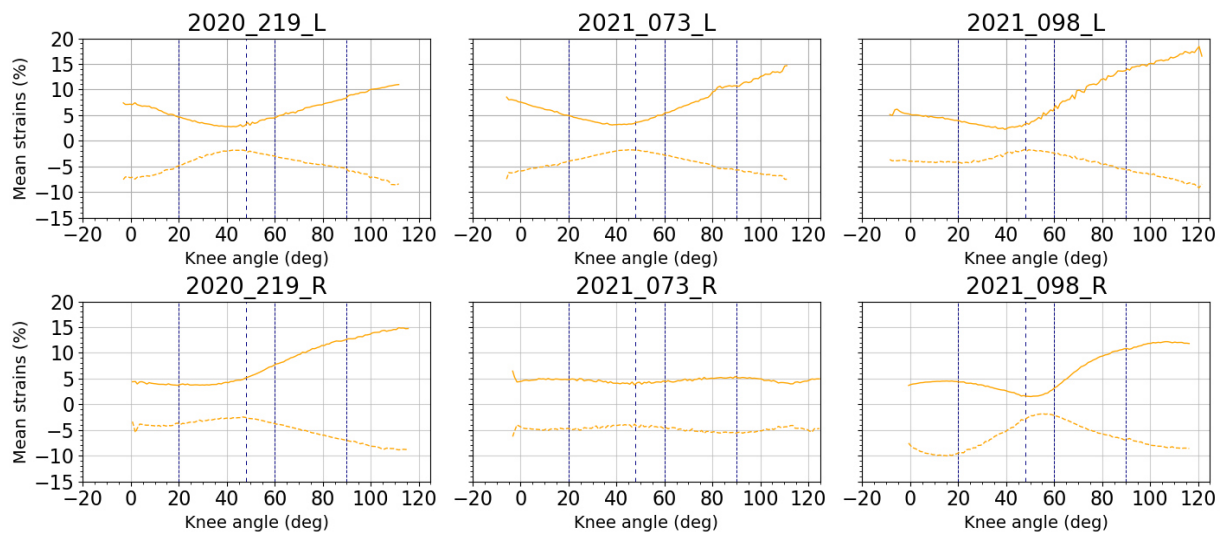


Figure 4. Average curves for mean major principal strain E_1 (bold) and mean minor principal strain E_2 (dashed) over the knee angles on the ITT.

Strain Mechanisms

To analyze the possible pure shear effect in the ITT, which is presumed by looking on the $\max E_{xy}$ and E_1 curves on the *Figure 3* we plotted E_1 as a function of E_2 in absolute value (*Figure 5*). On this figure, the data is colored in blue for strains corresponding to the knee position before 47° (extension) which is chosen as the reference image, and in red for the strain after it (flexion). All the subjects show similar strain mechanisms, including the subject 2021_073_R with very low strain values. When the knee is flexed (above 47°), the strains are higher compared to those when the knee flexion angles are under 47° . Pure shear strain can be noticed for the case when the leg is flexed under 47° (left leg for all subjects). Considering all the tests, the maximum tensile and compressive strains are respectively 4 – 18% and 4 – 10%.

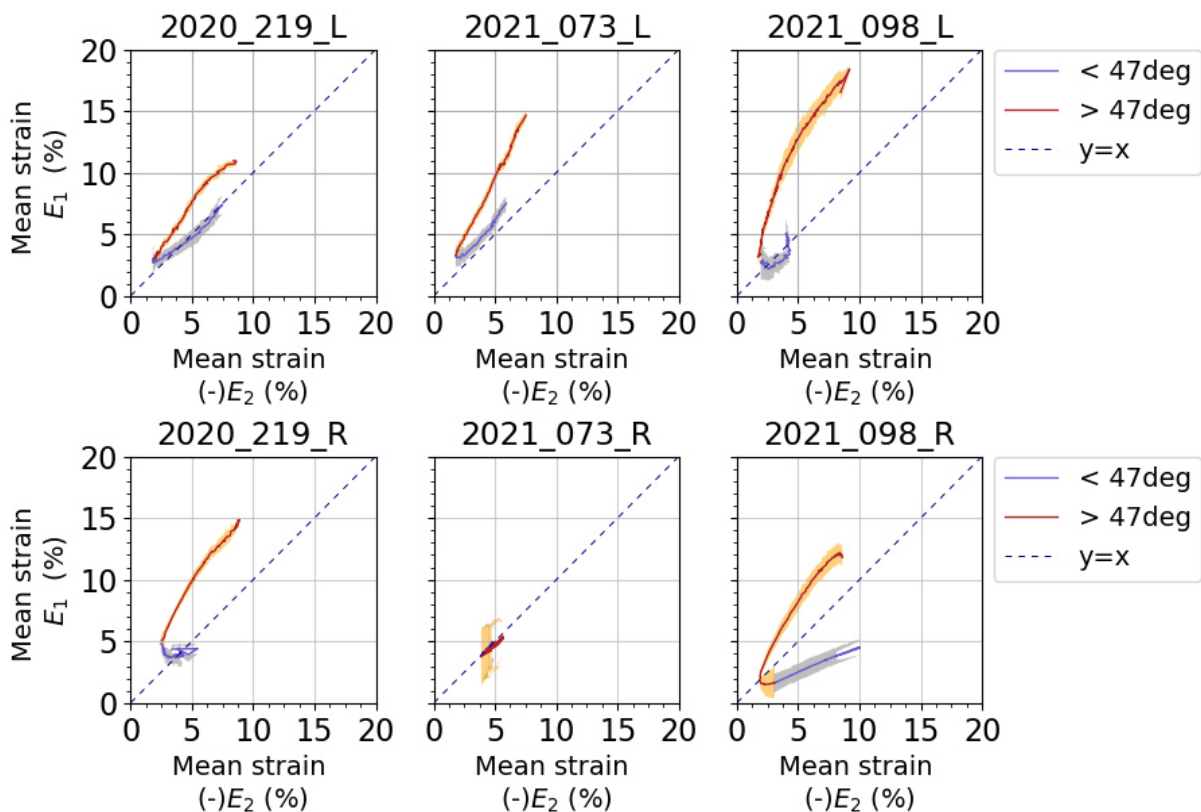


Figure 5. Average curves for mean major principal strain E_1 against negative mean minor principal strain E_2 for ITT. Results are presented for each subject and average of the test. Blue curves and light blue areas correspond respectively to average values and standard deviation obtained for a knee angle lower than the reference position of 47° : extended knee. Red curves and orange areas correspond respectively to average values and standard deviation obtained for a knee angle greater than the reference position of 47° : flexed knee. Dashed line represents the $y = x$ curve, when points are along this line, pure shear can be observed.

Strain rates

Strain rates measured on the ITT averaged for all tests of each subject are close in absolute value for the movement from extension to flexion (positive strain rates) and from flexion to extension (negative strain rates) (*Figure 6*). The average difference is between 0.07 and 1.6%/sec for dE_1 , 0.14 and 0.54%/sec for dE_2 . The maximum strain rate is the highest (more

than 30%/sec) for the subject 2021_073_L, and for the others (in absolute value) it is between 4.5 and 20%/sec for dE_1 , and 4.5 and 15%/sec for dE_2 .

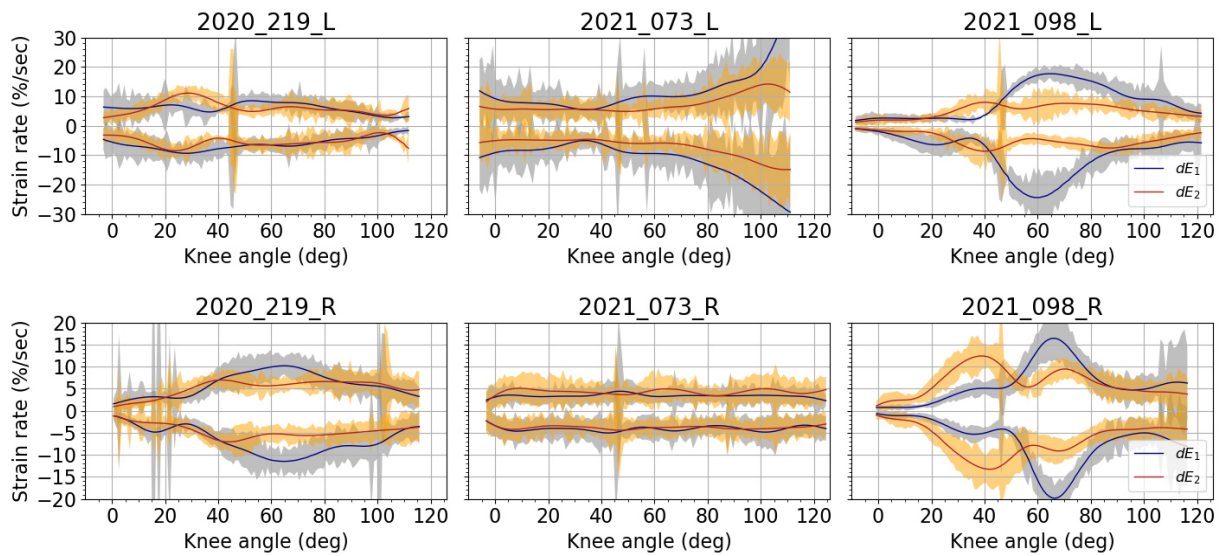


Figure 6. Averaged strain rates and corresponding standard deviation over the knee angles for all subjects on the ITT. Blue curves and grey areas correspond respectively to average strain rate and standard deviation for major strain E_1 . Red curves and orange areas correspond respectively to average strain rate and standard deviation for minor strain E_2 . Data was filtered using a forward-backward linear filter. Filter coefficients were obtained from a low-pass digital Butterworth filter (3rd order, cut off frequency of 2Hz) that was first applied on data.

Discussion

All the results are consistent with those presented in the published article. However, showing a little bit higher strain levels, but the strain mechanisms are remaining the same. The strain values can be explained by the anthropometry of the new subjects, which have higher BMI, and may have better quality of soft tissues and muscles volume.

APPENDIX II

Additional results to the Chapter III

The rest of the samples studied in the large band and biaxial tests are presented correspondingly on the *Figure 1* and *Figure 2*.

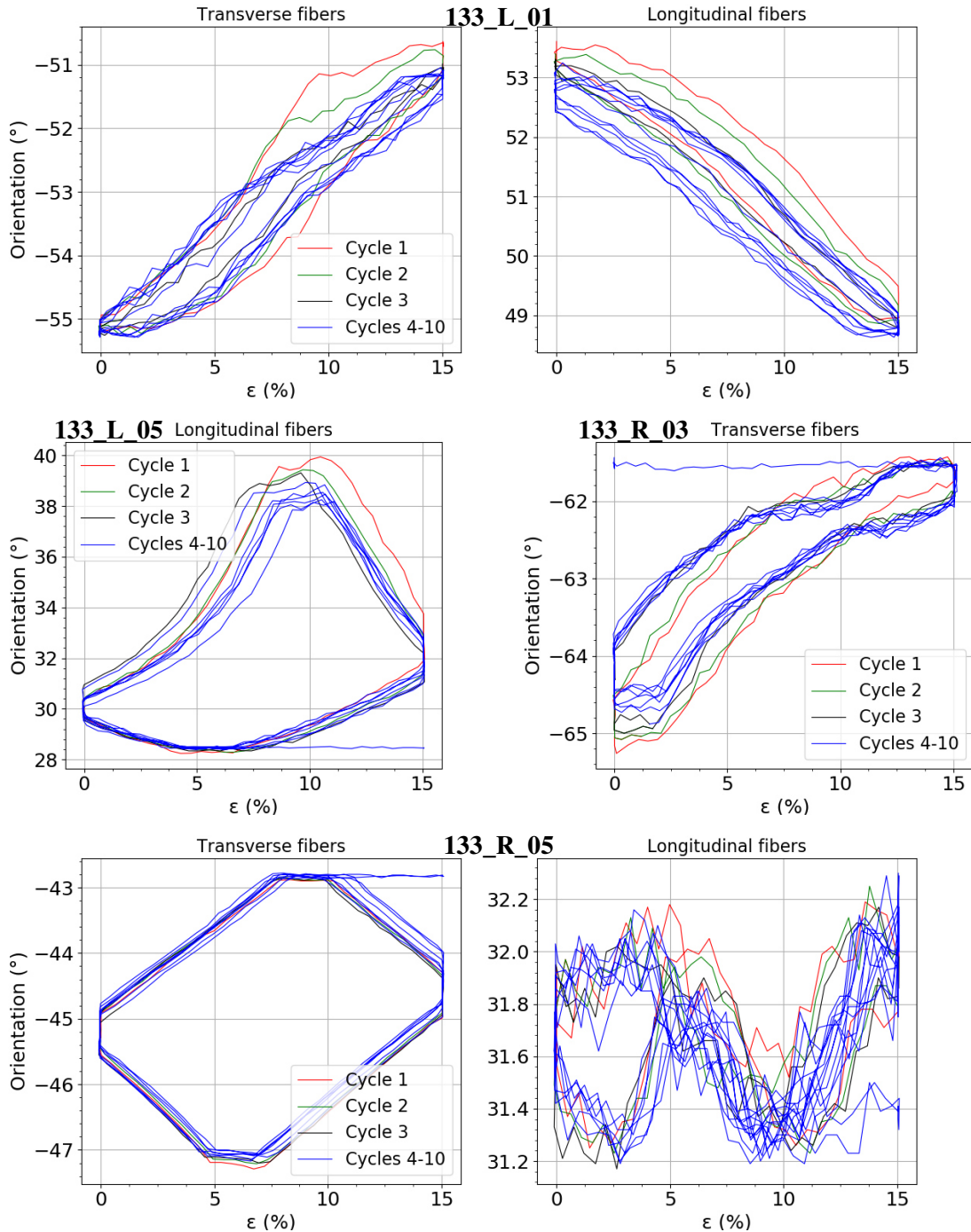


Figure 1. Reorientation of the main fibers along the global stretch measured on the front and (or) on the back faces of the large band samples. * A synchronization error may give this curve shape for samples 133_L_05 and 133_R_05.

107_L_01 and 107_L_03 samples, harvested from the posterior fascia lata were not possible to post process because no fibers were recognized, as the samples were very thin (0.3 mm), and they folded during the applied stretch.

Samples 107_L_09 and 107_L_11 were harvested from the anterior fascia lata, therefore, the thickness of the samples was 0.5 mm, and fibers on the back face of the samples were not visible. For the first sample, on the front face the software recognized partly the transverse fibers only.

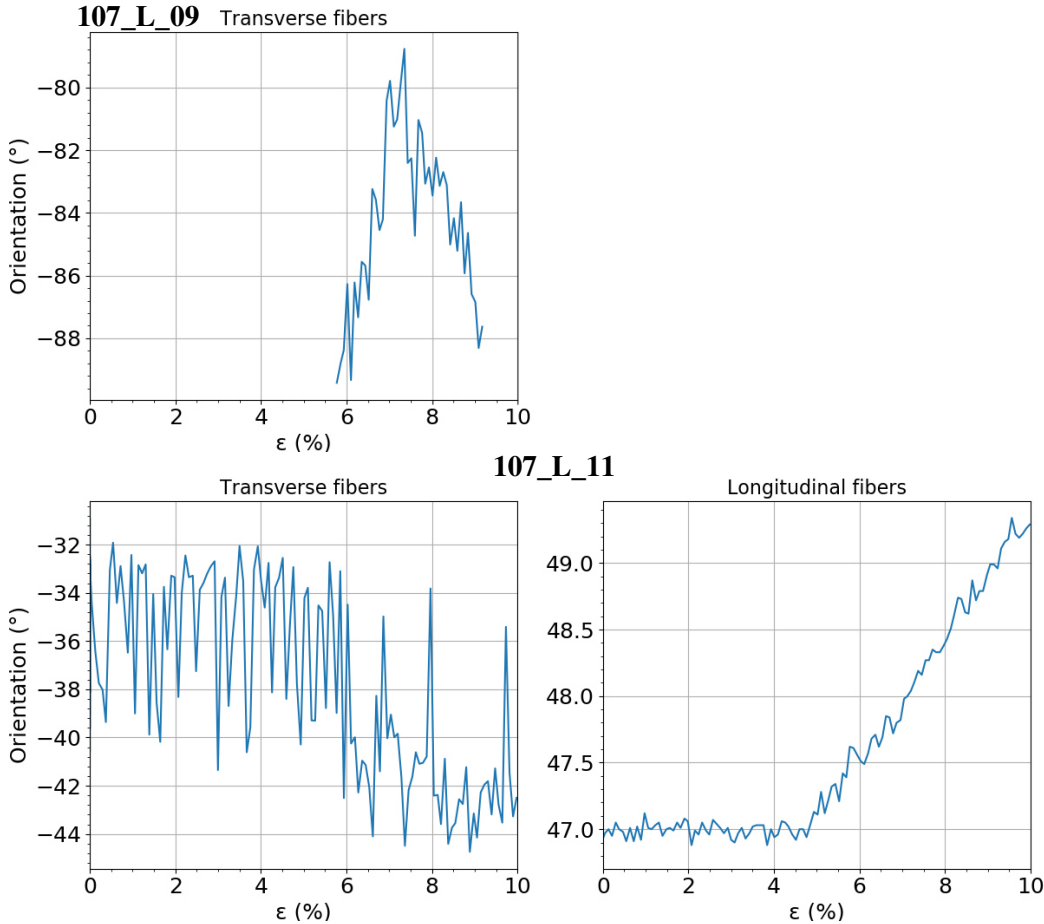


Figure 2. Reorientation of the main fibers along the global stretch measured on the front and (or) on the back faces of the bias samples.

APPENDIX III

Additional results to the Chapter V

*Table 1. Average of principal and maximal shear strains range, mean, and standard deviation values from all subjects on both areas of the interest for all cases and both rotation and varus-valgus knee movements. * Cases I, A, and B corresponds to the initial, after pie-crusting, and after ITT dissection from the tibial insertion, respectively. Std – standard deviation.*

Strain	Case	Knee flexion angle [°]	Rotation						Varus-valgus					
			area 2			area 3			area 2			area 3		
			range	mean	std	range	mean	std	range	mean	std	range	mean	Std
average E_1 [%]	I	0	7,8	3,9	2,0	11,3	5,9	2,7	4,9	3,1	0,8	8,3	5,4	1,6
	A		7,4	3,6	1,9	13,5	6,7	3,1	6,3	3,4	1,3	9,1	5,2	1,9
	B		8,0	3,7	2,2	13,8	6,7	3,6	5,6	2,7	1,1	8,3	4,1	1,9
	I	20	7,7	3,5	2,1	10,9	5,8	2,8	6,7	4,3	1,2	10,7	6,5	2,4
	A		7,8	3,7	1,6	11,7	5,8	2,3	7,3	3,9	1,5	9,7	5,0	2,0
	B		9,7	4,7	1,9	14,2	6,3	3,4	7,2	3,8	1,4	10,1	5,0	2,1
	I	50	8,9	4,5	2,3	13,1	7,2	3,0	6,3	4,1	1,1	11,0	6,5	2,2
	A		8,5	4,1	2,1	14,3	7,7	3,1	8,0	4,4	1,9	11,7	7,0	2,3
	B		8,0	4,5	1,3	14,4	7,2	3,3	9,4	5,4	1,5	12,7	7,0	2,1
average E_2 [%]	I	0	3,3	-1,7	0,7	3,7	-1,9	0,8	1,9	-1,1	0,3	2,6	-1,6	0,5
	A		5,1	-2,4	1,1	8,3	-3,6	2,0	6,8	-3,5	1,7	10,5	-5,6	2,7
	B		7,6	-3,6	1,9	10,1	-4,6	2,5	8,2	-3,6	2,0	10,1	-4,5	2,7
	I	20	3,5	-1,7	0,8	3,3	-1,6	0,8	2,5	-1,6	0,5	3,0	-1,7	0,7
	A		5,1	-2,3	1,1	7,7	-3,8	1,8	7,1	-4,2	1,4	9,4	-4,9	2,5
	B		10,6	-4,4	2,4	12,3	-5,6	2,6	9,7	-4,7	2,5	13,0	-6,6	3,1
	I	50	3,4	-2,0	0,8	3,3	-1,8	0,7	3,2	-1,9	0,6	3,7	-1,9	0,8
	A		5,4	-2,8	1,2	7,3	-3,5	1,5	5,9	-3,1	1,4	9,1	-5,0	2,3
	B		8,2	-4,1	1,9	11,6	-5,9	2,7	10,4	-4,7	2,6	14,8	-6,9	3,5
average $maxE_{xy}$ [%]	I	0	5,4	2,8	1,3	7,1	3,9	1,6	3,4	2,1	0,5	5,3	3,5	1,0
	A		6,0	3,0	1,4	9,7	5,2	2,2	5,7	3,4	1,2	8,9	5,4	2,0
	B		7,0	3,6	1,7	10,6	5,7	2,6	6,0	3,2	1,2	8,0	4,3	1,9
	I	20	5,3	2,6	1,4	6,7	3,7	1,6	4,5	3,0	0,8	6,8	4,1	1,6
	A		5,9	3,0	1,1	8,5	4,8	1,8	6,1	4,0	1,1	8,5	5,0	2,0
	B		8,7	4,5	1,7	11,5	6,0	2,4	7,7	4,3	1,7	10,4	5,8	2,3
	I	50	6,0	3,3	1,5	7,6	4,5	1,8	4,5	3,0	0,8	6,9	4,2	1,4
	A		6,2	3,5	1,3	9,7	5,7	2,0	6,1	3,8	1,3	8,9	6,0	1,8
	B		7,8	4,3	1,4	11,6	6,6	2,5	8,7	5,1	1,7	12,3	6,9	2,3

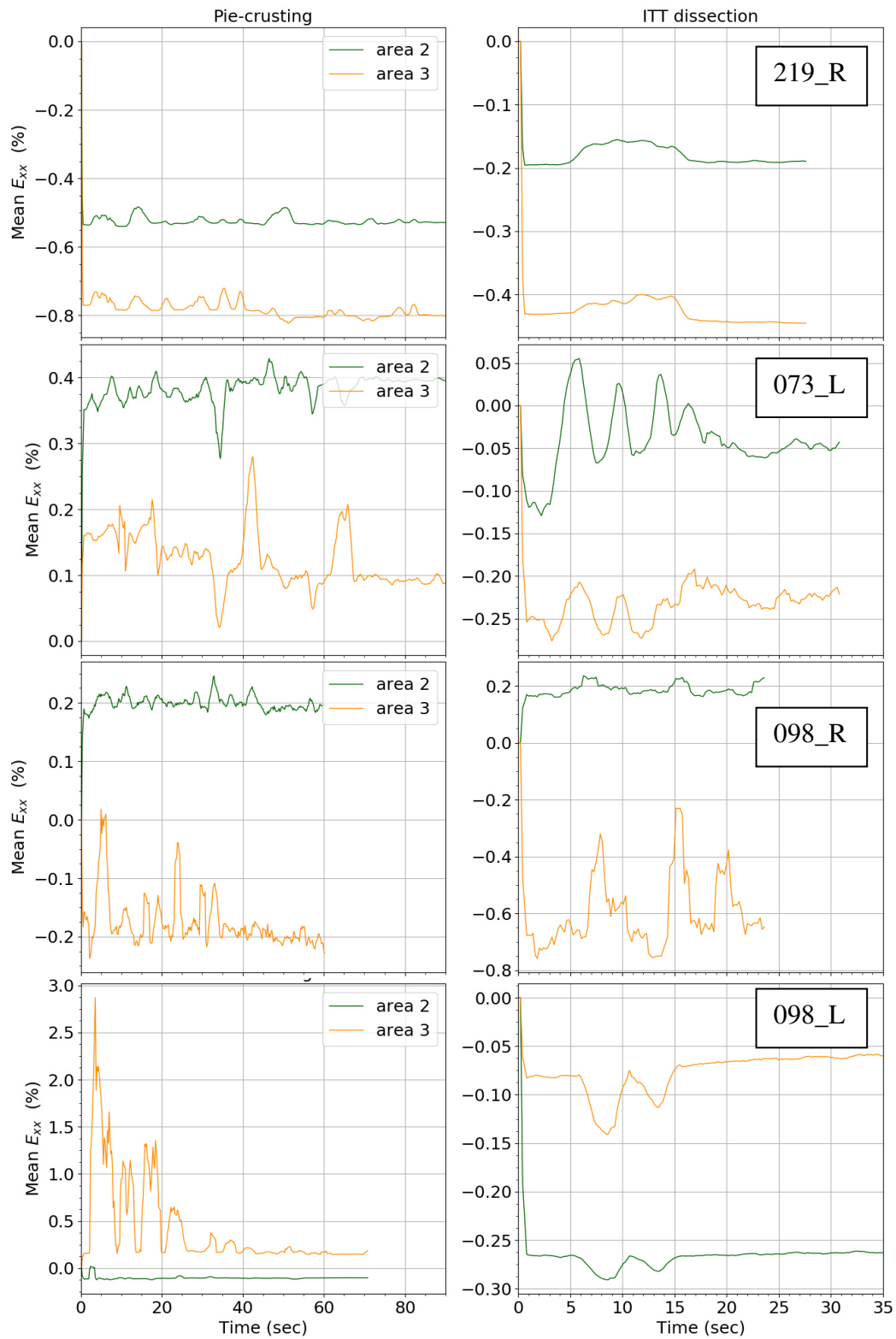
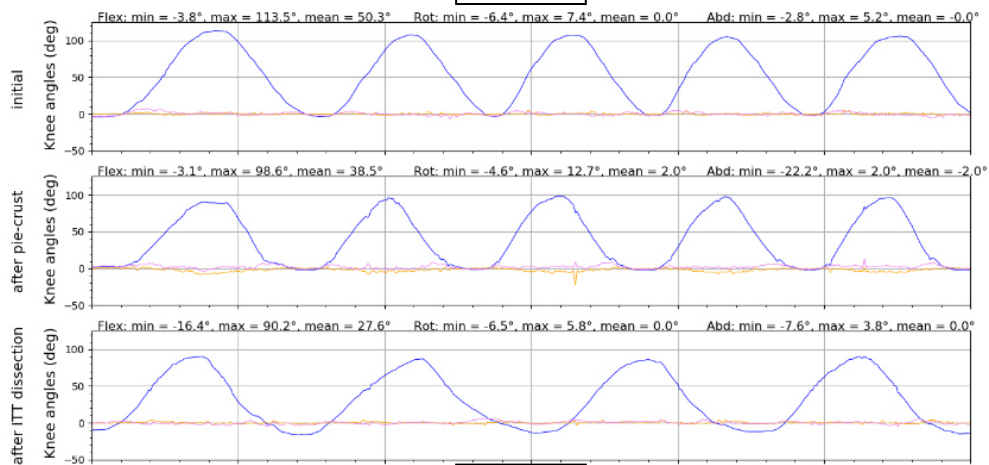
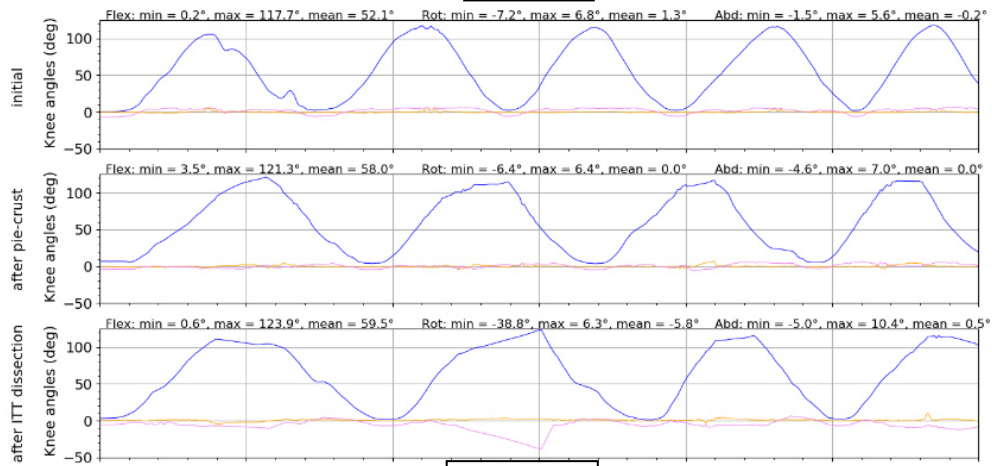


Figure 1. X-axis strains evolutions along the time during the pie-crusting technique and ITT dissection on areas 2 (green) and 3 (orange) for remaining subjects. Scale range is the same for pie-crusting (on the left) and ITT dissection (on the right) plots.

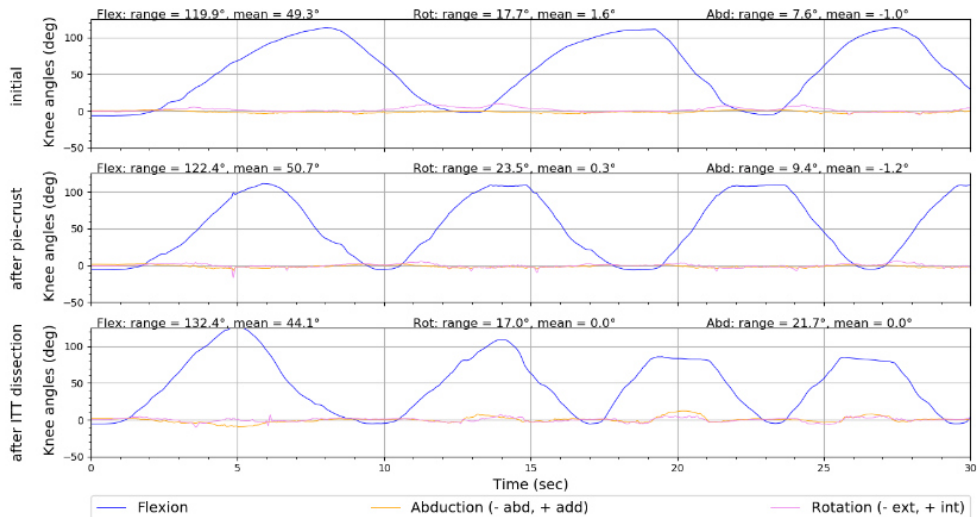
219 L



219 R



073_L



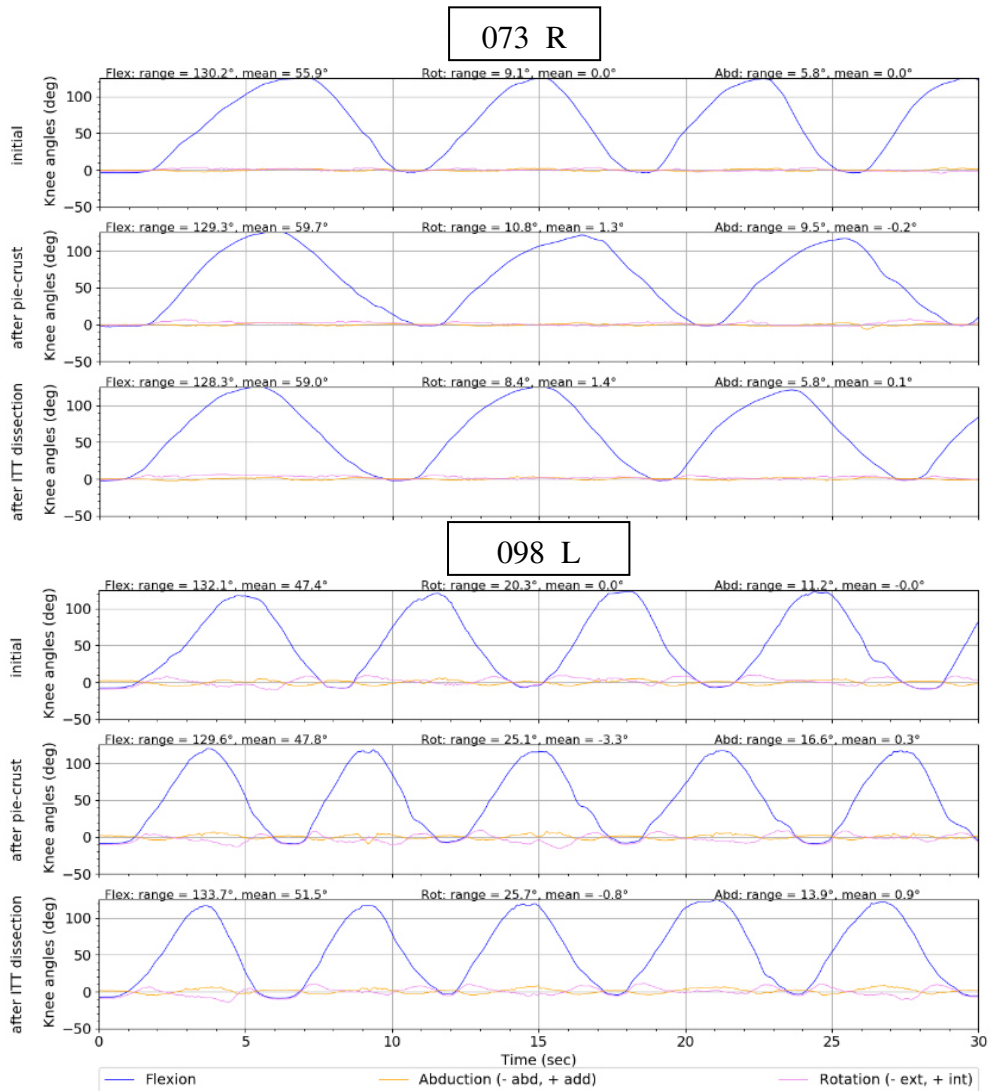
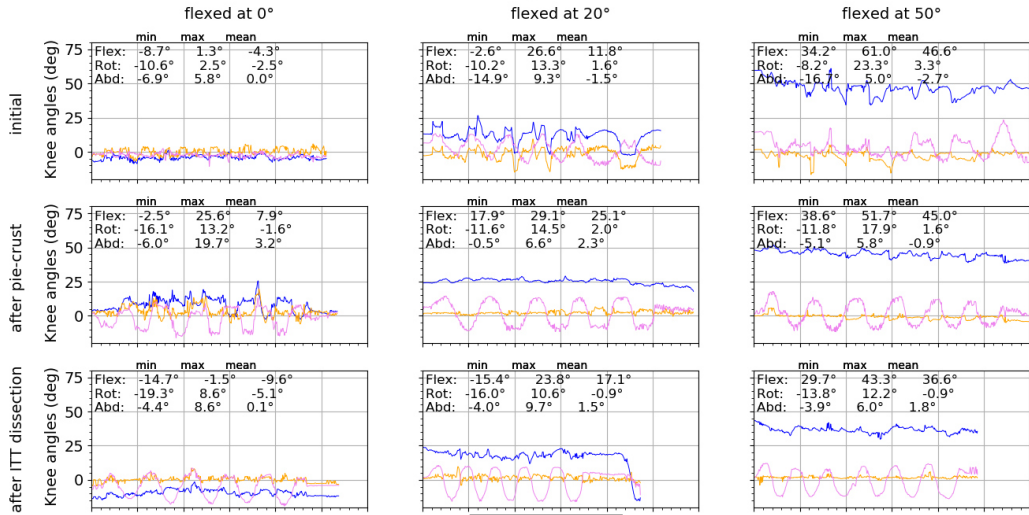
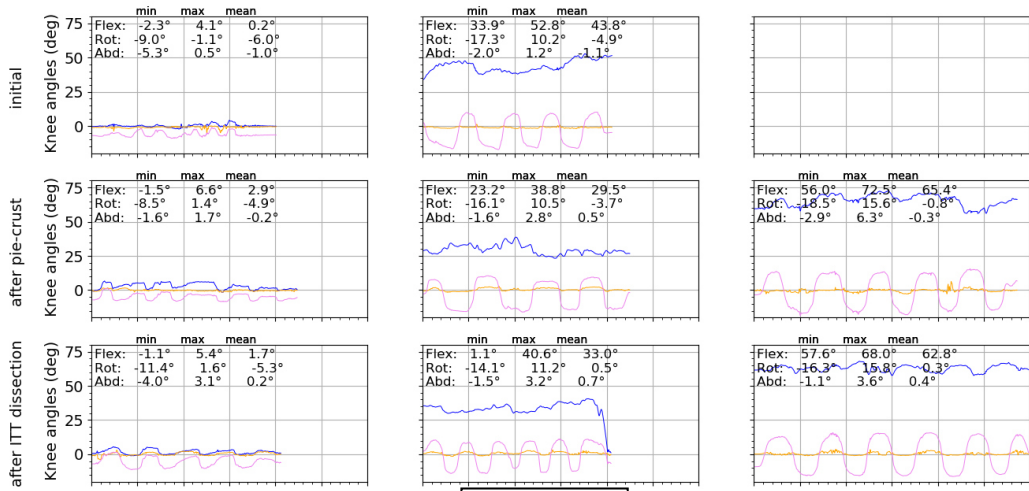


Figure 2. Flexion-extension movements knee joint angles with statistical data (range, mean values) during the initial, after pie-crusting, after ITT dissection cases for all remaining subjects.

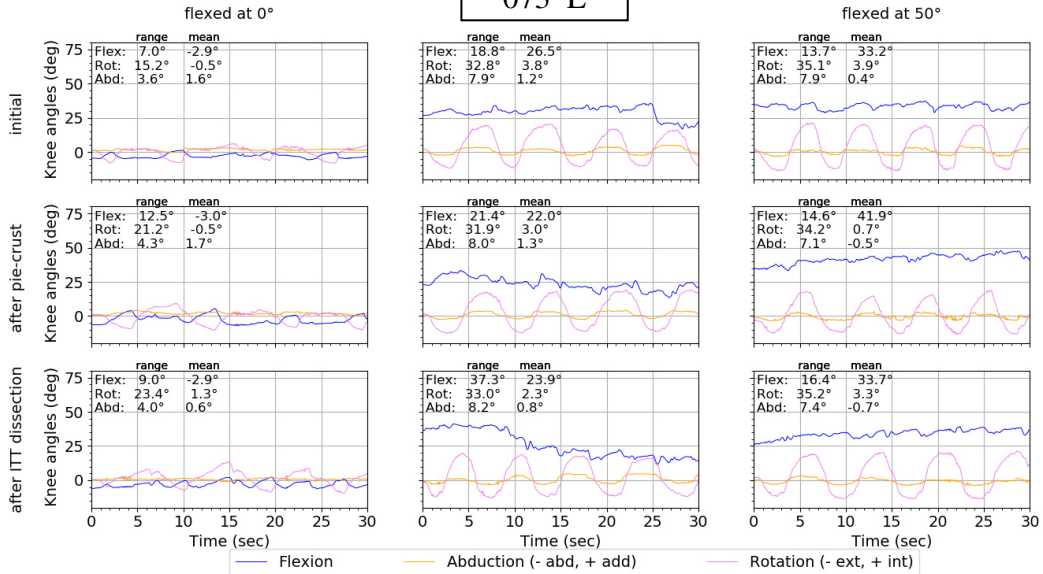
219 L



219 R



073 L



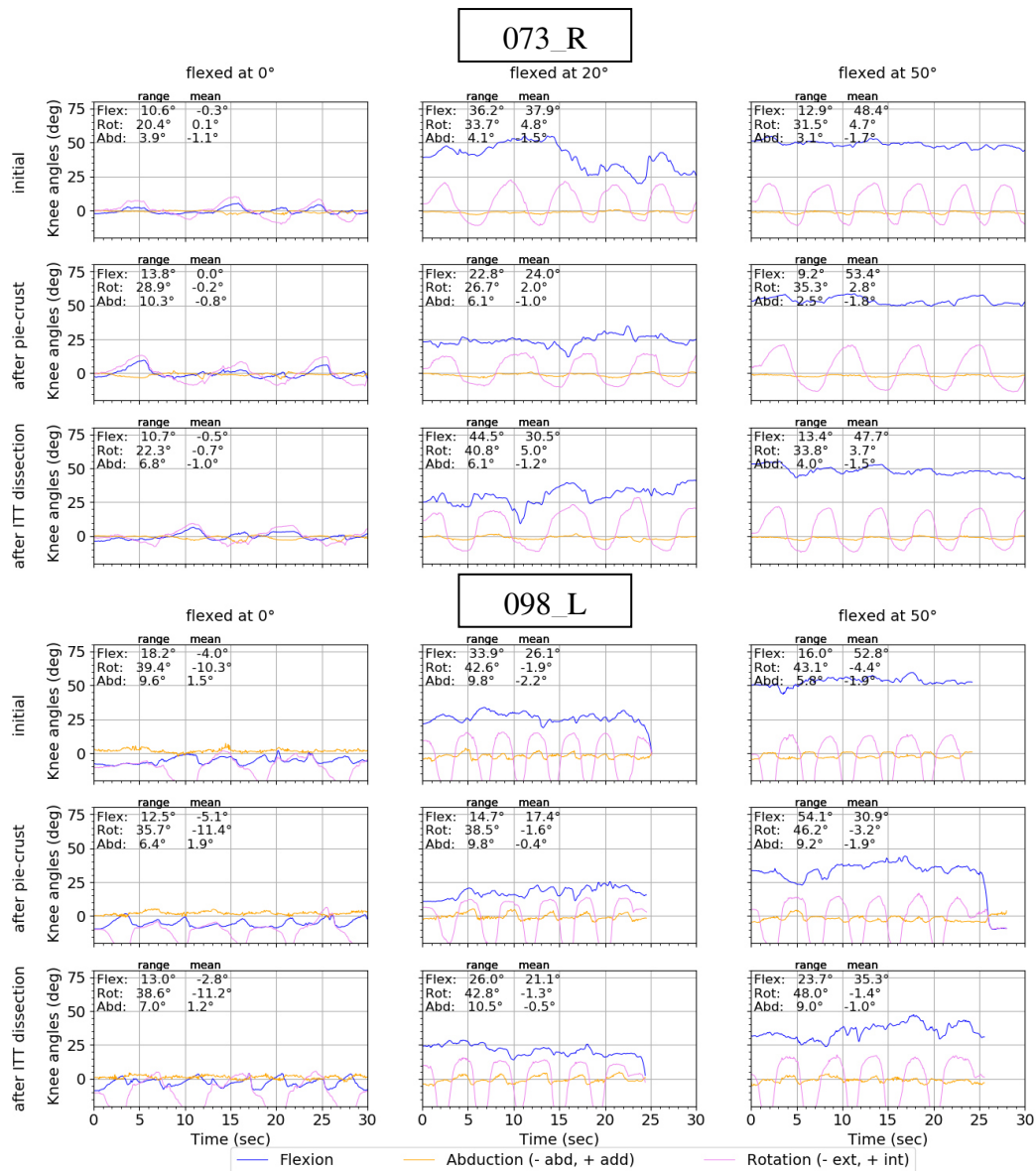
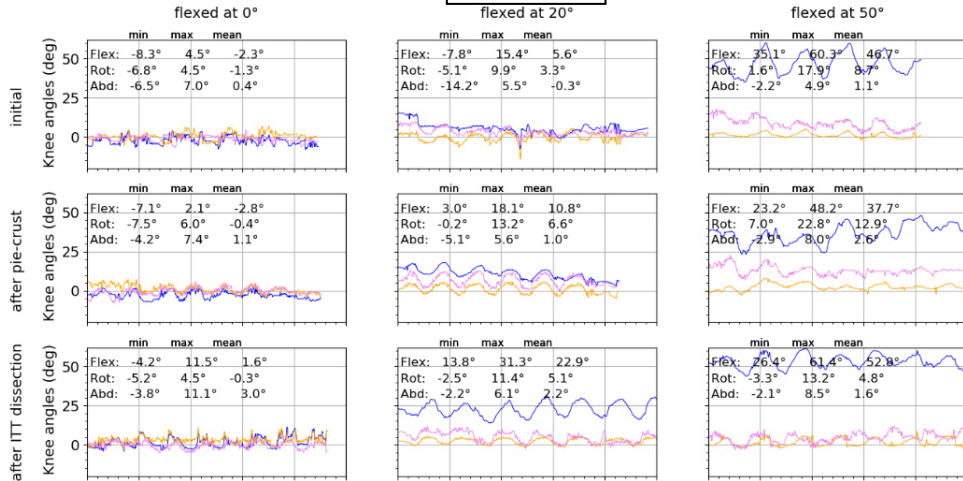
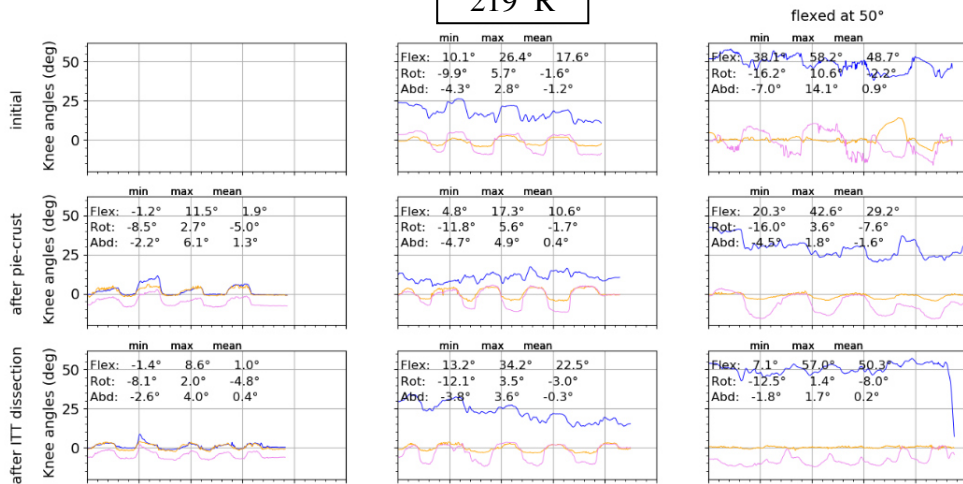


Figure 3. Rotation movements knee joint angles' with statistical data (range and mean values) when the leg was flexed at approximately 0°, 20°, and 50° during the initial, after pie-crusting, and after ITT dissection cases for all remaining subjects.

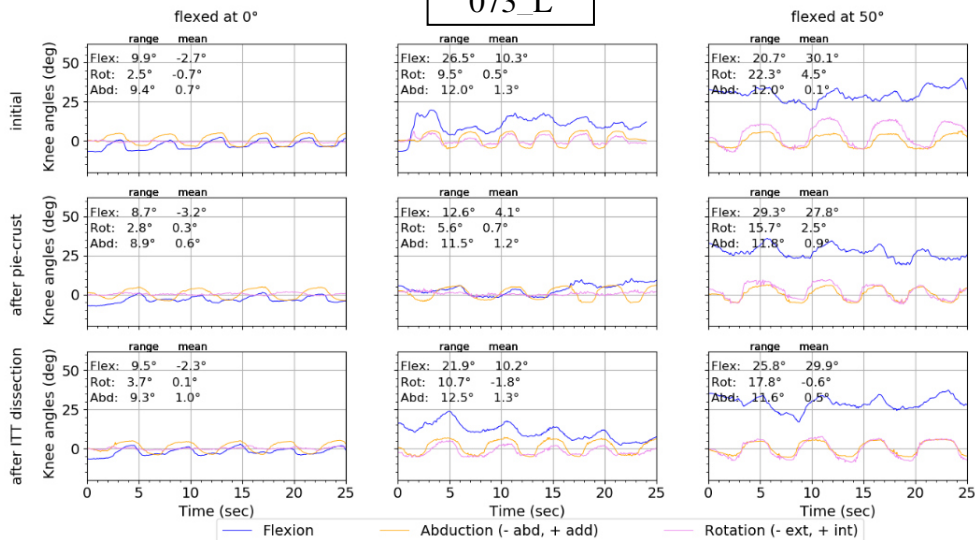
219_L



219_R



073_L



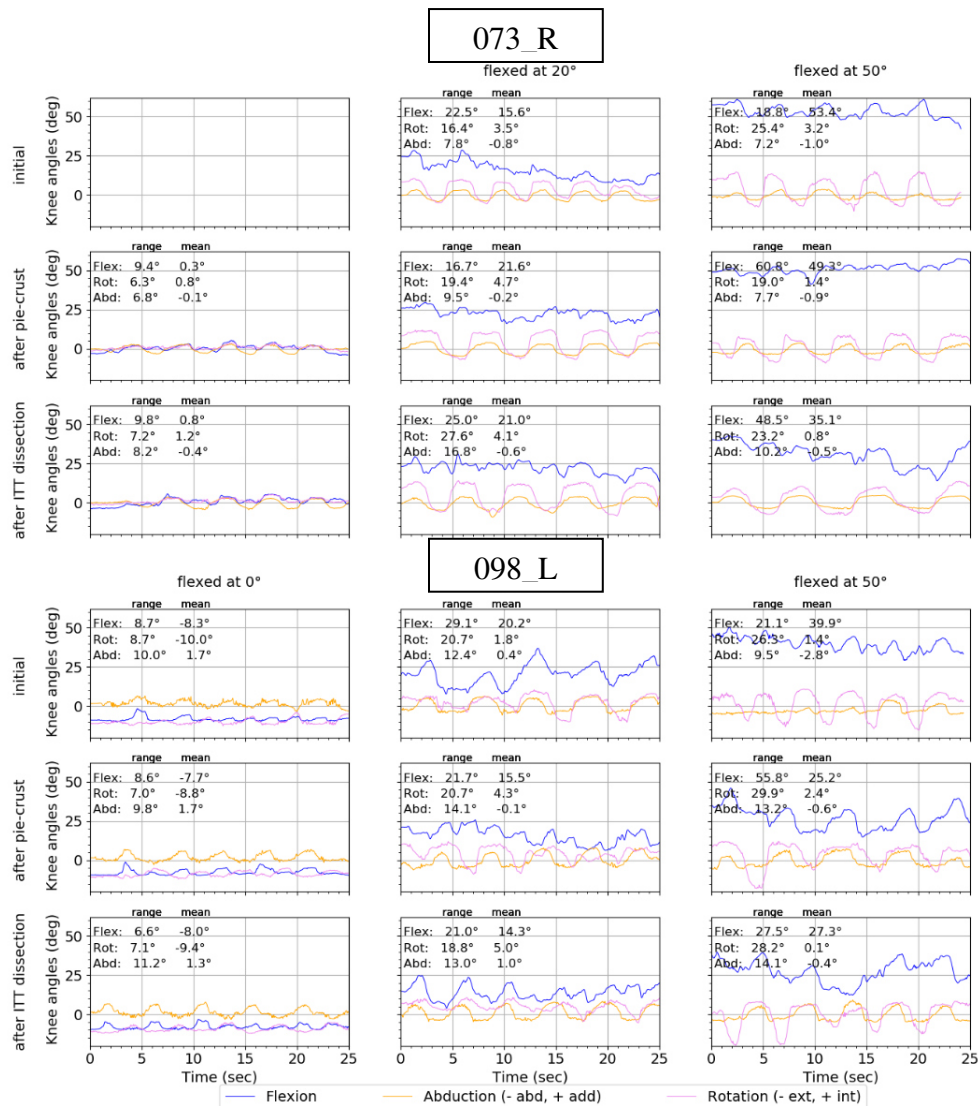


Figure 4. varus-valgus movements' knee joint angles with statistical data (range, mean values) when the leg was flexed at approximately 0°, 20°, and 50° during the initial, after pie-crusting, and after ITT dissection cases for all remaining subjects.

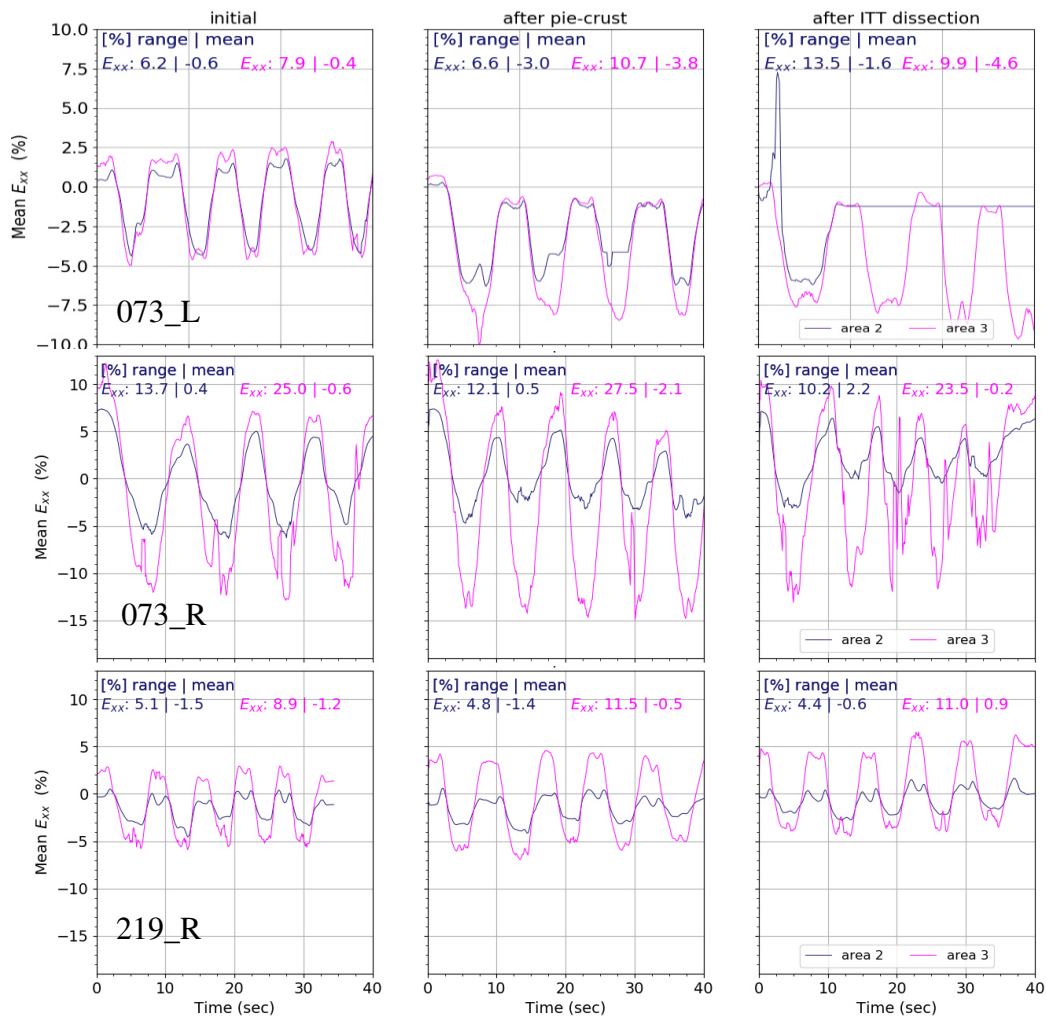
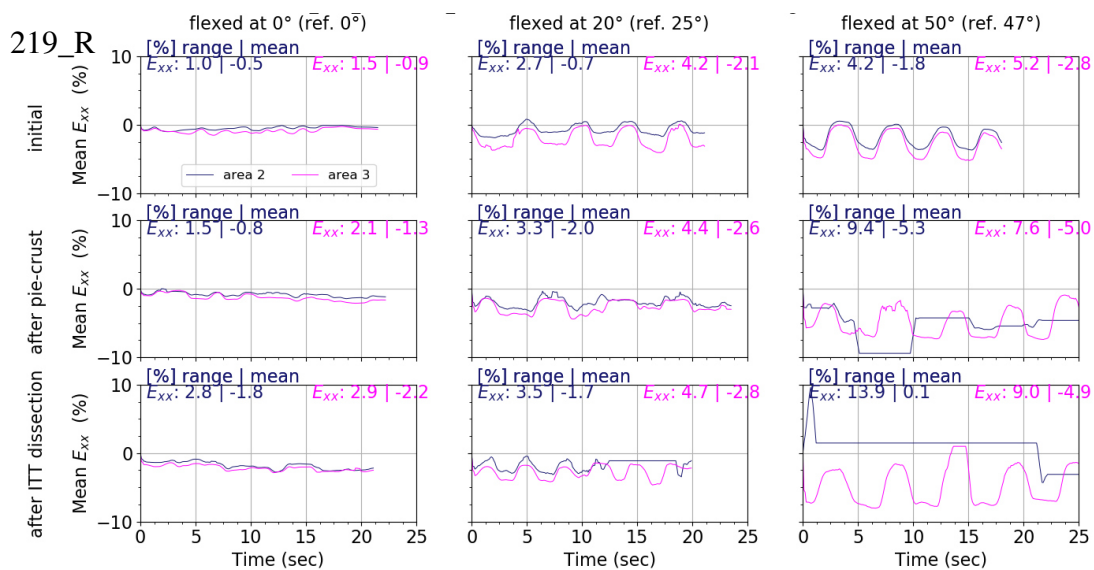
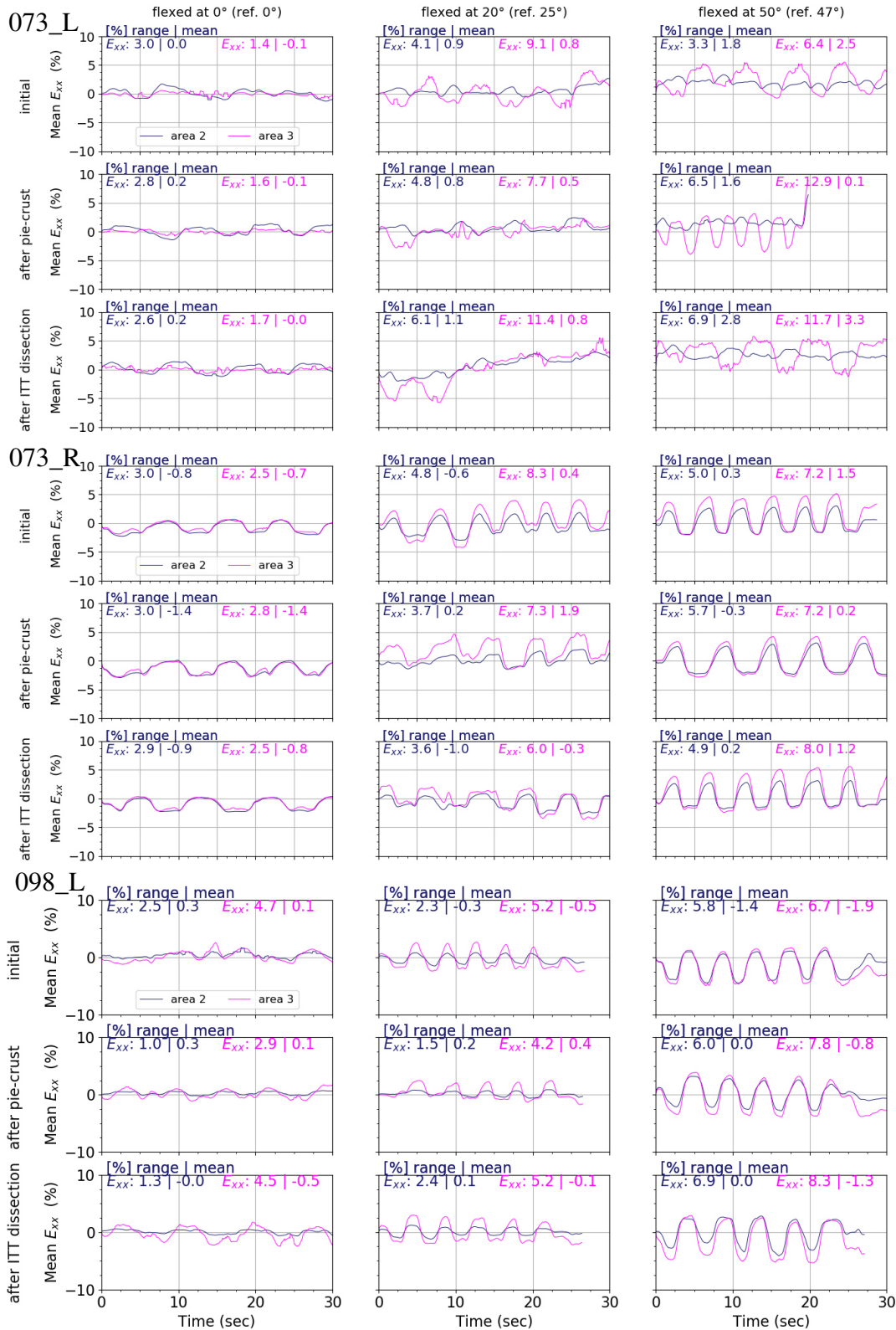


Figure 5. Mean E_{xx} strain along time (top) and along flexion knee angle (bottom) during leg flexion movements on both areas. The curves in blue color are representing the results on the area 2, and the curves in magenta color are representing the results on the area 3 for all remaining subjects.





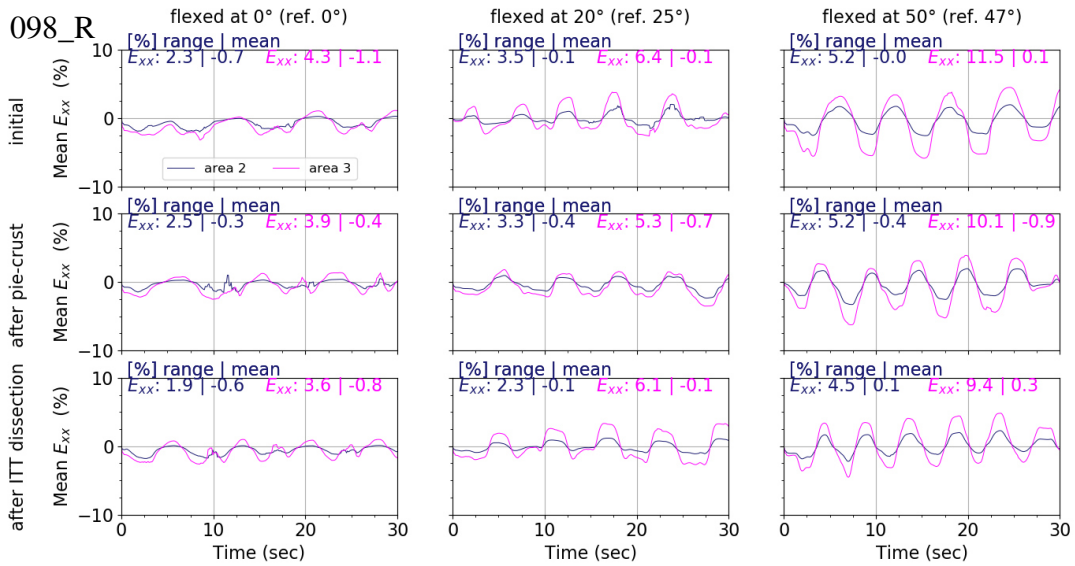
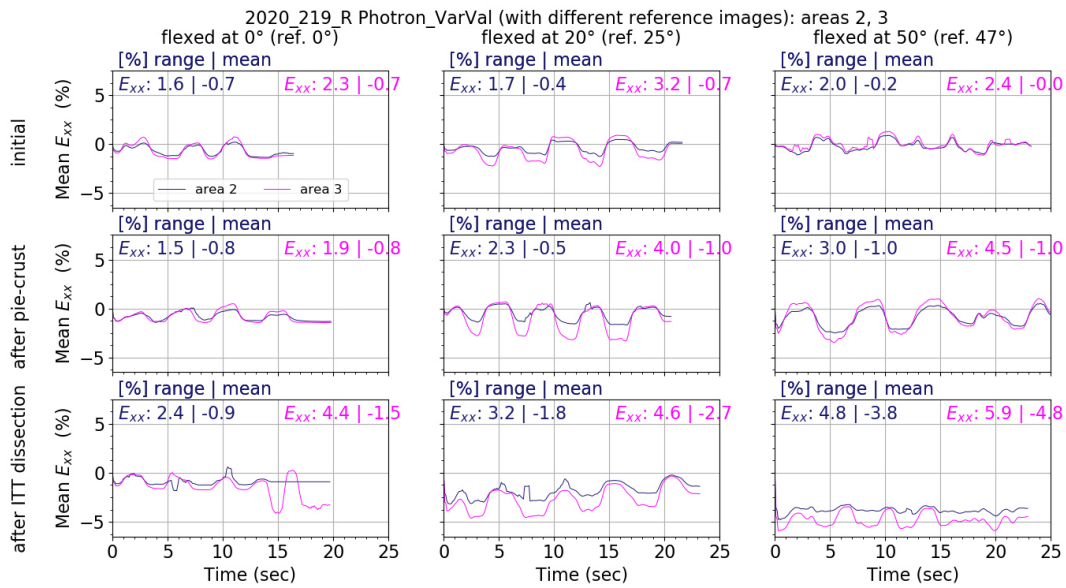
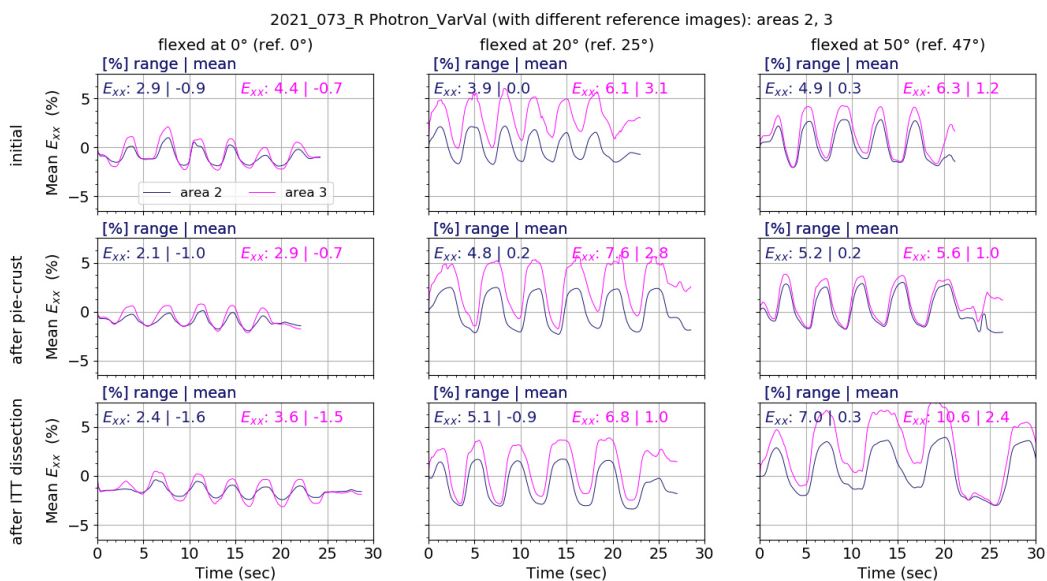
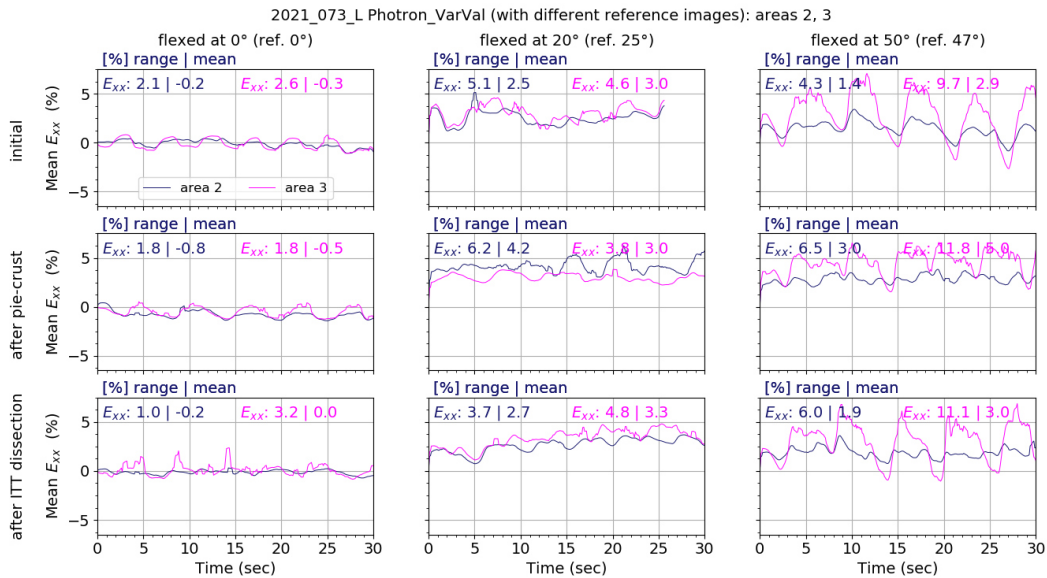
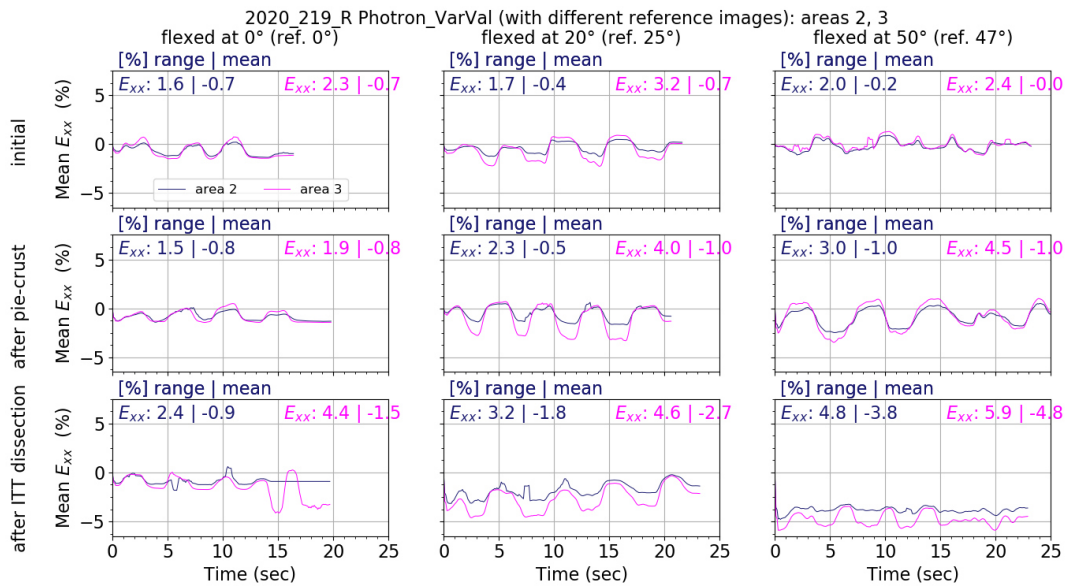


Figure 6. Knee rotation movements for all remaining subjects: mean value of x-axis– strain (E_{xx}) along the time on the area 2 (mid-thigh) and area 3 (closer to the pie-crust zone)s that are closer and further from the pie-crusting and ITT dissection, corresponding to area 3 (magenta) and area 2 (blue).





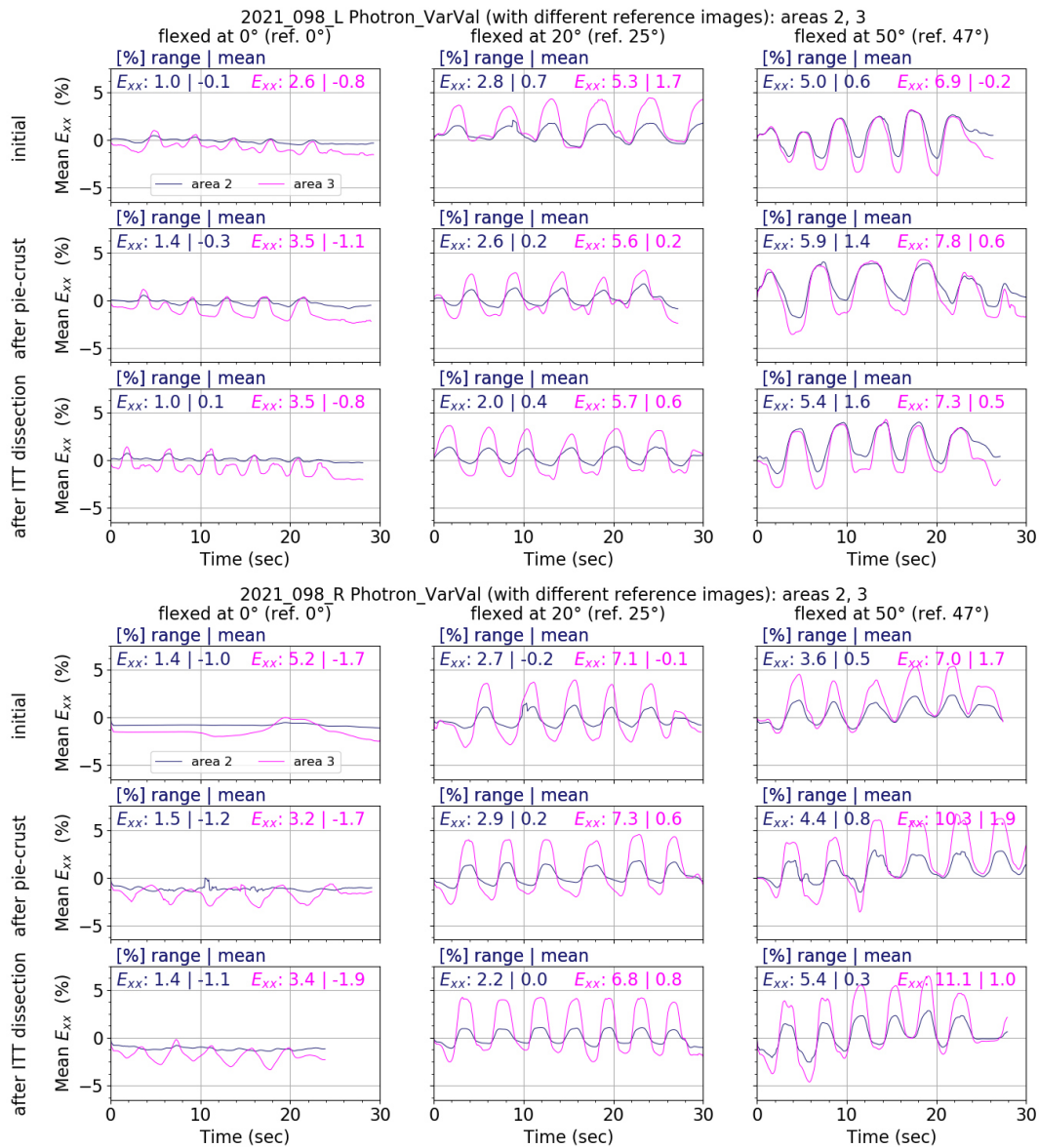


Figure 7. Knee varus-valgus movements for all subjects: mean value of x-axis– strain (E_{xx}) along the time on the area 2 (mid-thigh) and area 3 (closer to the pie-crust zone)s that are closer and further from the pie-crusting and ITT dissection, corresponding to area 3 (magenta) and area 2 (blue).

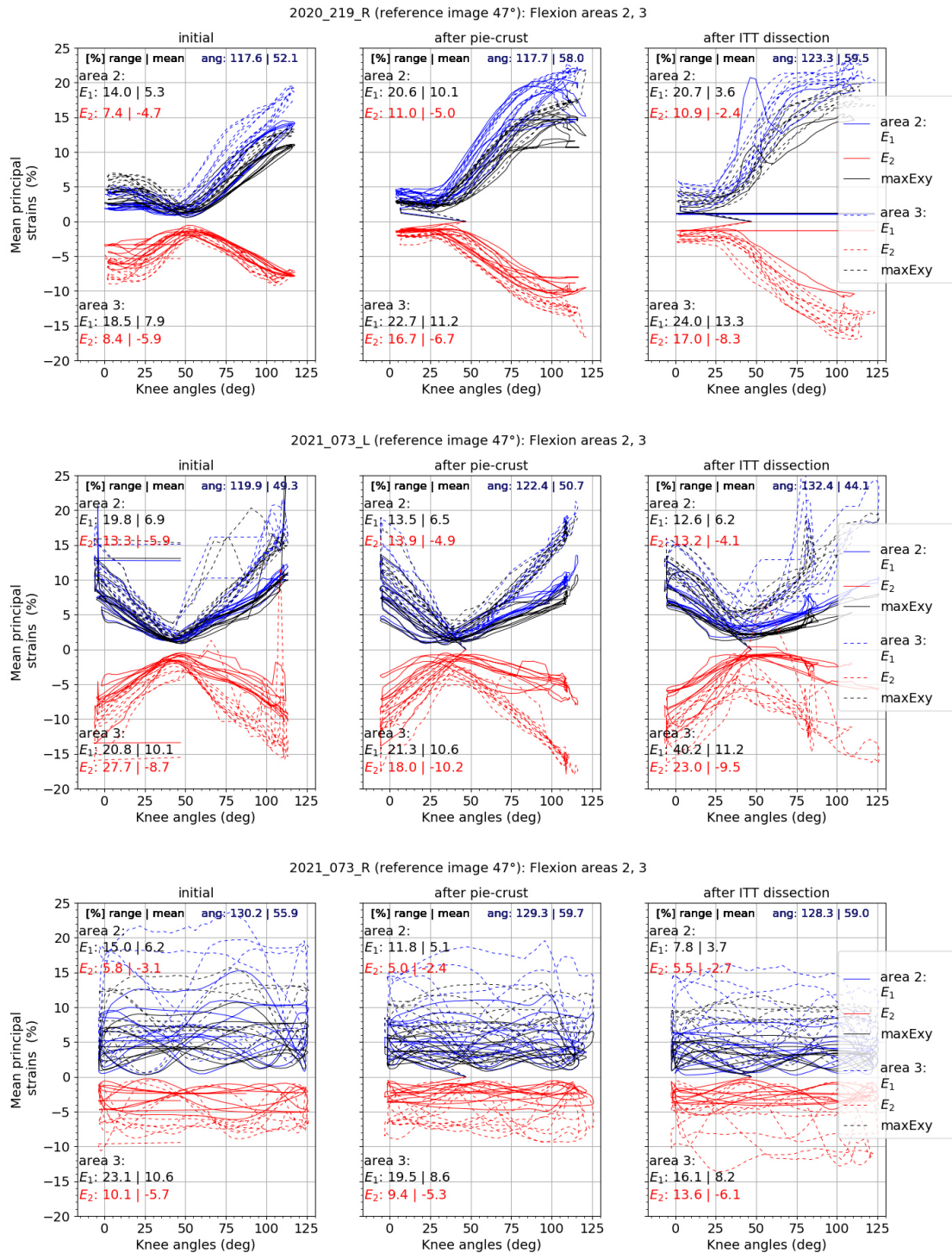
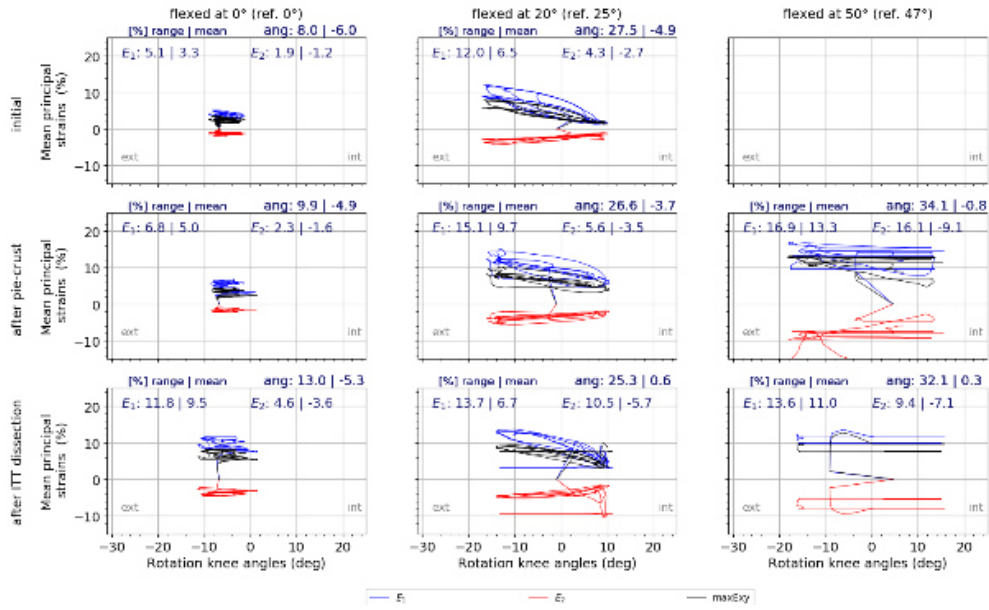
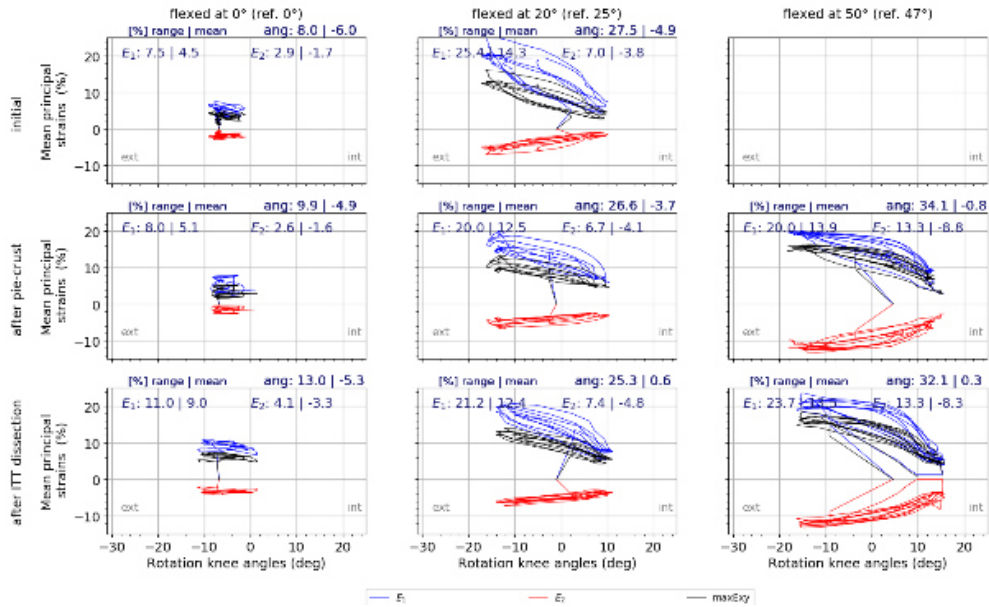


Figure 8. Principal strains and maximal shear strain distributions with the knee flexion angles during flexion-extension movement for areas 2 and 3. Bold and dashed lines are corresponding to the strains from the area 2 and 3, respectively for all remaining subjects. In blue – minor principal strain E_1 , in red – major principal strain E_2 , in black - maximal shear strain $maxE_{xy}$. The range and mean values of corresponding strain and of angles is on the top of the graphs.

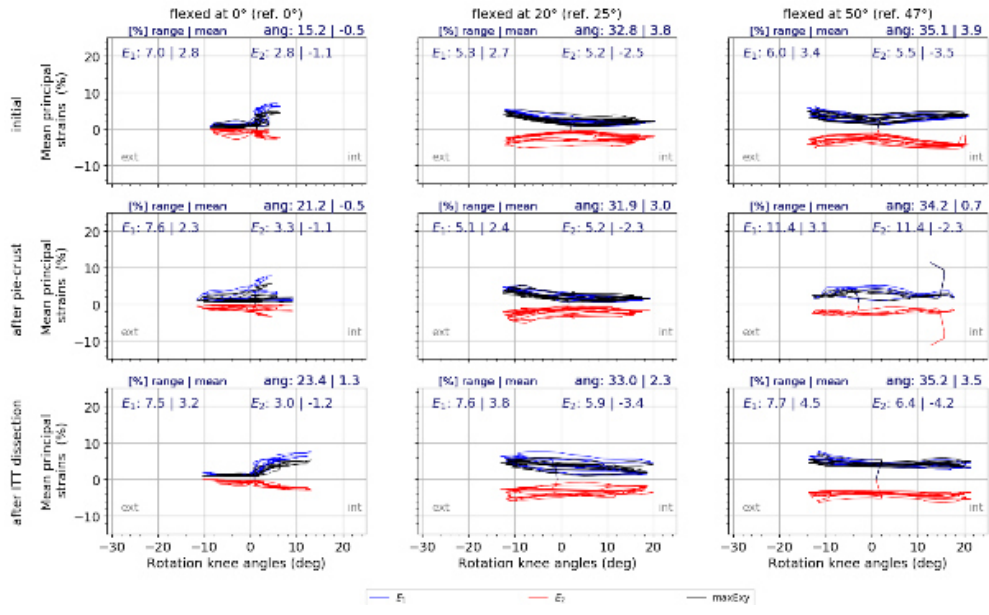
2020_219_R_Photron_Rotation (with different reference images): area 2



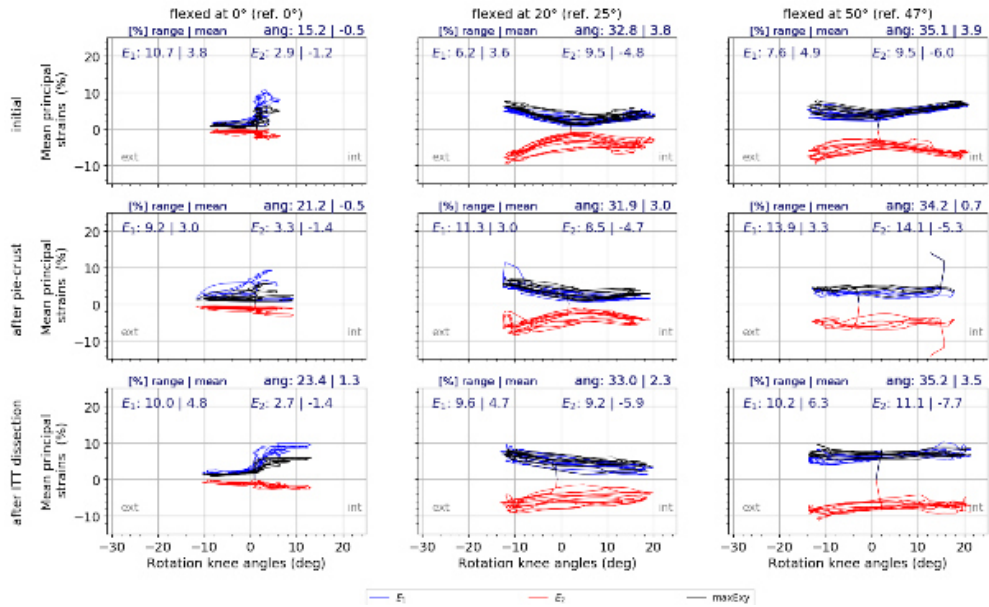
2020_219_R_Photron_Rotation (with different reference images): area 3



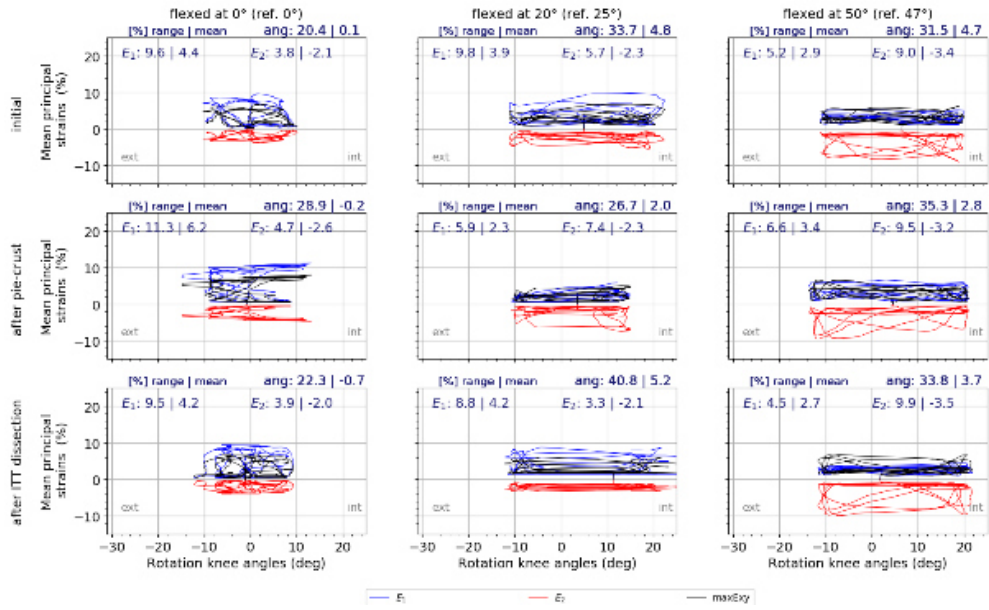
2021_073_L_Photron_Rotation (with different reference images): area 2



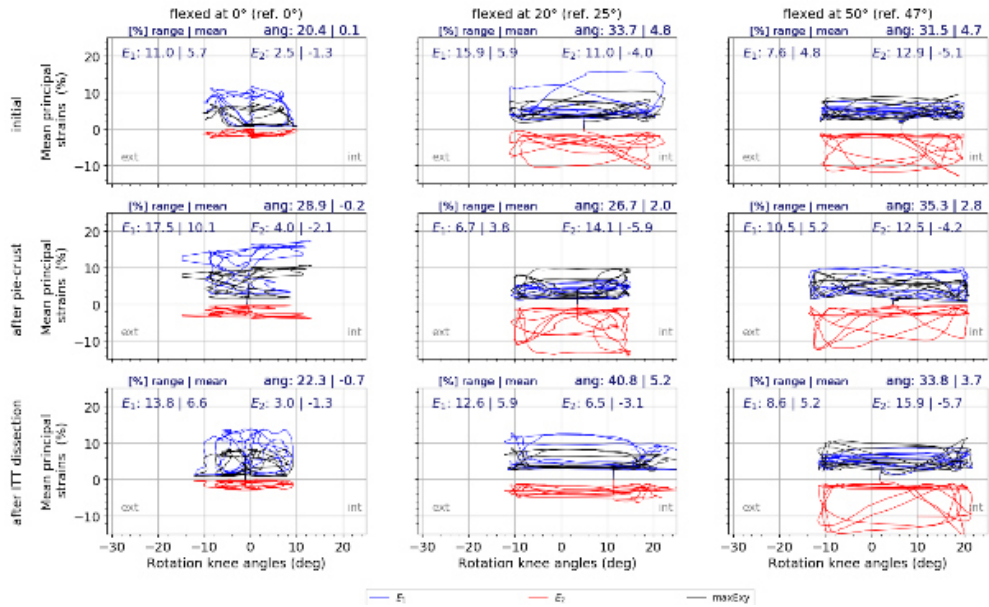
2021_073_L_Photron_Rotation (with different reference images): area 3



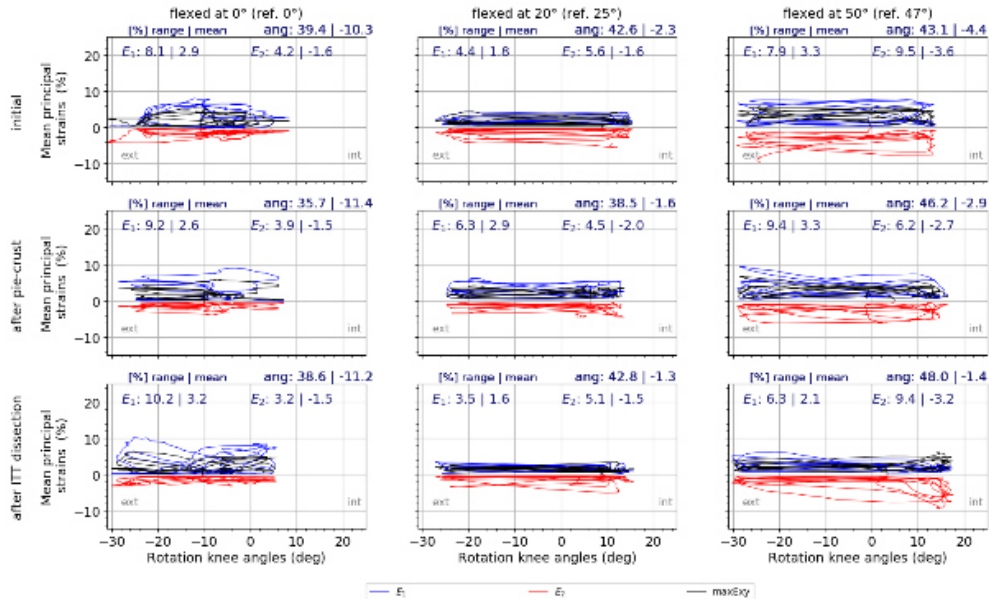
2021_073_R Photron_Rotation (with different reference images): area 2



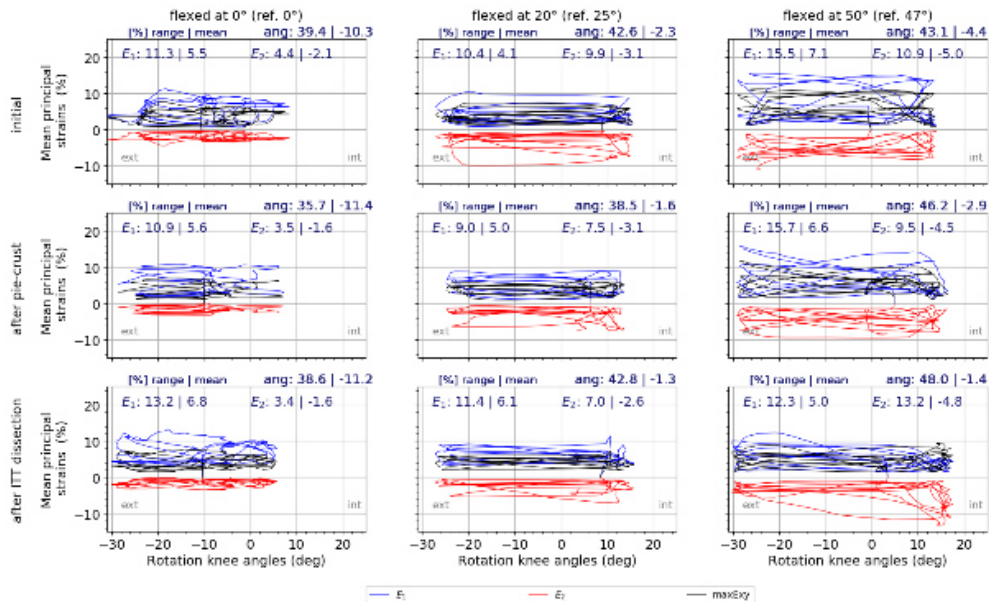
2021_073_R Photron_Rotation (with different reference images): area 3



2021_098_L_PhoBron_Rotation (with different reference Images): area 2



2021_098_L_PhoBron_Rotation (with different reference Images): area 3



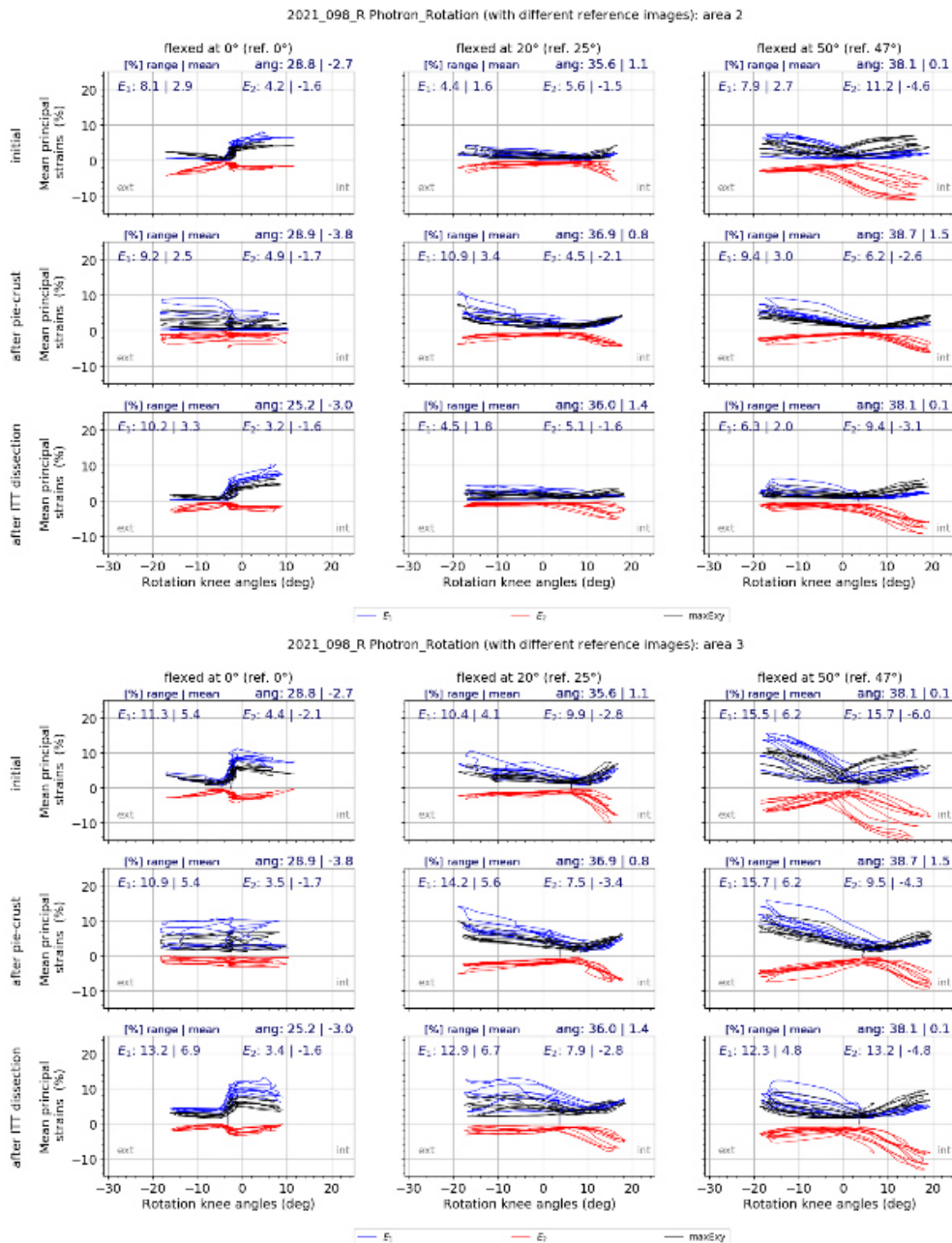
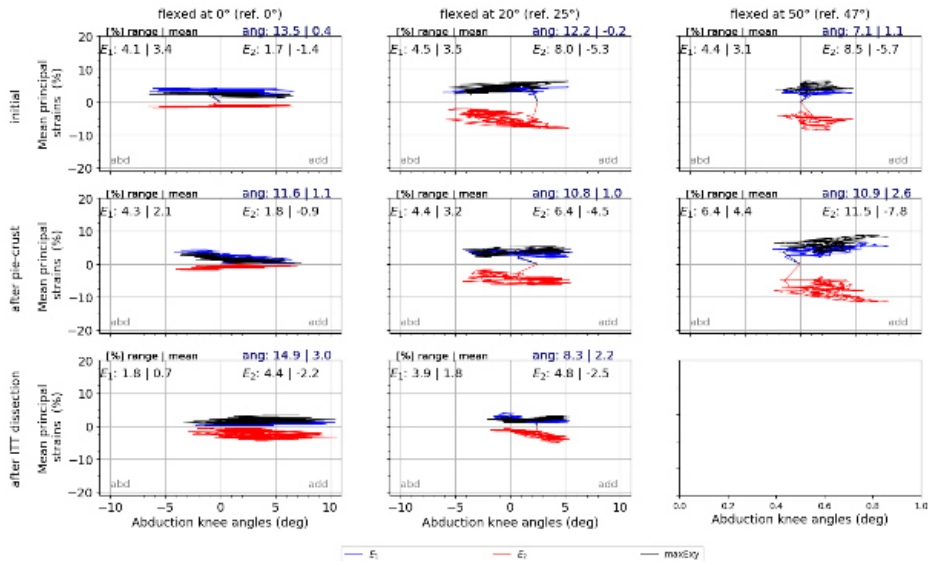
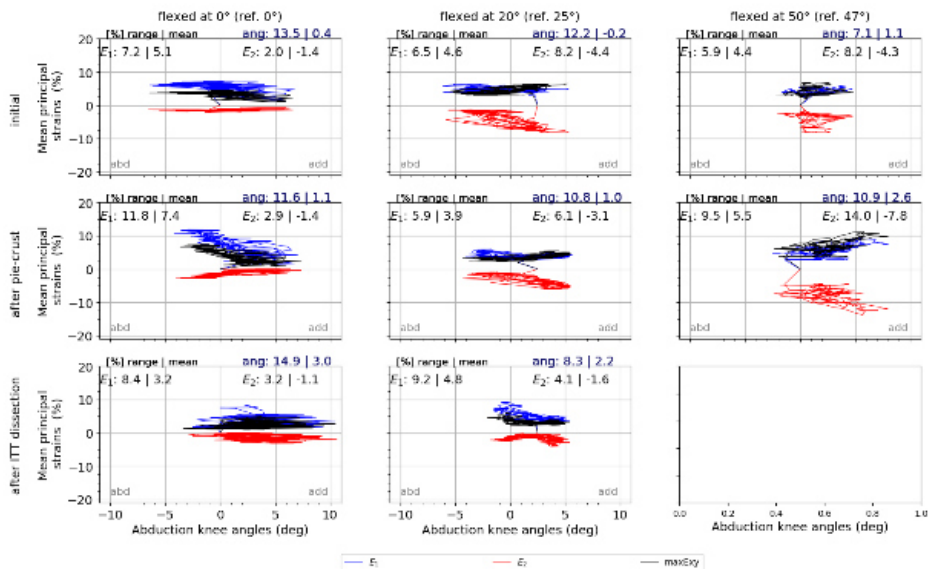


Figure 9. Average maximal shear $maxE_{xy}$, principal major E_1 and minor E_2 strains change with the rotation and adduction-abduction knee angle during rotation movement. Rotations and varus-valgus movements with different knee flexion angles (0° , 20° , and 50°) for initial, after pie-crusting, and after ITT dissection cases on the areas 2 and 3 along the ITT. * E_1 – maximum principal strain (blue), E_2 – minimum principal strain (red), $maxE_{xy}$ – maximal shear strain (black).

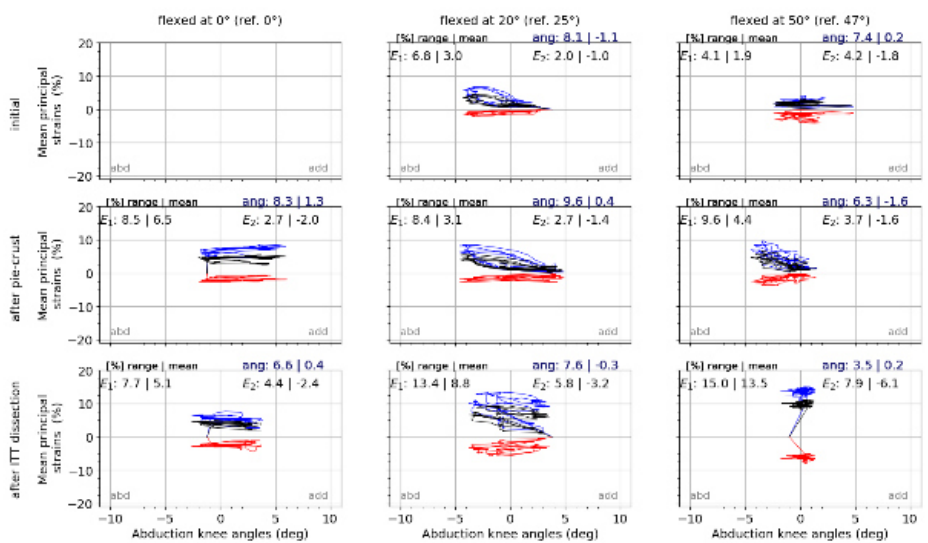
2020_219_L Photron_VarVal (with different reference images): area 2



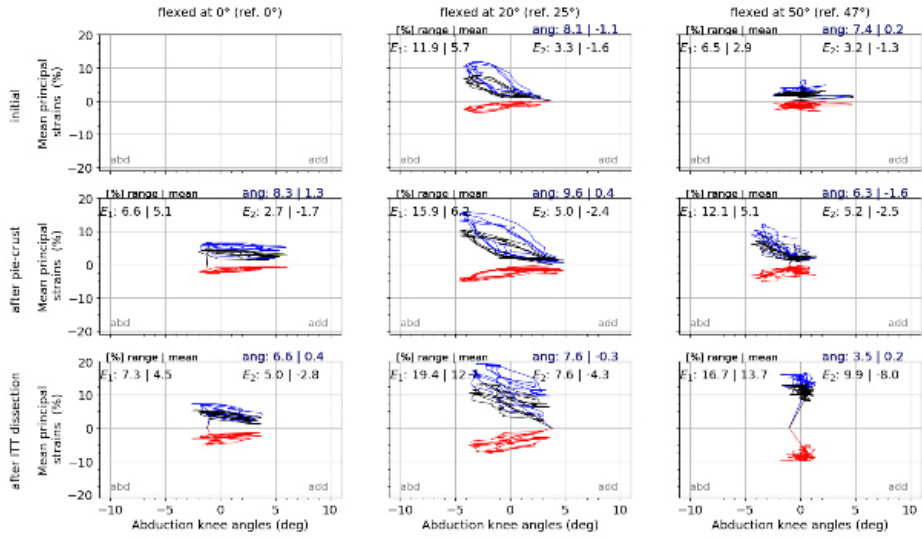
2020_219_L Photron_VarVal (with different reference images): area 3



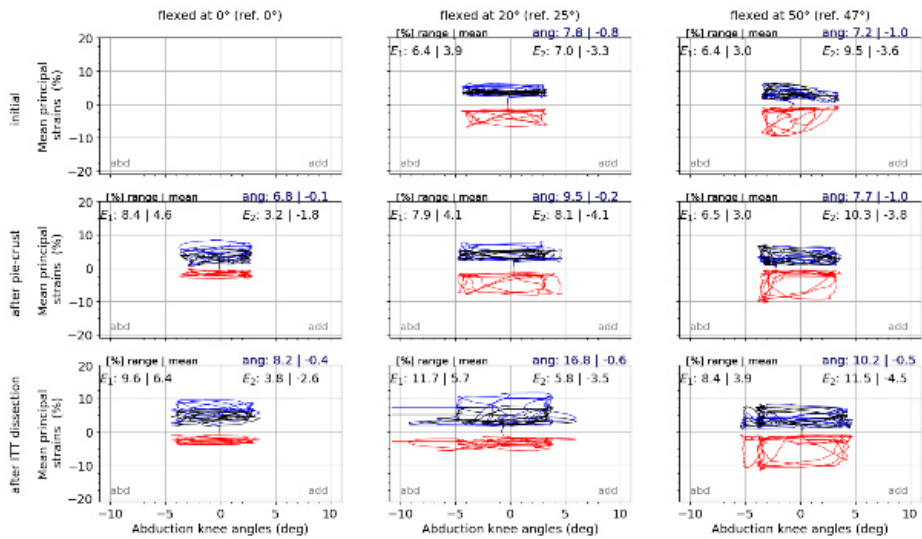
2020_219_R Photron_VarVal (with different reference images): area 2



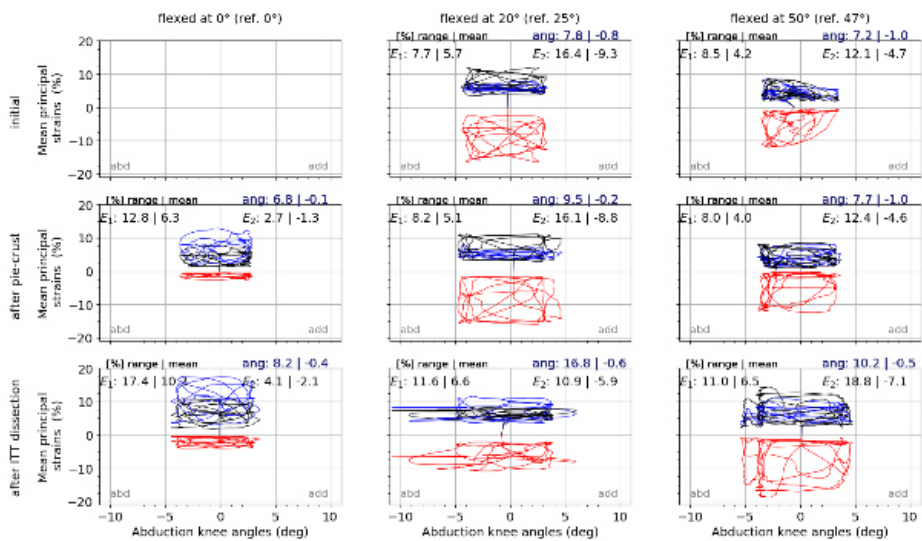
2020_219_R Photon_VarVal (with different reference images): area 3



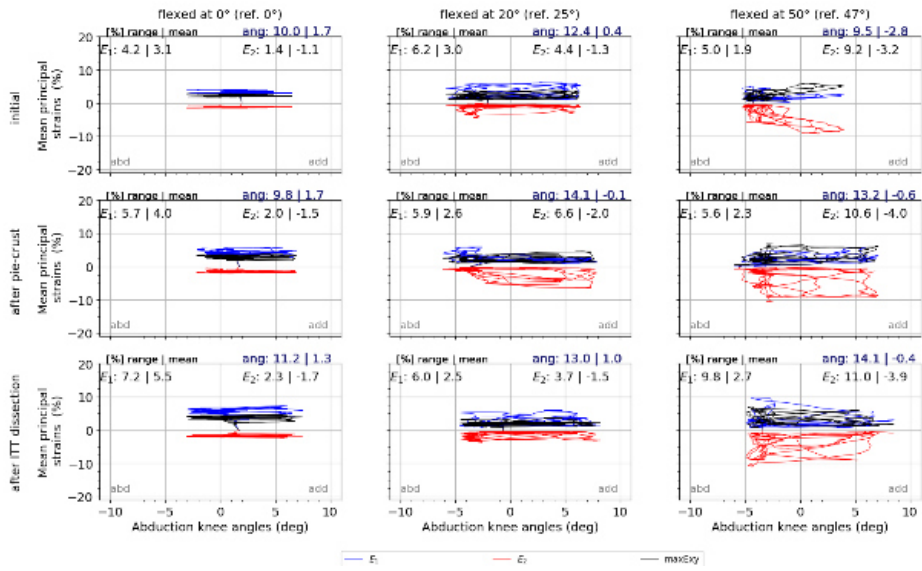
2021_073_R Photon_VarVal (with different reference images): area 2



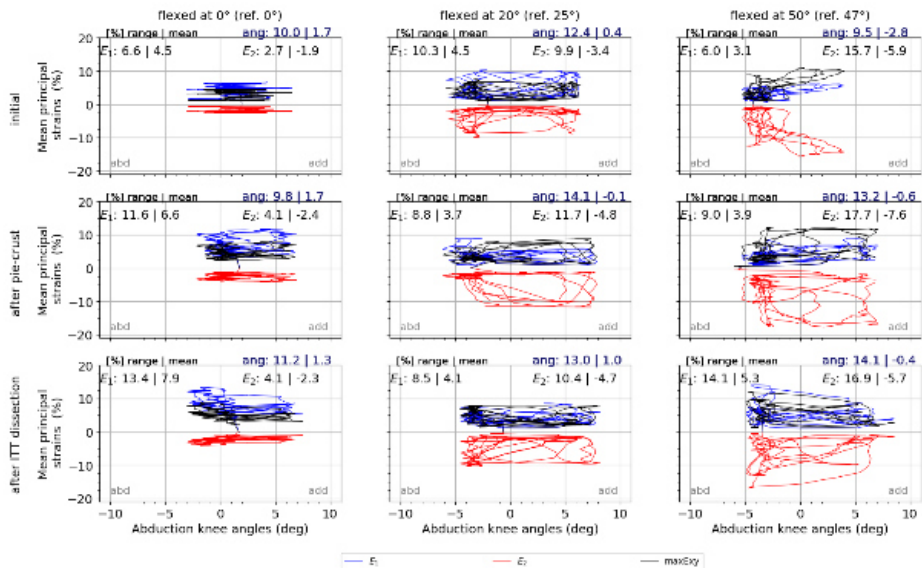
2021_073_R Photon_VarVal (with different reference images): area 3



2021_098_L Photron_VarVal (with different reference images): area 2



2021_098_L Photron_VarVal (with different reference images): area 3



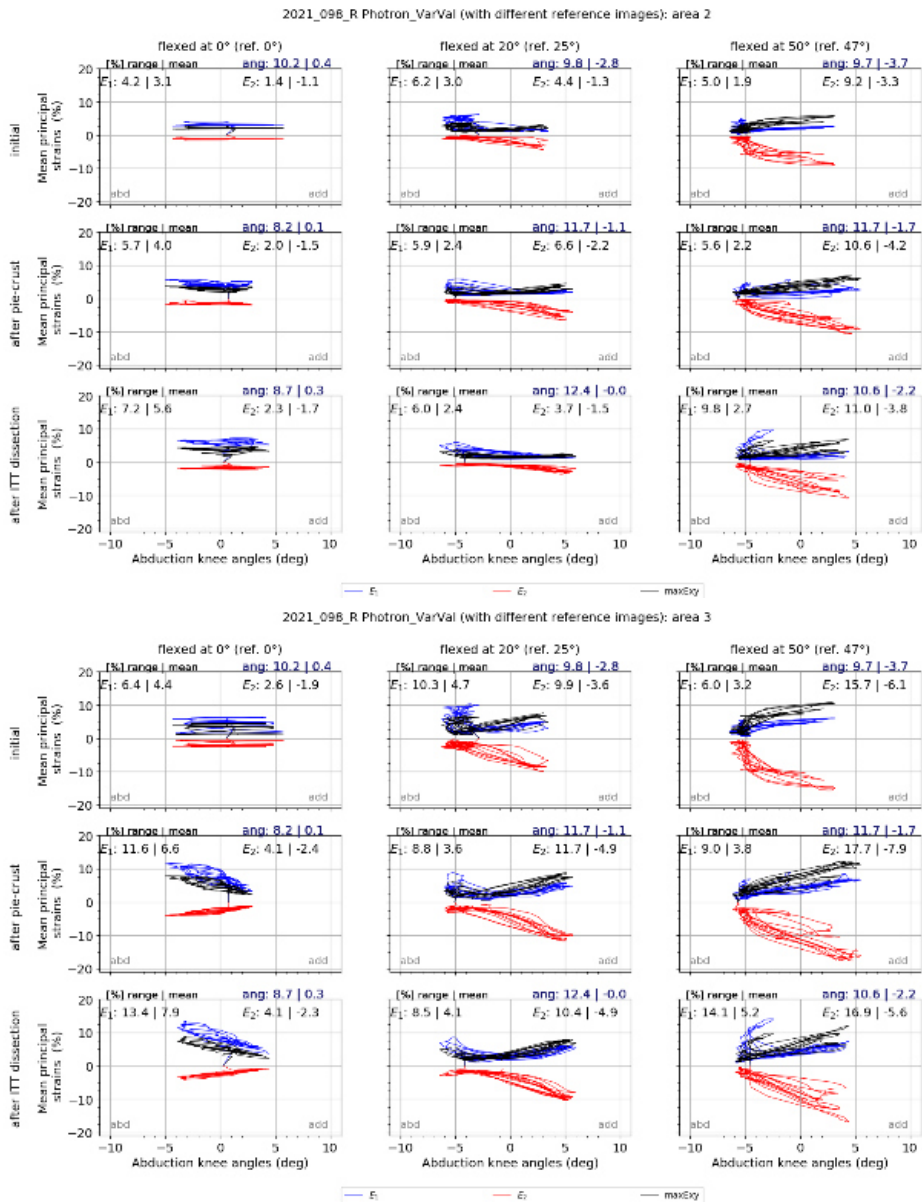
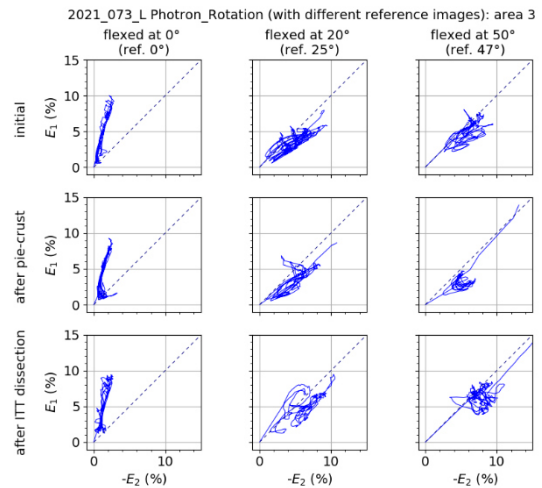
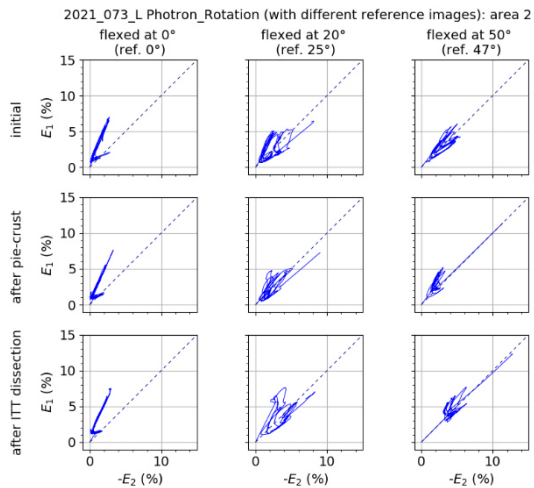
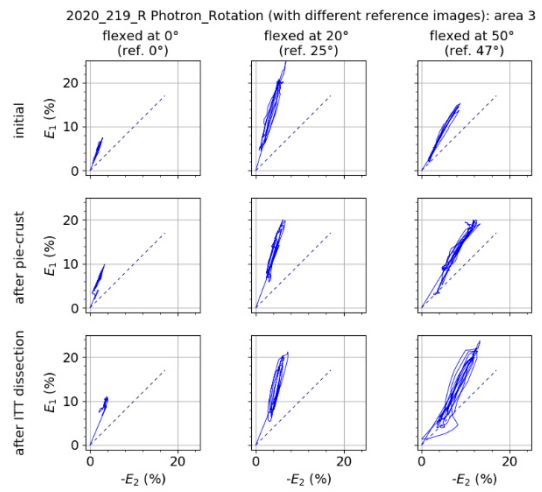
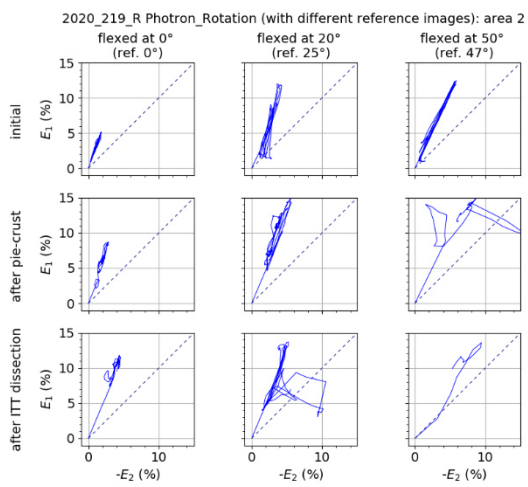
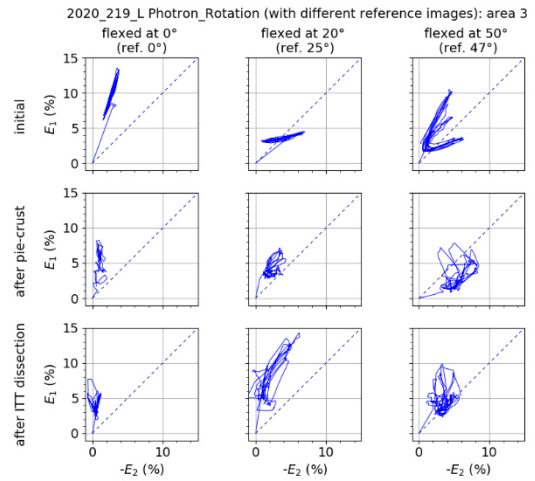
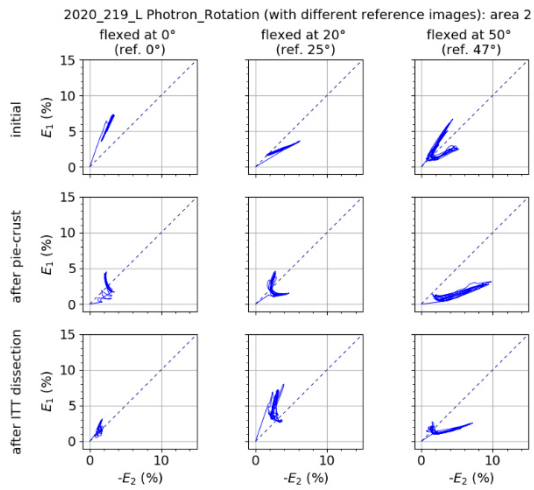


Figure 10. Average maximal shear $maxE_{xy}$, principal major E_1 and minor E_2 strains change with the rotation and adduction-abduction knee angle during varus-valgus movement. Rotations and varus-valgus movements with different knee flexion angles (0° , 20° , and 50°) for initial, after pie-crusting, and after ITT dissection cases on the areas 2 and 3 along the ITT. * E_1 – maximum principal strain (blue), E_2 – minimum principal strain (red), $maxE_{xy}$ – maximal shear strain (black).



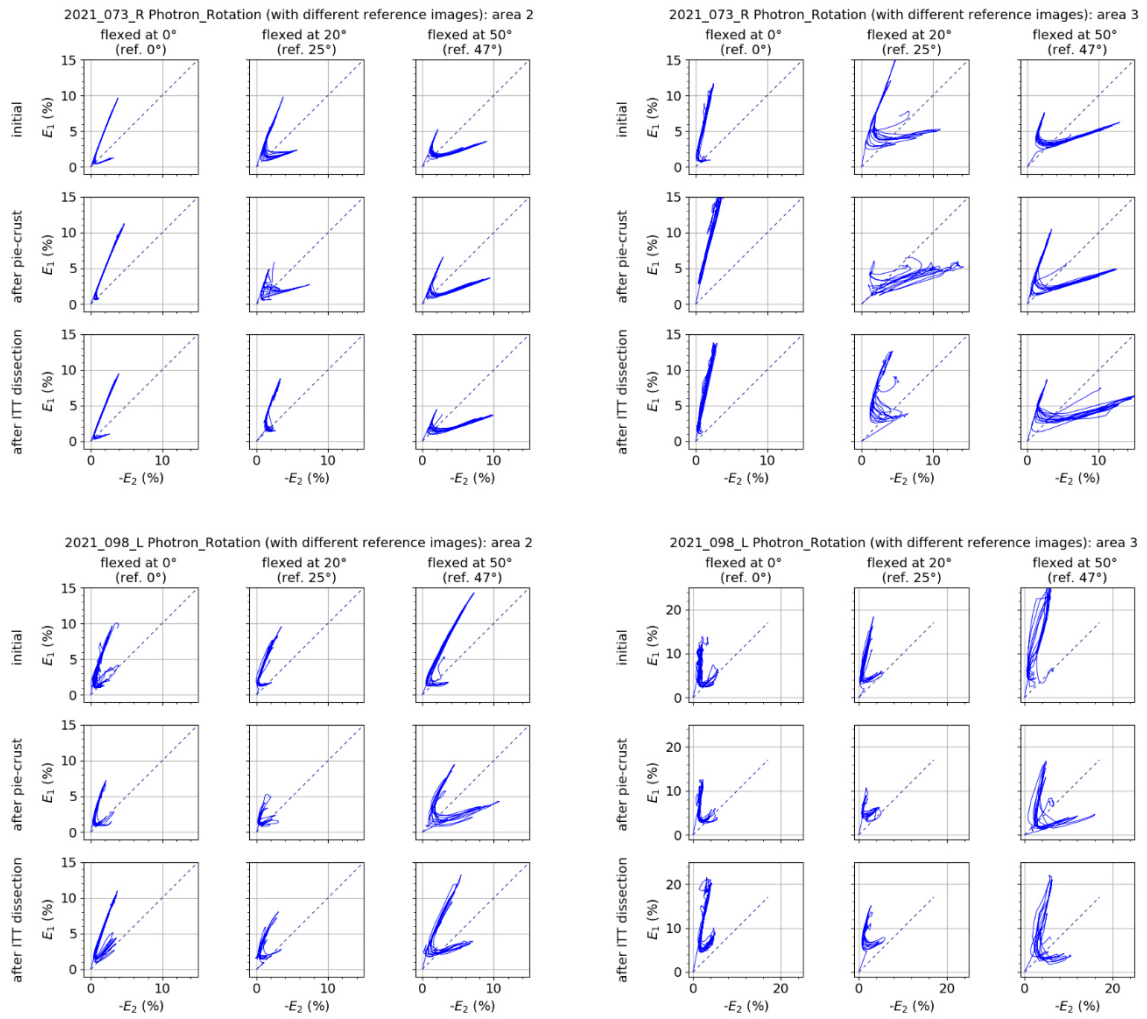
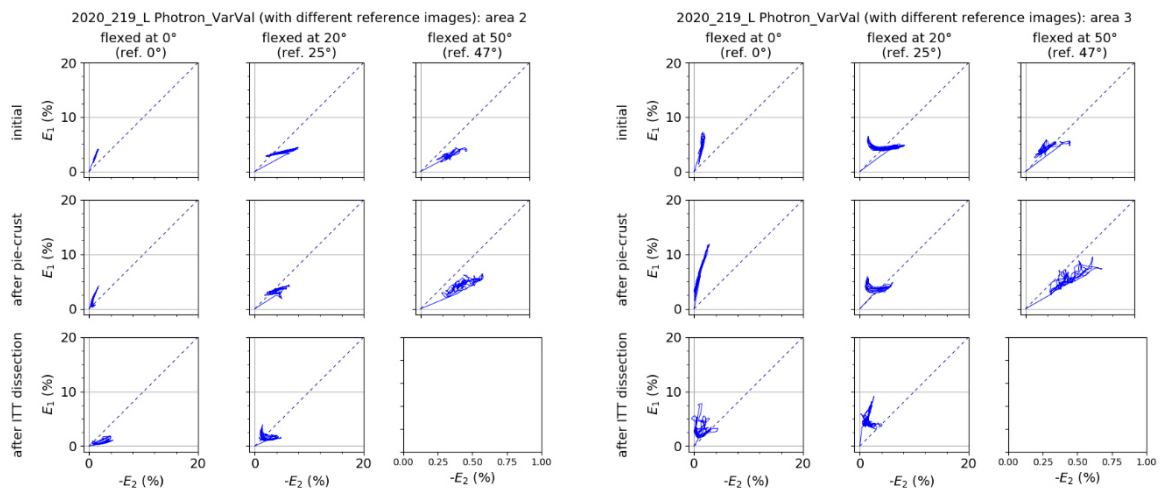
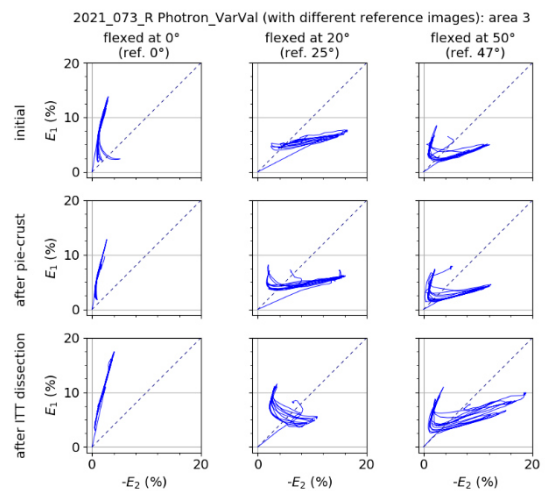
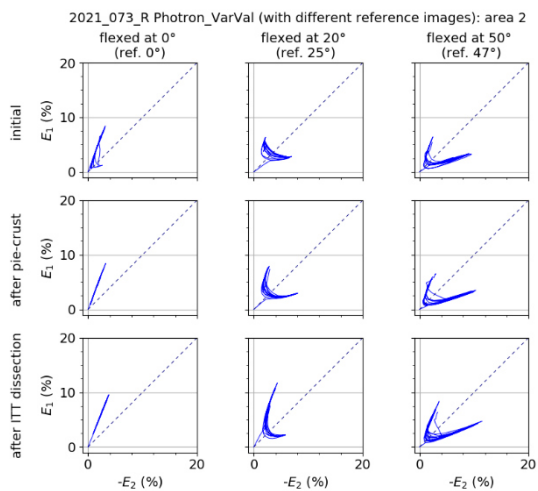
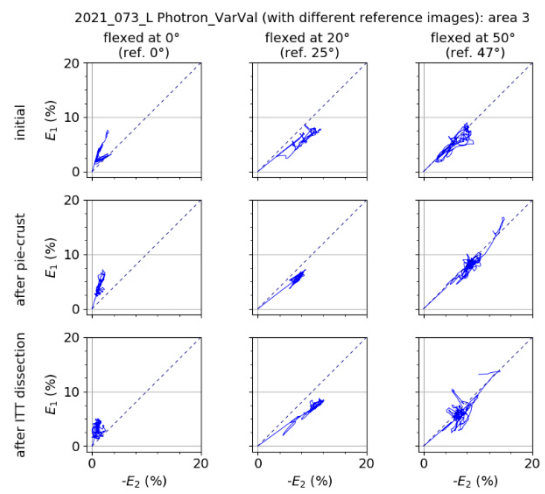
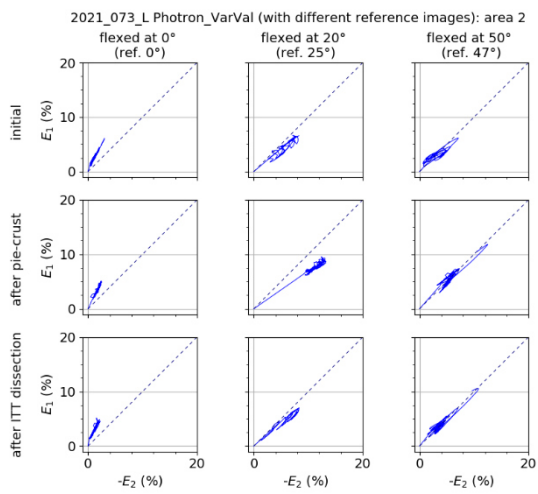
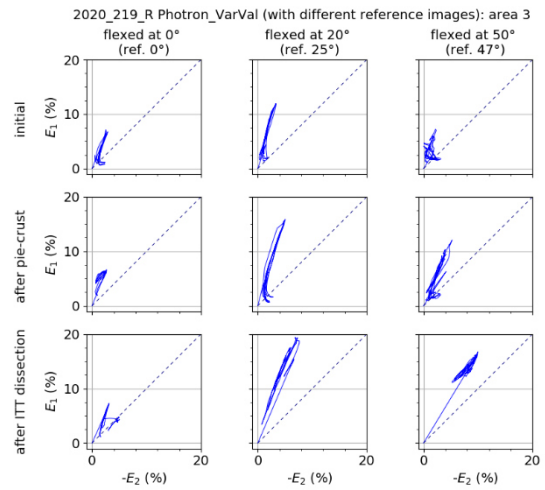
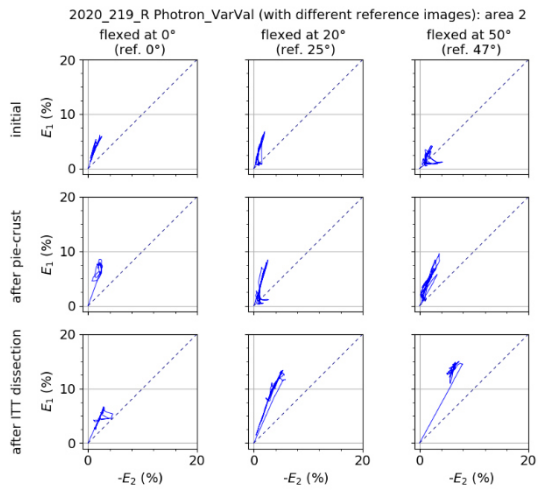


Figure 11. E_1 strain against E_2 strain in absolute value during rotation movement with flexed knee at 0° , 20° , and 50° along the areas 2 and 3 on the ITT for all remaining subjects.





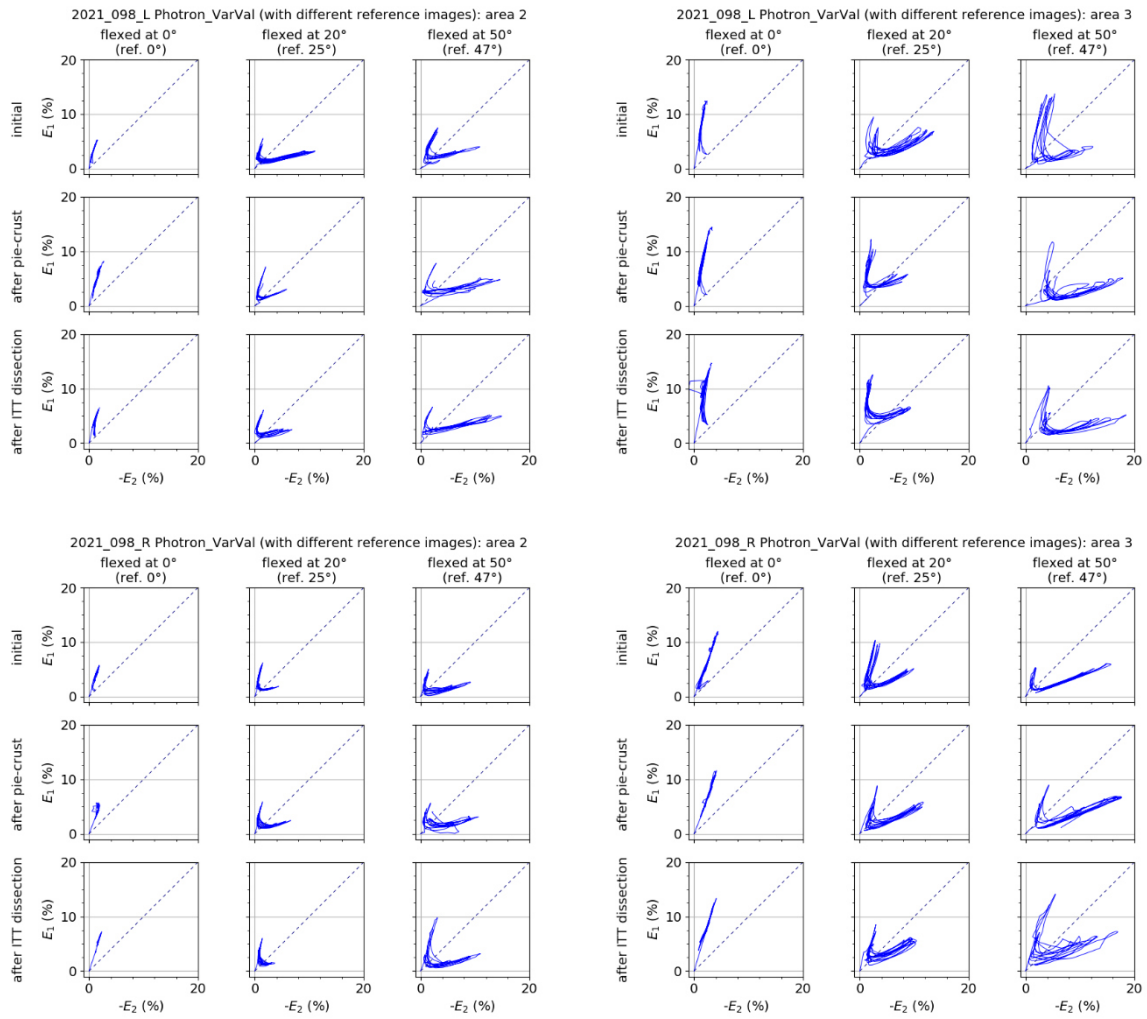


Figure 12. E_1 strain against E_2 strain in absolute value during varus-valgus movement with flexed knee at 0° , 20° , and 50° along the areas 2 and 3 on the ITT for all remaining subjects.